

54/1/2022

ISSN 1338-3523

ISSN 0369-2086

Mineralia Slovaca



Štátny geologický ústav Dionýza Štúra Bratislava



PRESEDA VYDAVATELSKEJ RADY – CHAIRMAN OF EDITORIAL BOARD

IGOR SLANINKA

Štátny geologický ústav Dionýza Štúra Bratislava

VEDECKÝ / VEDÚCI REDAKTOR – SCIENTIFIC AND MANAGING EDITOR

ZOLTÁN NÉMETH

Štátny geologický ústav Dionýza Štúra
Regionálne centrum Košice
Jesenského 8, 040 01 Košice
zoltan.nemeth@geology.sk

REDAKČNÁ RADA – EDITORIAL BOARD

KLEMENT FORDINÁL, Štátny geologický ústav D. Štúra Bratislava

ĽUBOMÍR HRAŠKO, Štátny geologický ústav D. Štúra Bratislava

JOZEF KORDÍK, Štátny geologický ústav D. Štúra Bratislava

PETER MALÍK, Štátny geologický ústav D. Štúra Bratislava

JOZEF MICHALÍK, Ústav vied o Zemi SAV Bratislava

ĽUBOMÍR PETRO, Štátny geologický ústav D. Štúra Košice

DUŠAN PLAŠIENKA, Prírodovedecká fakulta UK Bratislava

MARIÁN PUTIŠ, Prírodovedecká fakulta UK Bratislava

JÁN SOTÁK, Ústav vied o Zemi Banská Bystrica

LADISLAV ŠIMON, Štátny geologický ústav D. Štúra Bratislava

PAVEL UHER, Prírodovedecká fakulta UK Bratislava

REDAKCIA – EDITORIAL STAFF

Vedúci oddelenia vydavateľstva ŠGÚDŠ a propagácie – Head of the Department of ŠGÚDŠ Publishers and Promotion

LADISLAV MARTINSKÝ

ladislav.martinsky@geology.sk

Jazykoví redaktori – Lingual editors

Janka Hrtusová – Zoltán Németh

janka.hrtusova@geology.sk

Grafická úprava a technické spracovanie – DTP processing

Slávka Žideková

slavka.zidekova@geology.sk

Mineralia Slovaca (Web ISSN 1338-3523, ISSN 0369-2086), EV 3534/09, vychádza dvakrát ročne. Vydavateľ a tlač: Štátny geologický ústav Dionýza Štúra, Mlynská dolina 1, 817 04 Bratislava, IČO 31 753 604. Dátum vydania čísla 54/1/2022: júl 2022.

Predplatné v roku 2023 vrátane DPH, poštovného a balného pre jednotlivcov 22,00 €, pre členov SGS a geologických asociácií 20,90 €, pre organizácie v SR 31,90 €, pre organizácie v ČR 55,00 €. Cena jednotlivého čísla pri osobnom nákupe v predajniach ŠGÚDŠ v Bratislave a v Košiciach je 6,05 € vrátane DPH. Časopis možno objednať v redakcii a v knižnici regionálneho centra v Košiciach.

Adresa redakcie: Štátny geologický ústav D. Štúra – RC Košice (Mineralia Slovaca), Jesenského 8, 040 01 Košice. Telefón: 055/625 00 43; fax: 055/625 00 44, e-mail: mineralia.slovaca@geology.sk, e-mail knižnica: secretary.ke@geology.sk

Mineralia Slovaca (Web ISSN 1338-3523, ISSN 0369-2086) is published twice a year by the State Geological Institute of Dionýz Štúra Bratislava, Slovak Republic. The date of issuing of the number 54/1/2022: July 2022.

Subscription for the whole 2023 calendar year (two numbers of the journal): 66.00 € (Europe), 77.00 € (besides Europe), including VAT, postage and packing cost. Claims for nonreceipt of any issue will be filled gratis.

Order of the Editorial Office: Štátny geologický ústav D. Štúra – RC Košice (Library), Jesenského 8, SK-040 01 Košice, Slovak Republic. Phone: +421/55/625 00 43; fax: +421/55/625 00 44, e-mail: mineralia.slovaca@geology.sk, library: secretary.ke@geology.sk

© Štátny geologický ústav Dionýza Štúra Bratislava

PŮVODNÉ ČLÁNKY – ORIGINAL PAPERS

Danková, Z., Bekényiová, A., Čechovská, K., Fedorová, E., Nováková, J., Uhrinová, K., Briančin, J. & Kúšik, D.
Experimental study of polluted sediment and As elimination from the pit water in the locality of Zlatá Idka-Rieka, Slovakia

Štúdium kontaminovaných sedimentov a eliminácie As z podzemnej banskej vody na lokalite Zlatá Idka-Rieka 3

Valovičová, V., Dolinská, S., Vaculíková, L., Plevová, E., Znamenáčková, I. & Danková, Z.

Characterization of fine-grained montmorillonite fractions for preparing polymer-clay nanocomposites

Charakteristika jemnozrnej frakcie montmorillonitu na prípravu polymérových ílovitých nanokompozitov 17

Čičáková, C., Tóth, R., Horváthová, H., Drábik, A., Jurkovič, L. & Kravchenko, D.

Electroremediation in low-hydraulic conductivity zones – current stage of knowledge and small-scale laboratory experiment

Elektroremediácia v zónach s nízkou hydraulickou vodivosťou – súčasný stav poznatkov a laboratórny experiment 29

Bajtoš, P.

Use of analysis of seasonal hydrochemical regime for better understanding of mine water genesis and more accurate estimate of its impact on stream water quality at flooded Rudňany ore mine (North-Gemeric zone, Slovakia)

Využitie analýzy sezónneho hydrochemického režimu vody v zatopenej rudnej bani Rudňany na lepšie pochopenie jej genézy a presnejší odhad jej vplyvu na kvalitu vody v povrchovom toku 47

Phu, H., Tuan, L. C., Thao, N. L. N. & Han, H. T. N.

Relation of groundwater quality and peat deposits in Tay Ninh province, Vietnam

Vzťah kvality podzemnej vody a ložísk rašeliny na príklade monitorovacieho výskumu v provincii Tay Ninh, Vietnam 69

Eftimi, R., Basha, G., Tafilaj, I. & Sheganaku, X.

Hydrogeological map of Albania at a scale of 1:200,000, principles of compilation and content – a document of Albanian pioneering hydrogeological research since the 1960s

Hydrogeologická mapa Albánska v mierke 1 : 200 000, princípy jej zostavenia a obsah – dokument priekopníckeho prístupu k hydrogeologickému prieskumu v Albánsku od šesťdesiatych rokov minulého storočia 81

COVER: Mountain ridges in the area of Zlatá Idka village (Spiš-Gemer Ore Mts., Slovakia, dark forest zone on both sides of the valley with the position of Zlatá Idka village in its central part, middle photo of the composition) represented an important source of Au, Ag and Sb ores already from the end of the 15th century. Currently, this area is no longer active in mining, but pit waters from numerous abandoned adits represent a significant environmental load (upper positioned two images in the composition). The paper by Danková et al. (this issue, pp. 3–16) presents the results of laboratory investigation of possibilities of As elimination from pit water in locality Zlatá Idka-Rieka (the lower two photos in the composition). Authors of photographs: Z. Németh, Z. Danková and A. Bekényiová.

OBÁLKA: Horský masív v oblasti Zlatej Idky (Spišsko-gemerské rudohorie, tmavé pásmo lesov po oboch stranách údolia s pozíciou Zlatej Idky v centrálnej časti, stredná fotografia kompozície) bol už od konca 15. storočia významným zdrojom Au, Ag a Sb rúd. V súčasnosti už táto oblasť nie je bansky aktívna, ale banská voda z početných opustených štôlní predstavuje výraznú environmentálnu záťaž (horné dva obrázky kompozície). Článok Dankovej et al. na str. 3 – 16 prezentuje výsledky laboratórneho výskumu možnosti eliminácie As z banskej vody na lokalite Zlatá Idka-Rieka (dve spodné fotografie kompozície). Autori fotografií: Z. Németh, Z. Danková a A. Bekényiová.

Experimental study of polluted sediment and As elimination from the pit water in the locality of Zlatá Idka-Rieka, Slovakia

ZUZANA DANKOVÁ^{1,*}, ALEXANDRA BEKÉNYIOVÁ¹, KATARÍNA ČECHOVSKÁ¹,
ERIKA FEDOROVÁ¹, JARMILA NOVÁKOVÁ², KATARÍNA UHRINOVÁ², JAROSLAV BRIANČIN³
and DUŠAN KÚŠIK⁴

¹State Geological Institute of Dionýz Štúr, Regional Center Košice, Department of Applied Technology
of Raw Materials, Slovak Republic; *zuzana.dankova@geology.sk

²State Geological Institute of Dionýz Štúr, Regional Center Spišská Nová Ves,
Division of Geoanalytical Laboratories, Slovak Republic

³Slovak Academy of Sciences, Institute of Geotechnics, Košice, Slovak Republic

⁴State Geological Institute of Dionýz Štúr, Department of Raw Minerals and Geophysics, Bratislava,
Slovak Republic

Abstract: The study presents introductory laboratory and in-situ experiments focused on elimination of As from the pit water in locality Zlatá Idka-Rieka, Slovakia, as well as on characterization of the sediment parameters in this locality from the viewpoint of their eventual toxicity. The mobility of As from the sediment is dependent on the chemical bonds with non-stable Fe oxides/hydroxides, creating surface coatings on the grains of minerals and soil, present in the lake of pit water. Leachates after the Simply Bioavailability Extraction Test contained high concentrations of Fe (223 mg.l⁻¹), Mn (165 mg.l⁻¹), as well as As (11.1 mg.l⁻¹), which are potential toxic for people in case of contamination of the soil attached to vegetables, or from coarse dust that can be inhaled and then swallowed. The batch adsorption experiments were performed in the laboratory and next in in-situ conditions. As adsorbents natural zeolite, terra rossa and their mixture were used. In laboratory the As adsorption was fast, reached equilibrium almost after 4 hours. The adsorption capacity of zeolite and terra rossa was 18.3 and 25,3 µg.g⁻¹, respectively. Effect of in-situ As removal was the highest for terra rossa (almost 85 %) and the concentration of As in leachate after the experiment was slightly higher than required limited value. The promising results for future in-situ applications brought laboratory column experiments, where after 4 cycles of adsorption the effectivity of columns was still 95 % independently on the columns filling (layers or mixture of studied adsorbents).

Key words: pit water, adsorption, zeolite, terra rossa

Graphical abstract



Highlights

- Arsenic present in the sediment in studied locality is easy mobile and potential toxic for local population.
- Laboratory adsorption experiments decreased the As content in the pit water to concentration applicable for irrigation waters.
- Laboratory experiments in dynamic conditions demonstrated high potential of column filling – beds of zeolite and terra rossa for in-situ applications.

1 Introduction

In Slovakia, the source of contamination of the natural environment with arsenic is mainly anthropogenic or caused by mining activity, which adversely affects the ore deposits in all components of the environment. Its impact may appear immediately, but also with a delay of several years. The presence of arsenic (As) in surface water and

groundwater, and associated stream sediments and soils represents a serious environmental concern. In territory of Slovakia the highest concentrations of As contaminant are present in the ore deposits areas of Slovenské rudohorie Mts., Nízke Tatry Mts. and Malé Karpaty Mts. (Fľaková et al., 2017).

In old mining village of Zlatá Idka the silver and antimony ores were extensively mined and processed. Waters,

soil and stream sediments in this area are contaminated by arsenic. High contents of this potential toxic element are present especially in the outflows of pit waters and consequently in surface water of the Ida creek. Exploration was realized within the frame of geological project of the State Geological Institute of Dionýz Štúr (SGIDS) Evaluation of potential impact of the geochemical environment on the health state of inhabitants in the area of the Spiš-Gemer Ore Mts. (Rapant et al., 2004). Chemical analyses of water proved high concentrations of As in almost all water sources used in area, with the exception of some shallow based mines (adits) and springs. The arsenic is present in less toxic form of pentavalent ions, what suggests the presence of **oxidizing conditions** – probably in the final stage of pit water outflow to the surface (Cicmanová & Baláz, 2007).

Arsenic and its compounds represent persistent mobile pollutants, which cannot be destroyed, but their negative impact can be reduced by immobilization (adsorption). Between pH 2.2 to 11.5 the arsenate oxyanion ($pK_a = 2.2, 7.0, 11.5$) dissociates in aqueous solutions in two forms: $H_2AsO_4^-$ (pH 2.2–7.0 and $HAsO_4^{2-}$ (pH 7.0–11.5) (Ho & McKay, 1999).

Oxidation-reduction potential (Eh) and pH are the most important factors that control the forms of As occurrence. Both parameters must be measured directly in the field and simultaneously. Arsenic is a special element among the elements forming complex anions (e.g. As, Se, Sb, Mo, V, Cr) in its sensitivity to mobilization at pH values that are typical for the groundwater (6.5–8.5), and this in both oxidation and reduction conditions (Smedley and Kinniburgh, 2002; Sracek et al., 2004a, b). Arsenic can occur in the natural environment in several oxidation stages (– III, 0, + III and + V), but in natural waters it is predominantly found as an inorganic form in a complex anion such as trivalent arsenite (As (+ III)) or pentavalent arsenate [As (+ V)]. Under oxidizing conditions, $H_2AsO_4^-$ is dominant at low pH (less than 6.9), whilst at higher pH, the $HAsO_4^{2-}$ becomes dominant.

The work of Cicmanová and Baláz (2007) showed that in terms of the level of content and bioavailability of As in river sediments of streams, the whole Ida stream can be described as an area of high environmental risk. These are indicated results of the sequential extraction method of metals, where decisive proportions of As in the sediment is in the 5th residual fraction (41–54 %) and the 3rd reducible fraction (33–53 %). Particularly problematic is the high proportion of the 3rd reducible fraction, representing the metal content bound to the thermodynamically unstable Fe and Mn oxides. For this reason, there is a probability of variability in the processes of metal binding in the sediment and its release into water depending on changes in the redox conditions of the aqueous environment. These changes are directly related to seasonal regime conditions – strength of pit and surface water flows.

The study is focused in the characterization of sediment contaminated by arsenic containing pit water in locality Zlatá Idka-Rieka. The mobility and bioavailability of potential toxic elements in living environment were tested and evaluated by known methods for contaminated soils and sediments. The elimination of high content of arsenic (concentration changed in dependence on climate and weathering conditions from 300 up to 380 $\mu\text{g.l}^{-1}$) from the pit water was studied in laboratory within static and dynamic regimes, as well as in-situ in batch conditions using natural adsorbent of zeolite and decorative clay terra rossa. For all test both materials were used separately, as well as applied was also their mixture.

2 Materials and methods

2.1 Pit water sample

Laboratory, as well as, in situ experiments were performed applying the pit water, flowing out from the Hauser adit in the Zlatá Idka-Rieka locality. The pit water in this locality is characterized by very high concentrations of As and Fe, what is expressed by the rusty red colour



Fig. 1. Regulated flow of pit water on the locality of Hauser adit with formed lake under the drain of pit water.

of precipitates in drained water and coatings on the surrounding rocks and soil. The concentration of As in the pit water varied depending on the year season and climate conditions. The As concentrations of 200 up to 360 $\mu\text{g.l}^{-1}$ were measured on the locality, what is several times higher than required value applicable for irrigation waters 50 $\mu\text{g.l}^{-1}$ (according to the Regulation of Government of the Slovak Republic No. 269/2010 Coll. (next only “regulation”) – Part B – Surface waters for irrigation. Except of As and Fe, other analysed elements (Ba, Co, Cr, Cu, Mn, Ni, Zn, Pb, Sb, Cd) in the pit water did not exceed the limit value (not shown here). The flow of pit water is regulated and the water is cumulated in the plane under the previous heap forming small lake.

2.2 Sediment sample

The sediment sample, denoted as H1, was taken from the lake with pit water under its drain in the Hauser adit locality. The sample of sediment was wet sieved to grain size below 2 mm. The oversized product and product of fraction 1.0–2.0 mm consisted of organic material (leaves, springs, cons). The sludge below 1 mm was analysed by laser granulometer (defined below) to determine the particle size distribution and used for the experimental purposes.



Fig. 2. Fractions of sediment H1: fraction +2.0 mm and 1.0–2.0 mm created by organic matter, fraction below 1.0 mm consisted of fine particles with high content of Fe.

2.3 Adsorbents

As the adsorbents, domestic natural materials with good adsorption expectations were chosen: zeolite from the Majerovce locality and decoration clay terra rossa from the Včeláre locality.

2.4 Adsorbents and sediment characterization

The powder X-ray diffraction (XRD) patterns of adsorbent samples and sediment sample were recorded

using a diffractometer D2 Phaser (Bruker, Germany), equipped with a $\text{CuK}\alpha$ radiation source (30 kV, 10 mA) and Lynxeye detector. The data were qualitatively and quantitatively analysed using Software DIFFRAC.EVA with PDF-2 Database.

Differential thermal analysis (DTA) was carried out using the derivatograph STA 449 F3 Jupiter (Netzsch, Germany). Measurement was done in real atmosphere up to the temperature 1000 °C with heating gradient 10 °C/min. Obtained data were processed by the Proteus software.

Particle size distribution of sediment sample in the range 0.01–1000 μm was analysed by laser light scattering analyser Mastersize 3000 (Malvern, UK)

The iron oxide coatings of sediment were studied by scanning electron microscopy FE MIRA 3 (Tescan, Czech Republic) equipped by XRD energy-dispersive (EDX) analyser of chemical composition (Oxford Instruments).

2.5 Mobility of toxic elements and bioassessability testing

Mobility of toxic elements present in the sediment was tested using Synthetic Precipitation Leaching Procedure (SPLP), Method 1312 based on the acid rain leaching (Method 1312, 1994; Fey et al., 2011). The sediment sample of 5 grams was extracted by solution of H_2SO_4 and HNO_3 (weight ratio 3 : 2). The sediment and extraction solution were placed into the extraction bottle and shaken for 18 hours on the laboratory shaker. Then the leachate was filtered and analysed.

The bioassessability of the toxic elements present in the sediment H1 was tested by Simply Bioavailability Extraction Test (SBET). The sediment sample of 5 grams was extracted by solution of 0.4 M glycine of pH 1.5 (adjusted by HCl) under the vigorous stirring for 1 hour at 37 °C (Report No.: 1542820-003-R-Rev0, 2016; Kim et al., 2009).

2.6 Adsorption experiments

First, the laboratory adsorption experiments were made by batch technique. The adsorbents dose was 10 g. l^{-1} . 1 g of adsorbents was added into the glass bottles containing 100 ml of pit water. The initial pH of the pit water was 7.15. The suspensions were shaken for 20 hours at the ambient temperature (25 °C) at 200 rpm to reach equilibrium and then consequently filtered using the filter paper. The experiments were performed duplicate.

In situ batch adsorption experiments were realized during one day on locality Zlatá Idka. The plastic bottles were filled by adsorbents: zeolite (fraction 1.0–2.0 mm), terra rossa and mixture of both (adsorbents concentration 10 g. l^{-1}). The pit water of 500 ml was added into bottles and shaken onto terrain shakers for 15 up to 120 minutes.

The experiments were performed duplicate. The effect of contact time was studied to determine the rate constant as well as possible mechanism of adsorption.

All column experiments in laboratory conditions were performed using glass columns: inner diameter of 5 cm and 18 cm high. The columns were filled by different layers: quartz sand (60 g), zeolite from the Majerovce locality (20 g) and terra rossa from the Včeláre locality (20 g). During one adsorption cycle, 150 ml of pit water was percolated through the columns at constant flow 2.8 ml per minute. The initial As concentration of pit water varied from 104 to 387 $\mu\text{g.l}^{-1}$ for different cycles, pH from 7.07 up to 7.8. The initial As concentration changed in dependence of time of its storage in plastic bottles. The higher precipitation of iron hydroxides with As occurred, leading to the increase of pH value. The experiments were performed duplicate. For each cycle, the initial As concentration of pit water was analysed.

For all adsorption experiments the supernatant solutions were analysed by the inductively coupled plasma mass spectrometry ICP-MS (Agilent 7900).

3 Results

3.1 Sediment characterization

Particle size analyses of sediment sample showed wide distribution in the range of 1–500 μm , with the maximum at 63 μm , Fig. 3. The results of analyses are listed also in Tab. 1.

The sediment sample was processed by wet magnetic separation and dried at 60 °C for the purpose of mineralogical characterization. The X-ray diffraction analyses (XRD) of magnetic and non-magnetic fractions of this sample are in Fig. 4. Both fractions contained quartz, muscovite, plagioclase and in the case of magnetic fraction also chlorite. But, the XRD analysis did not confirm the presence of expected iron oxide or hydroxide crystalline phases. Therefore the rusty red coatings of rocks and sediment surfaces were further investigated by EDX analyses by scanning electron microscope.

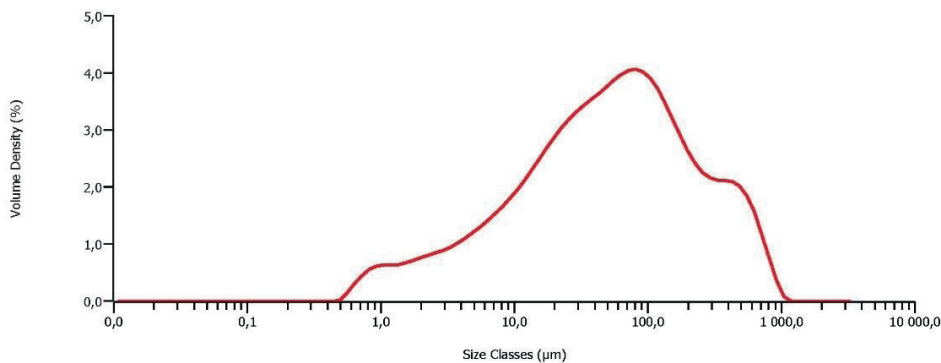


Fig. 3. Particle size distribution of sediment sample H1.

Tab. 1
Particle size analyses of sediment sample H1.

Sample	H1 below 1 mm		
Specific surface area ($\text{m}^2.\text{kg}^{-1}$) of sample of grain size below 1mm	203.2		
Granular class [μm]	volume [%]		
	fraction	over	below
over 2 000	–	0.00	–
2 000–1 000	0.04	0.04	100.00
1 000–500	5.23	5.27	99.96
500–250	9.64	14.91	94.73
250–125	13.12	28.03	85.09
125–63	17.73	45.76	71.97
63–31	17.03	62.79	54.24
31–16	12.98	75.77	37.21
16–8	9.35	85.12	24.23
8–4	6.03	91.15	14.88
4–2	4.04	95.19	8.85
2–1	3.04	98.23	4.81
1–0.010	1.77	100.00	1.77
below 0.010	–	–	0.00
Sum	100.00		

The point EDX analyses showed the presence of Fe and O (41.6 and 40.1 weight %, respectively), as well as expressed higher content of As in the analysed sample (Fig. 5). The content of Mn is also interesting from the environmental point of view.

On the basis of results of XRD and EDX analyses it can be assumed that rusty red colour of sediment as well as surface coatings of rocks in the surrounding lake is caused by amorphous phases of iron compounds (hydroxides, oxyhydroxides), also binding negligible content of As from the outflowing pit water.

During the water sampling also the presence of small precipitates was observed, that were unstable under the water stirring. Longer term of water accumulation (in the lake) and its slower drain into local stream lead to the precipitation of iron compounds caused the expressed sediment colouring.

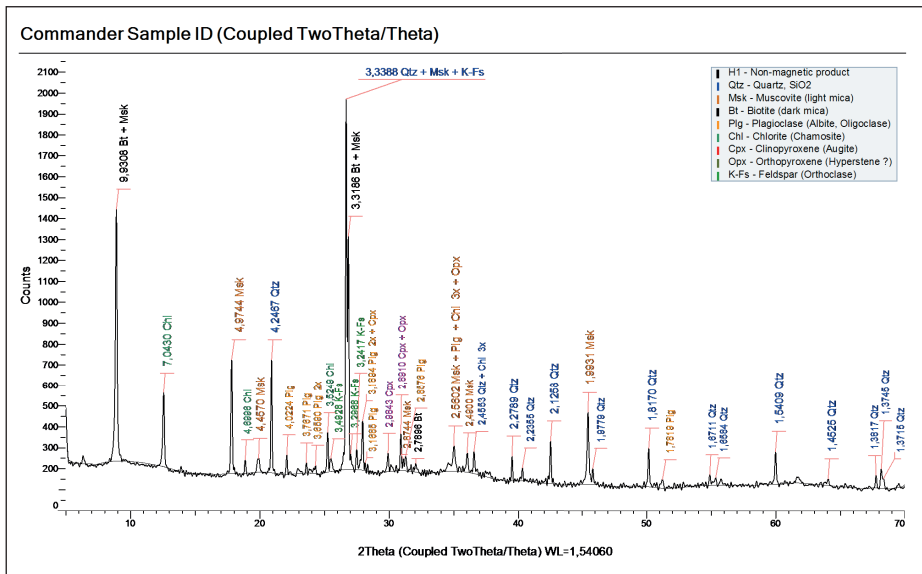


Fig. 4. XRD patterns of magnetic and non-magnetic fraction of sediment sample H1.

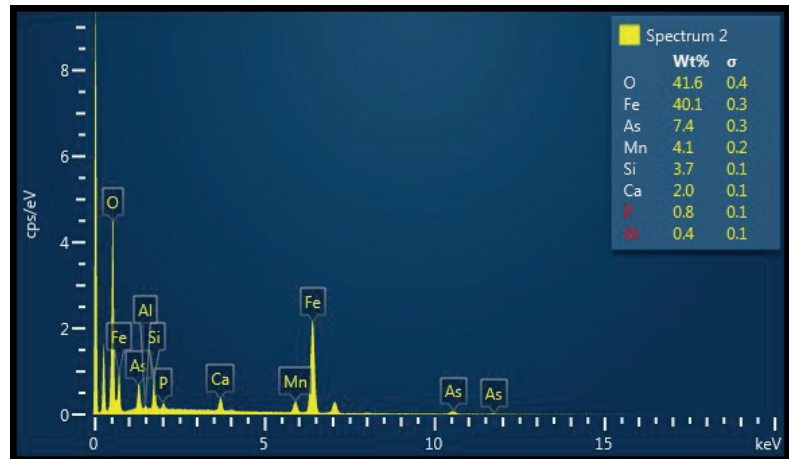
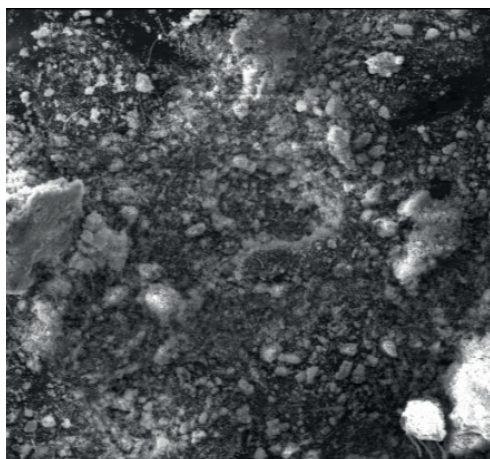
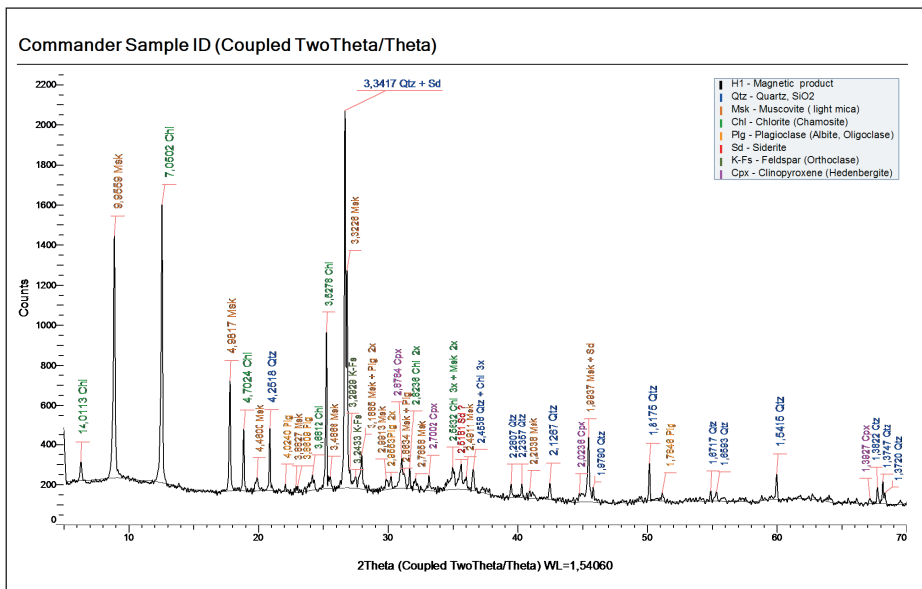


Fig. 5. Point EDX analysis of iron oxide surface coatings.

Tab. 2
Concentration of potential toxic elements in sediment and comparison with the permissible and critical limits according to the guideline.

Element	Permissible limit (ID)	Critical limit		H1 sediment
		Residential districts	Industrial districts	
	[mg.kg ⁻¹]	[mg.kg ⁻¹]	[mg.kg ⁻¹]	[mg.kg ⁻¹]
As	65	70	140	26 032
Ba	900	1 000	2 800	330
Cd	10	20	30	3
Co	180	300	450	28
Cr	12	20	50	34
Cu	500	600	1 500	46
Ni	180	250	500	25
Pb	250	300	800	624
Sb	25	40	80	444
Zn	1 500	2 500	5 000	411

- ID – Permissible limit of contaminant concentration in soils according to the Methodical Instruction of Ministry of Environment of the Slovak Republic, No. 1/2012-7
- IT – Critical limit of contaminant concentration in soils according to the Methodical Instruction of Ministry of Environment of the Slovak Republic, No. 1/2012-7
- 34 – value of contaminant over the critical limit (IT) according to the Methodical Instruction of Ministry of Environment of the Slovak Republic, No. 1/2012-7 for residential districts
- 444 – value of contaminant over the critical limit (IT) according to the Methodical Instruction of Ministry of Environment of the Slovak Republic, No. 1/2012-7 for industrial districts

The presence of potential toxic elements in the sediment represents a risk of their liberation and mobilization. They can be considerable toxic also at low concentrations and should negatively influence the living environment.

Concentrations of risk elements in sediment were evaluated on the basis of chemical analyses according with the Appendix No. 12 of the “Methodical Instruction of Ministry of Environment of the Slovak Republic from the January, 28th 2015, No.1/2015-7” (next only “guideline”).

According the chemical analyses, the concentrations of Cr and Pb provide the values over the critical limits of contaminant in soil in residential districts. The concentration values of As and Sb were over the critical limits of contaminant in soil in industrial districts, Tab. 2.

High concentration of As should be released from the soil matrix by the biological-chemical processes and lead to gradual contamination of plants and groundwaters. Together with other elements it should expose the living environment.

Next the mobility of contaminants in sediment was studied – case study for potential acidification of sediment by acid rains. Acid-forming matters as SO₂ and nitrogen oxides (NO_x) in the atmosphere and on the surface of vegetation react with the air humidity forming the sulphuric and azotic acid. Presence of both acids in the rainfall water leads to decreasing of pH and to reactions causing the acidification of waters and soils (Hruška et al., 1996).

The mobility of sediment contaminants was tested in laboratory conditions according to the Method 1312. Average values of cumulative concentrations of contaminants (mg.g⁻¹) in sediment after the leaching were used to calculate the mobility of indicators (%), Fig. 6.

Mobility of studied contaminants was not very expressive and ranged from 0.02 up to 0.38 %. The most

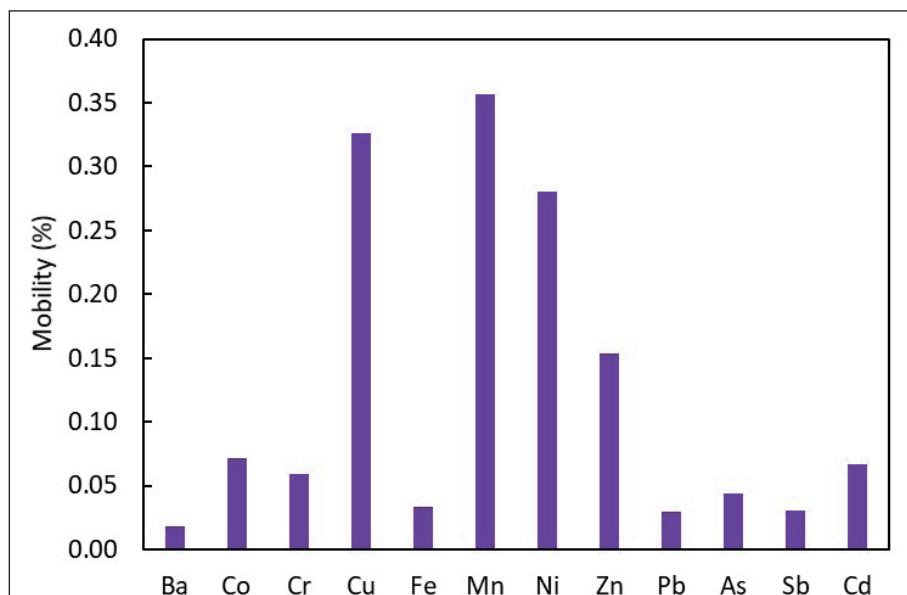


Fig. 6. Mobility of contaminants in studied sediment sample.

mobile seems to be Mn, the least Ba (Fig. 6). In spite of low mobility of As and Fe (0.03 and 0.04 %, respectively), their concentration in leachate after the test represented high values (2.602 mg_{Fe}·l⁻¹ and 0.568 mg_{As}·l⁻¹) due to initial As and Fe concentrations in sediment. It pointed at unstable forms of Fe (Fe, Mn) oxy-hydroxides/hydroxides in sediment binding As.

The bioavailability of a trace element is the proportion of that element being absorbed from soil by the digestive system into body. Laboratory-based extraction procedures

have been developed by researchers to mimic biological extraction using simulated digestive fluids. The bioaccessibility of a trace element is the proportion of that element that can be extracted under simulated digestive conditions. Soil ingestion is thought to be the dominant health risk exposure pathway for many trace elements in soils, including arsenic. Small amounts of contaminated soil and soil-derived dust can adhere to children's hands and to toys, which are then intentionally or accidentally put in the mouth. For both children and adults, some

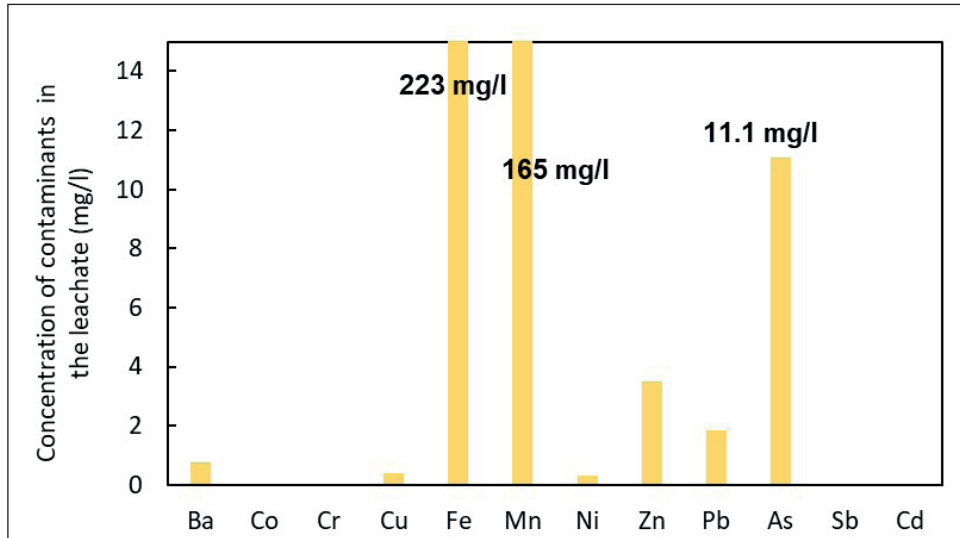


Fig. 7. Concentration of studied contaminants in leachates after the SBET test.

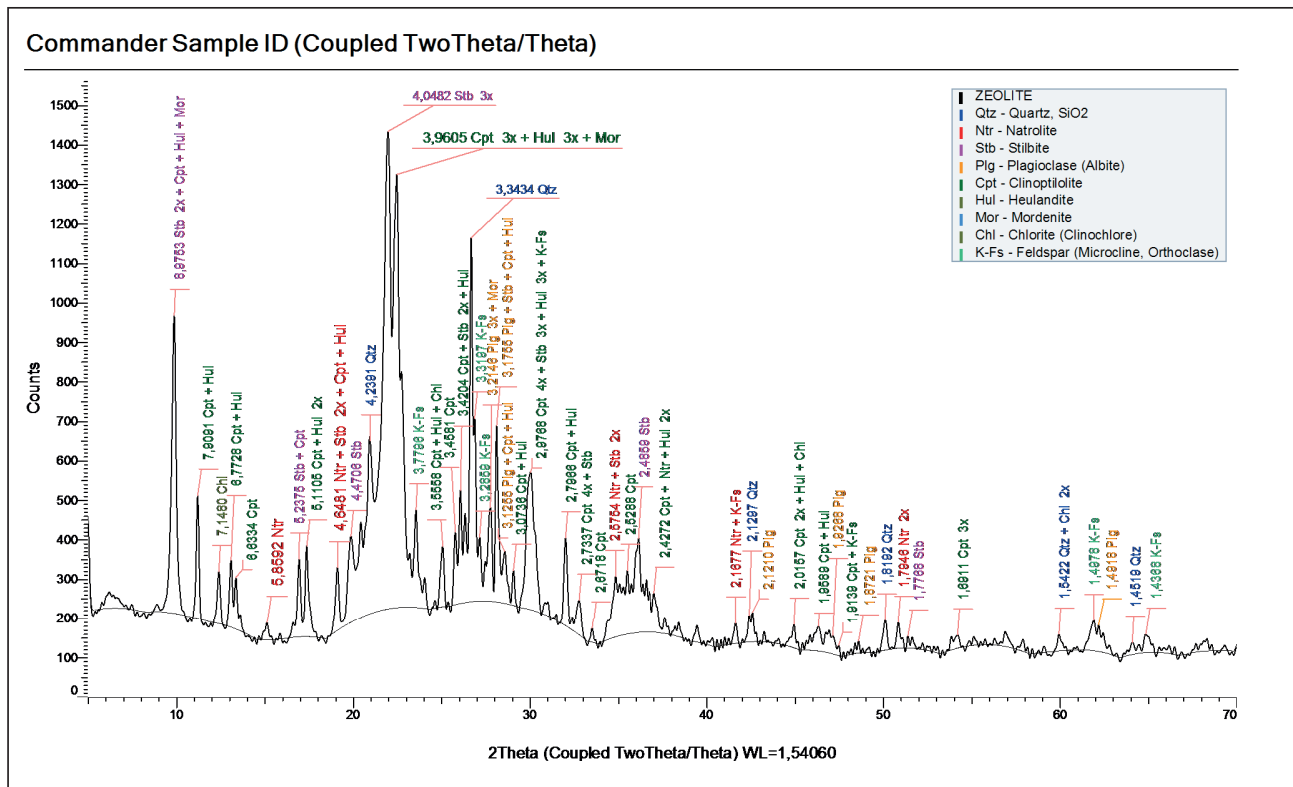


Fig. 8. XRD pattern of zeolite.

contribution may come from soil attached to vegetables, and from coarse dust that is inhaled and then swallowed.

Method Physiologically Based Bioavailability Extraction Test, PBET, is based on two sequential extractions simulating parameters for gastric and small intestinal pH, soil mass, fluid volume, stomach mixing and emptying rate, and small intestinal transit time. Simplified method Simply Bioavailability Extraction Test, SBET simulates only the stomach activity.

Leachates after the SBET test contained high concentrations of Fe (223 mg.l⁻¹), Mn (165 mg.l⁻¹), as well as As (11.1 mg.l⁻¹), also smaller concentrations of Zn, Pb, Ba, Cu (Fig. 7). Expressive acid environment led to the extraction of Fe, Mn and As into the leachate. Obtained results of chemical analyses correspond with the EDX analyses. Hereby, also pointed at the weak stability of Fe (Fe, Mn) precipitated bonding As.

3.2 Adsorbents characterization

For sorption experiments, two types of adsorbents were selected, zeolite and decorative clay terra rossa. X-ray diffraction patterns of used materials are shown in Figs. 8–9. Main mineralogical phases of zeolite sample are represented by clinoptilolite, stilbite, natrolite, present are also plagioclase, chlorite and mordenite. Main mineralogical phases detected in terra rossa sample were kaolinite, hematite and goethite. This material was

selected due to the presence of Fe oxides, known as good adsorbents of As from the water environment. Except drying and fraction grading these adsorbents were not modified or activated for experimental purposes.

3.3 Batch sorption-experiments in laboratory conditions

First, the kinetic of the sorption process was studied in the batch conditions. From the reason that As is considered as potential toxic element, the elimination of this selected indicator was solved and discussed. Sorption capacity of zeolite and terra rossa increased rapidly during the first minutes of experiment and reached equilibrium after 240 minutes. It stayed unchanged up to the end of experiment (Fig. 11), where higher sorption capacity was obtained for the terra rossa.

Adsorption kinetics controls the rate of adsorption, which determines the time required for reaching equilibrium for the adsorption process. Kinetic models can give information regarding adsorption pathways and probable mechanism involved. This is also an important data for the development of the process and the adsorption system design.

It was found, that the Lagergren-first-order kinetic model is not suitable to describe these adsorption systems (not shown here). Therefore the pseudo-second-order (PSO) model was used to interpret the experimental data:

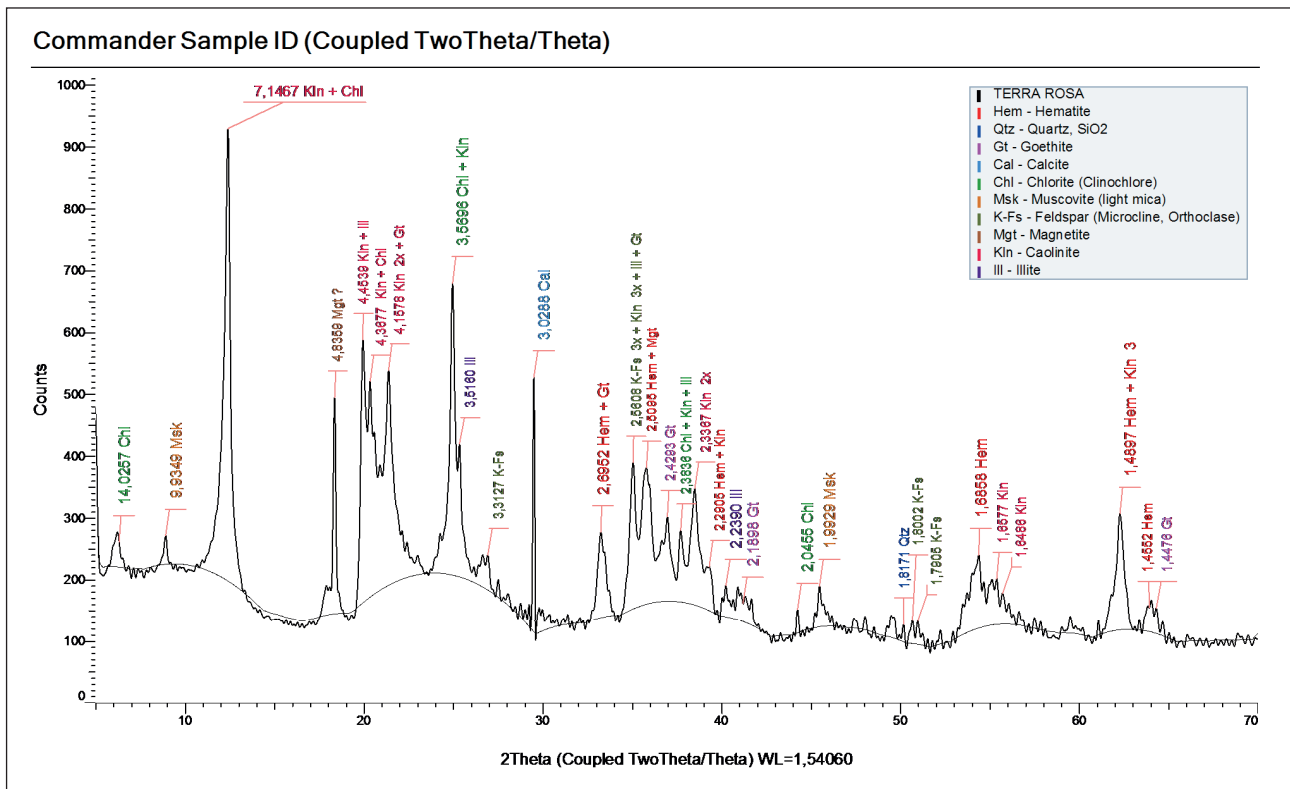


Fig. 9. XRD pattern of terra rossa.

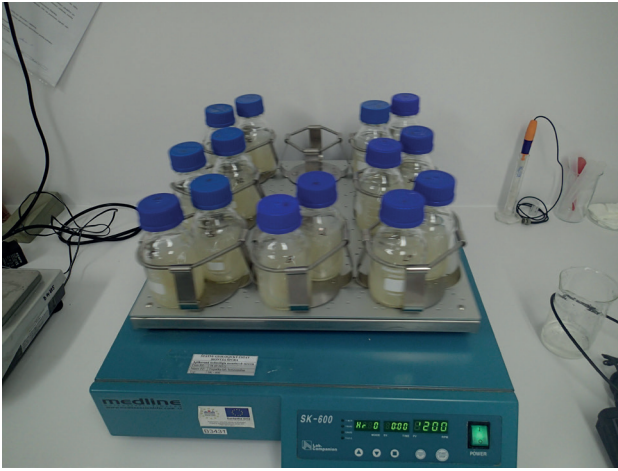


Fig. 10. Kinetic study of As sorption onto zeolite in batch conditions.

$$\frac{t}{q_t} = \frac{1}{kq_e^2} + \frac{1}{q_e}t,$$

where q_e and q_t are the amounts of ions adsorbed on the adsorbent at equilibrium and at various times t ($\text{mg}\cdot\text{g}^{-1}$), k is the rate constant of the pseudo-second-order model for the adsorption process ($\text{g}\cdot\text{mg}^{-1}\cdot\text{min}^{-1}$) (Erdem et al., 2009).

Tab. 3

Kinetic parameters of pseudo-second-order model for the adsorption of As onto studied adsorbents.

Adsorbent	k [$\text{g}\cdot\mu\text{g}^{-1}\cdot\text{min}^{-1}$]	q_e [$\mu\text{g}\cdot\text{g}^{-1}$] cal.	q_e [$\mu\text{g}\cdot\text{g}^{-1}$] exp.	R^2
Zeolite	0.0466	22.42	18.3	0.9999
Terra rossa	0.0078	29.49	25.3	0.9985

q_e [$\mu\text{g}\cdot\text{g}^{-1}$] – equilibrium amount of ions adsorbed per unit mass, k – rate constant [$\text{min}\cdot\text{g}\cdot\mu\text{g}^{-1}$], R^2 – correlation coefficient

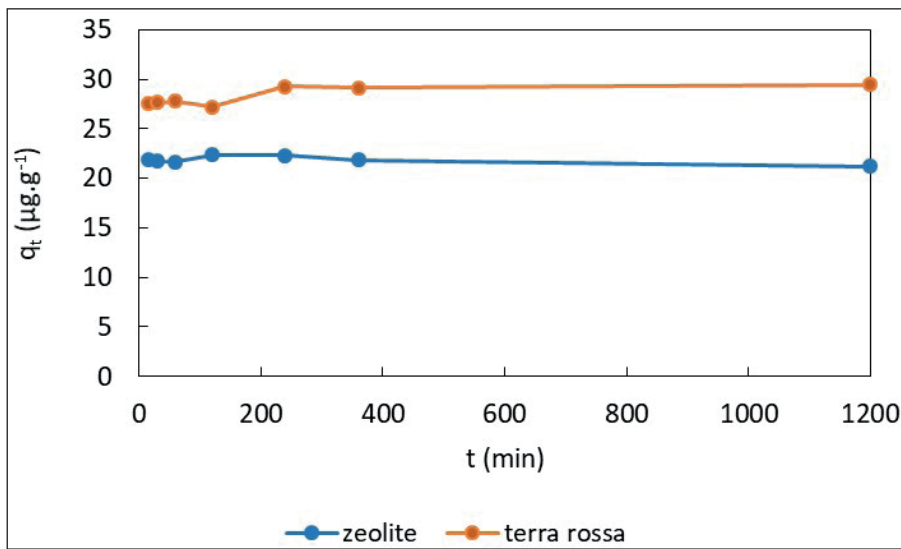


Fig. 11. Dependence of As adsorption on time in batch conditions.

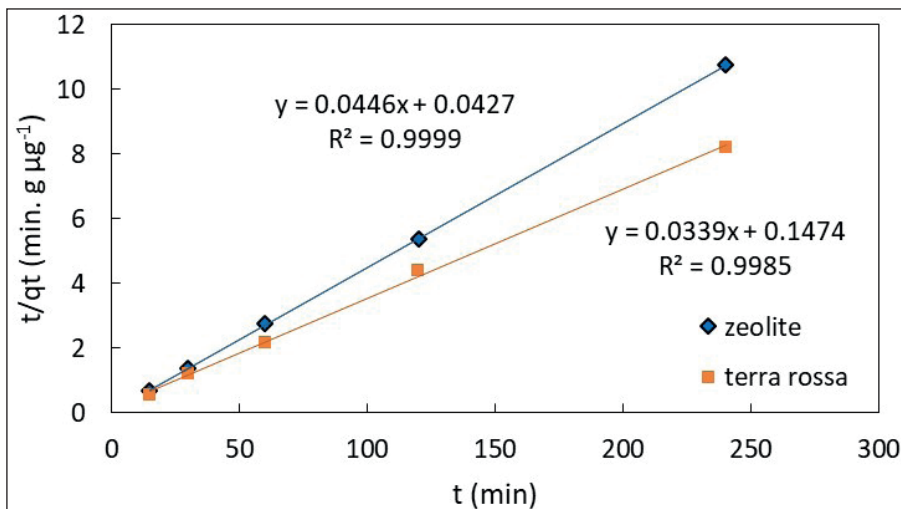


Fig. 12. Pseudo-second-order kinetic plots for the adsorption of As onto zeolite and terra rossa.

The kinetics parameters of As adsorption onto zeolite and terra rossa were calculated from the plots shown in Fig. 12 and are given in Table 3. From the obtained results it can be concluded that the dominant mechanism is external surface adsorption. Kinetic process was not evaluated from a diffusion point of view in regard to small calculated values of intercept. Higher values of intercepts suggests that surface diffusion has a larger role as the rate-limiting step (Boparai et al., 2011).

According to the kinetic study, zeolite (Z), terra rossa (TR) and mixture of both adsorbents (Z + TR) were tested for As elimination in batch sorption experiment. After 20 hours of adsorption the highest effect of removal was obtained for the mixture of adsorbents, where more than 90 % of As was removed from the pit water in laboratory conditions (Fig. 13).

The kinetic study of As removal was also tested in-situ, using terrain shaker (Fig. 14). The pit water was added into the plastic bottles with adsorbents and shaken for selected time periods. Then the leachates were filtered

and stabilized for chemical analyses. Three bottles with each kind of adsorbent were after 120 minutes of shaking taken into laboratory and storage in refrigerator to remain the in-situ temperature up to 24 hours. Then they were also filtered and sent for chemical analyses.

The in-situ adsorption experiment was performed in January, when the pit water flow was quite strong, the As concentration was $380 \mu\text{g.l}^{-1}$, temperature varied between -7 up to -4 °C and temperature of pit water decreased in dependence of shaking time from 7.5 up to 0 °C.

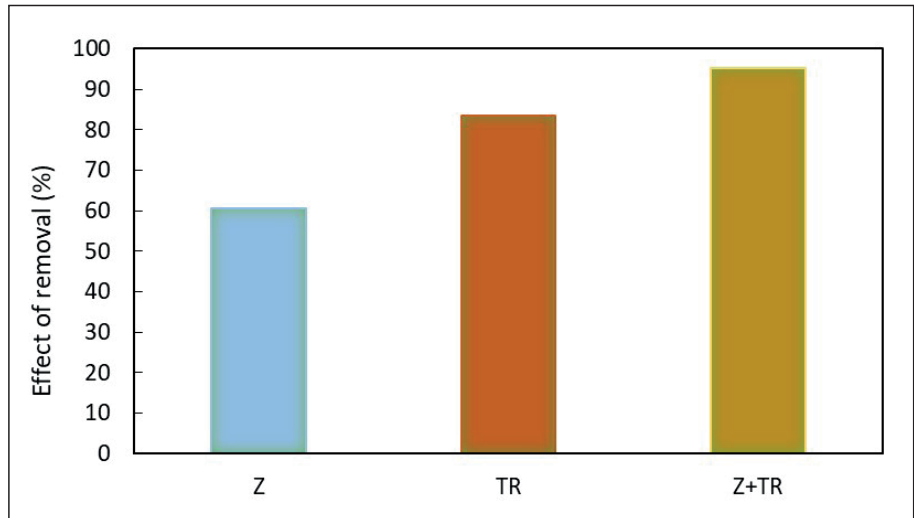


Fig. 13. Effect of As removal from the pit water by selected adsorbents.

Tab. 4

Kinetic parameters of pseudo-second-order model for the in-situ adsorption of As onto studied adsorbents.

Adsorbent	k [$\text{g} \cdot \mu\text{g}^{-1} \cdot \text{min}^{-1}$]	q_e [$\mu\text{g} \cdot \text{g}^{-1}$] cal.	q_e [$\mu\text{g} \cdot \text{g}^{-1}$] exp.	R ²
Zeolite	0.0009	20.2	19.5	0.9982
Terra rossa	0.0036	30.2	32.0	1
Zeolite + terra rossa	0.0022	29.3	31.0	0.9999

Also as in laboratory, in-situ As adsorption was fast for both adsorbents as well as for their mixture. The adsorption capacity for TR and Z + TR was higher in comparison to zeolite. After 90 minutes of adsorption the effectivity of zeolite decreased. The kinetic curves obtained for terra rossa and combined adsorbent were similar, slight higher adsorption capacity was shown by TR (Fig. 15). After 24 hours of experiment the effect of As elimination increased for all studied materials.

The kinetic parameters, Table 4, calculated from the applied PSO kinetic model (Fig. 16), pointed again at the external surface adsorption.

From the selected adsorbents, the most effective in As elimination, in spite of results of laboratory experiments, was TR. Slightly lower efficiency was obtained for



Fig. 14. In-situ batch adsorption experiment.

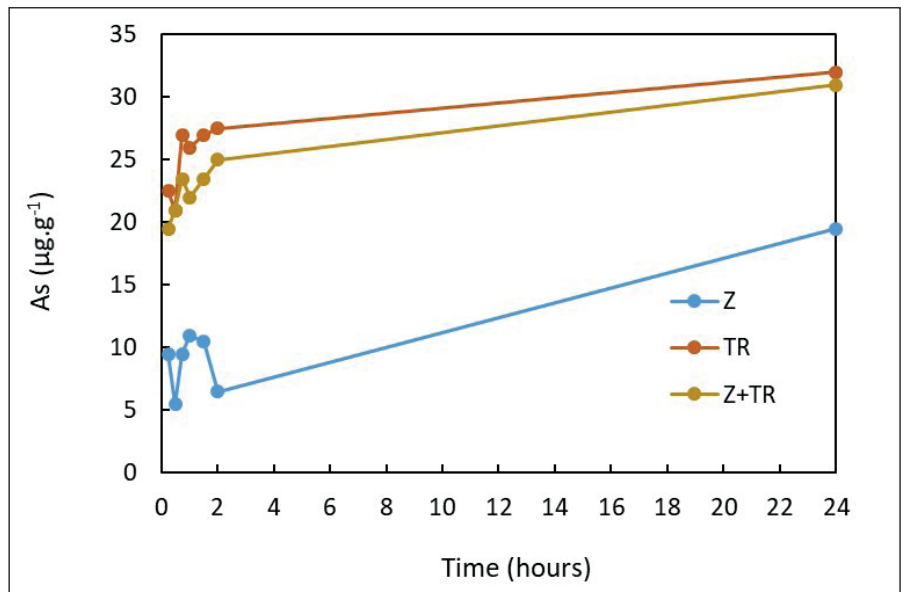


Fig. 15. Dependence of As adsorption on time in in-situ batch conditions.

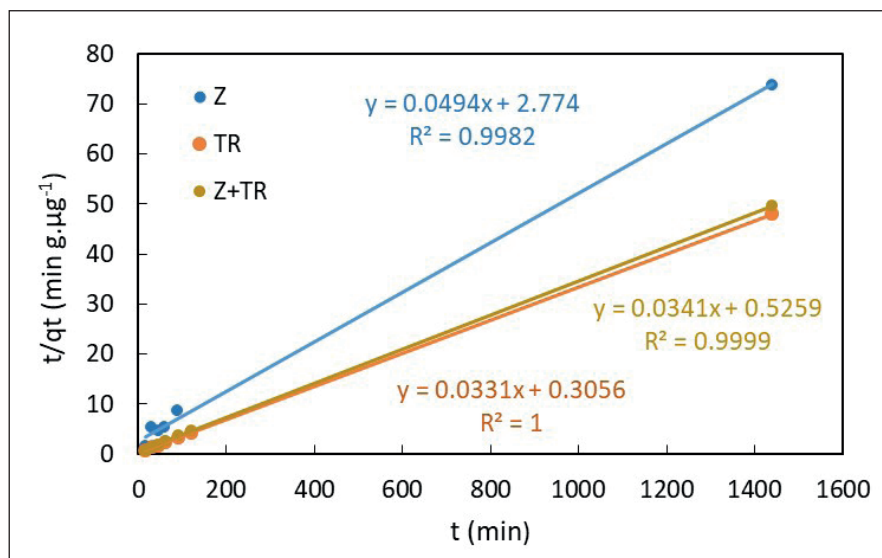


Fig. 16. Pseudo-second-order kinetic plots for the adsorption of As onto studied adsorbents.

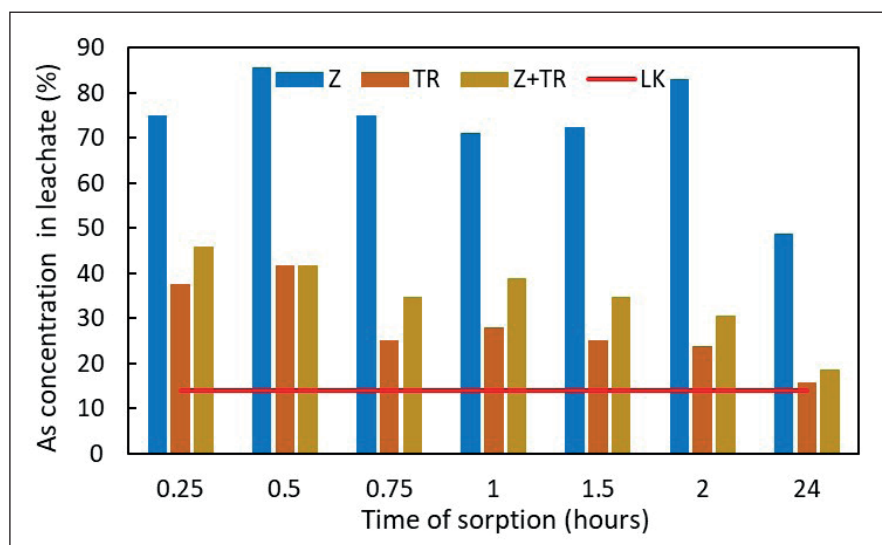


Fig. 17. Decrease of As concentration in leachates after in-situ adsorption in selected time periods in comparison with limited value of As concentration for irrigation waters.

TR + Z. During two hours of experiment non adsorbent was able to decrease the As concentration on the required value, even if it was more than 50 % lower for suspensions with TR and Z + TR (Fig. 17). The highest removal effect of all adsorbents was observed after 24 hours of experiment, where the As concentration in suspension with TR was the lowest and very close to required value. In regard to natural and weathering conditions, the obtained results were good input for realization of column experiments.

The column experiments were performed in laboratory conditions. The columns were filled with layers of zeolite and terra rossa (Fig. 18)



Fig. 18. Sorption column filled with zeolite and terra rossa in layers.



Fig. 19. Parallel test of As elimination in columns with mixture of adsorbents in laboratory conditions.

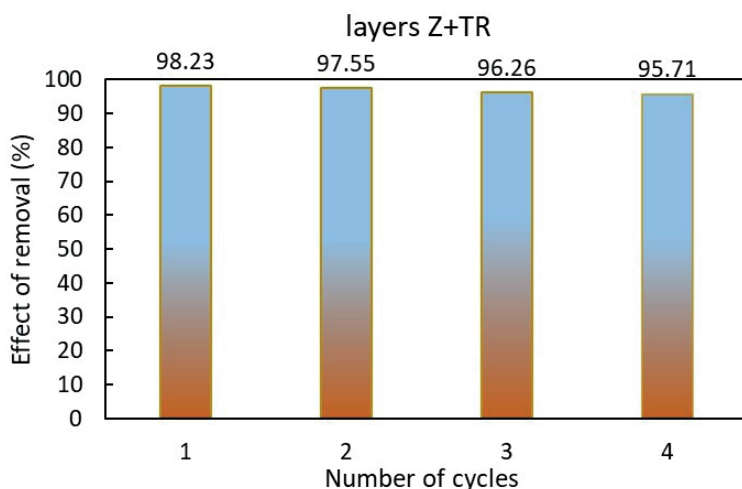


Fig. 20. Effect of As removal by column filled by zeolite and terra rossa layers, 4 cycles of experiment.

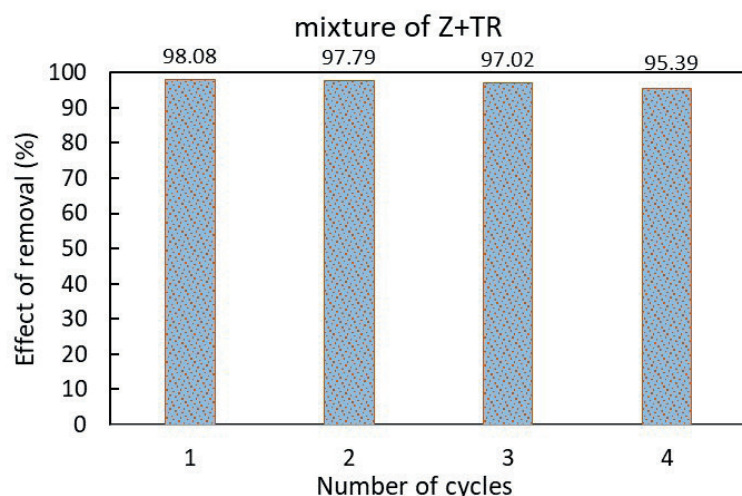


Fig. 21. Effect of As removal by column filled by mixture of zeolite and terra rossa, 4 cycles of experiment.

in second one, with their mixture (Fig. 19). As a permeable layer, quartz sand was used. The As elimination was studied in four cycles for both types of columns to prove their sorption capacity for longer utilization.

The first percolation of pit water led to almost 100 % of As elimination for both types of used columns (Figs. 20–21). After the fourth cycle the effectivity of columns decreased to approximately 95 %, no depending on the columns filling. Slight decrease in effectivity signified that the columns were not saturated yet and could be used for more adsorption cycles again (without need of exchange of the filling or its regeneration).

These results are positive for future columns applications directly on the studied locality. In next experiments, bigger columns of higher adsorbents amounts will be tested in-situ with the aim to suggest the method for pit water

cleaning and its following use for plants irrigating in local gardens.

4 Conclusion

The introductory experiments on selected locality of Zlatá Idka-Rieka, Slovakia, loaded by arsenic after previous mining activity confirm presence of high content of As in the lake sediment caused by the outflow of pit water. As is easy mobile depending on the chemical bonds with non-stable Fe (Fe, Mn) oxides/hydroxides creating surface coatings on the grains of minerals and soil present in the lake of pit water. From this reason it is also potential toxic for local population through contamination of vegetables or contaminated coarse dust inhalation.

Laboratory batch adsorption experiments and following in-situ experiments showed high effect of terra rossa in As removal. In spite of high efficiency, the required concentration value was not reached in solutions after adsorption (it was slightly higher), probably also due to not very favourable climate conditions during the in-situ testing. Also higher adsorbent doses should lead to expected results for As concentration.

Laboratory column experiments verified the repeated usage of adsorption columns with slight decreasing removal effect, not depended on the adsorbents bedding (layers or mixture), what is promising result for future in-situ testing of As elimination from the pit water in dynamic regime.

Acknowledgement

The presented results were obtained thankful the financial support of project from the Operational Programme Quality of Environment “Monitoring of environmental burdens in selected localities of the Slovak Republic, Part 2”, being co-funded by the European Union / Cohesion fund (code: NFP310010AXF2). Authors are grateful to reviewers of primary manuscript – Darina Štyriaková from Zavod za gradbeništvo Slovenije, and Silvia Dolinská from Slovak Academy of Sciences.

References

- BOPARAI, H. K., JOSEPH, M. & O’CARROL, D. M., 2011: Kinetics and thermodynamics of cadmium ion removal by adsorption onto nano zerovalent iron particles. *J. Hazard. Mater.*, 186, 458–65. <https://doi.org/10.1016/j.jhazmat.2010.11.029>.

- CICMANOVÁ, S. & BALÁŽ, P., 2007: Historical ore mining and quality of the environment in the surrounding of Zlatá Idka village. *Podzemná voda*, XIII, 1 (in Slovak).
- ERDEM, B., ÖZCAN, A., GÖK, Ö. & ÖZCAN, A. S., 2009: Immobilization of 2,2'-dipyridyl onto bentonite and its adsorption behavior of copper(II) ions, *J. Hazard. Mater.*, 163, 418–426.
- FEY, D. L., CHURCH, S., DRISCOLL, R. & ADAMS, M. G., 2011: Multiple applications of the U.S. EPA 1312 leach procedure. *Geochemistry: Exploration, Environment, Analysis*, 11, 163–178.
- FEAKOVÁ, R., ŽENIŠOVÁ, Z., KRČMÁŘ, D., ONDREJKOVÁ, I. & SRACEK, O., 2017: Occurrence of antimony and arsenic at mining sites in Slovakia: Implications of their mobility. *Carpath. J. Earth Environ. Sci.*, 12, 1, 41–48 (in Slovak).
- HO, Y. S. & MCKAY, G., 1999: Pseudo-second order model for sorption processes. *Process Biochem.*, 34, 451–65. [https://doi.org/10.1016/S0032-9592\(98\)00112-5](https://doi.org/10.1016/S0032-9592(98)00112-5).
- HRUŠKA, J., KRÁM, P. & MOLDAN, F., 1996: Vplyv kyslého dažďa na povrchové vody. Modelovanie vývoja minulosti a budúcnosti povodí Lysina vo Slavkovskom lese. *Vesmír*, 75, 373 (in Slovak).
- KIM, K. R., OWENS, G. & NAIDU, R., 2009. Heavy metal distribution, bioaccessibility and phytoavailability in long-term contaminated soils from Lake Macquarie, Australia. *Australian J. Soil Res.*, 47, 166–176.
- Method 1312, 1994: Synthetic Precipitation Leaching Procedure, 30 ps.
- Methodical Instruction of Ministry of Environment of the Slovak Republic from the January, 28th 2015, No.1/2015-7.
- RAPANT, S., CICMANOVÁ, S., MACKOVÝCH, D., LUČIVJANSKÁ, V. & BODIŠ, D., 2004: Zhodnotenie potenciálneho vplyvu geochemického prostredia na zdravotný stav obyvateľstva v oblasti Spišsko-gemerského rudohoria. *Manuscript. Bratislava, archive St. Geol. Inst. D. Štúr* (in Slovak).
- Regulation of Government of the Slovak Republic No. 269/2010 Collection of Laws, Part B – Surface waters for irrigation waters.
- Report Number: 1542820-003-R-Rev0, 2016: Accounting for bioavailability in contaminated land site – specific health risk assessment. Golder Associates, Wellington, New Zealand.
- SMEDLEY, P. L. & KINNIBURGH, D. G., 2002: A review of source, behaviour and distribution of arsenic in natural waters. *Appl. Geochem.*, 17, 5, 17–568.
- SRACEK, O., BHATTACHARYA, P., LACKS, G., GUSTAFSSON, L. P. & BRÄMSSEN VON, M., 2004a: Behaviour of arsenic and geochemical modelling of arsenic enrichment in aqueous environments. *Appl. Geochem.*, 19, 2, 169–180.
- SRACEK, O., CHOQUETTE, M., GÉLINAS, P., LEFEBRE, R. & NICHOLSON, R. V., 2004b: Geochemical characterization of acid mine drainage from waste rock pile, Mine Doyon, Québec, Canada. *J. Contamin. Hydrogeol.*, 69, 2, 45–7.

Štúdium kontaminovaných sedimentov a eliminácie As z podzemnej banskej vody na lokalite Zlatá Idka-Rieka

Cieľom štúdie bolo charakterizovať sediment z jazierka tvoreného vytekajúcou banskou vodou na lokalite Zlatá Idka-Rieka z hľadiska mobility a bioprístupnosti potenciálne toxických prvkov nachádzajúcich sa v sedimente a experimentálne overiť možnosti in-situ odstránenia/eliminácie obsahu As z vytekajúcej podzemnej banskej vody zo štôlne Hauser.

Vzorka sedimentu (označená H1) na granulometrickú analýzu a magnetickú separáciu bola podrobená zrnitostnému rozboru za mokra, sušená a analyzovaná. Frakciu väčšiu ako 2 mm tvoril len organický materiál (listy, šišky, konáriky). Granulometrická analýza potvrdila prítomnosť častíc menších ako 1 mm a poukázala na širokú distribúciu veľkosti častíc v rozsahu 1 až 500 µm, s maximom na distribučnej krivke v prípade frakcie 63 µm. Vzorka sa potom spracovala na kalovom magnetickom separátore a jej produkty boli podrobené rtg. analýze. Okrem hlavnej minerálnej fázy, kremeňa, obe frakcie sedimentu (magnetická aj nemagnetická) obsahovali muskovit a plagioklas, v prípade magnetickej frakcie aj chlorit. Röntgenovou analýzou sa však prítomnosť predpokladaných oxidov železa (kryštalických fáz) nepotvrdila.

Vzorka hnedočerveného nánosov, jemných usadenín z horninových povrchov, po ktorých banská voda vyteká do jazierka, sa analyzovala na rastrovom elektrónovom mikroskope. Bodová EDX analýza preukázala prítomnosť Fe a O (41,6 hm. % a 40,1 hm. %), ako aj výrazne vyšší obsah As a Mn.

Chemické analýzy sedimentu poukázali na zvýšenú koncentráciu Cr a Pb, ktorých hodnoty prekročovali intervenčné kritérium (IT) pre obytné zóny, a zvýšenú koncentráciu As a Sb, ktorých hodnoty prekročovali IT pre priemysel v zmysle prílohy č. 12 smernice Ministerstva životného prostredia Slovenskej republiky z 28. januára 2015 č. 1/2015-7. Preto sa v ďalšom kroku testovala mobilita kontaminantov obsiahnutých vo vzorke sedimentu v prípade potenciálnej acidifikácie nánosov sedimentu v okolí výpustu banskej vody kyslými zrážkami v laboratórnych podmienkach (Metóda U.S. EPA 1312).

Mobilita potenciálne toxických prvkov po lúhovaní vzorky sedimentu simulovaným kyslým dažďom nebola veľmi výrazná a pohybovala sa v rozsahu 0,02 až 0,38 %. Najviac mobilným prvkom sa javil Mn, najmenej Ba. Aj napriek nižšej mobilite Fe a As (0,03 a 0,04 %) ich

koncentrácia vo výluhu po teste aj vzhľadom na ich vstupnú koncentráciu v sedimente predstavovala relatívne vysoké hodnoty. Mobilita As závisí aj od pevnosti väzieb As, ako aj samotnej stability Fe (Fe, Mn) oxyhydroxidov a hydroxidov, čo korešponduje aj s výsledkami EDX analýz.

Výluhy po teste bioprístupnosti (SBET metóda) s využitím kyseliny chlorovodíkovej obsahovali vysokú koncentráciu Fe ($223 \text{ mg} \cdot \text{l}^{-1}$), Mn ($165 \text{ mg} \cdot \text{l}^{-1}$) a As ($11,1 \text{ mg} \cdot \text{l}^{-1}$) a nižšiu koncentráciu Zn, Pb, Ba a Cu. Výrazne kyslé prostredie viedlo k uvoľneniu vysokej koncentrácie Fe, Mn a As do výluhu. Stabilitu precipitátov Fe a Mn oxidov s As ovplyvňuje zmena pH vody v jazierku, ale aj sezónne poveternostné podmienky. As sa tak stáva ľahko mobilným a môže byť potenciálne toxický pre miestnych obyvateľov, ktorí sú vystavení jeho expozícii vo forme kontaminovanej pôdy využívanaj na pestovanie zeleniny, ale aj priamemu vdychovaniu kontaminantu vo forme prachových častíc.

Na adsorpčné experimenty boli zvolené prírodné adsorbenty zeolit (Majerovce, označ. Z), terra rosa (Včeláre, TR) a ich zmes (Z + TR). Sledoval sa vplyv času na elimináciu As z podzemnej banskej vody. Všetky experimenty sa realizovali duplicitne. Adsorpcia As na zeolit a terra rosa mala rýchly priebeh, rovnováha nastala po približne 240 minútach experimentu. Vyššia sorpčná kapacita bola pozorovaná v prípade TR. Adsorpčný proces sa riadil kinetickým modelom pseudodruhého poriadku, čo naznačuje, že ide o mechanizmus adsorpcie na externých povrchoch materiálov. V ďalšom laboratórnom experimente sa sledoval vplyv množstva adsorbentu ($10 \text{ g} \cdot \text{l}^{-1}$) na odstránenie As. Po 20 hodinách najvyššiu účinnosť (viac ako 90 %) dosiahla zmes Z + TR. Časová závislosť adsorpcie a adsorpčná kapacita použitých prírodných adsorbentov sa následne testovala priamo v teréne s cieľom znížiť koncentráciu As na limitnú hodnotu, prípustnú pre povrchovú vodu určenú na závlahy ($50 \mu\text{g} \cdot \text{l}^{-1}$ v zmysle nariadenia vlády SR č. 269/2010 Z. z., ďalej nariadenie). Vzorky suspenzií sa premiešavali na terénnej trepačke priamo na lokalite počas dvoch hodín. Výluhy po adsorpcii sa odoberali vo vybraných časových intervaloch a filtrovali na následnú chemickú analýzu. Tri suspenzie s obsahom jednotlivých

sorbentov boli po 2 hodinách miešania prinesené z terénu do laboratória a ponechané v chladničke (na zabezpečenie podmienok podobných prírodným v čase priebehu experimentu – zimné obdobie s teplotou okolo $0 \text{ }^\circ\text{C}$) a filtrovali sa až po 24 hodinách.

Podobne ako v prípade laboratórnych testov, aj adsorpcia As bola rýchla. Adsorpčná kapacita TR a Z + TR bola vyššia ako v prípade zeolitu. Po 24 hodinách experimentu sa zaznamenalo jej zvýšenie pri všetkých použitých adsorbentoch. Počas dvoch hodín experimentu in-situ sa ani napriek viac ako 50 % účinnosti odstránenia As z podzemnej banskej vody nedosiahla požadovaná hodnota koncentrácie ukazovateľa vo výluhoch. Až po 24 hodinách sa efektívnosť zmesového sorbentu Z + TR zvýšila a koncentrácia As vo výluhu len mierne prekročovala limitnú hodnotu v zmysle nariadenia. Aj napriek takýmto výsledkom boli získané poznatky veľmi dobrým vstupom na nastavenie adsorpcie v dynamických podmienkach v kolónach.

Adsorpčné experimenty sa uskutočnili v laboratórnych podmienkach v sklenených kolónach s rozmermi 5 cm (vnútorný priemer) a 18 cm (výška kolóny). Jednotlivé kolóny boli naplnené kremenným pieskom (60 g) na zabezpečenie ľahšej perkolácie podzemnej banskej vody a vrstvou zeolitu (20 g) a terra rosy (20 g), resp. ich zmesou. V jednom cykle pretieklo kolónami 150 ml banskej vody pri konštantnej prietokovej rýchlosti $2,8 \text{ ml} / \text{min}$ v priebehu 50 minút.

Po prvej perkolácii dosiahli oba typy kolón (vrstvy, zmes) takmer 100 % účinok odstránenia As. Po štvrtom prietokovom cykle klesla ich účinnosť na približne 95 %, bez závislosti od typu kolóny. Ešte stále to predstavovalo účinné zníženie koncentrácie ukazovateľa na požadovanú limitnú hodnotu v zmysle nariadenia. Uloženie adsorbentov v kolóne nemalo vplyv na množstvo odstráneného arzenu. Ani po 4 cykloch nedošlo k nasýteniu kolóny, čo umožňuje jej opätovné použitie bez potreby výmeny náplne, resp. jej regenerácie.

Doručené / Received: 3. 5. 2022

Prijaté na publikovanie / Accepted: 21. 6. 2022

Characterization of fine-grained montmorillonite fractions for preparing polymer-clay nanocomposites

VĚRA VALOVIČOVÁ¹, SILVIA DOLINSKÁ^{2*}, LENKA VACULÍKOVÁ¹, EVA PLEVOVÁ¹,
INGRID ZNAMENÁČKOVÁ² and ZUZANA DANKOVÁ³

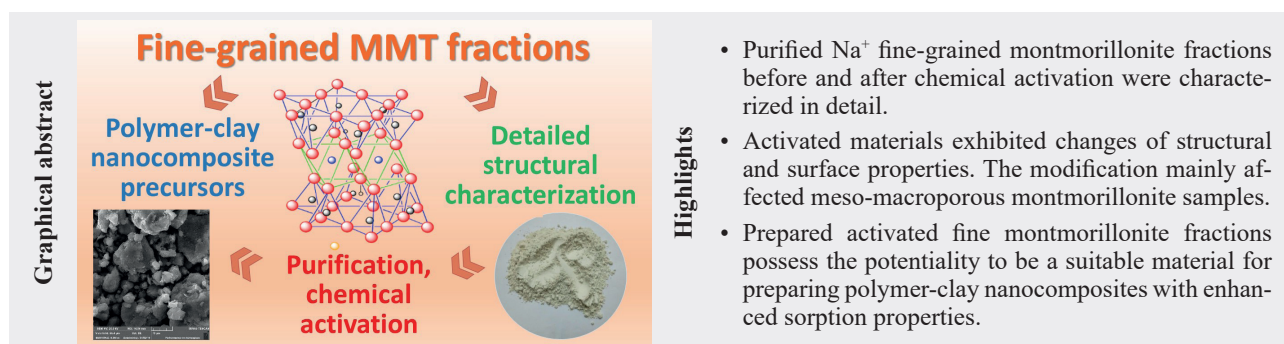
¹Institute of Geonics of the Czech Academy of Sciences, Studentská 1768, CZ–708 00 Ostrava-Poruba, Czech Republic

²Slovak Academy of Sciences, Institute of Geotechnics, Watsonova 45, SK–040 01 Košice, Slovak Republic; *sdolinska@saske.sk

³State Geological Institute of Dionýz Štúr, Department of Applied Technology of Raw Materials, Jesenského 8, SK–040 01 Košice, Slovak Republic

Abstract: Detailed structural characterization of clay minerals contributes to a better understanding of their behavior and physico-chemical properties, making it possible to fully exploit their potential for polymer-clay nanocomposite preparation and their future industrial applications. The object of this study was to characterize fine-grained fractions of four montmorillonite samples and compare them with untreated montmorillonite. The gained results confirmed that fine montmorillonite fractions would be more appropriate precursors for successive preparing of composite materials with sorption property enhancement, useable for environmental remediation.

Key words: montmorillonite, source clays activation, characterization



1 Introduction

Nanoclays are nanoparticles of layered silicates that can be used in the design and preparation procedure of polymer/clay nanocomposites (Ray & Okamoto, 2003). The integration of nanoclays into polymeric matrixes improves the physico-chemical and mechanical properties of polymers (Kanmani & Rhim, 2014; Gautam & Komal, 2019; Qin et al., 2021). Among the reasons for wide research of nanocomposite precursors founded on clay and layered silicates belong their easy availability as well as the fact that their intercalation chemistry was investigated for a long time (Ray & Okamoto, 2003; Pavlidou & Papaspyrides, 2008; Kanmani & Rhim, 2014). Advantages of nanoclays include high specific surface area, easy processability, good performance, and lower cost. Nanoclays used as a fillers of nanocomposites are usually in the form of 2-dimensional platelets with a thickness of ca. 1 nm and a length of several

micrometers (Ruitz & Van Meerbeek, 2006; Brantseva et al., 2018). A layered silicate montmorillonite (MMT) can be designated as one of the most commonly used nanoagents for preparing nanocomposites (de Azeredo, 2013). Its chemical general formula (without structural substitutions) is $(\text{OH})_4\text{Si}_8\text{Al}_4\text{O}_{20} \cdot n\text{H}_2\text{O}$ (Parekh & Rule, 2002). Generally, montmorillonite can be classified by the types of interlayer cations in montmorillonite into sodium and calcium montmorillonite. Calcium montmorillonite (CaMMT) has two H₂O molecular layers in the interlayer whereas sodium montmorillonite (NaMMT) contains typically single layer of water molecules. Important properties of CaMMT associated with their use include especially high absorption capacity, bleaching ability and bonding strength, NaMMT is characterized by higher swelling and viscosity (Tombacz & Szekeres, 2004; Wiess & Kužvart, 2005; Murray, 2007; Shah, 2018; Hayakawa et al., 2019).

Many industries (engineering, petroleum discovery, recovery and refining, etc.) use the clay minerals due to their composition and structure (Wiess & Kužvart, 2005; Ruitz & Van Meerbeek, 2006; Murray, 2007). Particle size, layer charge, swelling capacity, surface area and surface chemistry belong to the important characteristics connecting with applications of clay minerals. Modification of clays has a significant effect on the structural properties – very often causing an improvement in their sorption capacities (Sanqin et al., 2014; Kotal & Bhowmick, 2015; Alves et al., 2017; Tomić et al., 2018; Guo et al., 2020). This further functionalization of clay minerals is possible through substituting the exchangeable cations with organic molecules (Abollino et al., 2003; Hong & Rhim, 2008), by pillaring (Bergaya et al., 2006) or acid activation (Komadel & Madejová, 2006). Another possibility may be a magnetic modification in which the layered silicates are coated with iron oxides (Mockovčiaková et al., 2010). Modified and functionalised nanoclays are widely used for remediating environmental contaminants (Abollino et al., 2003; Al-Degs et al., 2006; Guerra et al., 2013; Akpomie & Dawodu, 2014; Schütz et al., 2016; Abdellaoui et al., 2017; Uddin, 2017; Galamboš et al., 2012; Galamboš et al., 2013), they show promise as advanced sorbents or biodegradation enhancers (Biswas et al., 2019).

Clay minerals are also used as a catalysts, their activity has been demonstrated in a number of reactions. Last but not least, application of montmorillonite clays as green catalysts plays role in developing eco-friendly chemical processes (Kaur & Kishore, 2012). The catalytic properties of natural clays are enhanced by acid activation, which causes an increase in nitrogen surface area and adsorptive capacity of activated materials. The activation process can sometimes lead to the destruction of clay mineral structure as it removes Fe, Al and Mg cations from the octahedral layer. Generally, the clay minerals having a high octahedral magnesium or iron content leach more easily than such materials with high octahedral aluminium content. Moreover, the hydrophilic surface of swelling clay material can become organophilic through the exchange of inorganic cations (naturally occurring) with organocations. It caused the extension of the layers for access the non-polar molecules to the interlamellar space (Breen & Moronta, 2001).

This paper is aimed at detailed structural characterization of fine-grained MMT fractions for preparing polymer-clay nanocomposites. Natural montmorillonite clays can consist of fine-grained elements of clay minerals accompanied by crystals of various minerals including quartz, carbonates, feldspars and also metal oxides (Ruitz & Van Meerbeek, 2006). This impurities presented in the natural montmorillonite composition can negatively influence the adsorption characteristic of the future synthesized nanomaterials.

2 Materials and methods

2.1 Materials

The four montmorillonite samples (Tab. 1) used in this study were: SWy-2, SAz-2, STx-1b (from the Source Clays Repository, the Clay Minerals Society, USA) and Kunipia-F (from Kunimine Industries Co. Ltd., Japan). The SAz-2 and STx-1b samples contain calcium in the interlayer, the SWy-2 sample shows the presence of both Na⁺ and Ca²⁺ cations and Kunipia-F belongs to sodium type clay. Na₂CO₃ was of analytical purity from Merck Ltd., Germany.

Tab. 1

Overview of used montmorillonite samples.

Sample	Description	Locality	Impurities XRD ^a	Impurities FT-IR ^b
SAz-2	CaMMT	Arizona, USA	–	opal*
STx-1b	CaMMT	Texas, USA	opal	cristobalite
SWy-2	Ca, NaMMT	Wyoming, USA	mica, quartz	quartz (mica), carbonate*
Kunipia-F	NaMMT	Kunimine Co., Japan	mica, quartz	quartz (mica), carbonate*

Notes: ^aDetected by XRD analysis. ^bDetected by FT-IR spectroscopy analysis. *The impurity occurs in traces.

The detailed study of these MMT standard samples by Infrared and Raman spectroscopy were performed by the authors Ritz and Vaculíková (Ritz et al., 2016; Vaculíková et al., 2019) in previous study. Some of the necessary information obtained from these analytical methods can be found in Tab. 1 and 2.

Tab. 2

Major elemental composition of montmorillonitic clay samples.

Sample	CaO	Na ₂ O	SiO ₂	Al ₂ O ₃	MgO	Fe ₂ O ₃	K ₂ O	TiO ₂
SAz-2	2.42	<0.05	51.5	14.8	5.0	1.4	0.2	0.2
STx-1b	1.6	0.2	65.4	12.6	2.6	1.0	0.2	0.2
SWy-2	1.5	1.4	61.2	17.8	2.5	3.7	0.6	0.1
Kunipia-F	0.4	3.0	58.5	19.0	3.0	1.8	0.1	0.2

The SWy-2, SAz-2, STx-1b and Kunipia-F samples in their natural form were first purified by sedimentation to eliminate inorganic mineral impurities. Clay fractions

with particle size below 5 μm were collected according to Stokes law, the sedimentation time was derived from the selected particle size. To improve the sorption properties of fine montmorillonites, their monoionic chemical activation was performed. The fractions of montmorillonite samples containing calcium in the interlayer were modified by the saturation with Na_2CO_3 : SWy-2, SAz-2, STx-1b fine fractions were mixed with 0.5 M aqueous solution of Na_2CO_3 by shaking for 24 h. After intensive mixing the mixture was separated by centrifugation. Sedimented Na-clay mineral fine fractions were rinsed repeatedly with distilled water. After that the fine clay productions were dried at 100°C for 24 h. The activated samples were labeled as NaSAz-2, NaSTx-1b and NaSWy-2.

2.2 Methods characterization

The X-ray powder diffraction (XRD) analysis was obtained by the X-ray diffractometer Bruker D8 Advance (40 kV, 40 mA), using $\text{CuK}\alpha$ radiation. For interpretation of the diffraction phases was used the Joint Committee for Powder Diffraction Data – International Centre for Diffraction Data (the JCPDS database).

Infrared spectra of montmorillonites were obtained using Fourier transform infrared (FT-IR) spectrometer Nicolet 6700. The configuration of FT-IR spectrometer and experimental conditions were as follows: middle infrared (MIR) region (4 000–400 cm^{-1}): ETC EverGlo IR source, KBr beam splitter and DTGS KBr detector. For sample preparation was used KBr pressed disk technique: approximately 1 mg of sample and 200 mg dried KBr pressed under pressure into a transparent disc. For each sample, 64 scans were measured in the abs mode with a resolution of 4 cm^{-1} .

Thermal curves were collected by simultaneous thermogravimetry and differential thermal analysis (TG/DTA) with thermal device Setsys Evolution 24, Setaram, France. Measurements were recorded under argon atmosphere with heating rate 10 $^\circ\text{C}\cdot\text{min}^{-1}$, final temperature 1 200 $^\circ\text{C}$ and cca 15 mg of sample.

Textural properties of studied montmorillonites were determined by method of physical adsorption of nitrogen at -196 $^\circ\text{C}$ by NOVA 1 200e Surface Area & Pore Size Analyzer (Quantachrome Instruments, USA). The samples were degassed at 100 $^\circ\text{C}$ in a vacuum oven under a pressure lower than 2 Pa for 18 hours. The specific surface (S_{BET}) was calculated from the adsorption isotherms following the BET (Brunauer, Emmett, Teller) method in the range of relative pressure 0.05–0.2. The volume of micropores

(V_{micro}) and the external surface (S_{e}) were gained by use of the t-plot method analysis using the Harkins-Jura standard isotherm. The value of total pore volume (V_{tot}) was estimated from the maximum adsorption at relative pressure close to saturation pressure. The total pore volume was derived from the nitrogen volume adsorbed at the relative pressure $p/p_0 \rightarrow 1$. The pore size distribution was determined using the BJH (Barrett, Joyner, Halenda) method from the desorption part of the isotherms.

The overview morphologies of the investigated samples were acquired by field emission scanning electron microscope TESCAN MIRA 3 FE SEM with an accelerating voltage of 20 kV. The sample particles were examined at magnifications of 5 000x.

3 Results

3.1 X-ray diffraction analysis

The X-ray diffraction analysis (XRD) shows the changes in a structure of fine-grained MMT fractions before and after their monoionic chemical activation (Fig. 1, Tab. 3).

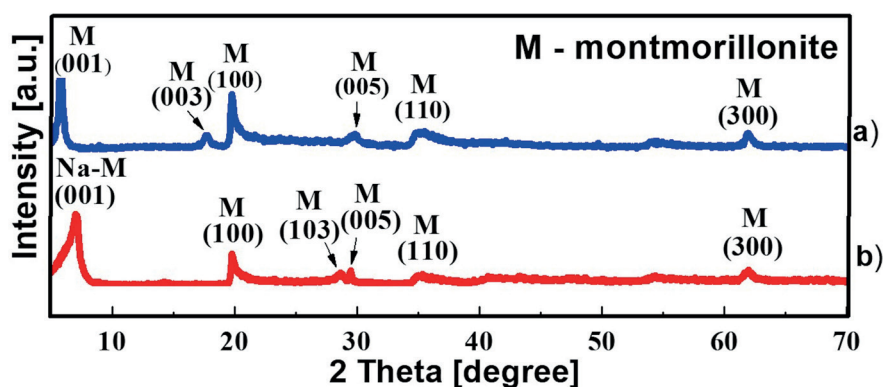


Fig. 1. XRD diffraction patterns of montmorillonite samples: a) CaMMT; b) NaMMT.

The basal reflections 001 in original samples with the interlayer space values (d) vary from 12.43 \AA to 15.24 \AA . It is caused by presence of exchangeable inorganic cations in the interlayer space of the samples. The SAz-2 sample shows the most intensive basal reflection 001 with the higher interlayer space value 15.24 \AA which confirms the presence of Ca^{2+} in the interlayer space (Iwasaki & Watanabe, 1988). The basal reflection 001 in sample STx-1b with the interlayer space of $d(001) = 14.63$ \AA is characteristic for the presence of Ca^{2+} in the interlayer (Önal et al., 2007). The diffractogram of SWy-2 shows that the basal reflection with interlayer space of $d(001) = 13.55$ \AA was reduced in comparison to the Kunipia-F. This change is probably due to the presence both Na^+ and Ca^{2+} in the interlayer space. The Kunipia-F is the sample with the interlayer space value of $d(001) = 12.43$ \AA , which

Tab. 3

Interlayer space values of original and activated fine montmorillonite fractions.

Sample	Description	d(001) [Å]	Activated sample	d(001) [Å]
SAz-2	CaMMT	15.24	NaSAz-2	12.83
STx-1b	CaMMT	14.63	NaSTx-1b	12.08
SWy-2	Ca,NaMMT	13.55	NaSWy-2	11.92
Kunipia-F	NaMMT	12.43	–	–

Tab. 4

Fundamental vibration frequencies of original montmorillonite samples.

Assignment	MMT SWy-2	MMT STx-1b	MMT SAz-2	MMT Kunipia-F
OH stretching of structural hydroxyl groups	3 627	3 624	3 621	3 626
OH stretching of water	3 427	3 429	3 425	3 440
OH deformation of water	1 636	1 636	1 637	1 638
Si-O of quartz	1 170	–	–	–
Perpendicular Si-O stretching	1 120	1 089	1 091	–
In plane Si-O-Si stretching	1 048	1 042	1 032	1 041
Al-Al-OH deformation	917	916	915	915
Al-Fe-OH deformation	884	–	–	–
Al-Mg-OH deformation	848	845	842	844
Si-O of quartz	798	–	–	798
Si-O of cristobalite	–	794	–	–
Si-O of silica (opal)	–	–	789	–
Si-O of quartz	779	–	–	779
Si-O of quartz	695	–	–	695
Coupled Al-O and Si-O, out-of-plane and Si-O of cristobalite	–	627	–	–
Coupled Al-O and Si-O, out-of-plane	622	–	622	622
Al-O-Si bending	524	521	519	522
Si-O-Si bending	467	469	466	467

is typical for the occupation of the interlayer space by calcium cations (Önal et al., 2007). The effect of chemical activation can be observed by comparison of MMT basal reflections 001. The shift of d(001) MMT reflection (Fig. 1, Tab. 3) to the right on the axis x for activated samples shows to the ion exchange in the interlayer space (Ca⁺ replaced by Na⁺).

3.2 Fourier transform infrared spectroscopy

The absorption spectra of the original montmorillonite forms obtained by the KBr-pressed technique are shown in Fig. 2. The absorption bands observed in these spectra are described in detail in Tab. 4. Individual types of montmorillonites differ not only in the type of mineral admixtures, but also in their chemical composition. It is evident, that the SAz-2 is a nearly pure specimen. Only slight shoulder occurring at 789 cm⁻¹ indicates traces of amorphous silica. The quartz admixture was confirmed by doublet of bands at 798 and 779 cm⁻¹ in SWy-2 and Kunipia-F. Sample STx-1b contains only cristobalite (794 cm⁻¹). The absorption band located at 884 cm⁻¹ in sample SWy-2 demonstrates the presence of Fe in the octahedral structure of this clay mineral. After treatment of the mineral samples with a natrifying agent, typical carbonate bands (1 430 and 880 cm⁻¹) appear in all IR spectra of used montmorillonites. Simultaneously, the position of the band corresponding to the vibrations of the surface-bound water molecules changes, the band shifts to higher wavenumbers (3 445 cm⁻¹).

3.3 Thermal analysis

The samples of fine-grained montmorillonite fractions as well as the samples of their activated sodium forms were measured by TG/DTA to get an overview of their thermal behaviour. The studied samples exhibit the same trend as shown in the Fig. 3. The thermal curves of montmorillonite samples generally show two temperature intervals. The first interval ranges from 100 to 300 °C and involves the release of adsorbed water from the interlayer. The second interval ranges from 500 to 1 100 °C and involves the release of hydroxyl groups and subsequent phase

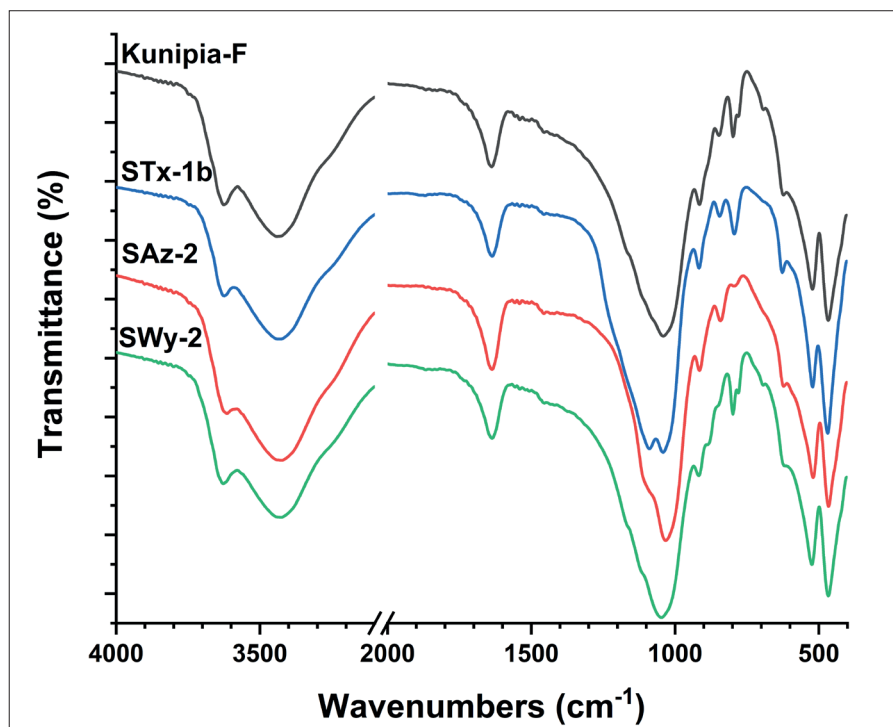


Fig. 2. FTIR spectra of original montmorillonite forms.

transformations. The temperatures, shapes and intensities of the endotherm peak in lower temperature interval are related to cations present in the sample (Hatakeyama & Liu, 1998). The doubled peak associated with loss of adsorbed water is connected to Ca-montmorillonite form, whereas after activation process there was obtained only one stage peak typical for Na-montmorillonite form (Blažek, 1974). Also the character of DTA curves for modified samples slightly differed in contrast to origin minerals. Moreover the temperature of phase transformation for STx-1b sample increased, but for SWy-2 and SAz-2 no phase transformation was observed.

3.3 Textural properties

The textural properties of MMT samples (SWy-2, SAz-2, STx-1b, Kunipia-F) and their natrified forms (NaSWy-2, NaSAz-2, NaSTx-1b) were studied by comparison their adsorption and desorption isotherms. The measured isotherms of all as-obtained MMT samples showed the hysteresis loop between the adsorption and desorption branches of isotherms. The hysteresis loop is generally related with the capillary condensation in mesopores, therefore their presence in the structure of studied samples is predicted. Adsorption isotherms of SWy-2, SAz-2 and Kunipia-F are very similar, slow increase of adsorbed gas volume in the whole range of relative pressure

with sharp increase at $p/p_0 \approx 0.95$, associated with the presence of larger pores, macropores, Fig. 4. For the sample Kunipia-F more regular increase of adsorbed gas volume with increasing relative pressure can be detected. The hysteresis loops of SWy-2, STx-1b and Kunipia-F as-obtained MMT samples correspond with Type H3, which relates with the presence of slit-like shape pores typical for aluminosilicate materials. The loop of SAz-2 sample is Type H4 also associated with presence of slit-like shape pores, but the initial part of the isotherm is connected with the presence of micropores, what was also confirmed from the processing of measured data by BET method, Tab. 5.

For the SAz-2 sample the BET isotherm exhibited the convex shape with the negative intercept indicating the occurrence

of higher volume of micropores. Based on negative value of intercept and C_{BET} constant acquired from the mathematical model (Tab. 5), the value of specific surface area is not of real physical significance. The BET method is suitable for mesoporous to macroporous materials (pores size bigger than 2 nm). For microporous samples should be employed data evaluations from other technique than BET. Therefore, allowing apparatus options, the texture of sample was gained applying the t -plot method using the

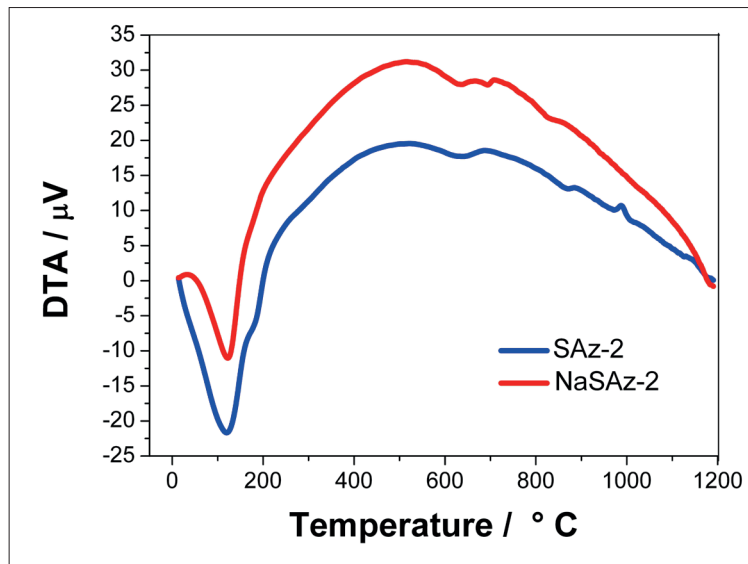


Fig. 3. DTA curves of CaMMT and NaMMT.

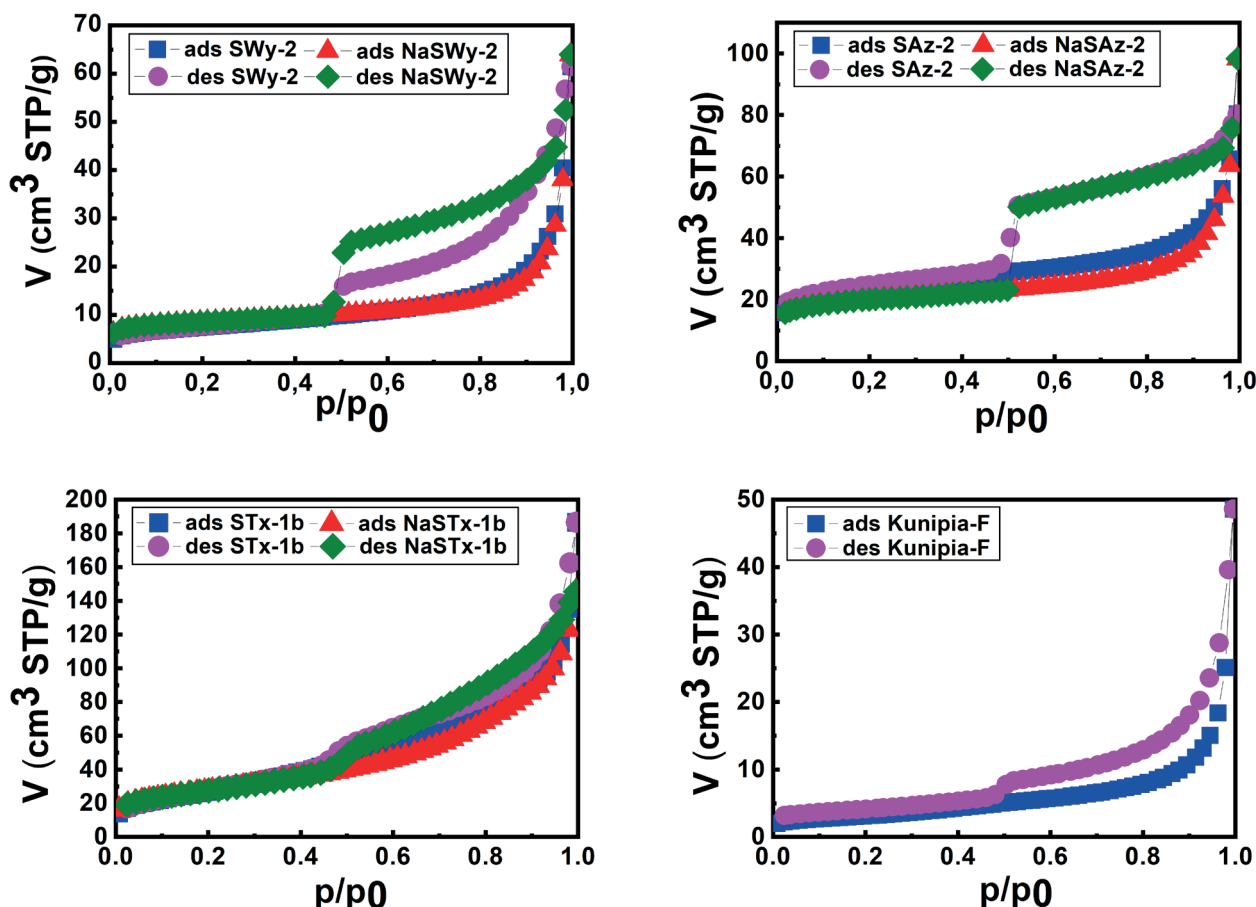


Fig. 4. Low temperature nitrogen adsorption – desorption isotherms of studied MMT samples.

Harkins-Jura isotherm. That permits to define the micropore volume and external surface area plus specific surface area of mesopores. While the STx-1b and Kunipia-F samples do not contain micropores, for the SAz-2 sample relative high volume of them was calculated. From the as-obtained MMT samples, the highest value of specific surface area was obtained for the STx-1b sample.

Modification of as-obtained montmorillonites did not change the shape of their isotherms significantly. The hysteresis loop got wider for all studied samples, Fig. 4. While for the SWy-2 and STx-1b samples similar gas volume was adsorbed at low relative pressure, for the SAz-2 sample slight decrease can be observed. For the SAz-2 sample the modification did not influence the textural properties as in case of other studied MMT samples. This sample was strongly microporous comparing with other studied materials and after the modification the volume of micropores only slight increased. In case of NaSWy-2 sample more than twice higher value of micropore volume was obtained. Increase from the zero value up to significant value of $0.004 \text{ cm}^3 \text{ STP/g}$ (STP – standard temperature and pressure, $t = 0 \text{ }^\circ\text{C}$, $p = 101.325 \text{ kPa}$) was detected for the

NaSTx-1b sample. For all samples, increase of micropore volume relates with the decrease in value of external surface area, Tab. 5.

The changes in textural properties of the as-obtained MMT samples after their modification can be observed also from the differential pore size distribution curves derived from the desorption branches of isotherms (Fig. 5).

The SWy-2 sample showed wider distribution in the range from 4.3 nm to 44.7 nm with maximum $R_{\text{max}} = 9.8 \text{ nm}$ (pore radius) what corresponds with the presence of meso- and macropores. The sharp maximum of pore radius at $R \approx 1.9 \text{ nm}$ correlates with the jump on the desorption isotherm, as called forced close of hysteresis loop and does not correspond with real pores. This maximum can be observed for all studied samples, therefore it was not regarded as significant data and the y axis of graphs were customized to better illustrate the differences between the curves. After the modification the distribution curve did not shown significant maximum, but also the volume of meso- and macropores decreased. The sample SAz-2 and NaSAz-2 have very similar distribution curves, slight difference can be observed only in the range of large

mesopores and macropores what can be associated with the lower value of adsorbed gas volume on the adsorption isotherm discussed above. As was mentioned, the SAz-2 sample was more microporous and the modification did not influence its textural properties significantly. Therefore, almost similar run of distribution curves was obtained for these studied samples. The STx-1b as-obtained sample did not contain micropores. It was mainly meso-macroporous, with higher content of larger mesopores ($R_{\max} = 21.6$ nm). After the sample modification, the shift of the distribution curve to left to the values of lower mesopores was observed ($R_{\max} = 3.05$ nm). This fact corresponds with the decrease of its value of total pore volume. The as-obtained Kunipia-F sample showed wide distribution from 3.03 nm to 143.3 nm with two maxima $R_{\max1} = 15.7$ nm and $R_{\max2} = 46.5$ nm, what confirmed its

Tab. 5
Textural parameters of MMT samples.

Sample	S_{BET} [m ² /g]	C const.	V_{tot} [cm ³ /g]	S_t [m ² /g]	V_{micro} [cm ³ /g]
SWy-2	26.2	1 662.0	0.095 04	17.6	0.003 82
NaSWy-2	29.6	-2 101.9	0.098 91	11.9	0.008 12
SAz-2	84.4	-1 031.0	0.124 30	48.8	0.015 94
NaSAz-2	69.3	-209.3	0.152 00	32.7	0.016 72
STx-1b	99.4	73.0	0.288 40	99.4	0.000 00
NaSTx-1b	97.2	149.3	0.224 80	86.3	0.004 47
Kunipia-F	11.1	170.5	0.075 15	9.5	0.000 67

predominantly mesoporous character with small value of specific surface area.

3.4 Scanning electron microscopy

Montmorillonite samples (MMT) were characterized by particles assembled into aggregates up to a few tens

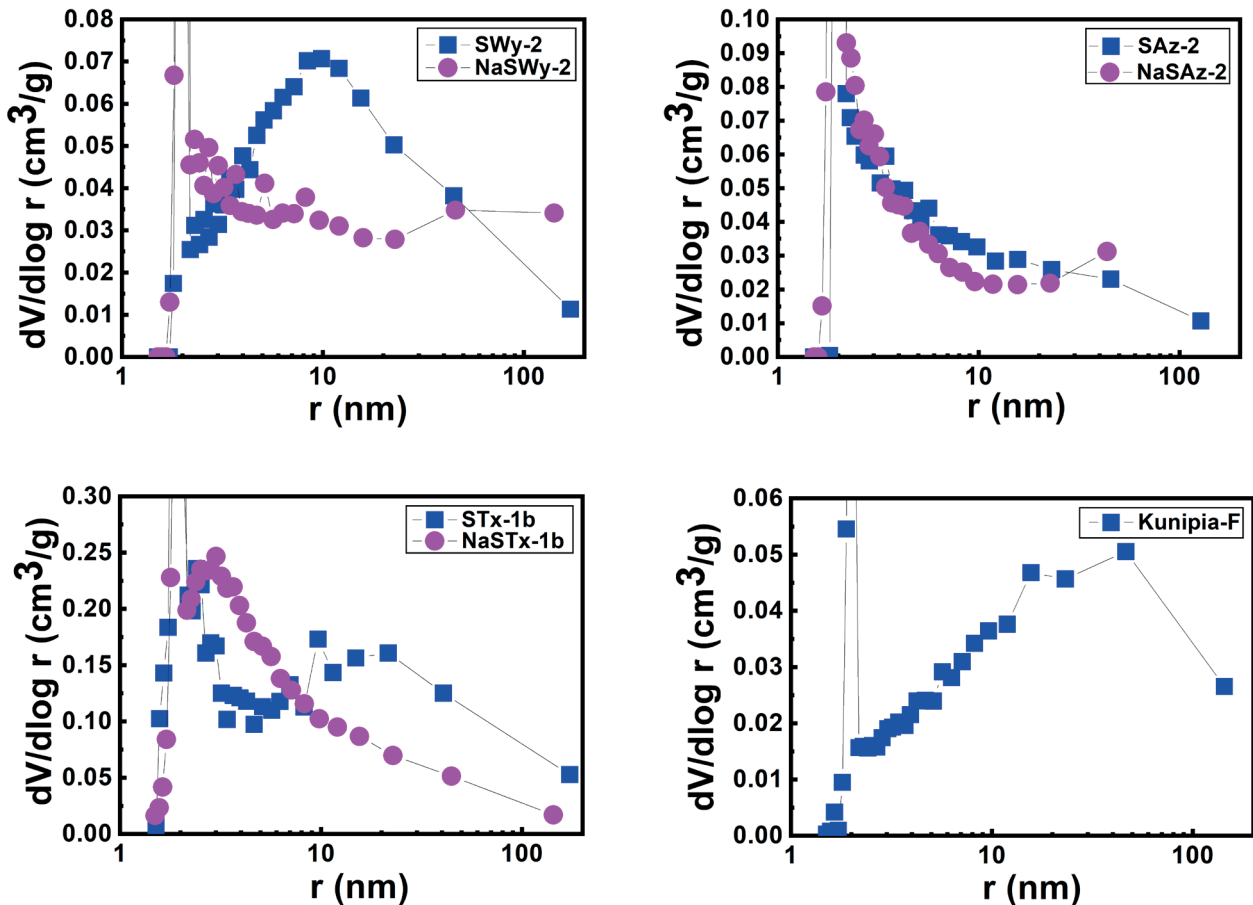
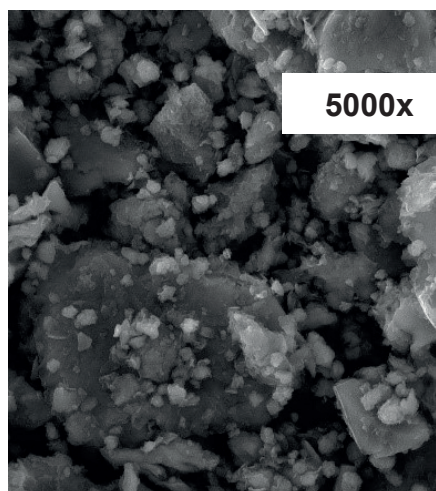
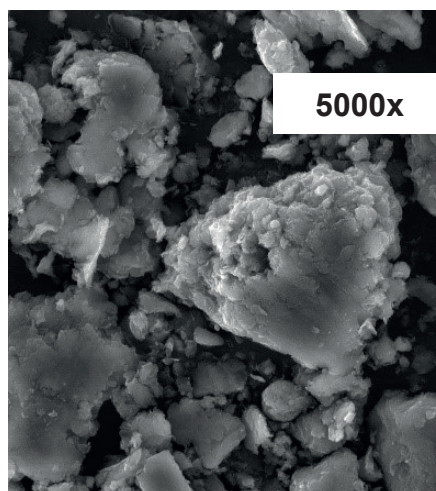


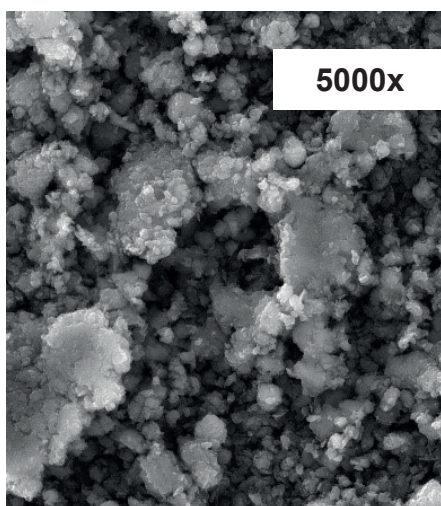
Fig. 5. Differential pore size distribution curves of studied MMT samples.



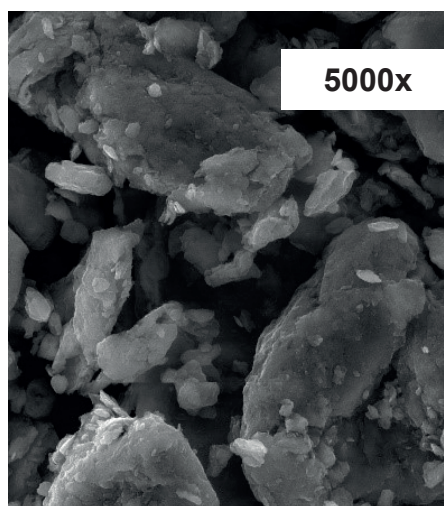
NaSWy-2



NaSAz-2



NaSTx-1b



Kunipia-F

Fig. 6. SEM images of MMT samples – magnification 5 000x.

of μm . The montmorillonite natrification had a dispersing effect on montmorillonite which meant grain refinement (Fig. 6). The bonds in the structure of montmorillonite are mainly influenced by the presence of water molecules. Water absorption is directly related to the presence of the two most common Na^+ and Ca^{2+} cations in the interlayer space of the MMT structure. Divalent Ca^{2+} cations keep the structural layers more stable and compact than their monovalent (Na^+) competitors. Upon entering Na^+ cations into the structure of smectite (montmorillonite), weaker bonds within the structural layers allow water molecules (but also other foreign cations or molecules) easier access to the layered structure. Hydration with water molecules leads to the expansion of the interlayer space immediately upon contact with water. A radical increase of the interlayer volume (up to 10 times) will affect the cation exchange

capacity of the montmorillonite (Kawatra & Ripke, 2003). In addition, monovalent Na^+ cations cannot compensate for the negative target charge of the phyllosilicate, as the presently ordered divalent Ca^{2+} cations.

This results in the structure being refined by increasing the repulsive forces between the montmorillonite particles. This phenomenon, together with the increase in volume, leads to an increase in the specific surface area and to changes in the adsorption properties of montmorillonite (Fig. 6).

4 Conclusion

In this study, the detailed characterization of fine-grained fractions of the montmorillonites samples SWy-2, SAz-2, STx-1b and Kunipia-F (in their natural state and after modification) was performed. The XRD analysis

confirmed montmorillonite as dominant mineral phase and demonstrated the structural changes of purified activated samples. The above mentioned changes affected the movement of montmorillonite main (001) reflection to the right on x axis. This phenomenon was caused by cation exchange between Ca^{2+} and Na^+ from interlayer space of montmorillonite structure.

The absorption bands observed in the IR spectra of the original montmorillonite forms were described in detail. After chemical activation, typical carbonate bands appear in all IR spectra of used montmorillonites. Simultaneously, the position of the band corresponding to the vibrations of the surface-bound water molecules changes, the band shifts to higher wavenumbers.

Thermal stability was determined for both fine-grained montmorillonite fractions and the samples of their activated sodium forms. Studied samples exhibit the same trend. The doubled peak on DTA curve associated with loss of adsorbed water is connected to Ca-montmorillonite form, whereas after activation process there was obtained only one stage peak typical for Na-montmorillonite form.

Based on the obtained data it can be concluded that modification influenced the structural and porous properties of SWy-2 and STx-1b samples (meso-macroporous samples). For microporous montmorillonites (SAz-2) such kind of treatment has not significant effect.

The activation of MMT samples with sodium led to a smaller grain sizes caused by the dispersive effect of sodium cations on the montmorillonite morphology seen on SEM.

These obtained results indicate that prepared activated fine montmorillonite fractions possess the potentiality to be a suitable material for preparing polymer-clay nanocomposites with enhanced sorptive properties usable for environmental remediation.

Acknowledgement

The authors would like to thank the Czech Academy of Sciences and the Slovak Academy of Sciences for supporting this study (Mobility Plus Project, project ID number SAV- AV ČR-21-08). This work was also supported by the Slovak Grant Agency for Science VEGA grant No. 2/0167/21. This work was supported by the Slovak Research and Development Agency under the contract No. APVV-19-0302. Authors are grateful to Alexandra Bekényiová and one anonymous reviewer for inspiring suggestions improving primary manuscript.

References

ABDELLAOUI, Y., OLGUÍN, M. T., ABATAL, M., ALI, B., MÉNDEZ, S. E. D. & SANTIAGO, A. A., 2017: Comparison of the divalent heavy metals (Pb, Cu and Cd) adsorption behavior

by montmorillonite-KSF and their calcium-and sodium-forms. *Superlatt. Microstruct.*, 127, 165–175.

ABOLLINO, O., ACETO, M., MALANDRINO, M., SARZANINI, C. & MENTASTI, E., 2003: Adsorption of heavy metals on Na-montmorillonite. Effect of pH and organic substances. *Water Res.*, 37, 7, 1619–1627.

AKPOMIE, K. G. & DAWODU, F. A., 2014: Efficient abstraction of nickel (II) and manganese (II) ions from solution onto an alkaline-modified montmorillonite. *J. Taibah Univ. Sci.*, 8, 4, 343–356.

AL-DEGS, Y. S., EL-BARGHOUTH, M. I., ISSA, A. A., KHRAISHEH, M. A. & WALKER, G. M., 2006: Sorption of Zn (II), Pb (II), and Co (II) using natural sorbents: equilibrium and kinetic studies. *Water Res.*, 40, 14, 2645–2658.

ALVES, J. L., ROSA, P. D. T. V. & MORALES, A. R., 2017: Evaluation of organic modification of montmorillonite with ionic and nonionic surfactants. *Appl. Clay Sci.*, 150, 23–33.

BERGAYA, F., AOUAD, A. & MANDALIA, T., 2006: Pillared Clays and Clay Minerals. In: Bergaya, F., Theng, B. K. G. & Lagaly, G. (Eds.): *Handbook Clay Sci.*, Elsevier, Amsterdam, 1, 393–421.

BISWAS, B., WARR, L. N., HILDER, E. F., GOSWAMI, N., RAHMAN, M. M., CHURCHMAN, J. G., VASILEV, K., PAN, G. & NAIDU, R., 2019: Biocompatible functionalisation of nanoclays for improved environmental remediation. *Chem. Soc. Rev.*, 48, 14, 3740–3770.

BLAŽEK, A., 1974: *Book of Thermal Analysis*. Prague, SNTL.

BRANTSEVA, T. V., ANTONOV, S. V. & GORBUNOVA, I. Y., 2018: Adhesion properties of the nanocomposites filled with aluminosilicates and factors affecting them: A review. *Int. J. Adhesion Adhesives*, 82, 263–281.

BREEN, C. & MORONTA, A. J., 2001: Influence of exchange cation and layer charge on the isomerization of α -pinene over SWy-2, SAz-1 and Sap-Ca. *Clay Miner.*, 36, 467–472.

DE AZEREDO, H. M., 2013: Antimicrobial nanostructures in food packaging. *Trends Food Sci. Technol.*, 30, 1, 56–69.

GALAMBOŠ, M., DAŇO, M., ROSSKOPFOVÁ, O., ŠERŠEŇ, F., KUŤÁKOVÁ, J., ADAMCOVÁ, R. & RAJEC, P., 2012: Effect of gamma-irradiation on adsorption properties of Slovak bentonites. *J. Radioanal. Nucl. Chem.*, 292, 481–492.

GALAMBOŠ, M., KRAJŇÁK, A., ROSSKOPFOVÁ, O., VIGLAŠOVÁ, E., ADAMCOVÁ, R. & RAJEC, P., 2013: Adsorption equilibrium and kinetic studies of strontium on Mg-bentonite, Fe-bentonite and illite/smectite. *J. Radioanal. Nucl. Chem.*, 298, 1031–1040.

GAUTAM, A. & KOMAL, P., 2019: Synthesis of montmorillonite clay/poly(vinyl alcohol) nanocomposites and their mechanical properties. *J. Nanosci. Nanotechnol.*, 19, 12, 8071–8077.

GUO, Y. X., LIU, J. H., GATES, W. P. & ZHOU, Ch. H., 2020: Organo-modification of montmorillonite. *Clays Clay Mine.*, 68, 6, 601–622.

GUERRA, D. J. L., MELLO, I., RESENDE, R. & SILVA, R., 2013: Application as absorbents of natural and functionalized Brazilian bentonite in Pb^{2+} adsorption: Equilibrium, kinetic, pH, and thermodynamic effects. *Water Res. Industry*, 4, 32–50.

HATAKEYAMA, T. & LIU, Z., 1998: *Handbook of Thermal Analysis*. New York, Wiley.

- HAYAKAWA, T., OYA, M., MINASE, M., FUJITA, K. I., TEPAKAKORN, A. P. & OGAWA, M., 2019: Preparation of sodium-type bentonite with useful swelling property by a mechanochemical reaction from a weathered bentonite. *Appl. Clay Sci.*, 175, 124–129.
- HONG, S. I. & RHIM, J. W., 2008: Antimicrobial activity of organically modified nano-clays. *J. Nanosci. Nanotechnol.*, 8, 11, 5818–5824.
- IWASAKI, T. & WATANABE, T., 1988: Distribution of Ca and Na ions in dioctahedral smectites and interstratified dioctahedral mica/smectites. *Clays Clay Mine.*, 36, 1, 73–82.
- KANMANI, P. & RHIM, J. W., 2014: Physical, mechanical and antimicrobial properties of gelatin based active nanocomposite films containing AgNPs and nanoclay. *Food Hydrocolloids*, 35, 644–652.
- KAUR, N. & KISHORE, D., 2012. Montmorillonite: An efficient, heterogeneous and green catalyst for organic synthesis. *J. Chem. Pharmaceut. Res.*, 4, 2, 991–1015.
- KOMADEL, P. & MADEJOVÁ, J., 2006: Acid activation of clay minerals. In: Bergaya, F., Theng, B. K. G. & Lagaly, G. (Eds.): Handbook of Clay Science, *Amsterdam, Elsevier*, 1, 263–287.
- KOTAL, M. & BHOWMICK, A. K., 2015: Polymer nanocomposites from modified clays: Recent advances and challenges. *Progress Polymer Sci.*, 51, 127–187.
- KAWATRA, S. K. & RIPKE, S. J., 2003: Laboratory studies for improving green ball strength in bentonite-bonded magnetite concentrate pellets. *Int. J. Mineral Process.*, 72, 1–4, 429–441.
- MOCKOVČIAKOVÁ, A., OROLÍNOVÁ, Z. & Škvarla, J., 2010: Enhancement of the bentonite sorption properties. *J. Hazard. Mater.*, 180, 1–3, 274–281.
- MURRAY, H. H., 2007: Applied Clay Mineralogy. *Amsterdam – Oxford, Elsevier*.
- ÖNAL, M., KAHRAMAN, S. & SARIKAYA, Y., 2007: Differentiation of α -cristobalite from opals in bentonites from Turkey. *Appl. Clay Sci.*, 35, 1–2, 25–30.
- PAREKH, S. B. & RULE, A. U., 2002: Teaching Clay Science, In: Rule, A. U. & Guggenheim, S. (Eds.): *Clay Mineral Soc., Aurora*, 11, 22.
- PAVLIDOU, S. & PAPANAYIDES, C. D., 2008: A review on polymer-layered silicate nanocomposites. *Progress Polymer Sci.*, 33, 111–1198.
- QIN, Z., PENG, T., SUN, H., ZENG, L. & ZHOU, C., 2021: Effect of montmorillonite layer charge on the thermal stability of bentonite. *Clays Clay Miner.*, 69, 328–338.
- RAY, S. S. & OKAMOTO, M., 2003: Polymer/layered silicate nanocomposites: a review from preparation to processing. *Progress Polymer Sci.*, 28, 11, 1539–1641.
- RITZ, M., VACULÍKOVÁ, L., KUPKOVÁ, J., PLEVOVÁ, E. & BARTOŇOVÁ, L., 2016: Different level of fluorescence in Raman spectra of montmorillonites. *Vibrational Spectrosc.*, 84, 7–15.
- RUITZ, E. & VAN MEERBEEK, A., 2006: Clay Mineral and Organoclay – Polymer Nanocomposites. In: Bergaya, F., Theng, B. K. G. & Lagaly, G. (Eds.): Handbook of Clay Science, *Amsterdam, Elsevier*, 1, 583–621.
- SANQIN, W., ZEPENG, Z., YUNHUA, W., LIBING, L. & JIANGSHENG, Z., 2014: Influence of montmorillonites exchange capacity on the basal spacing of cation-anion organo-montmorillonites. *Mater. Res. Bull.*, 59, 59–64.
- SCHÜTZ, T., DOLINSKÁ, S., HUDEC, P., MOCKOVČIAKOVÁ, A. & ZNAMENÁČKOVÁ, I., 2016: Cadmium adsorption on manganese modified bentonite and bentonite–quartz sand blend. *Int. J. Miner. Process.*, 150, 32–38.
- SHAH, L. A., 2018: Effect of Na_2CO_3 activation and sedimentation on surface area, particle size, and pore size distribution of Pakistani Ca-bentonite. *Arab. J. Geosci.*, 11, 15, 399.
- TOMBACZ, E. & SZEKERES, M., 2004: Colloidal behavior of aqueous montmorillonite suspensions: the specific role of pH in the presence of indifferent electrolytes. *Appl. Clay Sci.*, 27, 1–2, 75–94.
- TOMIĆ, M., DUNJIĆ, B., NIKOLIĆ, M. S., MALETAŠKIĆ, J., PAVLOVIĆ, V. B., BAJAT, J. & DJONLAGIĆ, J., 2018: Dispersion efficiency of montmorillonites in epoxy nanocomposites using solution intercalation and direct mixing methods. *Appl. Clay Sci.*, 154, 52–63.
- UDDIN, M. K., 2017: A review on the adsorption of heavy metals by clay minerals, with special focus on the past decade. *Chem. Eng. J.*, 308, 438–462.
- VACULÍKOVÁ, L., PLEVOVÁ, E. & RITZ, M., 2019: Characterization of montmorillonites by infrared and Raman spectroscopy for preparation of polymer-clay nanocomposites. *J. Nanosci. Nanotechnol.*, 19, 5, 2775–2781.
- WIESS, Z. & KUŽVART, M., 2005: Jílové minerály – jejich struktura a použití. *Praha, Karolinum*.

Charakteristika jemnozrnej frakcie montmorillonitu na prípravu polymérových ílovitých nanokompozitov

Cieľom štúdia bola detailná charakterizácia ílových minerálov (pred ich chemickou aktiváciou a po nej) na prípravu nanokompozitov polymér-íl v porovnaní s prírodným neupraveným materiálom. Komplexná štruktúrna charakterizácia jemnozrnných frakcií prispieva k lepšiemu pochopeniu fyzikálno-chemických vlastností a správania ílových minerálov a umožňuje plne využiť ich potenciál pri príprave ílových nanokompozitov s vyššími úžitkovými vlastnosťami na budúce priemyselné aplikácie.

Vzorky montmorillonitu sú charakteristické časticami spojenými do agregátov až do veľkosti niekoľkých desiatok mikrometrov. Natrifikácia má na montmorillonit dispergačný účinok, čím sa dosiahne zjemnenie zrna. Väzby v štruktúre montmorillonitu sú ovplyvnené najmä prítomnosťou molekúl vody. Absorpcia vody priamo súvisí s prítomnosťou dvoch najbežnejších katiónov, Na^+ a Ca^{2+} , v medzivrstvovom priestore. Dvojmocné katióny Ca^{2+} udržiavajú štruktúrne vrstvy stabilnejšie a kompaktnšie ako ich monovalentné (Na^+) ióny. Po vstupe katiónov Na^+ do štruktúry smektitu (montmorillonitu) slabšie väzby v rámci štruktúrnych vrstiev umožňujú molekulám vody (ale aj iným cudzím katiónom alebo molekulám) ľahší prístup k vrstvenej štruktúre. Radikálne zvýšenie objemu medzivrstvy (až 10-násobne) ovplyvní katiónovú výmennú kapacitu montmorillonitu. Tento jav spolu so zväčšením objemu vedie k zväčšeniu špecifického povrchu a k zmenám adsorpčných vlastností montmorillonitu.

Boli použité štyri vzorky ílového minerálu montmorillonitu: SWy-2, SAz-2, STx-1b a Kunipia-F. Vzorky SAz-2 a STx-1b obsahujú katióny Ca^{2+} v medzivrstve, vzorka SWy-2 katióny Na^+ aj Ca^{2+} a Kunipia-F iba katióny Na^+ . Montmorillonity v prírodnom stave boli purifikované sedimentáciou podľa Stokesovho zákona (získaná jemná frakcia, veľkosť častíc $< 5 \mu\text{m}$). Na zlepšenie povrchových vlastností jemnozrnných frakcií sa urobila monoiónová chemická aktivácia vzoriek montmorillonitov obsahujúcich vápnik v medzivrstve (SAz-2, STx-1b a SWy-2). Aktivované vzorky boli pripravené saturáciou 0,5 M vodným roztokom Na_2CO_3 intenzívnym trepaním počas 24 hodín, oddelením zmesi centrifugáciou, následným premývaním destilovanou vodou a sušením pri $100 \text{ }^\circ\text{C}$ počas 24 hodín. Následne sa vykonala fyzikálno-chemická charakterizácia získaných materiálov, ako aj vstupných vzoriek metódami rtg. práškovej difrakcie, infračervenej spektroskopie, termickej analýzy, SEM analýzy a analýzy povrchu pomocou sorpcie plynov.

Röntgenová prášková difrakcia potvrdila prítomnosť montmorillonitu ako dominantnú minerálnu fázu a preukázala štruktúrne zmeny aktivovaných vzoriek, ktoré

ovplyvnili posun hlavnej bazálnej difrakcie montmorillonitu (001) na osi x doprava. Tento jav bol spôsobený výmenou katiónov medzi Ca^{2+} a Na^+ z medzivrstvového priestoru montmorillonitovej štruktúry.

Infračervená spektroskopia charakterizovala absorpčné pásy pozorované v infračervených spektrách pôvodných foriem montmorillonitu. Jednotlivé typy montmorillonitov sa líšia typom minerálnych prímies aj svojím chemickým zložením. Montmorillonit SAz-2 predstavoval takmer čistú vzorku. Iba nepatrný pás nachádzajúci sa v blízkosti 789 cm^{-1} indikoval stopy amorfného oxidu kremičitého. Prímes kremeňa sa potvrdila dubletom pásov v oblasti vlnovej dĺžky 798 a 779 cm^{-1} vo vzorkách SWy-2 a Kunipia-F. Vzorka STx-1b obsahovala prímes cristobalitu (794 cm^{-1}). Absorpčný pás pri vlnovej dĺžke 884 cm^{-1} vo vzorke SWy-2 potvrdil prítomnosť Fe v oktaédrickej štruktúre tohto ílového minerálu. Po chemickej aktivácii sa vo všetkých infračervených spektrách použitých montmorillonitov zistili typické karbonátové pásy (1430 a 880 cm^{-1}). Súčasne bola pozorovaná zmena polohy pásu zodpovedajúceho vibráciám povrchovo viazanej vody. Pás sa posúva k vyšším vlnovým dĺžkam.

Pri hodnotení tepelnej stability jemnozrnných frakcií montmorillonitov a ich aktivovaných sodných foriem simultánnou termogravimetriou a diferenčnou termickou analýzou mali študované vzorky rovnaký trend. Teplotné krivky vykazovali dva teplotné intervaly. Prvý interval ($100 - 300 \text{ }^\circ\text{C}$) zodpovedá uvoľňovaniu adsorbovanej vody z medzivrstvy. Druhý interval ($500 - 1100 \text{ }^\circ\text{C}$) predstavuje uvoľňovanie hydroxylových skupín a následné fázové premeny. Zdvojený pík na DTA krivke zodpovedajúci strate adsorbovanej vody je spojený s Ca formou montmorillonitov. Po aktivačnom procese bol získaný jednodušový pík, typický pre Na montmorillonitovú formu. Teplota fázovej premeny sa pri vzorke STx-1b zvýšila, zatiaľ čo pri vzorkách SWy-2 a SAz-2 fázová premena nebola pozorovaná.

Podrobné analýzy adsorpčných izoteriem sa uskutočnili na porovnanie povrchových vlastností študovaných vzoriek. Namerané izotermy všetkých vzoriek montmorillonitov ukázali hysteréznú slučku medzi adsorpčnými a desorpčnými vetvami izoteriem. Adsorpčné izotermy SWy-2, SAz-2 a Kunipia-F boli veľmi podobné, pomalé zvyšovanie objemu adsorbovaného plynu v celom rozsahu relatívneho tlaku s prudkým nárastom pri $p/p_0 \approx 0,95$ bolo spojené s prítomnosťou väčších pórov, makropórov. Hysterézne slučky vzoriek SWy-2, STx-1b a Kunipia-F korešpondujú s typom H3 potvrdzujúcim prítomnosť pórov typických pre hlinitokremičitanové materiály.

Slučka vzorky SAz-2 je typu H4, spojená s prítomnosťou štrbinovitých pórov, ale počiatočná časť izotermy je spojená s prítomnosťou mikropórov. Najvyššia hodnota špecifického povrchu bola v prípade vzorky STx-lb (99,4 m²/g).

Zmeny vlastností po modifikácii vzoriek montmorillonitov boli pozorované aj z distribučných kriviek diferenciálnej veľkosti pórov odvodených z desorpčných vetiev izoteriem. Vzorka SWy-2 vykázala širšiu distribúciu, v rozsahu od 4,3 do 44,7 nm s maximom $R_{\max} = 9,8$ nm (polomer pórov). Zodpovedá to prítomnosti mezo- a makropórov. Ostré maximum polomeru pórov pri $R \approx 1,9$ nm zodpovedá skoku na desorpčnej izoterme, ktorý sa nazýva vynútené uzavretie hysteréznej slučky a nezodpovedá skutočným pórom. Toto maximum možno pozorovať pri všetkých študovaných vzorkách. Vzorky SAz-2 a NaSAz-2 majú veľmi podobné distribučné krivky, mierny rozdiel možno pozorovať iba v rozsahu veľkých mezopórov a makropórov. Môže to byť spojené s nižšou hodnotou objemu adsorbovaného plynu na adsorpčnej izoterme. Vzorka

SAz-2 bola mikroporéznejšia a modifikácia významne neovplyvnila jej textúrne vlastnosti. Vzorka STx-lb neobsahovala mikropóry, bola hlavne mezoporézno-makroporézna, s vyšším obsahom väčších mezopórov ($R_{\max} = 21,6$ nm). Po modifikácii vzorky sa pozoroval posun distribučnej krivky doľava k hodnotám nižších mezopórov ($R_{\max} = 3,05$ nm). Táto skutočnosť zodpovedá zníženiu hodnoty celkového objemu pórov. Vzorka Kunipia-F vykázala širokú distribúciu, od 3,03 do 143,3 nm s dvomi maximami, $R_{\max1} = 15,7$ nm a $R_{\max2} = 46,5$ nm. Potvrdilo to prevažne mezoporézny charakter s malou hodnotou špecifického povrchu. Získané jemné frakcie montmorillonitu majú potenciál byť vhodným materiálom na prípravu ílových nanokompozitov s lepšími sorpčnými vlastnosťami využiteľnými v environmentálnych oblastiach.

Doručené / Received: 19. 5. 2022

Prijaté na publikovanie / Accepted: 21. 6. 2022

Electroremediation in low-hydraulic conductivity zones – current stage of knowledge and small-scale laboratory experiment

CLAUDIA ČIČÁKOVÁ¹, ROMAN TÓTH^{1,2}, HANA HORVÁTHOVÁ^{1,2}, ANTON DRÁBIK²,
EUBOMÍR JURKOVÍČ¹ and DENYS KRAVCHENKO²

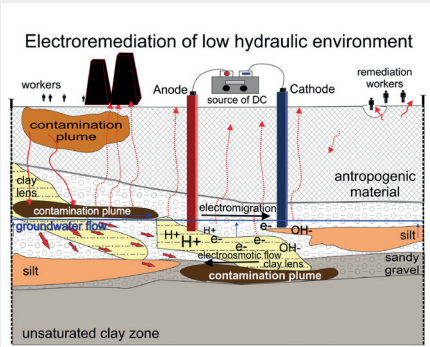
¹ Comenius University in Bratislava, Faculty of Natural Sciences, Department of Geochemistry Ilkovičova 6, SK 842 15 Bratislava, Slovakia; cicakova13@uniba.sk; hana.horvathova@uniba.sk; roman.toth@uniba.sk; lubomir.jurkovic@uniba.sk

² The Centre of Environmental Services, Ltd., Kutlíkova 17, SK 852 50 Bratislava, Slovakia; toth@cenvis.sk; horvathova@cenvis.sk; drabik@cenvis.sk; kravchenko@cenvis.sk

Abstract: Over past decades, the rapid increase of industrial activities has caused vast environmental pollution by different types of contaminants. Groundwater sources belong to the most vulnerable parts of the environment. Zones, especially aquifers with low hydraulic-conductivity (mainly clayey, silty soils with gravels) represent a considerable challenge for scientists to remediate due to their low transmissivity values. Conventional remediation methods (i.e. pump and treat) are ineffective in such conditions; therefore, new and effective methods are required. Electroremediation appears to be a suitable technique in aquifers with low-hydraulic conductivity. Although, this method has been known for decades, there is still a lack of field applications. This article summarizes the current stage of knowledge in electrokinetic remediation of contaminants (e.g. hydrocarbons, metals) in low-hydraulic conductivity aquifers and presents information from certain available field application studies. The aim was to focus on optimizing and enhancing approaches in the electroremediation method and summararily bring useful information to future researchers in their practical utilization. Furthermore, a small-scale laboratory experiment was conducted to prove the efficiency of electroremediation of chlorinated hydrocarbons in groundwater from the model locality (environmental burden), intended for large-scale pilot decontamination by this approach.

Key words: electroremediation, low permeability aquifer, laboratory experiment, field applications

Graphical abstract



The diagram illustrates the electroremediation process in a low-hydraulic environment. It shows a cross-section of the ground with an anode (left) and a cathode (right) connected to a DC source. The ground consists of several layers: an unsaturated clay zone at the top, followed by a layer with clay lenses, silt, and sandy gravel. A contamination plume is shown in the groundwater, with arrows indicating the direction of groundwater flow and electroosmotic flow towards the cathode. The diagram also shows the migration of ions (H⁺, OH⁻, e⁻) and the presence of anthropogenic material and workers near the site.

Highlights

- To summarize the current stage of knowledge in electroremediation of contaminants in low-hydraulic conductivity aquifers during field application studies
- Electroremediation of chlorinated aliphatic hydrocarbons from the native contaminated groundwater sample was verified under laboratory condition

1 Introduction

Water, groundwater, and soil pollution belong among the most important concerns for scientific and engineering society. Relentless, increasing demand on quality of life forces the scientific community to investigate the newest and more effective treatment methods and techniques to provide the best results in the remediation of contaminated sites.

The conventional water contaminants vary from organic substances, such as chlorinated hydrocarbons (Černíková

et al., 2020; Rajic et al., 2014; Sáez et al., 2009); petroleum hydrocarbons (Korolev & Nesterov, 2018; Moussavi et al., 2011; Song et al., 2018), herbicides (Risco et al., 2016), polycyclic aromatic hydrocarbons (Fan et al., 2016; Yukselen-Aksoy & Reddy, 2013), nitrate (Lee et al., 2011), to inorganic contaminants such as metals (Kim et al., 2012) or radionuclides (Purkis et al., 2021). Significant contamination sources originate primarily from anthropogenic activities, e.g. mining activities, agriculture, manufacturing industries, or even households.

The contaminated substances differ in the varying levels of their natural degradability in the aquifer (groundwater environment). Some contaminants prefer to transform into another state rather than undergo degradation. Contaminated groundwater is often characterized by a deficiency in oxygen content (limited oxygen concentration), thus, in situ remediation processes focus on improving contaminant degradation in anaerobic conditions. This applies especially to chlorinated hydrocarbons, which are recalcitrant to oxidation (microbial or chemical), and preferably reduced (Fallgren et al., 2018).

Field application of different remediation techniques can be generally limited by the difficulties of measuring and defining the highly variable hydrological and hydrogeological features (e.g. permeability, porosity, saturation, hydraulic flow, oxygen content) of the geological environment (Hyldegaard, 2019; Lee et al., 2000).

Hydrogeological and geological conditions of the geological environment considerably affect in situ remediation, including the type of in situ remediation, selection of the reaction materials, remediation efficiency, and the cost (Zhao et al., 2022). The primary constraint of current in situ remediation technologies in low-hydraulic conductivity aquifers using conventional hydraulic recirculation or injection techniques is the often insufficient delivery of the required amendments to the target contaminated matrix (Cox et al., 2018).

The study of the efficiency of aquifer remediation provided by Lee et al. (2000) showed that permeability heterogeneities can vastly affect the length of time required to remove the pollutants. This study mentioned the ability of clays and clay beds with low conductivity zones $< 10^{-7} \text{ m.s}^{-1}$ (Hyldegaard & Ottosen, 2021; Nazaroff & Alvarez-Cohen, 2000) to trap significant amounts of pollutants, with their later slow-release into the aquifer. As a result of long-term leakage of trapped contaminants (“back diffusion effect”) from clays, they may persist in the groundwater systems and significantly affect the time required for remediation and financial demands. Contaminated low-permeability geological environments pose a long-term threat (Hyldegaard & Ottosen, 2021; Parker et al., 2008; Scheutz et al., 2010) due to geological and hydrogeological complexity in lithology, stratigraphy, and structure. The optimal remediation designs are site-specific and differ by variations in permeability fields (Lee et al., 2000).

On the other hand, saturated high-permeability soils (gravels, sands, limestones) can comprise of heterogeneous and homogeneous layers (Gill et al., 2014; Hansen et al., 2015; Hyldegaard & Ottosen, 2021; Ottosen et al., 2019). The grain sizes in such environments are commonly large and also bedrock may be fractured, which contributes to higher hydraulic conductivities until $>10^{-4} \text{ m.s}^{-1}$ (Appelo & Postma, 2010; Hyldegaard & Ottosen, 2021; Nazaroff

& Alvarez-Cohen, 2000), therefore some pollutants (e.g. chlorinated ethenes) can easily spread and distribute through soil pores and contaminate aquifers (Hyldegaard & Ottosen, 2021). The issues of clay materials and their specific properties are covered in a detailed review published by Janeni and Adassooriya (2021).

By the conventional in situ treatment methods, e.g. pump-and-treat (Banerjee et al., 1991; Fountain et al., 1996), in situ chemical reduction (ISCR) (Fallgren et al., 2018), or in situ chemical oxidation (ISCO) (Fan et al., 2014; Yukselen-Aksoy & Reddy, 2013), hydraulic conductivity and low permeability of geological environment play a key role (Cox et al., 2018). Pump-and-treat is considered an economical process; however, the desired results may be limited, particularly in low-permeability soils and aquifer areas where contaminants tend to be sorbed (Banerjee et al., 1991). These conventional methods are usually not efficient in LNAPL (light nonaqueous phase liquid) and DNAPL (dense nonaqueous phase liquid) degradation in contaminated aquifers (Starr & Cherry, 1994) and require the delivery of additional agents or solvents or other kinds of enhancements.

In comparison with an advective hydraulic delivery, the electrokinetic-enhanced delivery is considered as more efficient due to the effective uniform amendments distribution at contaminated sites where heterogeneous layers in the geological environment often constrain the applications of hydraulic methods (Cox et al., 2018).

Electrokinetics can achieve relatively uniform transport in inter-bedded clays and sands. Electrokinetically-enhanced transport, which relies primarily on the electrical properties of aquifer materials instead of the hydraulic properties, represents a solution for the limitations of preferential pathways, which are facing the conventional advective-based hydraulic technologies (Cox et al., 2018).

The scientific community has to come up with new technologies to remediate contaminated sites with specific hydrogeological properties (such as silt and clay materials, or combination of sand with low permeability materials). The electroremediation method has been confirmed in removing water- and soil-contaminants from low permeability environments with limited hydraulic conductivity, e.g. in clay aquifers (Fallgren et al., 2018; Liu et al., 2020; Reddy et al., 2010; Reddy & Saichek, 2003; Yin et al., 2022).

2 Electroremediation basic principles

Electroremediation is a group of remediation techniques belonging to the category of direct current technologies (DCT) (Niroumand et al., 2012; Streche et al., 2018), including electrokinetic remediation, electrochemical processes, electrodeposition, electrocoagulation, electrodewatering, etc. The principle of this technology is in

the application of an electric current into the remediated matrix with subsequent creation of electric field.

The electroosmosis process was mentioned for the first time by Reuss (1809). Since the 1950's development of the technology continued with several studies (Casagrande et al., 1986; Casagrande, 1949; Gray & Mitchell, 1967; Segall et al., 1980). Acar and Alshawabkeh (1993) and Alshawabkeh and Acar (1992) set up the theoretical background of principal processes. Since then, several publications in field applications were published (Ho et al., 1999a, b; Lageman, 1993).

The natural electric current generally appears on sediments, mineral, and rock surfaces in groundwater systems as a consequence of natural abiotic and microbial processes. At a mineral surface, anode and cathode-like reactions occur and affect the redox potential in the pore water of a saturated matrix (Fallgren et al., 2018; Revil et al., 2012). The external application of electric current into the saturated zone (aquifer) leads to the increase of electron activity and subsequent lowering of redox potential of the pore water (Fallgren et al., 2018). The surfaces of the minerals in sedimentary rocks contain protonic and hydroxyl groups, which create an electric charge on the sediment surface, that depends on the pH and ionic strength of the surrounding electrolyte (Černík et al., 2020; Saleh et al., 2007).

The application of direct current (DC) and subsequent creation of electric field leads to several changes in the electric double layer – an interface layer between solid (clay particles) and the liquid (electrolyte). Detailed information about the impact of electric current behaviour of diffused double layer and point of zero charges are discussed in Pamukcu et al. (2014). Diffuse double layer

(or Helmholtz double layer – consists of two layers of opposite polarity or charge) and possible redox reaction at a soil particle surface under electric current are depicted in Fig. 1. As Fig 1 shows, redox reactions are formed along the outer Helmholtz plane. The hygroscopic water in the inner Helmholtz plane plays a role of a dielectric media and the hydrated cations interface with the redox reaction zones (Jin & Fallgren, 2010).

The in situ electroremediation method is usually based on application of DC or low voltage among a pair or series of electrodes (anode and cathode) inserted into the geological environment, with the subsequent creation of the electric field. Under an electric field, several electrokinetic processes take place (see Fig. 2), such as electromigration, electroosmosis, and electrophoresis, responsible for contaminants transport in the subsurface environment. *Electromigration* (EM) describes the movement of dissociated ions through a bulk solution, along the electric field to the electrode of the opposite charge. It is used for ionic contaminants removals such as heavy metals (Banerjee et al., 1991) or radionuclides (Purkis et al., 2021). *Electroosmotic flow* (EOF) can be understood as water movement of contaminants dissolved in aquatic solution or the movement of pore fluid in stationary porous media. The significance of electroosmosis raises with increasing surface charge density, i. e., with decreasing grain size (Probstein & Hicks, 1993; Wiczorek et al., 2005). The general direction of electroosmotic flow is from anode to cathode. With increasing pH, phenomenon such as reverse osmosis may occur. Therefore, the direction of EOF is from cathode to anode (Cameselle & Reddy, 2012; Wiczorek et al., 2005). Electroosmosis occurs mainly in a low permeability environments (Hyldegaard & Ottosen, 2021). *Electrophoresis* (EP) includes the movement of charged colloids (clay minerals, dissolved organic matter) and solid particles in the stagnant fluid. This type of electrophoretic transport is limited by the pore size and ineffective in fine-textured soils (Probstein & Hicks, 1993; Wiczorek et al., 2005). Both electroosmosis and electrophoresis are applied for organic contaminants (e.g. chlorinated hydrocarbons, polycyclic aliphatic hydrocarbons) degradation.

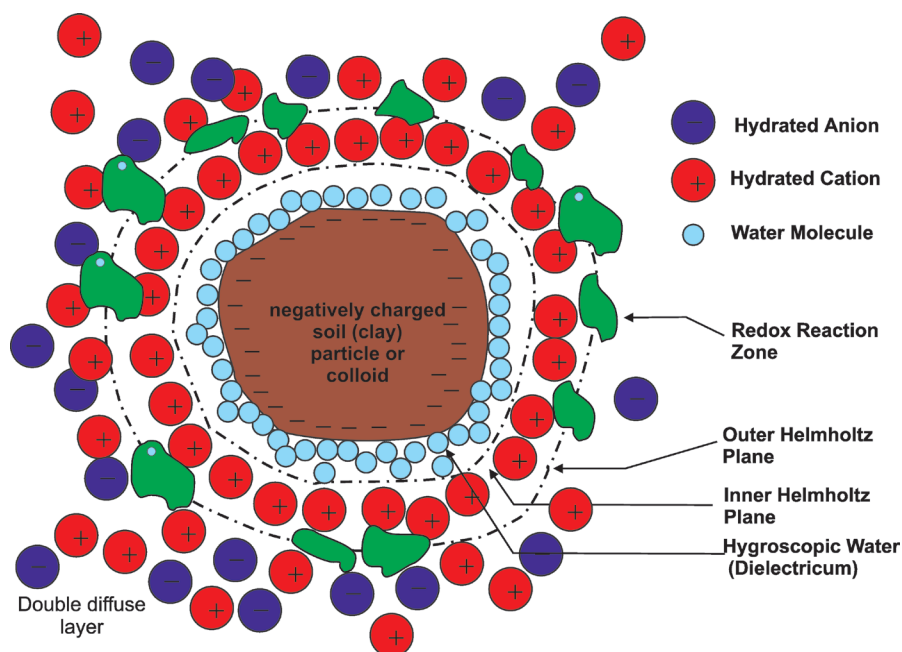


Fig. 1. Possible redox reaction at a soil particle surface under electric current [modified after Fallgren et al. (2018); Jin & Fallgren (2010)].

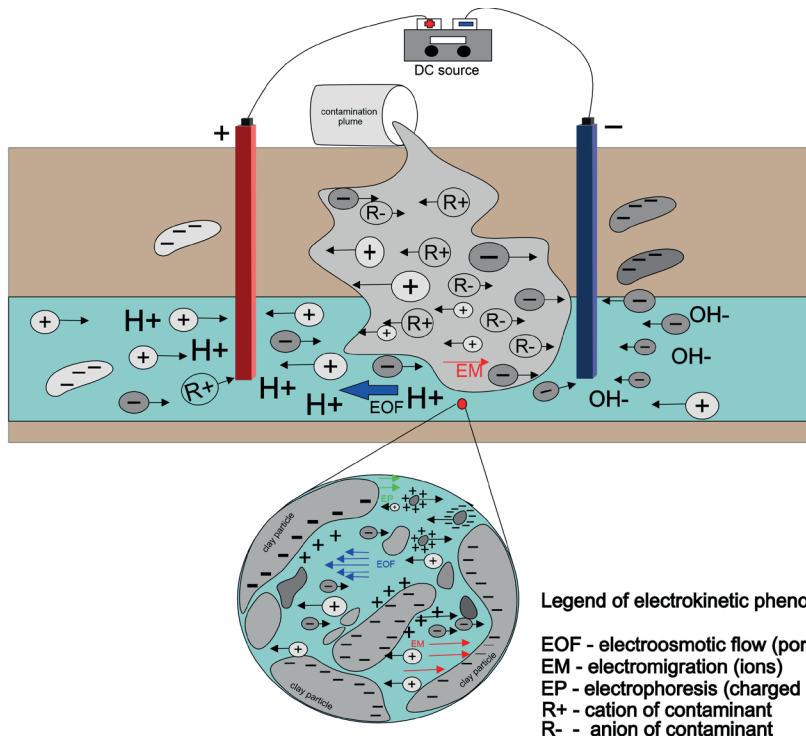
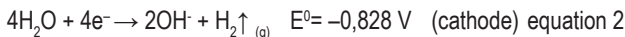
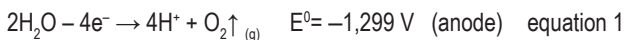


Fig. 2. Main mechanisms occurring during electrokinetic remediation, modified after Gill et al. (2014).

Both electrochemical processes, oxidation and reduction, occur at the anode and at the cathode electrode due to the *electrolysis of water*. These reactions are given below:



Where eq. (1) represents anodic oxidation with consequent pH decreasing due to H^+ production and redox-potential raising. Eq. (2) introduces reduction on the cathode, where pH is rising due to produced OH^- ions and redox potential is decreasing (Acar & Alshawabkeh, 1993; Cameselle & Reddy, 2012; Fallgren et al., 2018; Kim et al., 2005; Vocciante et al., 2021; Yin et al., 2022). Electrolysis of water can be understood as the redox process, which occurs when the voltage gradient is exceeded and redox reactions can lead to changes in acid-base equations (Pavelková et al., 2021). The critical point of water electrolysis is the donation of electrons into a geological environment through electric current. Exceeding voltage gradient at electrodes increases water conductivity and decreases the surrounding environment's resistance (Černík et al., 2020). Low pH contributes to the desorption and the dissolution of heavy metals, while higher pH values favour their sorption and precipitation (Acar & Alshawabkeh, 1993; Kim et al., 2005; Shen et al., 2007).

Electrochemical remediation also causes other processes, i.e. ionic diffusion, dissolution of electrode materials, advection, dispersion, precipitation of salts or minerals

and other chemical transformation (Acar & Alshawabkeh, 1993; Banerjee et al., 1991; Hyldegaard & Ottosen, 2021; Vocciante et al., 2021).

As Fallgren et al. (2018) mentioned, redox potential is not often taken into account by electroremediations since contaminants used to be transported through subsurface treatment zones filled with different sorbents; or contaminants are degraded at the electrodes or in their vicinities. However, in such way of contaminants disposal,

fouling of electrode materials is avoided. Another way of electroremediation use includes distribution of remediation agents, such as bacteria and nutrients through the geological environment (Fallgren et al., 2018; Mao et al., 2012). The primary purpose of this kind of technology is to overcome the solvent distribution problems in low permeable matrices in which chemical methods such as ISCO [e.g. persulfate (Wen et al., 2022)], ISCR [e.g. nZVI – nanozero valent iron (Černíková et al., 2020)] use to struggle, and simultaneously to improve mobility of contaminants through the electric field (Fallgren et al., 2018). Electroosmotic flow is more important in soils with low permeability, than in sandy and limestoned soils (Hyldegaard & Ottosen, 2021). High natural groundwater flow velocity in a more permeable environment may constrain the flow of electrokinetic transport against the direction of the natural groundwater flow (Cox et al., 2018).

The biggest advantage of electroremediation is to avoid the need for disturbing ground structure and expensive excavation procedures (Yükselen-Aksoy & Reddy, 2012). Inseparable condition for electroremediation is the necessity of submerging electrodes into the aquifer or saturated soil matrix, or in wells to reach the contact with groundwater.

In the past, the electrokinetic remediation used to be utilized in various ways, e.g. electroosmosis dewatering, consolidation and stabilization of soft soils (Adamson et al., 1966; Burnotte et al., 2004), electrical thickening, electrophoretic separation, and electrophoretic deposition

(Asavadorndeja & Glawe, 2005). At present, electrokinetic remediation finds application for injection and control of grouting in soils or aquifer (Banerjee et al., 1991; Esrig, 1968; Yamanouchi & Matsuda, 1975), remediation of soils and groundwater (Banerjee et al., 1991).

Advantages, that bring electroremediation into consideration are, that it is an in situ environmental-friendly degradation method with relatively easy and undemanding equipment for installation. Electrokinetically-enhanced transport, which depends mainly on the electrical characteristic of aquifer mass, not on the hydraulic properties, poses a solution to the restriction of preferential pathways facing conventional advective-based hydraulic technologies. The technology is safer and more controllable than the current high-pressure or fracturing injection and thermal approaches (Cox et al., 2018). Increased demands on time and energy and relatively challenging manageability in subsurface during process are among the drawbacks of the technique (Vocciante et al., 2021).

Since electrochemical remediation is based on chemical reactions at, and in the vicinity of electrodes, contaminants will be degraded by electrogenerated species and changes in redox potentials (Hyldegaard & Ottosen, 2021).

3 Pilot and field studies

The literature contains plenty of laboratory-scale oriented studies and bench-scale experiments of electroremediation either in the water or soils, but field applications are scarce. It is financially and technically demanding to provide large scale applications in real conditions. The

field applications may be limited by some discrepancies. Even though laboratory experiments bring more accurate observations of processes and phenomena, the main degradation processes in a natural geological environment may be different from those provided in laboratory conditions. The field degradation via electroremediation differs from site to site and depends on the specific features of each site, contaminant properties and the extent. Laboratory investigations may provide a false indication of the applicability of electrokinetic remediation to a specific site. Therefore, it is necessary to identify site-specific factors that could limit the performance of remediation technology. In the following section, key factors influencing the efficiency of electroremediation based on field or pilot application studies will be summarized and compared. Furthermore, the subsequent part will try to bring useful information to other researchers in their in situ field application attempts.

3.1 Key features in optimization of field application

The parameters significantly influencing the removal efficiency discussed in literature are:

- value of pH, redox potential, temperature and conductivity,
- electrode material and electrode arrangement,
- additives (agents, solvents),
- current density, resp. gradient voltage,
- soil composition, moisture, salt content.

To simulate the behaviour of contaminants or delivery of agents in the subsurface, numerical models, summarized in Ghazanfari and Pamukcu (2014), Gomes et al. (2015), Wu et al. (2012), are suitable to use. Second option is to imitate their behaviour under laboratory conditions (most of the available literature). To verify the current knowledge before large scale field application, the best approach is to use both.

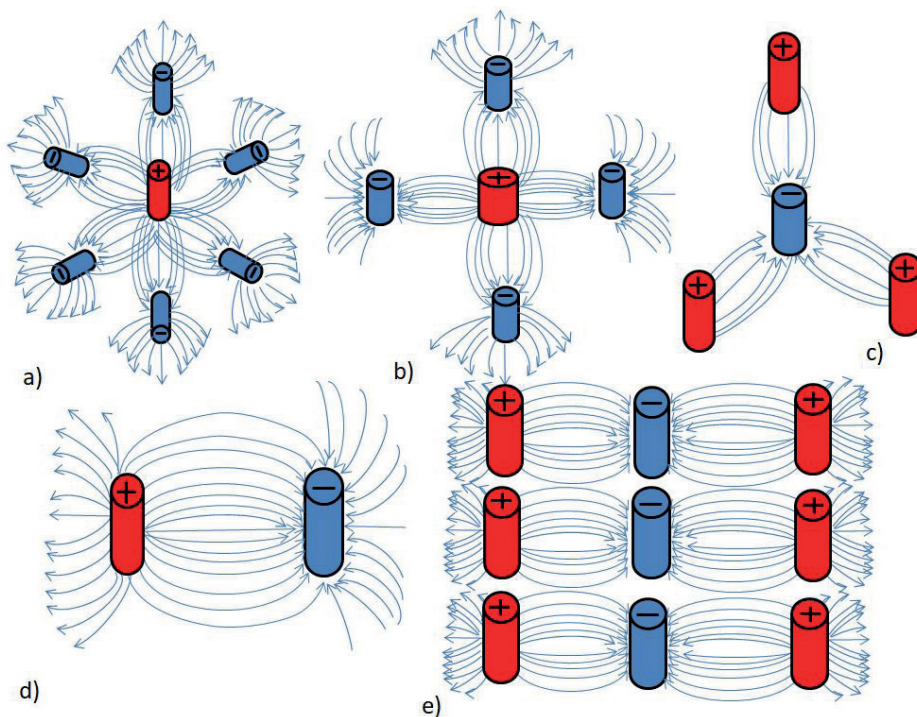


Fig. 3. Possible electrode arrangements: a) hexagonal; b) square; c) trigonal; d, e) linear (slightly modified after Alshwabkeh et al., 1999; Vocciante et al., 2016).

The development of electrokinetic soil remediation system models has raised during the last years. The complexity of the natural processes occurring in the soil matrix makes models predictions difficult. Hence, the existing models stay focused on contaminants behaviour predictions and simulations, not the whole geochemical systems containing the behaviour of natural soils and the porewaters (López-Vizcaino et al., 2017).

3.1.1 Design, operation and installation of electro-supported remediation

Material and configuration of electrodes in the soil or geological environment play a key role in successful remediation attempts. Based on the available final reports and field application studies, the electrodes' most used configuration and materials are given.

Design of electrode configuration

Configuration of electrode settings is a crucial part of the whole remediation process. One-dimensional (1D) (equal number of anodes and cathodes) electrode arrangement is routinely used in laboratory scale experiments to set a uniform electric field. On the other hand, in field application, it is suitable to operate with a two-dimensional (2D) electrode configuration (unequal number of anodes and cathodes). The critical factors for appropriate electrode configuration in large field applications depend on the extent of contamination, remediation costs, remediation proposal (stabilization of contamination, acceleration of the migration process, transport of ionic contamination or distribution of different kinds of agents and reagents, or direct degradation of contaminants in the vicinity of electrodes), and diverse soil properties (resistance, permeability, pH, porosity, buffer capacity, soil texture, conductivity). The electrode configuration may be distinguished into several patterns (see Fig. 3) (Alshawabkeh et al., 1999; Cang et al., 2021):

The most used electrode patterns include:

- a) the hexagonal pattern (conducted by Banerjee et al., 1991; Lageman & Godschalk, 2007),
- b) the square pattern (conducted by Černík et al., 2020),
- c) the circle pattern remediation (conducted by Czinnerová et al., 2020; Lageman, 2014),
- d) the row electrode sequence (conducted by Cox et al., 2018; Riis et al., 2012; U.S. EPA, 2000c, 2000a).

Banerjee et al. (1991) reported that the utilization of square-hexagonal array of cathodes with central anode is suitable, due to better enrichment of a more radially uniform potential field. Besides regular electrode sequencing,

other options of configuration of electrodes exist, e.g. electrokinetically induced barriers or fences (Lageman, 2014; Sale et al., 2005).

Authors Černík et al. (2020), Černíková et al. (2020), Czinnerová et al. (2020) employed various approaches in their investigations, either equal amounts of anodes and cathodes (Černíková et al., 2020) or exceed of cathodes (Czinnerová et al., 2020; Černík et al., 2020). Two of them (Černíková et al., 2020; Czinnerová et al., 2020) encompass the application of nanoparticles; therefore, they adjust electrode arrangement (more cathodes than anodes) to the fact that nano-zero iron particles prefer a reduced environment created predominantly by cathodes.

Linear arrangement showed decrease from 8800 $\mu\text{g.l}^{-1}$ of total chlorinated ethenes to 210 $\mu\text{g.l}^{-1}$ after the three-stage nZVI + DC remediation (Černíková et al., 2020), later cross-like arrangement proved 50 % efficiency (Černík et al., 2020), and square-like array of electrodes appears with 75 % effectivity (Czinnerová et al., 2020).

Shen et al. (2007) mentioned a new approach in electroremediation by approaching surrounding anodes to one fixed anode. Cathode's positions stay fixed. Authors stated that the nearer the anodes are, the faster the Cd removal is from the soils, due to raising H^+ concentration (and so lowering pH), and redox potentials. The low pH and high redox-potential help accelerate Cd removal through electromigration.

The investigation of the electrode arrangement influence on the electroremediation was demonstrated on soil (predominantly sandy soil) contaminated by Cu, As, and Pb in a pilot-scale field experiment near a zinc refinery plant in South Korea. However, the authors focused on distances between electrodes (respectively the density of the placement of electrodes), not on the specific shape of electrodes arrangement. The square pattern was employed during the whole treatment application. The higher density of electrodes, the higher temperatures were observed. They observed a significant relationship between temperature changes and applied current. The authors recommend monitoring groundwater flow to avoid complications (e.g. unnecessary consumption of electrical energy or transport of contaminants by water flow). Moreover, they stated that the transport of contaminants may not only be affected by electrokinetic phenomena (i.e. electromigration or electroosmosis), but it can also be influenced by the gravitational flow of groundwater flux, diffusion or evaporation of soil pore water as a result of rising temperature. In this research, the contaminants (metals) were accumulated in the bottom and top layers of the soil as a result of degradation (Kim et al., 2012).

Electrode placement

Hyldegaard and Ottosen (2021) stated two concepts of in situ electrochemical remediations (e.g. for chlorinated

ethenes). First concept includes “in-well treatment”, therefore the electrodes are placed in the same well which is a fully water-filled setting (e.g. setting in laboratory conditions) (Hyldegaard & Ottosen, 2021; Mao et al., 2011). In the second concept (“in-between well treatment”), the electrodes are installed separately in wells. The aim of the second concept is to create an electrochemical barrier in a porous matrix through which the contaminated plume will flow (Hyldegaard & Ottosen, 2021; Petersen et al., 2007).

Electrodes do not have to be inserted only vertically (applied in most field studies), but they can be placed also in a horizontal way (Lee et al., 2011) or, for example, e.g. in Lasagna treatment (Ho et al., 1999a, b; Roulier et al., 2000). However, also in the Lasagna method, electrodes can be installed in both ways vertically and horizontally. Gases (H_2 , O_2) generated during horizontally placed electrodes can cause problems with displacement of water, thereby reducing the contact between the electrodes, leading to the decrease of electrical conductivity. Therefore, the produced gases have to be properly vented (Lee et al., 2011).

One of the promising techniques represents the Provect-EBR® technology (Integrated Electrochemical-Biogeochemical Method for Remediation of Contaminated Groundwater) (Elgressy, 2018). The one-dimensionally stable anode is composed of mixed metal oxides to produce oxygen via electrolysis. Gradual electrode connections cause the formation of strong oxidants, such as H_2O_2 , $\bullet HO_2$, $\bullet O_2$, and $\bullet OH$ radicals. It is a field-proven system that efficiently connects ISCO, microbiological and geophysical mechanisms to treated contaminated aquifers by mineralizing chlorinated solvents, petroleum hydrocarbons and MTBE (methyl tert-butyl ether). Potentially, it would be useable to degrade perchlorate, 1,4-dioxane, pharmaceuticals or fluorinated compounds (Hyldegaard & Ottosen, 2021; Mandelbaum et al., 2019; Provectus Environmental Products, 2019) in the future. In 2019, this technique was used in Israel for degradation of chlorinated ethenes with an efficiency up to 99 % within 30 days. This technique operates in a large radius of the electric field, up to 2–4 m (Provectus Environmental Products, 2019).

The drop of groundwater level below the design of electrode construction can cause trouble with releasing electrolytes used in the electrode wells into the environment. To solve this problem, Gill et al. (2000) used a bentonite sealing membrane to prevent electrolyte emptying. However, as bentonite has a high sorption capacity, it absorbed a significant amount of degraded contaminant (chromium) during their pilot experiment; and therefore, it decreased the removal efficiency (Gill et al., 2000).

The application of electroremediation method in shallow zones, near to the ground surface or near to utilities (electrical wiring), can represent limitation of the techno-

logy, especially in case of electrokinetic-enhanced amendments delivery (Cox et al., 2018).

Spacing of electrodes

The number of electrodes and their spacing depends on the thickness (depth interval) of the contaminated area and the extent of the treatment area (Cox et al., 2018). Deployment of the electrodes closely relates to soil properties, e.g. porosity, conductivity, and resistance. The length among electrodes of both equal and opposite charges depends on site-specific conditions but is generally considered at a distance of 1.5 or 2.0 m (Lageman & Pool, 2009).

In conceptual layout by Reynolds et al. (2017), the electrodes were installed 3 m apart. In Černíková et al. (2020), two rows of three anodes and three cathodes were arranged perpendicular to each other at a 3 m apart distance. In Gill et al. (2000), the distance between electrodes of the same polarity was 2 m and 1 m among oppositely charged electrodes. Spacing of three anodes housed in a line and distributed 3 m apart with one cathode inserted 9 m from the anode in the middle was deployed in arsenic soil and groundwater remediation (U.S. EPA, 2000c). The larger space (5 m) was applied by Lageman et al. (2014) in Fukushima's Daiichi nuclear power plant. Cox et al. (2018) operated with 5.5 m spacing between electrode wells.

The geoelectrical survey conducts the measurement of electrical resistivities of the subsurface. These are needed to efficiently calculate the distance between electrodes and determine the amount energy for ions to migrate through the soil. The calculations are described in Lageman and Pool (2009).

Material of electrodes

Materials of electrodes should be considered with regard to the nature of contaminants. Research by Hyldegaard (2019) described the suitable electrode materials, their electrical properties, and overvoltage characterization in detail. Studies by Černík et al. (2020) and Torii (2006) also discussed the suitable electrode materials. Based on the review of the available literature, the most used materials of electrodes are ferrous or stainless steel electrodes followed by titanium coated mixed metal oxides.

In field studies by Černík et al. (2020), Černíková et al. (2020), and Czinnerová et al. (2020), several meters long steel rods were used as electrode material. Except cathodes in Černík et al. (2020), where Fe-Zn liners were used. The advantages of steel electrodes are affordability and accessibility. Additionally, steel electrodes form hydrated iron oxides during anodic oxidation, which can significantly assist in the chlorinated ethenes removal (Černíková et al., 2020; Mu et al., 2017). On the other hand, steel anodes

tend to corrode in an oxidizing environment leading to their disintegration and dysfunction. Therefore, they have to be replaced after certain time. Černíková et al. (2020) replaced anodes in 10 months interval, together three times during the pilot experiment. Moreover, the gradual dissolution of steel anodes contributes to the lowering of current flow what decrease the efficiency of remediation. In addition, it contributes also to the changes in Eh (redox potential) values, when increasing Eh value nearby the anode signalizes electrode passivation (Černíková et al., 2020). One of the disadvantages is, that stainless steel electrodes may release alloying materials (Cr, Mo, etc.) which might be dangerous for the environment (Černík et al., 2020).

In some cases, non-corrosive materials of electrodes are more preferred. Fallgren et al. (2018) used titanium electrodes (152 mm x 3 mm) coated with metal mixed oxides, due to their resistance to anodic corrosion. Due to aim of research (focus on changes in redox potential), the non-corrosive materials had to be used.

Likewise, Reynolds et al. (2017) used 1.5 m long titanium tube electrode coated with an MMO (mixed metal oxides electrodes) (with diameter of approx. 6 cm) to prevent passivation and corrosion of the electrodes. In electrokinetically induced degradation of contaminants (chlorinated ethenes – TCE), three titanium coated MMO electrodes were inserted into the redox barrier by Sale et al. (2005). Carbon steel cathodes and stainless steel anodes were used in the pilot scale experiment during remediation of arsenic in the soil and groundwater in the southern United States (U.S. EPA, 2000b).

3.1.2 Evaluation of physico-chemical parameters in field applications

At the beginning of the field application, physico-chemical parameters: pH, redox potential, dissolved oxygen content, and conductivity should be measured. Further, at sites contaminated by chlorinated hydrocarbons, concentrations of VOCs (volatile organic compounds), DHGs (dissolved hydrocarbon gases – methane, ethene and ethane), VFAs (volatile fatty acids), metals and anions (nitrate, sulfate, and chloride) should be monitored. Analysing of various carbon indicators, such as TOC (total organic carbon) and VFAs, allows the subsequent tracking of electron donor distribution, and should be monitored in soils as follows: Volatile Organic Compounds (VOCs), metals, microbial characterization and grain-size of soil mass (Cox et al., 2018).

Application of low-intensity DC causes changes in redox potential (oxidation-redox reaction). The in situ manipulation of redox potential improves the degradation and reduction of groundwater and sediment contaminants (e.g. TCE) (Fallgren et al., 2018).

The values of redox potential and pH of the groundwater reflect the effect of the electrochemical process in groundwater chemistry. In particular, the mobility and transport of inorganic substances depend on the redox potential and pH of the solution (Sale et al., 2005).

The relationship between pH and migration of heavy metals is well known and has been shown in Peng et al. (2013). Heavy metal distribution was tightly related to pH distribution, where heavy metal mobility was higher under acid conditions and their migration was retarded/reduced at the pH-jump zone (zone of the sharp interface of pH values created as a result of electrolytic decomposition of water).

According to the study presented by Fallgren et al. (2018), investigating the treatment of the contaminated aquifers with chlorinated aliphatic hydrocarbons, the electric field extends also outside the area between the electrodes; therefore, the redox potential changes are observable beyond the direct line between the electrodes. The external application of an electric field influenced redox potential in horizontal (> 7.9 m) and vertical directions (> 7.6 m). Based on this study, it was observed that the radius of electrical impact depends on the resistance of surrounding materials in the vicinity of electrodes. Furthermore, the authors stated that chemical manipulation of redox potentials is limited by properties of contaminated matrices, such as permeability, heterogeneity and groundwater flow velocity.

Electrochemical remediation is characterized by applying lower electrical potential < 12 V.m⁻¹ to the aquifer, compared to the electrokinetic remediation. It results in limited movement of contaminants, which on the other hand, enhance electrochemically induced redox reactions in the electric field. Certain soil compounds, such as soil particles and humic acids, can serve as “microelectrodes”. The microelectrodes principle was covered in the study of Rahner et al. (2002), where authors discussed a new approach to the remediation of the soil with organic contamination.

At the Hořice site, where electroremediation was applied for decontamination of aquifer by chlorinated ethenes, course of Eh and other physical-chemical parameters was monitored with 11 monitoring boreholes. In the cathodes area, the Eh values changed from the initial values of around +200 mV almost immediately after the electrical current was connected, and gradually decreased up to –400 mV. However, the increase in Eh was observed after electrode passivation (i.e. dissolving of sacrificial metal electrodes leads to decreasing performance of remedial process). On the contrary, there were no significant changes during the process in the anode area observed; the Eh values were kept around +200 mV. The pH values varied from 6 to 8 across the treatment area. Only in one borehole with cathode, the pH reached higher values, up to 12,

while conductivity also increased. Changes in pH were observed only after electrolytic decomposition of water (after exceeding the voltage decomposition). Groundwater flow with changed pH expanded through the aquifer due to dispersion, electromigration, and groundwater flow. Changes in Eh were not dependent on the groundwater flow (Černík et al., 2020).

Sale et al. (2005) observed the spread of oxidized conditions upstream and downstream from the barrier during operation of an electrokinetically induced redox barrier. The changes in both trends – redox potential and pH, led to the decrease of alkalinity and calcium concentration from upstream to downstream from the barrier. Several field applications of the pH control amendments – reagents to avoid significant pH-changes and simultaneous pH-jump, are mentioned below.

Reynolds et al. (2017) used buffer solutions (monobasic and dibasic potassium phosphate) in both (anode and cathode) electrode wells, and maintained the pH at neutral range (6 to 8). Potassium phosphate was introduced periodically into the anode well, when oxidant persulfate was electrokinetically delivered into geological environment. The pH control reagent – potassium carbonate (K_2CO_3), was used also in the field application performed by Cox et al. (2018). The buffer was added into the supply wells before the addition of the electric donor (potassium lactate) and also during the addition of lactate into subsurface environment. In Riis et al. (2012), water has been recirculated between cathodes and anodes for pH control in electrode wells. For further pH control, NaOH was added to the anode wells and lactic acid was added to the cathode wells. However, authors Černík et al. (2020), Černíková et al. (2020), and Czinnerová et al. (2020) did not use any buffer solution during their investigations, when they focused on integration of electrokinetic treatment coupled with nZVI. A special electrolyte system is used to improve conditions of physical parameters (pH, Eh) around the electrodes, and in order to collect the contaminants around the electrodes (Lageman & Pool, 2009). The amendment of buffer solution seems to be effective also by metal degradation process (Gill et al., 2000; U.S. EPA, 2000a) or to create stable conditions by delivering amendments, e.g. sodium persulfate into the soil (Reynolds et al., 2017).

3.1.3 Applied current density

The electrical current and voltage gradient established across a direct-current electric field provide the driving force for the transport of remediation amendments (incl. electron donors, chemical oxidants, and even bacteria) through the subsurface. Electrokinetic phenomena can achieve relatively uniform transport in low-permeability materials (Cox et al., 2018).

Depending on the contaminated site location, the technology should be placed with respect to the utilities that are electric interference sensitive or corrosion endangered. Some protecting measures (cathode grounding) or consultations with facility power or electrical suppliers are sometimes needed (Cox et al., 2018). The current density was calculated from the total current using the bulk area of the electrodes. Subsequently, the result DC was normalized to the wetted area of electrobarrier. The wetted surface of the electrolytic barrier (electrodes) was determined from the depth of groundwater measurements (Sale et al., 2005).

Observed variabilities in DC values may result from electrical conductivity variability of the groundwater, which is affected by the resistance to current flow inside the electric field (between electrodes) (Sale et al., 2005). Current density can be influenced by anodic passivation (Černíková et al., 2020), speed of ground water flow, temperature (Kim et al., 2012), and other specific properties of the treated environment.

As Grande and Gent (2002) stated, during electrochemical remediation of chlorinated hydrocarbons, current density should be lowered due to chlorine gas production (Cl_2) at anodes, which can subsequently form chloroform with organic carbon. Chloroform has to be vented out by air sparging (Niroumand et al., 2012).

Not just DC can be applied to remediate contaminated sites by electroremediation, but also the altering current (AC) can create suitable degradation conditions. When applying AC power to electrode configuration, the soil heats up, and the rising temperature thermally activates electrokinetically implemented amendments (e.g. persulfate's free radical $\bullet SO_4^-$) distributed by electromigration process (Reynolds et al., 2017).

Most of the available studies used lower voltages. Cox et al. (2018) used voltage < 30 V during electrokinetically-enhanced amendment delivery for in situ bioremediation via enhanced reductive dechlorination of a tetrachloroethene source area in clay. Černík et al. (2020) and Czinnerová et al. (2020) operated with 24 V current flow. Černíková et al. (2020) worked also with 24 V, when by applying 24 V to electrodes (at the resistance of the geological environment 0.4–1.2 Ω), created DC reached from 7 A to 15 A. Except for the research by Kim et al. (2012) and research by U.S. EPA (2000b), where they used 100 V, and 440 V respectively, it can be summarized that low voltage is most commonly applied.

3.1.4 Influence of native sulfate, iron, carbonates and chloride

Carbonates

The concentration of main cations (e.g. calcium, iron, magnesium) in groundwater could significantly influence the differences in costs of the construction system (Cox et

al., 2018). The buffering system of carbonates influences the evaluation and spatial distribution of pH in the environment. The effect of buffering by carbonates hinders the spread of so-called pH-jump (López-Vizcaino et al., 2017).

Since the presence of carbonates in the soil systems increases the buffering capacity, heavy metals are present in precipitated hydroxide or carbonate forms, which prevent the solubility and the releasement of heavy metals from soil into the pore flux and, therefore, decrease the efficiency of the treatment method (Ouhadi et al., 2010). However, the high content of carbonates does not impact the electroosmosis phenomena. Electrolysis of water occurs at electrodes. The production of OH⁻ ions at cathodes causes calcium precipitations, which clog the soil pores and prevent further transport of dissolved heavy metals ions (Ouhadi et al., 2010).

The presence of carbonate geology and aqueous phase liquid affected the performance of the Electrically Induced Redox Barrier. The high pH values at the cathode favour the precipitation of carbonate minerals (CaCO₃). The covering of the cathode surface available for contaminant degradation reactions limited the performance of the process. The current density and geochemical quality of water were used as indicators for scale formation, primarily due to the direct correlation between electrode areas and scale formation. Implementing a three-electrode configuration of the electrolytic barrier and subsequent regular polarity reversals hindered precipitate build-up at the cathodes. Polarity reversals are carried out remotely using a wireless connection to on-site data logging instrumentation. The polarity reversals were executed weekly every 12 hours. The process should be easily automated during a large full-scale operation (Sale et al., 2005).

Chloride, iron and sulfates

High levels of chloride and/or iron require particular engineering control measures (e.g., corrosion protection) or more operational maintenance efforts for fouling controls. Iron fouling is also a common challenge to other in situ remediation technologies (Cox et al., 2018).

Particular attention should be given to iron contents in the treated zone due to the possible concentration of iron ions around the cathode with subsequent fouling of the cathode surface (Cox et al., 2018). On the other hand, the presence of natural iron in the treated area can be utilized to reduce, e.g. chlorinated ethenes. Stainless steel anodes can create reduction conditions (Fe²⁺ stability) by anodic dissolution and also gradually dissolve iron from the geological matrix. Thereby, subsidizing environment with iron ions, which will react with the target contaminants (Černíková et al., 2020).

The mineral phases (siderite and ferrous hydroxide) are partially soluble at lower or normal pH values. Therefore, these mineral phases can re-introduce Fe²⁺ ions into the treated geological environment, thereby facilitating the reductive dechlorination of chlorinated hydrocarbons, primarily ethenes. Furthermore, the iron itself cannot be affected by cathodic reductive processes (Černíková et al., 2020).

In electrokinetically induced redox barrier field treatment, chloroform was detected as a result of DC application. This observation was not detected in the prior laboratory experiment. The presence of chloroform is ascribed to chloride oxidation to chlorine with subsequent reaction of carbon compounds with chlorine. The authors attributed this to higher content of oxygen in field treatment than in the laboratory study, and chlorine reaction with carbon compounds containing a methyl-keton functional group (Sale et al., 2005).

The observation that electrochemical remediation was the source of chloroform was confirmed also in the field electrokinetic extraction of metals at the contaminated site at Naval Air Weapons Station (NAWS) Point Mugu, California. The electrochemical transformation of naturally occurring chlorides into chlorine contributed to the further reaction of chlorine with organic material in the shallow soil layer. To avoid trihalomethanes production during treatment, the electrode wells were periodically pumped down, and air sparged the free chlorine generated in the anode wells. However, the authors do not confirm the high efficiency of the electrokinetic extraction of these metals. This research has just proven the mobility and transport of the contaminants through the electric field towards the cathode by application of DC (U.S. EPA, 2000c).

Very high concentrations of sulfate or nitrate may challenge the supply of electron donors for promoting and sustaining reductive dechlorination. This limitation is not specific to electrokinetic amendment delivery, instead, it is a limitation for anaerobic in situ bioremediation (Cox et al., 2018).

4 Laboratory experiment

The following section contributes with our investigation results of the DC application (alone) in degradation of target contaminants – chlorinated aliphatic hydrocarbons (CAH). The degradation was conducted in laboratory condition, in the sample of native groundwater, taken from the environmental burden in Zlaté Moravce (Slovakia). Groundwater in the area of the environmental burden is massively contaminated with chlorinated aliphatic hydrocarbons by industrial activities (e.g. manufacturing of fridges) conducted in the area in the past. Besides chlorinated hydrocarbons, contamination of groundwater with petroleum hydrocarbons was identified (Auxt et al., 2019).

4.1 Materials and methods

Samples of native groundwater from environmental burden were taken from borehole applying the Slovak Technical Norm STN EN ISO 5667 (2018). The laboratory analyses were conducted in the accredited laboratory ALS, s.r.o., Prague, Czech Republic. Concentration of volatile organic compounds in water samples was analysed by gas chromatography with FID and MS detection. Concentrations of the dissolved chlorides were determined by liquid chromatography. The concentration of chlorinated hydrocarbons (sum of 5 selected ethenes) in the sample of native groundwater, taken from the environmental burden before experiment, was $5\,900\ \mu\text{g}\cdot\text{l}^{-1}$.

The composition of the laboratory set-up designed for the electroremediation of chlorinated hydrocarbons consisted of two connected compartments, closed on the top with a lid (see Fig. 4). This set-up was designed for the observation of anodic and cathodic reactions.

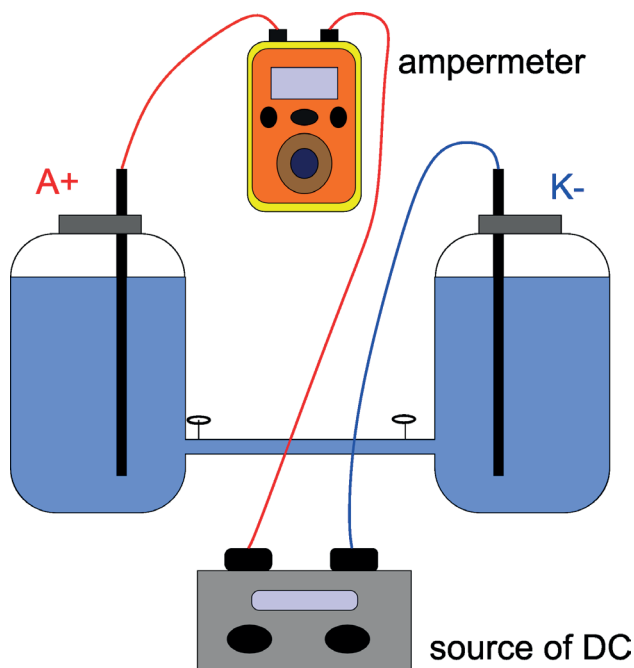


Fig. 4. Design of laboratory set up.

The length of the experiment was three weeks (21 days). During the experiment, gradual increase of DC (20 V, 40 V and 60 V) was applied, during which degradation of chlorinated hydrocarbons and changes in physical-chemical properties – values of pH, redox potential (Eh), conductivity (EC), and concentrations of iron (Fe^{2+} , Fe^{3+}) and chloride (Cl^-) were evaluated. Samples of groundwater from the compartments were collected at regular intervals – every second day for the first week, and two times per week in the second and third week. Both electrodes

(anode and cathode) were steel-alloy rods, containing a nonspecified amount of iron and other alloys.

4.2 Results and discussion

The reason for selecting the iron-containing electrodes was their affordability, specific surface, and, based on the available literature (Czinnerova et al., 2020; Černík et al., 2020, Pavelková et al., 2021), their proved efficiency in the degradation of chlorinated ethenes.

During the laboratory experiment, changes in groundwater properties were observed. Reductive conditions were recorded in the cathodic compartment (negative values of redox potential up to $-121.25\ \text{mV}$ from initial $188.25\ \text{mV}$) with pH values increased up to 9.12 (see Fig. 5a). On the other hand, in anodic compartment oxidizing conditions should be reached according to the equations of water electrolysis (see above eq. 1). However, due to the corrosion of reactive anodic material, reductive conditions occurred also in the anodic compartment, as a result of dissolved ferrous ions (Fig. 5b).

Pavelková et al. (2021) also reported a slight decrease in Eh and a significant increase in pH in the cathode compartment. Further, they state that after about 100 hours of experiment, iron reached the stability limit of $\text{Fe}(\text{OH})_3$, where $\text{Fe}(\text{OH})_3$ dissolves under strongly alkaline conditions (see below eq. 4).

The values of redox potential in our anodic compartment decreased from initial values of $188.25\ \text{mV}$ to $-105.6\ \text{mV}$. The values of pH in anodic compartment slightly decreased from initial pH 6.8 to pH 6.53, but no significant changes in pH were observed.

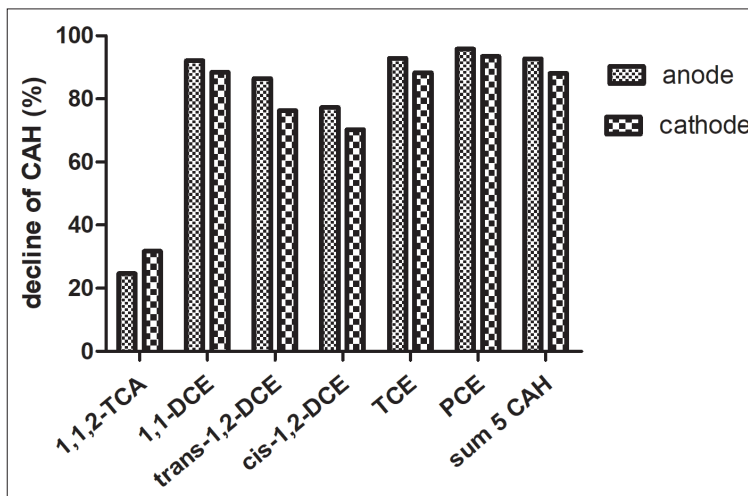
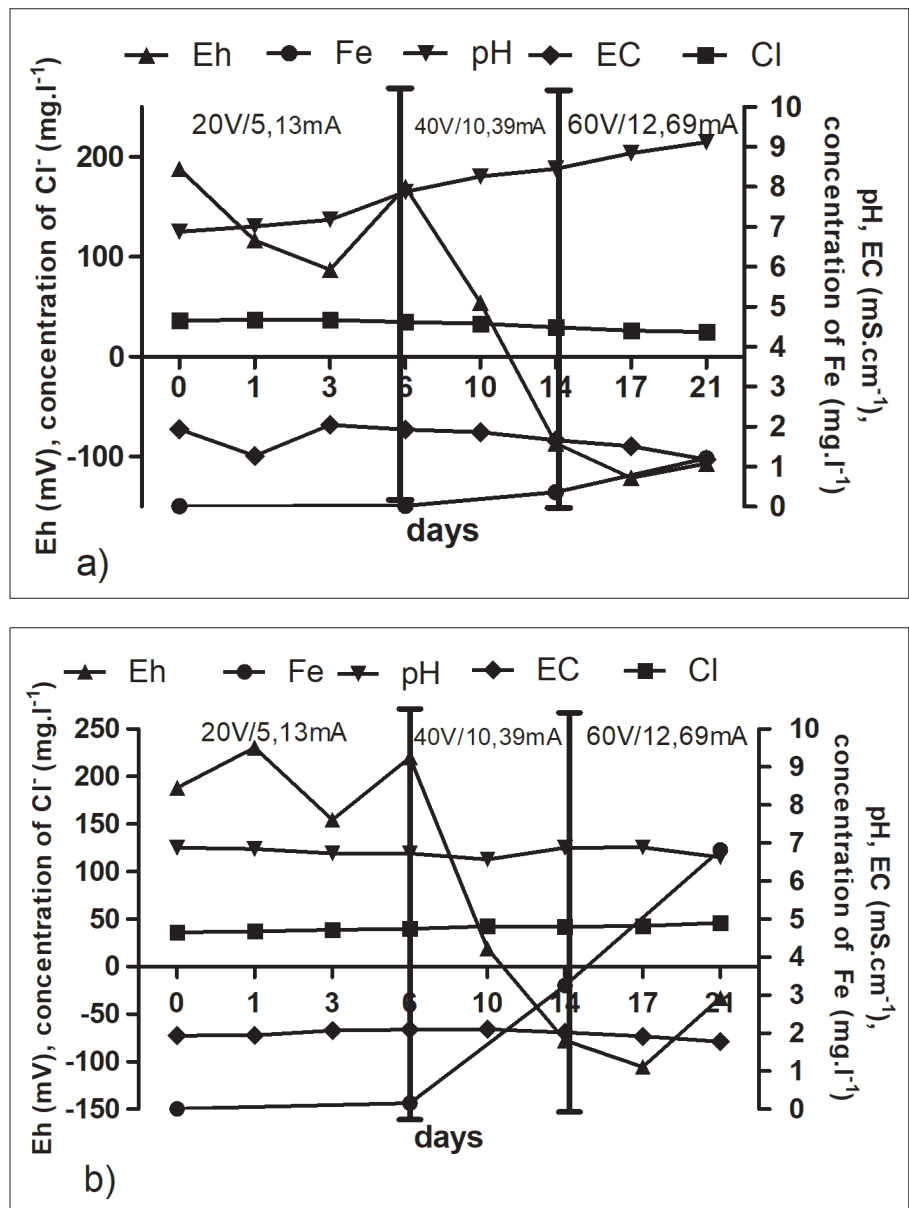
In the case of our laboratory experiment in the anode compartment, there were no significant changes in pH, as reported by Pavelková et al. (2021), where pH had a declining trend. The reason may be a slightly different electrode material, as steel-alloy rods were used in our experiment and Pavelková et al. (2021) used stainless steel. Another explanation for the slightly different pH development may be the fact that in our case, an ion membrane was not used to prevent the transfer of ions between the reactors, which was used by Pavelková et al. (2021). The cathodic development of pH and Eh is comparable to this study.

Concentrations of dissolved ferric ions Fe^{3+} ($6.82\ \text{mg}\cdot\text{l}^{-1}$) were recorded mainly in anodic compartment, where the water was coloured into the ochre due to electrode dissolution. In comparison, in the cathodic compartment mildly milk colour of water with a white film (coating) of precipitated carbonates on the surface of the cathode occurred. This precipitated crust occurred as a response to the mineralization of native groundwater samples with increased Ca-Mg HCO_3^- content.

Fig. 5. Diagram of the development of physical-chemical properties during the laboratory experiment in: a) cathode compartment (left), b) anode compartment (right).

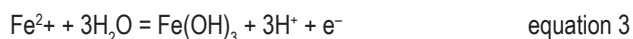
After three weeks of the laboratory experiment, higher efficiency of chlorinated ethenes degradation was achieved in anodic compartment than in the cathodic one. The degradation efficiency reached the average 92.7 % in anodic compartment and 88.12 % in cathodic compartment (total degradation efficiency can be seen in Fig. 6).

The results obtained indicate that the anodic reactions were more efficient in degradation of chlorinated aliphatic hydrocarbons. This is primarily due to acidic dissolution of anodic electrodes, which leads to the release of Fe^{2+} ions into the aqueous environment and the creation of reducing conditions (Mao et al., 2011; Pavelková et al., 2021), as Fe^{2+} ions are an important reductant involved in the reductive dechlorination of chlorinated hydrocarbons. Oxidation of Fe^{2+} to Fe^{3+} releases electrons that reduce chlorinated hydrocarbons.

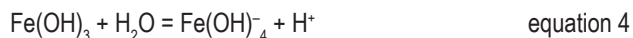


Increased Fe^{3+} concentrations analysed in anodic compartment indicate that the oxidation of Fe^{2+} ions into Fe^{3+} occurred quickly. During the oxidation of Fe^{2+} in an aqueous solution to soluble or precipitated forms of $Fe(OH)_3$, protons were formed, which are also involved in the degradation of chlorinated aliphatic hydrocarbons according to reaction eq. 3 (Pavelková et al., 2021):

Fig. 6. Total degradation efficiency of selected chlorinated aliphatic hydrocarbons (CAH) during electroremediation in the laboratory experiment.



The cathodic dechlorination of chlorinated hydrocarbons produces $\text{Fe}(\text{OH})_3$ compounds, which dissolve under strong alkaline conditions to form $\text{Fe}(\text{OH})_4^-$ compounds, releasing H^+ , which participates in the reduction of chlorinated aliphatic hydrocarbons according to reaction eq. 4 (Pavelková et al., 2021):



Final concentration of chlorinated hydrocarbons reached $432 \mu\text{g.l}^{-1}$ in anodic compartment and $701 \mu\text{g.l}^{-1}$ in cathodic compartment from initial $5\,900 \mu\text{g.l}^{-1}$. The higher anodic degradation can also be confirmed by an increased concentration of chloride ions from the dechlorination process in that compartment.

This laboratory experiment confirmed the efficiency of chlorinated hydrocarbons degradation in a native sample of contaminated groundwater, while a higher efficiency was recorded in the case of an anode (anodic reactions). The possibility and theoretical effectiveness of using chlorinated hydrocarbons electrodegradation directly at the contaminated site were confirmed. The results obtained in a laboratory experiment can be used to optimize chlorinated hydrocarbons degradation in situ on a contaminated site.

5 Conclusion

Electroremediation was proved as an effective treatment method for contaminated sites with low hydraulic conductivity. The application of DC highly affects the geochemical properties of the treated areas and subsequently creates specific pH and redox potential conditions in the environment. Laboratory scale studies, bench scale or ex situ pilot studies may seem to prove a high efficiency of degradation, however direct in situ application in real geological environment condition may be significantly different. In the case of effective use of electrodegradation, it is important to optimize the conditions and technical specifications of the electrodegradation intervention.

In conclusion, the high efficiency of this remediation method in chlorinated hydrocarbons degradation has been confirmed under laboratory condition. The highest degradation efficiency (92.7 %) was achieved by anodic reactions. In contrast, cathodic degradation achieved a lower efficiency of 88.12 %. Furthermore, high rate of chlorinated hydrocarbons degradation was observed already at a voltage of 20 V and subsequently highest degradation was observed at 40 V. The maximum applied current was 14.3 mA. During the experiment, anodic dissolution of the electrodes and the formation of white

coatings (carbonates) on the cathode were observed. The appearance of these carbonate coatings was probably also a consequence of lower chlorinated hydrocarbons degradation efficiency in the cathode compartment.

Based on literature review and small-scale laboratory experiment, the pilot-scale in situ degradation of chlorinated hydrocarbons in the groundwater of the contaminated site Zlaté Moravce was optimized. The results of the pilot scale experiment show relatively high removal efficiency (average ca. 88 %). At present, this pilot scale experiment is no longer taking place at the Zlaté Moravce site due to the permit's expiry to carry out this experiment.

Most reviews and scientific papers investigating the electrokinetic or electrochemical remediations are usually based on both laboratory and field or pilot applications. This short summary provides published field studies, final reports and terrain applications with the major technical optimizations for the in situ degradation of chlorinated hydrocarbons. As can be seen, there is only limited number of available field application studies of electroremediation treatment of chlorinated hydrocarbons. There still exist uncertainties in this developing approach.

Acknowledgement

Authors express their thanks to the Centre of Environmental Services, Ltd. (Bratislava) for financing this laboratory research. This study was also supported by the Operation Program of Integrated Infrastructure for the project, UpScale of Comenius University Capacities and Competence in Research, Development and Innovation ŽoNFP: NFP313020BUZ3, co-financed by the European Regional Development Fund. Authors express their thanks to Katarína Ďurčanská (ZVVS) and Jozef Kordík (SGUDS) for valuable notices and suggestions which improved the primary manuscript.

References

- ACAR Y. B. & ALSHAWABKEH, A. N., 1993: Principles of Electrokinetic Remediation. *Environ. Sci. Techn.*, 27, 13, 2638–2647.
- ADAMSON, L. G., CHILINGAR, G. V., BEESON, C. M. & ARMSTRONG, R. A., 1966: Electrokinetic dewatering, consolidation and stabilization of soils. *Eng. Geol.*, 1, 4.
- ALSHAWABKEH, A. N. & ACAR, Y. B., 1992: Removal of Contaminants from Soils by Electrokinetics: A Theoretical Treatise. *J. Environ. Sci. Health A. Part A: Environmental Science and Engineering and Toxicology*, 27, 7, 1835–1861.
- ALSHAWABKEH, A. N., YEUNG, A. T. & BRICKA, M. R., 1999: Practical Aspects of In situ Electrokinetic Extraction. *J. Environ. Eng.*, 125, 1, 27–35.
- APPELO, C. A. J. & POSTMA, D., 2010: Flow and transport. In: Appelo, C. A. J. & Postma, D. (Eds.): *Geochemistry, Groundwater and Pollution*. 2nd ed. *CRC Press LLC*, 63–118.

- ASAVADORNDEJA, P. & GLAWE, U., 2005: Electrokinetic strengthening of soft clay using the anode depolarization method. *Bull. Eng. Geol. Environ.*, 64, 3, 237–245.
- AUXT, A., INGÁR, K., POLČAN, I., OROSZLÁNY, J., ŠUCHOVÁ, M., JENČKO, P., MÁŠA, B., BAUER, K., FILO, J., TÓTH, R., ŠEVČÍKOVÁ, L., SCHERER, S., KOVÁCS, T., ŠPIROVÁ, V. & KRAKOVSKÝ, D., 2019: Čiastková záverečná správa s predšanačnou aktualizovanou analýzou rizika. Sanácia environmentálnej záťaže ZM (013)/Zlaté Moravce – bývalý areál Calexu (SK/EZ/ZM/1115). Sanácia vybraných environmentálnych záťaží Slovenskej republiky (1) – Časť 7: Sanácia environmentálnych záťaží na lokalitách Brezno a Zlaté Moravce. Final report of geological works. Manuscript. Bratislava, Ministry Environ. Slovak Republic (in Slovak), 1–178.
- BANERJEE, S., HORNG, J. J. & FERGUSON, J. F., 1991: Field Experience with Electrokinetics at a Superfund Site Superfund Site. *Transport. Res. Record*, 1312, 167–174.
- BURNOTTE, F., LEFEBVRE, G. & GRONDIN, G., 2004: A case record of electroosmotic consolidation of soft clay with improved soil-electrode contact. *Canad. geotechn. J.*, 41, 6, 1038–1053.
- CAMESELLE, C. & REDDY, K. R., 2012: Development and enhancement of electro-osmotic flow for the removal of contaminants from soils. *Electrochim. Acta*, 86, 10–22.
- CANG, L., HUANG, Q., XU, H. & ZHOU, M., 2021: The Integration of Electrokinetics and In Situ Chemical Oxidation Processes for the Remediation of Organically Polluted Soils. In: Electrokinetic Remediation for Environmental Security and Sustainability. First ed. *John Wiley*, 479–503.
- CASAGRANDE, D. R., CASAGRANDE, L. & CASTRO, G., 1986: Improvement of sensitive silty clay by electroosmosis: Discussion. *Canad. geotech. J.*, 23, 1.
- CASAGRANDE, L., 1949: Electro-osmosis in soils. *Geotechnique*, 1, 3.
- ČERNÍK, M., HRABAL, J. & NOSEK, J., 2020: Combination of Electrokinetics and nZVI Remediation. In: Filip, J., Cajthaml, T., Najmanová, P., Černík, M. & Zbořil, R. (Eds.): Advanced Nano-Bio Technologies for Water and Soil Treatment. *Springer Nature Switzerland*, 65–85.
- ČERNÍKOVÁ, M., NOSEK, J. & ČERNÍK, M., 2020: Combination of nZVI and DC for the in situ remediation of chlorinated ethenes: An environmental and economic case study. *Chemosphere*, 245.
- COX, E., WANG, J., REYNOLDS, D., GENT, D. & SINGLETARY, M., 2018: Electrokinetic-Enhanced Amendment Delivery for Remediation of Low Permeability and Heterogeneous Materials. *ESTCP. U.S. Depart of Defense*, 1–72.
- CZINNEROVÁ, M., VOLOČŠUKOVÁ, O., MARKOVÁ, K., ŠEVČŮ, A., ČERNÍK, M. & NOSEK, J., 2020: Combining nanoscale zero-valent iron with electrokinetic treatment for remediation of chlorinated ethenes and promoting biodegradation: A long-term field study. *Water Res.*, 175.
- ELGREGSY, E., 2018: Breakdown of fuel components and solvents in groundwater and contaminated soil (Patent No. US Patent 9,975,156 B2).
- ESRIG, M. I., 1968: Pore Pressures, Consolidation, and Electrokinetics. *J. Soil Mech. Found. Div., ASCE*, 94, 4, 899–921.
- FALLEGREN, P. H., EISENBEIS, J. J. & JIN, S., 2018: In situ electrochemical manipulation of oxidation-reduction potential in saturated subsurface matrices. *J. Environ. Sci. Health A., Toxic/Hazard.*, 53, 6, 517–523.
- FAN, G., CANG, L., FANG, G., QIN, W., GE, L. & ZHOU, D., 2014: Electrokinetic delivery of persulfate to remediate PCBs polluted soils: Effect of injection spot. *Chemosphere*, 117, 1.
- FAN, G., WANG, Y., FANG, G., ZHU, X. & ZHOU, D., 2016: Review of chemical and electrokinetic remediation of PCBs contaminated soils and sediments. *Royal Soc. Chem., Environ. Sci.: Processes Impacts*, 18, 9, 1140–1156.
- FOUNTAIN, J. C., STARR, R. C., MIDDLETON, T., BEIKIRCH, M., TAYLOR, C. & HODGE, D., 1996: A Controlled Field Test of Surfactant-Enhanced Aquifer Remediation. *Ground Water*, 34, 5, 910–916.
- GHAZANFARI, E. & PAMUKCU, S., 2014: Mathematical Modeling of Electrokinetic Transport and Enhanced Oil Recovery in Porous Geo-Media. In: Electrokinetics for Petroleum and Environmental Engineers. *John Wiley*, 177–236.
- GILL, M., DRUCKER, A., TRUITT, R. & BLOOM, M., 2000: Removal of Heavy Metals from Contaminated Soils at a Former Naval Air Station: A Demonstration of Electrokinetic Remediation. *Naval Facilities Engineering Service Center, California, TechData Sheet, TDS-2084-ENV*.
- GILL, R. T., HARBOTTLE, M. J., SMITH, J. W. N. & THORNTON, S. F., 2014: Electrokinetic-enhanced bioremediation of organic contaminants: A review of processes and environmental applications. *Chemosphere*, 107.
- GOMES, H. I., RODRÍGUEZ-MAROTO, J. M., RIBEIRO, A. B., PAMUKCU, S. & Dias-FERREIRA, C., 2015: Numerical prediction of diffusion and electric field-induced iron nanoparticle transport. *Electrochim. Acta*, 181.
- GRANDE, S. & GENT, D., 2002: Electrokinetic remediation of contaminated sediments. In: Hinchee, R. E., Porta, A. & Pelli, M. (Eds.): Remediation and Beneficial Reuse of Contaminated Sediments. Conference Proceedings. *Battelle Press*, 205–212.
- GRAY, D. H. & MITCHELL, J. K., 1967: Fundamental Aspects of Electro-Osmosis in Soils. *J. Soil Mech. Found. Div.*, 93, 6.
- HANSEN, B. H., NEDERGAARD, L. W., OTTOSEN, L. M., RIIS, C. & BROHOLM, M. M., 2015: Experimental design for assessment of electrokinetically enhanced delivery of lactate and bacteria in 1,2-cis-dichloroethylene contaminated limestone. *Environ. Technol. Innov.*, 4, 73–81.
- HO, S. V., ATHMER, CH., SHERIDAN, P. W., HUGHES, B. M., ORTH, R., MCKENZIE, D., BRODSKY, P. H., SHAPIRO, A., THORNTON, R., SALVO, J., SCHULTZ, D., LANDIS, R., GRIFFITH, R. & SHOEMAKER, S., 1999a: The lasagna technology for in situ soil remediation. 1. Small field test. *Environ. Sci. Technol.*, 33, 7.
- HO, S., ATHMER, C., SHERIDAN, P. W., HUGHES, B. M., ORTH, R., MCKENZIE, D., BRODSKY, P. H., SHAPIRO, A. M., SIVAVEC, T. M., SALVO, J., SCHULTZ, D., LANDIS, R., GRIFFITH, R. & SHOEMAKER, S., 1999b: The lasagna technology for in situ soil remediation. 2. Large field test. *Environ. Sci. Technol.*, 33, 7.
- HYLDEGAARD, B. H., 2019: Electrochemical zone for degradation of chlorinated ethenes in aquifers. *Technical University of Denmark*.
- HYLDEGAARD, B. H., & OTTOSEN, L. M., 2021: Electrokinetic and Electrochemical Removal of Chlorinated Ethenes: Application in Low- and High-Permeability Saturated Soils. In: Electrokinetic Remediation for Environmental Security and Sustainability. *Wiley*, 503–540.
- JANENI, J. & ADASSOORIYA, N. M., 2021: Clays and Clay Polymer Composites for Electrokinetic Remediation of Soil. In:

- Electrokinetic Remediation for Environmental Security and Sustainability (eds. Ribeiro, A. B. & Vara Prasad, M. N.), 1–16.
- JIN, S. & FALLEGREN, P. H., 2010: Electrically induced reduction of trichloroethene in clay. *J. Hazard. Mater.*, 173, 1–3, 200–204.
- KIM, W. S., KIM, S. O. & KIM, K. W., 2005: Enhanced electrokinetic extraction of heavy metals from soils assisted by ion exchange membranes. *J. Hazard. Mater.*, 118, 1–3.
- KIM, W. S., PARK, G. Y., KIM, D. H., JUNG, H. B., KO, S. H. & BAEK, K., 2012: In situ field scale electrokinetic remediation of multi-metals contaminated paddy soil: Influence of electrode configuration. *Electrochim. Acta*, 86, 89–95.
- KOROLEV, V. A. & NESTEROV, D. S., 2018: Regulation of clay particles charge for design of protective electrokinetic barriers. *J. Hazard. Mater.*, 358, 165–170.
- LAGEMAN, R., 1993: Electroreclamation. Applications in the Netherlands. *Environ. Sci. Technol.*, 27, 13, 2648–2650.
- LAGEMAN, R., 2014: Preliminary Assessment Of The Application Of An Electrokinetic Ring Fence For The Removal Of Radionuclides From Groundwater At Fukushima Daiichi Nuclear Power Plant. *Lambda Consult*, 1–12.
- LAGEMAN, R. & GODSCHALK, M. S., 2007: Electro-bioreclamation. *Electrochim. Acta*, 52, 10, 3449–3453.
- LAGEMAN, R. & POOL, W., 2009: Experiences with field applications of electrokinetic remediation. In: Reddy, K. R. & Cameselle, C. (Eds.): *Electrochemical Remediation Technologies for Polluted Soils, Sediments and Groundwater*. John Wiley.
- LEE, M. KUO., SAUNDERS, J. A. & WOLF, L. W., 2000: Effects of Geologic Heterogeneities on Pump-and-Treat and In Situ Bioremediation: A Stochastic Analysis. *Environ. Eng. Sci.*, 17, 3, 183–189.
- LEE, Y. J., CHOI, J. H., LEE, H. G., HA, T. H. & BAE, J. H., 2011: Pilot-scale study on in situ electrokinetic removal of nitrate from greenhouse soil. *Sep. Purif. Technol.*, 79, 2, 254–263.
- LIU, B., LI, G., MUMFORD, K. G., KUEPER, B. H. & ZHANG, F., 2020: Low permeability zone remediation of trichloroethene via coupling electrokinetic migration with in situ electrochemical hydrodechlorination. *Chemosphere*, 250.
- LÓPEZ-VIZCAÍNO, R., YUSTRES, A., LEÓN, M. J., SAEZ, C., CAÑIZARES, P., RODRIGO, M. A. & NAVARRO, V., 2017: Multiphysics Implementation of Electrokinetic Remediation Models for Natural Soils and Porewaters. *Electrochim. Acta*, 225, 93–104.
- MANDELBAUM, R., MANDELBAUM, G. & ELGREGSY, E., 2019: Integrated biogeochemical / electrochemical method for remediation of contaminated groundwater. 5th International Symposium on Bioremediation and Sustainable Technologies, (Battelle).
- MAO, X., CIBLAK, A., AMIRI, M. & ALSHAWABKEH, A. N., 2011: Redox control for electrochemical dechlorination of trichloroethylene in bicarbonate aqueous media. *Environ. Sci. Technol.*, 45, 15.
- MAO, X., WANG, J., CIBLAK, A., COX, E. E., RIIS, C., TERKELSEN, M., GENT, D. B. & ALSHAWABKEH, A. N., 2012: Electrokinetic-enhanced bioaugmentation for remediation of chlorinated solvents contaminated clay. *J. Hazard. Mater.*, 213–214, 311–317.
- MOUSSAVI, G., KHOSRAVI, R. & FARZADKIA, M., 2011: Removal of petroleum hydrocarbons from contaminated groundwater using an electrocoagulation process: Batch and continuous experiments. *Desalination*, 278, 1–3.
- MU, Y., JIA, F., AI, Z. & ZHANG, L., 2017: Iron oxide shell mediated environmental remediation properties of nano zero-valent iron. *Environ. Sci. Nano*, 4, 1, 27–45.
- NAZAROFF, W. W. & ALVAREZ-COHEN, L., 2000: Transport phenomena. *Environ. Eng. Sci.*, 159–206.
- NIROUMAND, H., NAZIR, R. & KASSIM, K. A., 2012: The Performance of Electrochemical Remediation Technologies in Soil Mechanics. *J. Electrochem. Sci.*, 7.
- OTTOSEN, L. M., LARSEN, T. H., JENSEN, P. E., KIRKELUND, G. M., KERNN-JESPERSEN, H., TUXEN, N. & HYLDEGAARD, B. H., 2019: Electrokinetics applied in remediation of subsurface soil contaminated with chlorinated ethenes – A review. *Chemosphere*, 235.
- OUHADI, V. R., YONG, R. N., SHARIATMADARI, N., SAEIDIJAM, S., GOODARZI, A. R. & SAFARI-ZANJANI, M., 2010: Impact of carbonate on the efficiency of heavy metal removal from kaolinite soil by the electrokinetic soil remediation method. *J. Hazard. Mater.*, 173, 1–3, 87–94.
- PAMUKCU, S., GHAZANFARI, E. & WITTLE, K., 2014: Reduction of Contaminants in Soil and Water by Direct Electric Current. In: *Electrokinetics for Petroleum and Environmental Engineers*. John Wiley, 33–101.
- PARKER, B. L., CHAPMAN, S. W. & GUILBEAULT, M. A., 2008: Plume persistence caused by back diffusion from thin clay layers in a sand aquifer following TCE source-zone hydraulic isolation. *J. Contam. Hydrol.*, 102, 1–2.
- PAVELKOVÁ, A., CENCEROVÁ, V., ZEMAN, J., ANTOS, V. & NOSEK, J., 2021: Reduction of chlorinated hydrocarbons using nano zero-valent iron supported with an electric field. Characterization of electrochemical processes and thermodynamic stability. *Chemosphere*, 265.
- PENG, C., ALMERIA, J. O. & GU, Q., 2013: Effect of electrode configuration on pH distribution and heavy metal ions migration during soil electrokinetic remediation. *Environ. Earth Sci.*, 69, 1, 257–265.
- PETERSEN, M. A., SALE, T. C. & REARDON, K. F., 2007: Electrolytic trichloroethene degradation using mixed metal oxide coated titanium mesh electrodes. *Chemosphere*, 67, 8, 1573–1581.
- PROBSTEIN, R. F. & HICKS, R. E., 1993: Removal of contaminants from soils by electric fields. *Science*, 260, 5107.
- Provectus environmental products, 2019: *Provect-EBR® ISCO Generator technical data sheet*.
- PURKIS, J. M., WARWICK, P. E., GRAHAM, J., HEMMING, S. D. & CUNDY, A. B., 2021: Towards the application of electrokinetic remediation for nuclear site decommissioning. *J. Hazard. Mater.*, 413.
- RAHNER, D., LUDWIG, G. & RÖ, J., 2002: Electrochemically induced reactions in soils-a new approach to the in situ remediation of contaminated soils? Part 1: The microconductor principle. *Electrochim. Acta*, 47.
- RAJIC, L., FALLAHPUR, N., YUAN, S. & ALSHAWABKEH, A. N., 2014: Electrochemical transformation of trichloroethylene in aqueous solution by electrode polarity reversal. *Water Res.*, 67, 267–275.
- REDDY, K. R., CAMESELLE, C. & ALA, P., 2010: Integrated electrokinetic-soil flushing to remove mixed organic and metal contaminants. *J. Appl. Electrochem.*, 40, 6, 1269–1279.

- REDDY, K. R. & SAICHEK, R. E., 2003: Effect of Soil Type on Electrokinetic Removal of Phenanthrene Using Surfactants and Cosolvents. *J. Environ. Eng.*, 129, 4, 336.
- REUSS, F. F., 1809: Notice sur un nouvel effet de l'électricité galvanique. *Mem. Soc. Imp. Nat., Moscou*, 2, 327–337.
- REVL, A., KARAOLIS, M., JOHNSON, T. & KEMMA, A., 2012: Review: Some low-frequency electrical methods for subsurface characterization and monitoring in hydrogeology. *Hydrogeol. J.*, 20, 4, 617–658.
- REYNOLDS, D., GENT, D. & COX, E., 2017: Pilot test of Electrokinetically Delivered Thermally Activated Persulfate, EK-TAPTUM Final Report. *The Capital Region of Denmark*.
- RUIS, C., BYMOSE, M., COX, E., WANG, J., GENT, D. & TERKELSEN, M., 2012: Successful pilot test of electrokinetic enhanced bioremediation (EK-BIO) as an innovative remedial approach for PCE/DNAPL source area. *NORDROCS 2012: 4th Nordic Joint Meeting on Remediation of Contaminated Sites*.
- RISCO, C., LÓPEZ-VIZCAÍNO, R., SÁEZ, C., YUSTRES, A., CAÑIZARES, P., NAVARRO, V. & RODRIGO, M. A., 2016: Remediation of soils polluted with 2,4-D by electrokinetic soil flushing with facing rows of electrodes: A case study in a pilot plant. *Chem. Eng. J.*, 285, 128–136.
- ROULIER, M., KEMPER, M., AL-ABED, S., MURDOCH, L., CLUXTON, P., CHEN, J.-L. & DAVIS-HOOVER, W., 2000: Feasibility of electrokinetic soil remediation in horizontal Lasagna™ cells. *J. Hazard. Mater.*, 77, 1–3, 161–176.
- SÁEZ, V., ESCLAPEZ VICENTE, M. D., FRÍAS-FERRER, Á. J., BONETE, P. & GONZÁLES-GARCÍA, J., 2009: Electrochemical degradation of perchloroethylene in aqueous media: An approach to different strategies. *Water Res.*, 43, 8, 2169–2178.
- SALE, T., PETERSEN, M. & GILBERT, D., 2005: *Final Report Electrically Induced Redox Barriers for Treatment of Groundwater (CU-0112)*.
- SALEH, N., SIRK, K., LIU, Y., PHENRAT, T., DUFOUR, B., MATYJASZEWSKI, K., TILTON, R. D. & LOWRY, G., 2007: Surface Modifications Enhance Nanoiron Transport and NAPL Targeting in Saturated Porous Media. *Environ. Eng. Sci.*, 24, 1, 45–57.
- SCHEUTZ, C., BROHOLM, M. M., DURANT, N. D., WEETH, E. B., JØRGENSEN, T. H., DENNIS, P., JACOBSEN, C. S., COX, E. E., CHAMBON, J. C. & BJERG, P. L., 2010: Field evaluation of biological enhanced reductive dechlorination of chloroethenes in clayey till. *Environ. Sci. Technol.*, 44, 13.
- SEGALL, B. A., O'BANNON, C. E. & MATTHIAS, J. A., 1980: Electro-Osmosis Chemistry and Water Quality. *J. Geotech. Eng. Div.*, 106, 10.
- SHEN, Z., CHEN, X., JIA, J., QU, L. & WANG, W., 2007: Comparison of electrokinetic soil remediation methods using one fixed anode and approaching anodes. *Environ. Pollut.*, 150, 2, 193–199.
- SONG, Y., CANG, L., FANG, G., ATA-UL-KARIM, S. T., XU, H. & ZHOU, D., 2018: Electrokinetic delivery of anodic in situ generated active chlorine to remediate diesel-contaminated sand. *Chem. Eng. J.*, 337, 499–505.
- STARR, R. C. & CHERRY, J. A., 1994: In Situ Remediation of Contaminated Ground Water: The Funnel-and Gate-System. *Groundwater*, 32, 3.
- STN EN ISO 5667-1, 2018: Kvalita vody. Odber vzoriek. Časť 1: Pokyny na návrhy programov odberu vzoriek a techniky odberu vzoriek (ISO 5667-1: 2006).
- STRECHE, C., COCĂRȚĂ, D. M., ISTRATE, I. A. & BADEA, A. A., 2018: Decontamination of Petroleum-Contaminated Soils Using the Electrochemical Technique: Remediation Degree and Energy Consumption. *Sci. Rep.*, 8, 1.
- TORII, S., 2006: Electroorganic reduction synthesis. *Weinheim, Wiley-VCH*, 1.
- U.S. EPA, 2000a: Electrokinetic Extraction at the Unlined Chromic Acid Pit Sandia National Laboratories. *New Mexico*.
- U.S. EPA, 2000b: Electrokinetics at an Active Power Substation (*Confidential Location*).
- U.S. EPA, 2000c: Electrokinetics at Site 5, Naval Air Weapons Station Point Mugu, *California*.
- VOCCIANTE, M., CARETTA, A., BUA, L., BAGATIN, R. & FERRO, S., 2016: Enhancements in ElectroKinetic Remediation Technology: Environmental assessment in comparison with other configurations and consolidated solutions. *Chem. Eng. J.*, 289, 123–134.
- VOCCIANTE, M., DOVI, V. G. & FERRO, S., 2021: Sustainability in electrokinetic remediation processes: A critical analysis. *Sustainability (Switzerland)*, 13, 2, 1–15).
- WEN, D., GUO, X., LI, Q. & FU, R., 2022: Enhanced electrokinetically-delivered persulfate and alternating electric field induced thermal effect activated persulfate in situ for remediation of phenanthrene contaminated clay. *J. Hazard. Mater.*, 423.
- WIECZOREK, S., WEIGAND, H., SCHMID, M. & MARB, C., 2005: Electrokinetic remediation of an electroplating site: Design and scale-up for an in situ application in the unsaturated zone. *Eng. Geol.*, 77, 3–4, spec. iss., 203–215.
- WU, M. Z., REYNOLDS, D. A., PROMER, H., FOURIE, A. & THOMAS, D. G., 2012: Numerical evaluation of voltage gradient constraints on electrokinetic injection of amendments. *Adv. Water Res.*, 38, 60–69.
- YAMANOUCHI, T. & MATSUDA, S., 1975: Stabilization of Sand Feasible to Liquefaction by Means of a Kind of Grouting Applying Electro-Osmosis. In: *Proc., Symposium on Recent Developments in the Analysis of Soil Behavior*, 411–421.
- YIN, C., JIANG, L., SUN, K., SUN, W. & LIANG, B., 2022: Influence of degree of compaction on electrokinetic remediation of unsaturated soil. *Korean J. Chem. Eng.*, 39, 4, 963–972.
- YUKSELEN-AKSOY, Y. & REDDY, K. R., 2013: Electrokinetic Delivery and Activation of Persulfate for Oxidation of PCBs in Clayey Soils. *J. Geotech. Geoenviron. Eng. – ASCE*, 139, 1, 175–184.
- ZHAO, B., SUN, Z. & LIU, Y., 2022: An overview of in situ remediation for nitrate in groundwater. *Sci. Total Environ.*, 804.

Elektroremediácia v zónach s nízkou hydraulickou vodivosťou – súčasný stav poznatkov a laboratórny experiment

Neustále sa zvyšujúce industriálne aktivity majú významný vplyv na kvalitu životného prostredia. V minulosti sa vo vzťahu k životnému prostrediu pristupovalo veľmi nedbalo. Dôsledkom takýchto činností boli úniky znečisťujúcich látok do okolitého prostredia. Mnohé lokality boli kontaminované a znečistené rôznymi potenciálne toxickými prvkami, organickými látkami a ďalšími znečisťujúcimi látkami, ktoré majú negatívny vplyv na kvalitu pôdy, podzemnej vody a okolitých ekosystémov. Zdroje podzemnej vody patria medzi najohrozenejšie časti životného prostredia. Konvenčné sanačné metódy v dobre hydraulicky priepustnom geologickom prostredí (štrkové nánosy, piesky s priepustnosťou $> 10^{-4} \text{ m} \cdot \text{s}^{-1}$) sú relatívne efektívne v degradácii znečisťujúcich látok. Naopak, slabo hydraulicky priepustné geologické prostredia (íly, silty s priepustnosťou $< 10^{-7} \text{ m} \cdot \text{s}^{-1}$) sú pomerne obtiažne sanovateľné konvenčnými spôsobmi v dôsledku obmedzeného hydraulického gradientu. Primárnou prekážkou sanačných metód *in situ* v slabo hydraulicky priepustných zónach je často neefektívny transport podporných sanačných činidiel a neefektívne hydraulické čerpanie znečistenej podzemnej vody. Preto sa už v minulosti vyvíjali nové a inovátné technológie a metódy, ktoré by efektívne odstraňovali znečisťujúce látky z týchto médií. Spôsob sanácie prostredníctvom jednosmerného elektrického prúdu sa preukázal ako vhodný a efektívny spôsob remediácie v slabo hydraulicky priepustných prostrediach. Táto práca predkladá základné charakteristiky a princípy elektroremediácie ako relatívne inovátnej a stále sa vyvíjajúcej metódy. V časti popisujúcej pilotné a terénne aplikácie v podmienkach *in situ* na iných lokalitách sú predstavené základné technické náležitosti týkajúce sa aplikovateľnosti tejto sanačnej metódy priamo v terénnych podmienkach. Diskutované sú najmä rôzne rozmiestnenia elektród (elektródové konfigurácie), aplikované napätia, voľba vhodných materiálov elektród pri vybraných, dosiaľ realizovaných terénnych aplikáciách *in situ* tejto metódy. Zhrnuté sú aj poznatky o vplyve aplikácie tejto metódy na zmeny fyzikálno-chemických parametrov, akými sú najmä pH a Eh (oxidačno-redukčný potenciál), konduktivita a teplota. Spomenuté sú aj komplikácie spojené s aplikáciou tejto metódy pozorované inými autormi, ktoré spôsobovali technické problémy počas sanácie (napríklad upchávanie povrchov elektród vyzrážanými povlakmi vodného kameňa) a ich spôsoby odstraňovania.

Degradácia chlórovaných uhl'ovodíkov (CIU) aplikáciou jednosmerného elektrického prúdu bola v rámci tejto práce testovaná v laboratórnych podmienkach. Cieľom tohto výskumu bolo štúdium degradácie chlórovaných uhl'ovodíkov v natívnej vzorke znečistenej podzemnej vody pochádzajúcej z priemyselného areálu – environmentálnej záťaže (Zlaté Moravce, Slovensko).

Statický experiment degradácie chlórovaných uhl'ovodíkov prebiehal v dvoch vzájomne prepojených tmavých a uzavretých nádobách, do ktorých boli umiestnené po jednej elektróde. Ako elektródový materiál boli použité železiarské materiály s nešpecifikovaným obsahom železa a ďalších prímiesí. Laboratórny experiment trval 21 dní s postupným zvyšovaním elektrického napätia – 20 V, 40 V a 60 V každých 7 dní. Z nádob sa po 1, 3, 6, 10, 14, 17 a 21 dňoch odobrali vzorky vody a merali sa základné fyzikálno-chemické parametre (pH, Eh, EC). Koncentrácia 5 CIU a ich suma v odobratých vzorkách bola stanovená v akreditovaných laboratóriách ALS, s. r. o., Praha, Česká republika. Počiatočná koncentrácia CIU (suma 5 vybraných chlórovaných eténov – tetrachlórétén, trichlórétén, *cis*-1,2- a *trans*-1,2-dichlórétén, 1,1-dichlórétén) bola $5\,900 \mu\text{g} \cdot \text{l}^{-1}$.

Počas laboratórneho experimentu boli pozorované zmeny vo fyzikálno-chemických parametroch. V katódovej časti sa vytvorili redukčné podmienky (pokles parametra Eh) a zásadité podmienky (nárast pH). V anódovej časti sa hodnoty pH výraznejšie nemenili. Pri parametri Eh boli zaznamenané redukčné hodnoty, ktoré pravdepodobne vyplývali z uvoľňovania železných iónov z rozpúšťajúcich sa anód. Z pozorovaní účinnosti degradácie CIU prostredníctvom aplikovania jednosmerného elektrického prúdu vyplynulo, že anódy preukázali vyššiu schopnosť degradácie CIU (priemerne 93 %) – najmä v dôsledku rozpúšťania železného materiálu anód a dotovania okolitého prostredia iónmi Fe^{2+} , ktoré slúžili ako redukčné činidlo. Pri oxidácii železných iónov Fe^{2+} na železité ióny Fe^{3+} sa do okolitého prostredia uvoľňujú elektróny, ktoré sa podieľajú na rozklade chlórovaných uhl'ovodíkov. V katódovej časti bola zaznamenaná nižšia účinnosť degradácie (priemerne 88 %), pravdepodobne v dôsledku zanášania povrchu katódy vyzrážanou vrstvou vodného kameňa, ktorá sa vytvárala z vyzrážania iónov Ca^{2+} a Mg^{2+} .

Účinná degradácia chlórovaných alifatických uhl'ovodíkov prostredníctvom jednosmerného elektrického prúdu v natívnej vzorke podzemnej vody bola preukázaná

laboratórnym experimentom. Tým sa potvrdil potenciál využitia elektrodegradačných účinkov na sanáciu chlórovaných uhl'ovodíkov na tejto modelovej lokalite. Výsledky získané v laboratórnom experimente možno použiť aj na ďalšiu optimalizáciu degradácie chlórovaných

uhl'ovodíkov v podmienkach in situ, priamo na modelovej lokalite environmentálnej záťaže.

Doručené / Received: 5. 5. 2022

Prijaté na publikovanie / Accepted: 21. 6. 2022

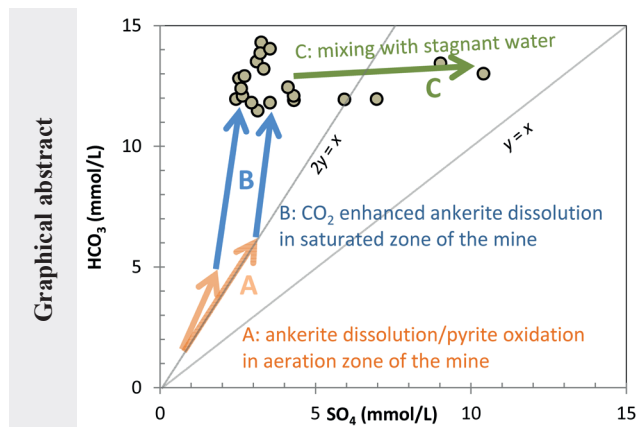
Use of analysis of seasonal hydrochemical regime for better understanding of mine water genesis and more accurate estimate of its impact on stream water quality at flooded Rudňany ore mine (North-Gemeric zone, Slovakia)

PETER BAJTOŠ

State Geological Institute of Dionýz Štúr, Markušovská cesta 1, SK-052 01 Spišská Nová Ves, Slovak Republic;
peter.bajtos@geology.sk

Abstract: Seasonal hydrochemical regime of water flowing out of the Rochus Fe-Cu mine in the Spiš-Gemer Ore Mts. was monitored by discharge measurements and laboratory analyses of mine water chemical composition. Regression analysis of these data showed a statistically significant dependence of concentration of many important chemical elements on mine water discharge. The obtained data made it possible to better understand the processes of mine water chemical composition genesis, as well as to determine in more detail the degree of its environmental impact. Geochemical calculations and forward geochemical modelling suggest that chemical composition of mine water is formed in three stages. First phase takes place in the aeration zone of the mine, where ankerite dissolution, intensified by pyrite oxidation, dominates. In saturated zone of the mine, ankerite dissolution is probably controlled by CO₂ input in open carbonate system. These two main geochemical processes take place permanently and at the time of low flow conditions they lead to relatively stable composition of water outflowing from mine. In time of higher flow conditions, concentration of SO₄, Mg, Ca, Na and As significantly increases, probably as a consequence of mixing with stagnant water from deeper or hydraulically more isolated parts of the flooded mine. Water flowing out from mine enters the Rudniansky potok creek and contaminates it mainly by manganese. The limit for Mn content in surface water is exceeded here at the time of low flow conditions – usually for 180 days a year. Anomalous concentrations of SO₄, Mg, As and Sb in mine water are sufficiently diluted in stream water where they do not exceed environmental limits.

Key words: mine water, hydrochemical regime, surface water pollution, geochemical modelling, manganese, arsenic contamination



Highlights

- Positive dependence of SO₄, Mg, Ca, Na and As concentrations in mine water discharge was revealed by observation of seasonal hydrochemical regime.
- Geochemical calculations and forward modelling based on mine water samples suggest three main phases of the mine water chemical composition formation.
- Water quality of the Rudniansky potok creek is endangered mainly by manganese – its surface water quality limit is usually exceeded for 180 days a year.
- The example clearly demonstrates that detailed knowledge of seasonal hydrochemical regime is necessary for understanding of mine water genesis.

Introduction

As remnants of historical and modern mining, hundreds of abandoned mines occur in the territory of Slovak Republic. Most of them are historic, but many were closed after the transition to a market economy in Slovakia after 1989, when the State declared attenuation in ore mining programme. Among allocated 14 mining-deposit regions, Gemeric zone in eastern Slovakia is the

largest one and richest in mine occurrences and as many as 656 mine water sources were documented here with total discharge of 663 L/s (Bajtoš, 2016). Of these, up to 535, with total discharge of 456 L/s, are connected to siderite-sulphidic veins hosted by Paleozoic metamorphites. As the chemical composition of these mine waters is very variable, some of them meet the conditions for the use as drinking water sources and some pose an environmental

risk, mainly due to their high As, Sb, Mn and SO₄ content. The chemical composition of the largest mine water outflows is generally known, but it is based only on repeated sampling. Therefore, their hydrochemical regime is practically unknown. However, detailed knowledge about the fluctuation in the content of hazardous elements over time is important for the evaluation of mine water sources in terms of possible use but also for assessing the risk of their negative environmental impact. In addition, it is useful for understanding of genesis of mine water chemistry.

The Rudňany mine is one of the largest mines in the Gemer zone, encompassing the Gemeric tectonic unit. Throughout all history of ore mining, but also since 1993, when it was flooded, it negatively affected the quality of the nearby Rudniansky potok creek. The presented study firstly describes the extent of seasonal fluctuations in the risk elements present in this mine water and evaluates its impact on stream water quality. Additionally, the presented interpretation of the acquired knowledge brings a better understanding of geochemical processes taking place in studied flooded mine. These findings can be applied in the study of mine water genesis at other mines, connected to siderite-sulphidic veins hosted by Paleozoic metamorphites, not only in Slovakia.

Study area

The Rudňany ore field is spread over an area of 20 km² in the north-eastern part of the Volovské vrchy Mts., in eastern Slovakia. The altitude of this area ranges from 430 to 870 m above sea level. Climate is relatively cold (annual air temperature 3–6 °C) and wet (annual precipitation total 630–800 mm), (Landscape Atlas of SR, 2002). The majority of area is dewatered by the Rudniansky potok creek to the Hornád river. Discharge of the Rudniansky potok creek is observed by Slovak Hydrometeorological Institute (SHMI) on gauge-discharge station No. 8425, situated close to its effluent into the Hornád river (Fig. 1). In the period 2012–2013 the discharge of this stream fluctuated from 0.05 to 5.8 m³/s, with median of 0.158 m³/s (Fig. 3). Stream discharge exceeded its average value of 0.351 m³/s for 26 % of the time.

In the Rudňany ore field there are 7 shafts with 13 main mining levels (Figs. 2, 3) with the deepest level in 120 m below the sea level. All mine workings are interconnected into one large mine. It is excavated in Paleozoic rocks of Gemeric unit, which crop out in the southern part of the Rudňany ore field. To the north, Paleozoic rocks are covered with Mesozoic and Paleogene sediments. For these reasons, mine workings that reach the land surface are concentrated in southern part of area, especially in headwater of the Rudniansky potok creek. Therefore this location represents the main infiltration area of the mine,

as it is documented by previous hydrogeological study (Bajtoš, 1999a, b). Here, main ore vein of the ore field – the Droždiak vein – reaches land surface and is accompanied by caving falls.

The Droždiak vein is hosted by metasandstones, phyllites and metamorphosed volcanic rocks (Zlatník Formation, Dobšiná Group of North-Gemic unit, Late Carboniferous; Grecula, 1982; Vozárová & Vozár, 1988) or by cover conglomerates of Knola Formation, Krompachy Group of North-Gemic unit, Early Permian). Common feature of these rocks is relatively low hydraulic conductivity ($k = 5.30 \cdot 10^{-9} - 8.99 \cdot 10^{-4}$ m/s, geometric mean $1.65 \cdot 10^{-6}$ m/s) and transmissivity ($T = 2.80 \cdot 10^{-7} - 1.65 \cdot 10^{-2}$ m²/s, geometric mean $3.13 \cdot 10^{-5}$ m²/s), decreasing with increasing depth (Bajtoš in Grecula et al., 2011). Under such conditions, shallow groundwater circulation prevails and slightly alkaline water of Ca–Mg–HCO₃ or Ca–Mg–HCO₃–SO₄ chemical types, with low TDS content of 0.1–0.4 g/L is formed. Dissolution of carbonate and aluminosilicate minerals is the main water chemistry forming process. Groundwater recharge occurs mainly in the spring due to snow melting, and also during colder rainy periods with low evapotranspiration. According to long term observation of snow chemical composition in sampling point in Dobšiná, atmospheric water is acid, pH = 5.5 in average (Bodiš et al., 2000), with average concentrations of Cl, SO₄, NO₃ of 1.45, 4.47 and 1.92, respectively.

Ore vein mineralization in the Gemeric region is a product of Permian metamorphic-magmatic and hydrothermal cycle (Radvanec & Gonda, 2019). Ore veins are of the siderite-barite-sulphidic type with developed transversal as well as vertical zonality (Grecula et al., 1995). Their uppermost parts consist of barite, siderite and variable content of sulphide minerals. Siderite proportion gradually increases downwards and it totally prevails in the middle parts of ore veins, while in their lower parts the siderite amount decreases at the expense of quartz and ankerite. Sulphides are represented mainly by tetrahedrite (schwartzite), chalcopyrite and pyrite. The relative contents of chalcopyrite and pyrite increase proportionally with depth. Siderite contains relatively high portion of magnesium and also non-negligible portion of calcium and manganese – the formula (Ca_{0.01}Fe_{0.82}Mg_{0.13}Mn_{0.04})CO₃, calculated from 156 siderite samples taken from Droždiak vein (Cambel & Jarkovský, 1985), gives its average stoichiometry. Beside that the average contents of microelements were determined: 13.7 ppm Ti, 13.8 ppm V, 63.4 ppm Ni, 22.2 ppm Co, 6.1 ppm Sc, 15.5 ppm Cr and 78.8 ppm Sr. Those authors also state that other carbonate minerals most represented in ore veins (instead of siderite) are ankerite, Fe-dolomite and Mg-dolomite; minerals of isomorphic series magnesite-siderite often occur and calcite is rarely present. Typical formula for

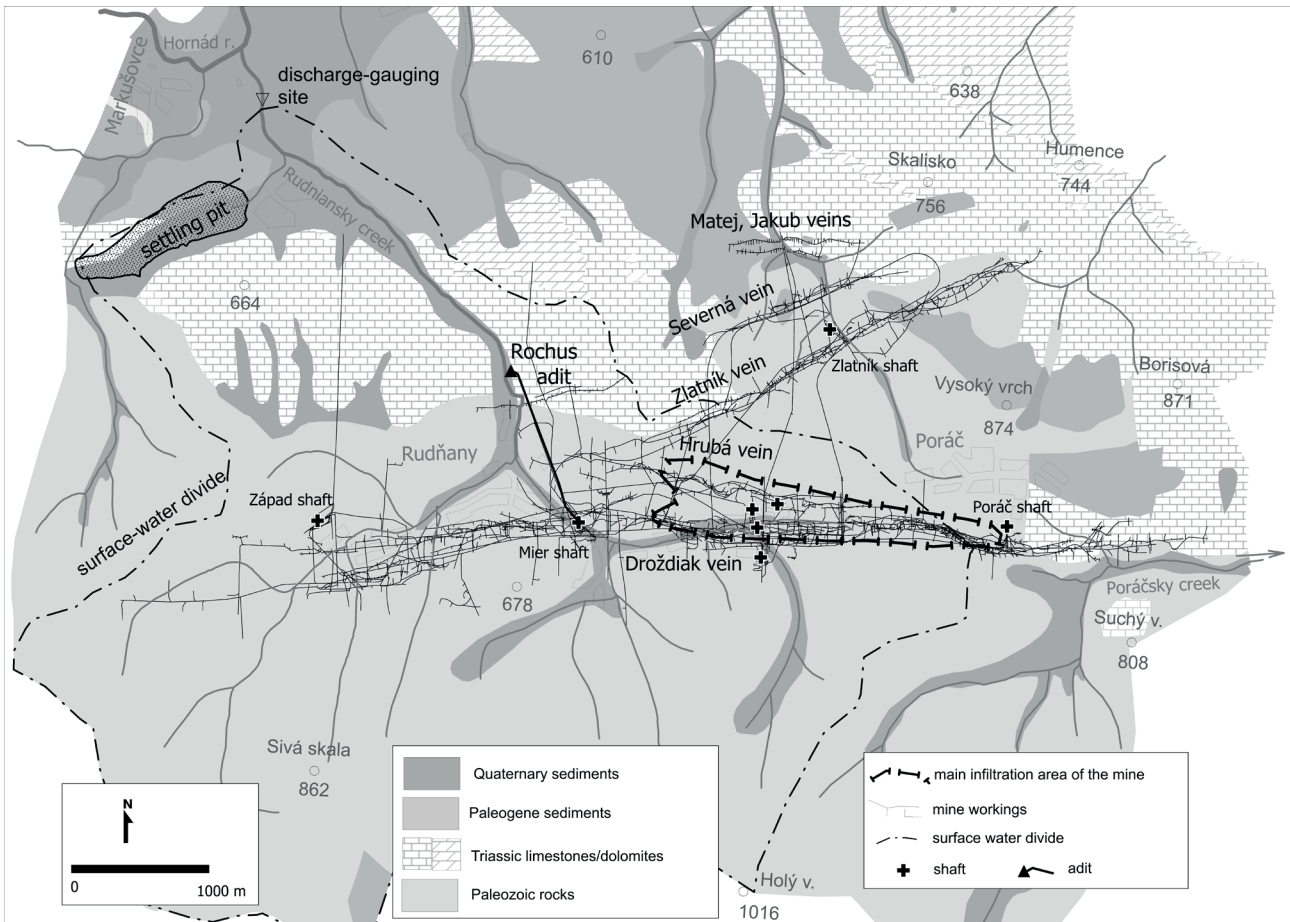


Fig. 1. Geological situation of the Rudňany mine (compiled on the basis of geological map of Mello et al., 2000).

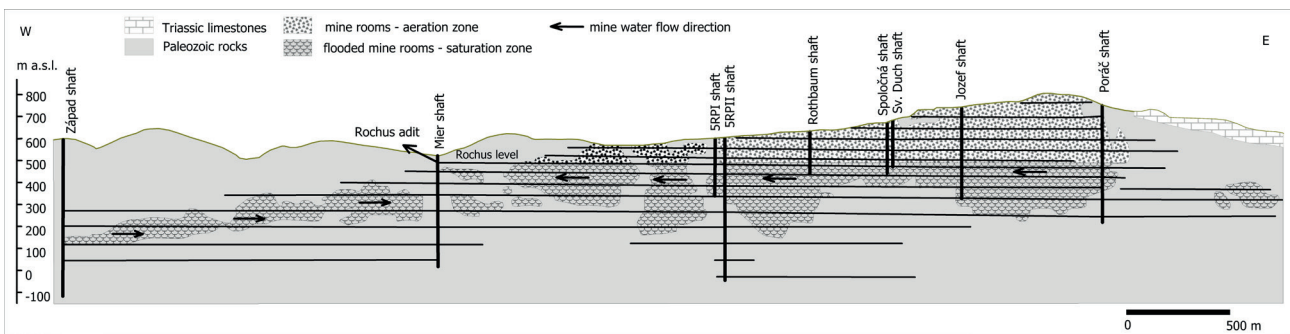


Fig. 2. Longitudinal cross-section through the Droždiak.

ankerite from Rudňany calculated from 11 samples is $\text{Ca}_{1.008}(\text{Fe}_{0.372}\text{Mg}_{0.574}\text{Mn}_{0.046})(\text{CO}_3)_2$, for calcite from 3 samples $(\text{Ca}_{0.915}\text{Fe}_{0.019}\text{Mg}_{0.052}\text{Mn}_{0.013})\text{CO}_3$ and for Fe-dolomite from 10 samples $\text{Ca}_{1.033}(\text{Fe}_{0.242}\text{Mg}_{0.705}\text{Mn}_{0.020})(\text{CO}_3)_2$.

The Rudňany mine was flooded in 2006. Since then, all water drained by the mine flows out of the Mier shaft and from it flows to the surface through a 1.2 km long Rochus adit by gravity. According to measurements performed 2–6 times a year the mine water discharge fluctuated from

12 to 40 L/s in the period 2007–2011 and it contributed to contamination of the Rudňany creek mainly by high Mn, SO_4 , TDS and Sb concentrations (Bajtoš et al., 2012).

Data and methods

Sampling

Mine water samples were collected on the mouth of Rochus gallery in 2012 and 2013. Sampling frequency

was irregular (Fig. 4) – aimed on documentation of wide range of climate/discharge conditions. The water samples were filtered with a 0.45 µm Whatman filter using Nalgene vacuum hand-operated pump into PE sample bottles, which were prepared by lab. Water for Fe(II) measurement was sampled into 300 ml glass bottle and fixed with 6 ml of sodium acetate solution and 6 ml of dilute acetic acid. A WTW Multi 340i was used to quantify pH, specific conductance, temperature, dissolved O₂ and Eh (platinum electrode) in sampled water. In time of sampling, the mine water discharge was measured using A.OTT C1 current meter.

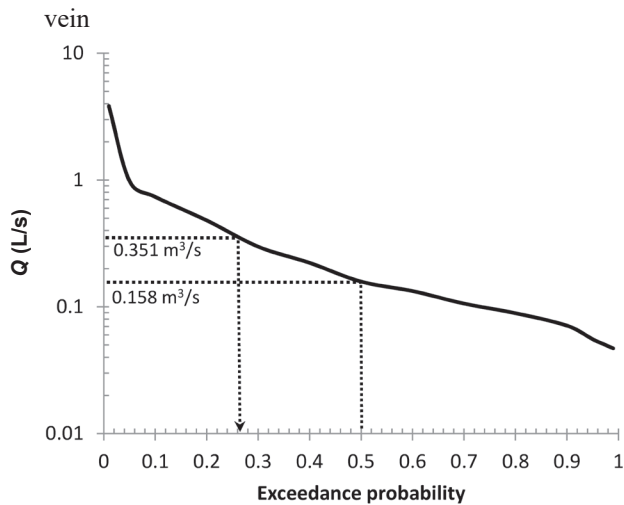


Fig. 3. Flow duration curve of the Rudniansky potok creek recorded in the period 2012–2013 by Slovak Hydrometeorological Institute on gauging station No. 8425 in Markušovce locality.

Chemical analysis

Bicarbonate and carbonate anions were measured using Titroline 7000 alkalinity titrator. Sulphate, chloride, fluoride and nitrate were measured by ion chromatography using DX-120 IC apparatus. Concentrations of Na, K, Al, Ba, Ca, Cu, Fe, Mg, Mn, Ni, SiO₂, Sr, Zn and U were determined by the ICP-OES technique using VARIAN Vista-MPX and CETAC Technologies Ultrasonic Nebulizer. Concentrations of As, Bi, Sb, and Se were measured by atomic absorption spectrometry using SPECTRAA-20 AAS-GH. Atomic absorption spectrometer AMA-254 was used for mercury determination. Using UV-VIS spectrophotometer Hach Lange DR 5000, concentrations of ammonium ion, nitrite and Fe(II) were determined. Mine water samples were delivered to the laboratory within 3 hours of collection. All chemical analyses were performed at the Geoanalytical Laboratories (GAL) of the State Geological Institute of Dionýz Štúr (SGIDS), located in Spišská Nová Ves. GAL is accredited by Slovak National Accreditation Service – regular member of

European Cooperation for Accreditation – for chemical and physical-chemical tests of all types of waters and water leachates, as well as for water sampling.

Geochemical calculations and geochemical modelling

The PHREEQC computer program with minteq.v4 database was used for speciation and saturation index (SI) calculations. These types of calculations, referred to as speciation calculation or speciation modelling, requires only a SOLUTION data block for each water analysis (Parkhurst & Appelo, 2013). Speciation calculation distributes total concentrations of element in solution among aqueous species by using an aqueous model – the results are the activities of all of the aqueous species including gas phases (CO₂, O₂). The activities are used for calculating saturation indices for minerals, relative to water. Carbonate minerals, gypsum and Fe and Mn hydroxides are considered to be most relevant for study of water-rock interactions in Rochus mine. The Eh measured in the field were employed to predict the speciation of Sb and As in mine water samples.

Forward geochemical modelling uses hypothesized geochemical reactions to predict water and rock compositions (Plummer, 1992). This approach allows to simulate mineral solubilities, mass transfers, reaction paths, pH and pe by using available solid-aqueous data in aqueous specification models. In this study, forward modelling is applied to simulate the evolution of mine water chemical composition at the Rochus mine. The hypothesis is that ore minerals (carbonates, pyrite) dissolution, precipitation of calcite, goethite, ferrihydrite, manganite and rhodochrosite, and consumption/release of carbon dioxide and oxygen are sufficient to account for the changes in water composition of all the major ions, iron and manganese. Taking into account the complexity of the modelled environment, results of presented simulation should be considered as indicative. The calculation uncertainty is mainly due to the variability of primary carbonate minerals composition combined with the lack of available values of $\log K$ for these minerals, as well as temporal and spatial variability of CO₂ and O₂ partial pressure in studied environment.

Some ore carbonate minerals present with documented average stoichiometry (Cambel & Jarkovský, 1985) were added to the thermodynamic database (minteq.v4) used for SI calculations and forward modelling. Due to the lack of data on their solubility product ($\log K$) in the literature, these data were estimated by linear interpolation between the $\log K$ values of main end-members of respective solid solutions. $\log K = -9.87$ was estimated for siderite(Ry) Ca_{0.01}Fe_{0.82}Mg_{0.13}Mn_{0.040}CO₃, by interpolation between siderite FeCO₃ (minteq.v4; $\log K = -10.89$) and magnesite

MgCO₃ (phreeqc database; $\log K = -7.46$). Similarly, $\log K = -8.48$ of calcite Ca_{0.916}Fe_{0.019}Mg_{0.052}Mn_{0.013}CO₃ was determined from data for calcite ($\log K = -8.475$, minteq.v4) and magnesite. $\log K = -17.31$ for ankerite(Ry) Ca_{1.008}(Fe_{0.372}Mg_{0.574}Mn_{0.046})(CO₃)₂ and of $\log K = -17.35$ for ankerite(f) Ca_{1.0}(Fe_{0.46}Mg_{0.5}Mn_{0.04})(CO₃)₂, were determined from data for ordered dolomite ($\log K = -17.09$; minteq.v4) and ankerite Ca(Fe_{0.6}Mg_{0.4})CO₃)₂ ($\log K = -17.40$; Al et al., 2000).

Statistical data treatment

Regression analysis was used to evaluate the direction and strength of relationship between mine water discharge as independent variable and content of observed chemical compounds dissolved in it, by using the software STATISTICA Cz version 10 (StatSoft CZ). The strength of a monotonic (Spearman correlation) relationship between those variables was also evaluated. The interdependence of

Tab. 1

Basic physico-chemical parameters and ion concentrations of mine water samples together with time corresponding mine water discharge Q at the Rudňany mine.

Date	Q [L/s]	T _{H2O} [°C]	EC [mS/m]	pH [-]	E _H [mV]	O ₂ [%]	Ba [mg/L]	Fe [mg/L]	Fe ²⁺ [mg/L]	Mn [mg/L]	As [µg/L]	Sb [µg/L]	Hg [µg/L]	SO ₄ [mg/L]
13. 9. 2011	14.7	11.7	143.9	7.55	511	56	0.03	0.216	< 0.1	1.37	5	8	0.1	244
28. 2. 2012	14.2	9.4	161.0	7.84	421	90	0.028	0.081	< 0.1	1.19	5	6	0.1	299
12. 3. 2012	13.4	10.0	163.1	7.69	389	91	0.03	0.064	< 0.1	1.38	5	4	0.3	313
21. 3. 2012	17.6	10.4	162.9	7.76	395	83	0.036	0.072	< 0.1	1.52	5	5	0.2	310
28. 3. 2012	20.8	10.8	165.0	7.70	446	79	0.035	0.087	< 0.1	1.54	3	3	0.1	323
4. 4. 2012	19.7	10.7	161.5	7.65	396	77	0.03	0.074	< 0.1	1.52	4	9	0.1	320
10. 4. 2012	20.9	9.7	158.4	7.70	435	78	0.033	0.079	< 0.1	1.21	5	8	< 0.1	297
17. 4. 2012	32.6	10.9	148.6	7.54	444	70	0.042	1.11	< 0.1	1.07	4	13	< 0.1	279
26. 4. 2012	31.9	10.8	154.5	7.48	85	74	0.035	0.137	< 0.1	1.35	3	14	< 0.1	271
3. 5. 2012	25.9	11.1	153.4	7.54	490	78	0.038	0.087	< 0.1	1.42	3	26	0.1	263
24. 5. 2012	20.3	11.4	154.9	7.67	500	82	0.03	0.012	< 0.1	1.41	5	6	0.1	261
29. 5. 2012	19.2	11.2	156.1	7.65	450	80	0.039	0.1	< 0.1	1.65	4	3	0.2	265
4. 6. 2012	17.6	11.7	158.5	7.67	350	79	0.039	0.1	< 0.1	1.65	5	4	0.2	271
13. 6. 2012	30.3	11.3	148.7	7.53	343	75	0.039	0.147	–	1.53	6	5	0.2	271
13. 9. 2012	20.4	11.7	159.7	7.72	411	75	0.03	0.099	–	1.37	5	6	< 0.1	340
5. 3. 2013	76.6	11.3	162.6	7.47	294	89	0.057	0.47	< 0.1	1.32	18	7	0.2	414
12. 3. 2013	127.4	11.5	201.2	7.50	238	99	0.028	2.15	–	1.16	18	6	0.2	867
19. 3. 2013	123.0	11.1	199.5	7.51	201	84	0.024	0.804	0.46	0.98	20	9	< 0.1	670
3. 4. 2013	52.1	10.7	147.9	7.53	364	57	0.035	0.33	–	1.36	11	9	0.3	302
9. 4. 2013	59.3	11.3	169.9	7.57	277	51	0.033	0.63	–	1.25	11	8	< 0.1	413
16. 4. 2013	65.0	12.9	254.9	7.60	176	29	0.026	1.41	0.77	0.90	6	21	–	1 000
23. 4. 2013	117.5	11.9	193.2	7.86	199	39	0.028	1.02	0.36	1.00	14	14	< 0.1	570
6. 5. 2013	70.0	11.3	141.6	7.53	481	59	0.032	0.193	< 0.1	1.24	9	9	< 0.1	235
14. 5. 2013	60.1	11.1	141.1	7.67	357	61	0.03	0.199	< 0.1	1.37	7	6	0.2	251
19. 6. 2013	59.4	11.2	143.5	7.27	531	73	0.041	0.161	< 0.1	1.57	6	6	0.1	255
11. 7. 2013	69.8	11.2	144.7	7.27	411	76	0.03	0.08	< 0.1	1.29	8	5	0.1	283
18. 9. 2013	29.8	11.6	165.8	7.46	326	77	0.042	0.166	< 0.1	1.64	8	20	< 0.1	395
3. 10. 2013	26.2	11.4	170.0	7.60	522	74	0.031	0.197	< 0.1	1.22	5	10	< 0.1	431

Tab. 1 (continued)

Date	Na [mg/L]	K [mg/L]	NH ₄ ⁺ [mg/L]	Ca [mg/L]	Mg [mg/L]	Sr [mg/L]	Zn [µg/L]	Cu [µg/L]	Ni [µg/L]	Co [µg/L]	Cl [mg/L]	NO ₂ [mg/L]	NO ₃ [mg/L]	HCO ₃ [mg/L]	SiO ₂ [mg/L]
13. 9. 2011	11.4	7.65	0.08	85.9	168	1.27	17	5	9	5	11.9	< 0.01	2.08	781	3.72
28. 2. 2012	9.8	6.21	0.09	69.8	156	1.05					15.3	0.01	1.2	824	3.51
12. 3. 2012	11.6	7.56	0.12	77.2	177	1.26	6	< 2	9	4	15.3	< 0.01	1.14	872	4.05
4. 4. 2012	12.4	7.65	0.06	84.8	183	1.42	8	2	6	4	17.2	< 0.01	2.3	805	4.07
24. 5. 2012	12.3	7.75	0.23	77.9	186	1.23	3	< 2	5	3	14.8	< 0.01	2.37	787	3.84
13. 9. 2012	11.7	7.79	0.32	78	171		9	3			14.9	0.01	1.98	856	3.43
5. 3. 2013	16.8	8.68	0.15	98.9	166	1.72	3	4	14	7	15.2	0.02	3.08	726	4.69
12. 3. 2013	59.8	14.1	0.27	116	259						15.7		1.2	819	4.92
19. 3. 2013	44.9	11.00	0.27	98.2	230	2.89	3	< 2	9	5	16.2	0.03	5.19	729	4.31
3. 4. 2013	12.8	6.28	0.57	82.2	146						15.6		6.2	700	3.53
9. 4. 2013	23.9	8.00	0.19	87.3	190						18		5.3	737	3.57
16. 4. 2013	68.7	16.7	0.34	114	280	4.06		2	8	5	18.5	0.02	3.62	793	4.14
23. 4. 2013	37.3	9.28	0.24	93.6	200						17.9		5.8	728	3.78
6. 5. 2013	10.7	5.82	0.29	74.2	144						16.2		5.76	729	3.48
14. 5. 2013	10.5	5.58	0.08	76.2	166	1.04	6	2	8	5	16.4	0.01	5.26	720	2.84
19. 6. 2013	12.7	7.40	0.25	93	172						18.3		6.7	737	4.01
11. 7. 2013	12.3	6.45	0.22	78.7	151	1.16	5	2	10	5	17.1	0.01	5.83	720	3.25
18. 9. 2013	10.6	6.51	0.31	95.5	167						18.2		3.01	759	3.64
3. 10. 2013	11.2	6.92	0.14	101	184	1.49	5	4	10	7	18.6	< 0.01	12.4	756	4.47

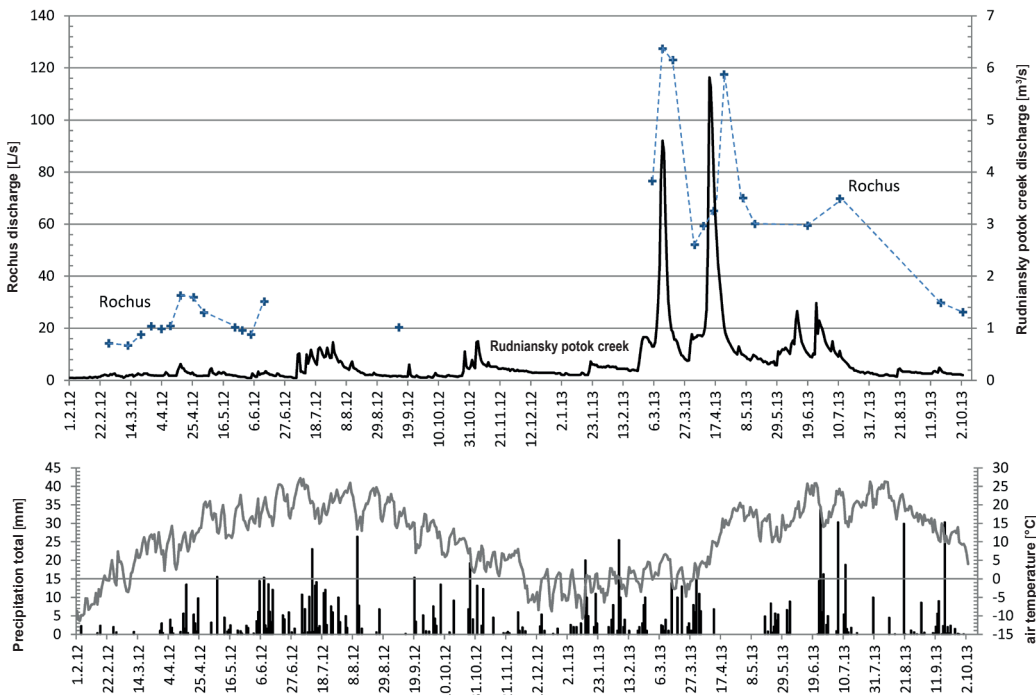


Fig. 4. Sampling frequency represented by discharge values of the Rochus mine water (plus marks) in the background of local climate and runoff regime. The Rudniansky potok creek discharge was measured on discharge-gauging station no. 8 425 in Markušovce village, daily precipitation totals measured at precipitation stations in the Rudňany vilage, air temperature measured at climatic station in Rožňava; measurements were performed by SHMI Bratislava.

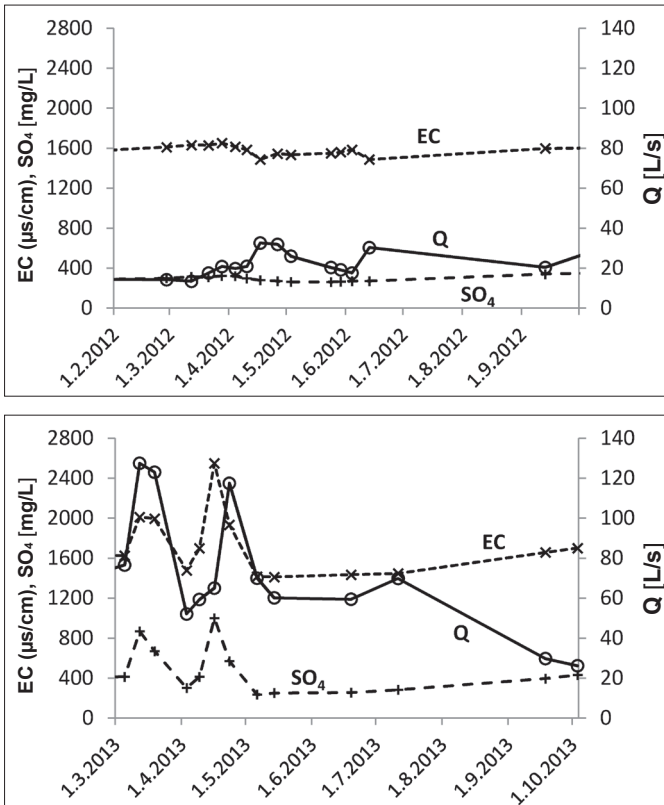


Fig. 5. Temporal changes of mine water discharge Q , EC value and sulphate concentration during sampling periods 2012 and 2013.

chemical compounds and some geochemical indicators is evaluated and presented by regression graphs by using the software MS EXCEL.

Results

Mine water chemistry

Water discharged from the Rochus gallery is slightly alkaline with pH values 7.3–7.9 (Tab. 1). The total dissolved solids (TDS) content in samples ranged from 1.2 to 2.3 g/L. Magnesium (70–75 eq %) is the most dominant cation, followed by calcium (18–30 eq %). Bicarbonate (38–70 eq %) and sulphate (28–60 eq %) are dominant anions. Therefore, samples represent Mg–Ca–HCO₃–SO₄, Mg–HCO₃–SO₄ or Mg–SO₄–HCO₃ type, according to water chemistry classification based on presence of major (> 20 eq %) ions. Sodium (2–9 eq %), potassium (1 eq %) and chloride (1–3 eq %) are secondary major ions. Concentration of nitrogen species is low – ammonium ion and nitrate do not exceed 0.6 mg/L and 12 mg/L, respectively. Among the trace elements, strontium and manganese is present in units of mg/L, iron in tenths of mg/L, antimony, barium in tens of µg/L, arsenic, zinc, cobalt, nickel and copper in units of µg/L and mercury in tens of µg/L. Concentrations of cadmium and beryllium are under

detection limits of analytical method used. In situ measured Eh values of 85–531 mV indicate aerobic conditions.

Hydrochemical regime

Hydrochemical regime of Rochus mine water was observed in two periods – 2012 and 2013. Most of samples were collected during the spring and summer months, when the most significant changes in mine water chemical composition are expected.

Spring warming in March 2012 did not bring much increase of runoff (Fig. 4), probably due to low snow and soil water storage. Low runoff increase on April 14–17 was caused by precipitation total of 20 mm and the Rochus mine water yield rose quickly from 20 to 32 L/s. This increase was accompanied by slight decrease in EC from 165 to 149 mS/m, SO₄ from 0.32 to 0.26 g/L (Fig. 5) and pH value decrease from 7.7 to 7.5. Since March 28 to May 3 the gradual increase of Sb content from 3 to 26 µg/L was recorded while As content remained at the level between 3 and 5 µg/L (Fig. 6).

On the other hand, spring warming in 2013 brought two big runoff increases. The first of them was cau-

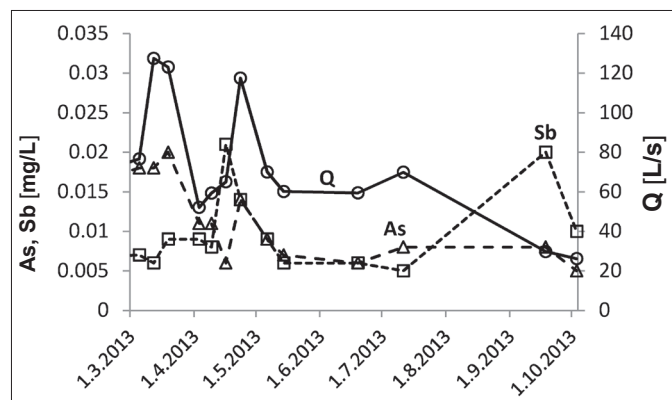
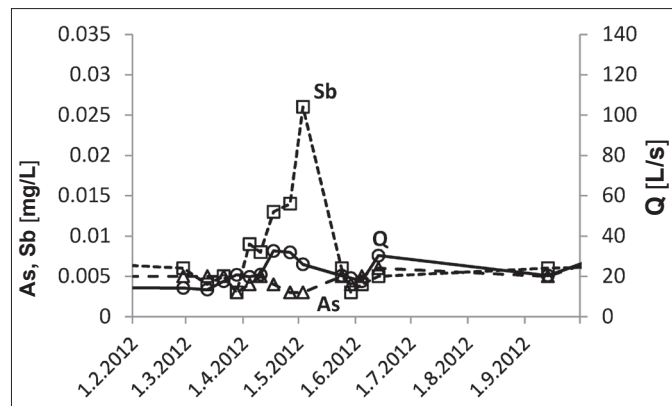


Fig. 6. Temporal changes of mine water discharge Q and arsenic and antimony concentration during sampling periods 2012 and 2013.

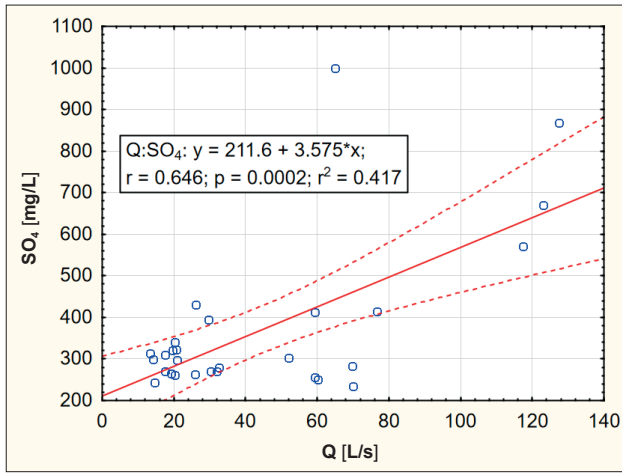


Fig. 7. Dependence of sulphate anion concentration on mine water discharge. Linear regression line fitted to the data and a 95 % confidence interval for that line.

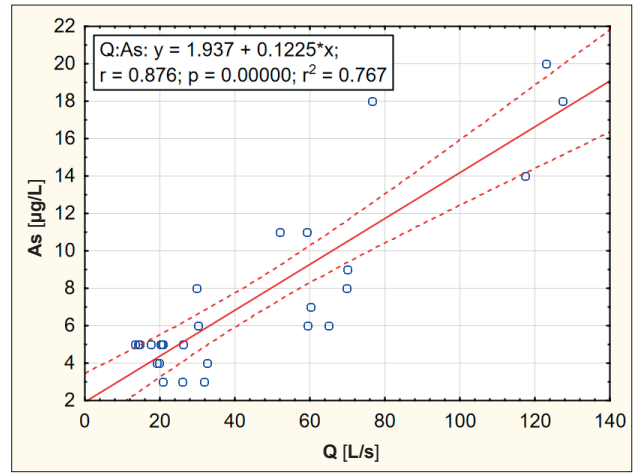


Fig. 8. Dependence of arsenic concentration on mine water discharge.

Tab. 2

Results of correlation and regression analysis of water chemical composition features and mine water discharge.

Q L/s	n	r – Spearman	r	r ²	t-value	p-value	y-intercept	Slope
pH	28	-0.554	-0.280	0.078	-1.485	0.150	7.64	-0.001 1
Eh	26	-0.431	-0.536	0.287	-3.110	0.005	455	-1.828 0
EC	28	0.101	0.471	0.222	2.723	0.011	1 490	3.301 5
O ₂ mg/L	28	-0.324	-0.226	0.051	-1.181	0.248	7.93	-0.011 2
As	28	0.719	0.876	0.767	9.242	0.000	1.9	0.122 5
Sb	28	0.429	0.121	0.015	0.624	0.538	8.1	0.020 0
Fe	25	0.616	0.594	0.353	3.546	0.002	-0.000 7	0.007 1
Mn	28	-0.507	-0.622	0.386	-4.047	0.000 4	1.514	-0.003 8
Ba	28	-0.129	-0.193	0.037	-1.002	0.326	0.036	-0.000 04
SO ₄	28	0.315	0.646	0.417	4.314	0.000 2	212	3.575
Ca	19	0.498	0.539	0.290	2.638	0.017	78	0.189
Mg	19	0.207	0.491	0.241	2.325	0.033	158	0.479
Na	19	0.584	0.681	0.464	3.836	0.001	3.2	0.329
K	19	0.362	0.506	0.256	2.418	0.027	6.2	0.039
NH ₄	19	0.427	0.295	0.087	1.274	0.220	0.17	0.001
Sr	11	0.445	0.556	0.309	2.005	0.076	1.02	0.015
Cl	19	0.284	0.256	0.065	1.090	0.291	15.7	0.012
NO ₃	19	0.412	0.174	0.030	0.727	0.477	3.53	0.013
HCO ₃	20	-0.604	-0.496	0.246	-2.423	0.026	807	-0.686
SiO ₂	19	0.211	0.326	0.106	1.421	0.173	3.61	0.004
Ni	10	0.389	0.393	0.154	1.208	0.261	7.50	0.026 6
Co	10	0.553	0.326	0.106	0.974	0.359	4.45	0.011 3
Zn	10	-0.648	-0.515	0.265	-1.698	0.128	9.14	-0.059 4

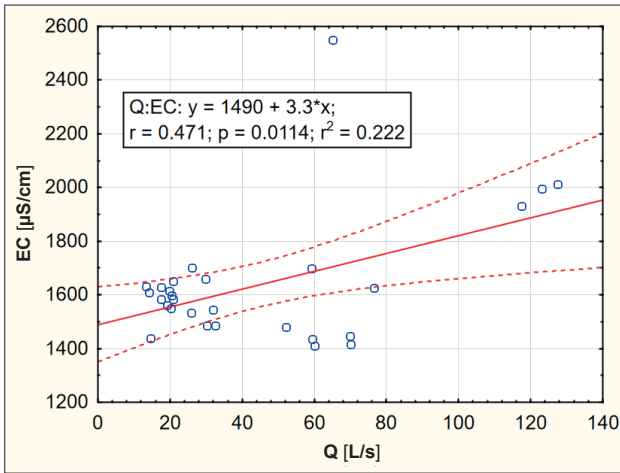


Fig. 9. Dependence of manganese concentration on mine water discharge.

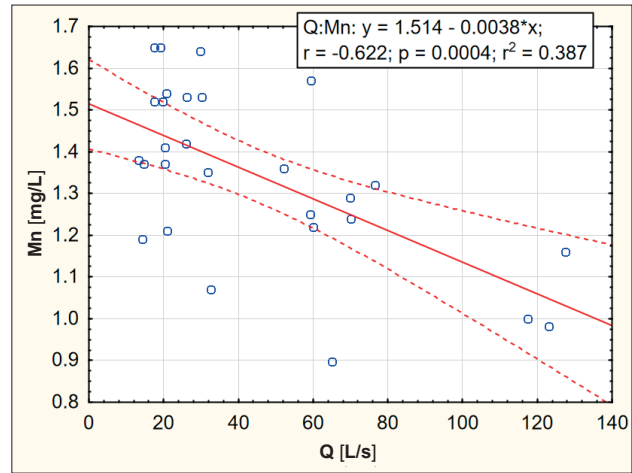


Fig. 10. Dependence of EC(25 °C) on mine water discharge.

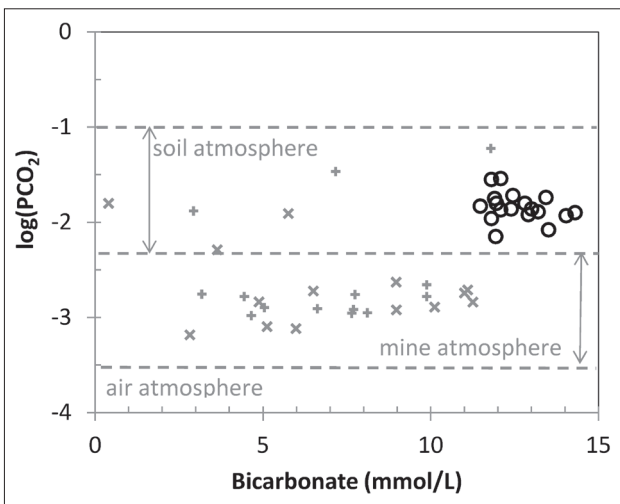


Fig. 11. Computed values of $P(\text{CO}_2)$ versus concentration of bicarbonate anion. Empty circles – new samples of mine water from Rochus adit; plus signs – samples of mine water pumped from the mine at the time of its operation 1992–1995, cross marks – seepage samples from mine rooms on the Droždiak vein taken in time of ore extraction, according data from Bajtoš (1993a, b).

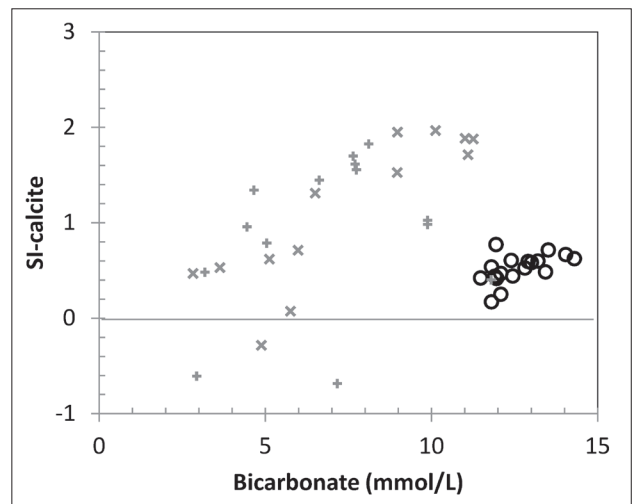


Fig. 12. Computed SI-calcite values versus concentration of bicarbonate anion. Explanations as in Fig. 11.

sed by short terming warming and snow melting in March 7–13, with 4.6 m³/s peak of the Rudňany potok creek discharge on March 12. In this time, maximum 128 L/s mine water yield was recorded. During following frosty days runoff dropped almost to its original level, but permanent warming that began on April 9 has brought another rapid increase of the Rudňany potok creek discharge, with its 5.4 m³/s peak on April 13. Mine water discharge also increased rapidly in this time, but its peak occurred a few days later – between 16 and 23 April. During these high mine water discharge stages, both EC values, sulphate and arsenic concentrations have significantly increased (Figs. 5, 6). Concentrations of antimony have increased only during second discharge peak, from 8 to 21 µg/L. In-

creases of EC values, SO₄ and As content reached up to 107 mS/m, 0.7 g/L and 14 µg/L, respectively. The pH value increased slightly during the first discharge peak from 7.5, reaching its maximum of 7.86 in time of the second discharge peak.

The relationship between mine water chemical composition features and mine water discharge

Regression analysis was applied to examine the relationships between mine water chemical composition features (dependent variables) and mine water discharge (independent variable). Its results reveal that many of them have statistically significant relationship (Tab. 2). All the major ions concentrations significantly depend on mine water discharge – most sulphate anion (Fig. 7), with 42 % of its variability explained ($r^2 = 0.42$), followed by calcium ($r^2 = 0.29$), bicarbonate anion ($r^2 = 0.25$) and magnesium ($r^2 = 0.24$). In accordance with EC ($r^2 = 0.22$), sul-

Tab. 3

Saturation indices of mine water samples with respect to selected mineral phases.

Saturation indices with respect to:								
	siderite	ankerite(Ry)	Fe-dolomite(Ry)	calcite	monohydrocalcite	dolomite	nesquehonite	rhodochrosite
	FeCO ₃	Ca(Fe _{0.37} Mg _{0.58} Mn _{0.05}) (CO ₃) ₂	Ca _{1.03} (Fe _{0.24} Mg _{0.71} Mn _{0.02}) (CO ₃) ₂	CaCO ₃	CaCO ₃ *H ₂ O	CaMg(CO ₃) ₂	MgCO ₃ *3H ₂ O	MnCO ₃
Average	-2.21	0.08	0.23	0.51	-0.85	1.50	-1.74	0.65
Minimum	-5.16	-1.32	-0.94	0.17	-1.19	0.79	-2.10	0.35
Maximum	-0.15	1.28	1.21	0.77	-0.59	2.05	-1.45	0.92

Tab. 4

Saturation indices of mine water samples with respect to selected mineral and gas phases.

Saturation indices with respect to:								
	manganite	ferrihydrite	goethite	K-jarosite	gypsum	quartz	CO ₂ (g)	O ₂ (g)
	MnOOH	Fe(OH) ₃	FeOOH	KFe ₃ (SO ₄) ₂ (OH) ₆	CaSO ₄ *2H ₂ O	SiO ₂	log(P _{CO2})	log(P _{O2})
Average	-0.98	2.88	5.69	1.63	-1.23	0.00	-1.84	-30.9
Minimum	-4.47	1.69	4.50	-2.55	-1.44	-0.13	-2.15	-43.7
Maximum	1.71	3.76	6.55	5.21	-0.82	0.12	-1.54	-20.0

Tab. 5

Predicted antimony (as % Sb_T), arsenic (as % As_T) and manganese (as % Mn_T) speciation in Rochus mine water based on measured Eh values (milivolts).

	Eh (mV)	Sb(OH) ₆ ⁻	SbO ₂ ⁻	HAsO ₄ ²⁻	H ₂ AsO ₄ ⁻	Mn ²⁺	MnHCO ₃ ⁺	MnSO ₄
13. 9. 2011	511	99.9	0.1	86.5	13.5	84.8	9.1	6.0
28. 2. 2012	421	99.9	0.1	92.4	7.6	83.9	9.5	6.6
12. 3. 2012	389	99.9	0.1	89.9	10.0	83.1	9.6	7.3
4. 4. 2012	396	99.9	0.1	89.1	10.8	83.7	8.9	7.4
24. 5. 2012	500	99.9	0.1	89.5	10.4	84.8	8.9	6.2
13. 9. 2012	411	99.9	0.1	90.6	9.4	82.4	9.5	8.1
5. 3. 2013	294	99.9	0.1	84.5	15.5	82.4	8.0	9.6
12. 3. 2013	238	99.9	0.1	86.8	13.2	78.1	7.3	14.6
19. 3. 2013	201	99.9	0.1	86.5	13.4	80.4	7.0	12.5
3. 4. 2013	364	99.9	0.1	85.7	14.3	83.9	8.2	7.8
9. 4. 2013	277	99.9	0.1	87.4	12.6	83.1	7.6	9.2
16. 4. 2013	176	99.9	0.1	89.2	10.8	75.5	6.9	17.5
23. 4. 2013	199	99.9	0.1	93.3	6.7	80.8	7.3	11.8
6. 5. 2013	481	99.9	0.1	85.6	14.4	84.8	8.8	6.3
14. 5. 2013	357	99.9	0.1	89.4	10.6	83.4	8.2	8.3
19. 6. 2013	531	99.9	0.1	77.2	22.8	85.3	8.5	6.2
11. 7. 2013	411	99.9	0.1	76.8	23.2	84.1	8.5	7.3
18. 9. 2013	326	99.9	0.1	84.2	15.8	82.4	8.4	9.2
3. 10. 2013	522	99.9	0.1	88.3	11.7	82.2	8.1	9.6

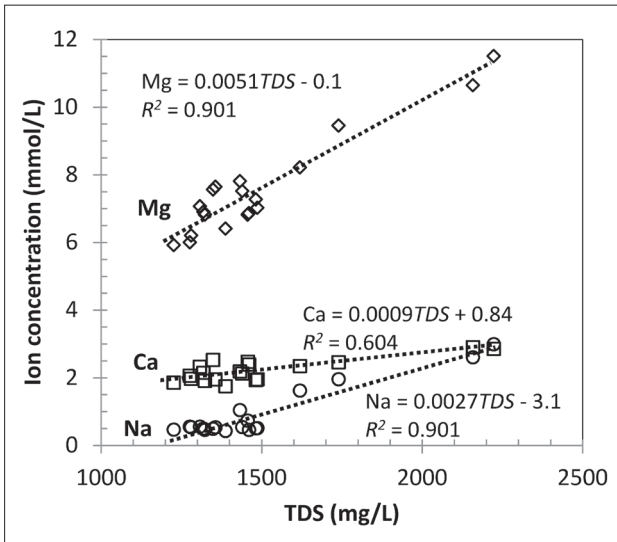


Fig. 13. Concentrations of main cations versus TDS content in mine water samples.

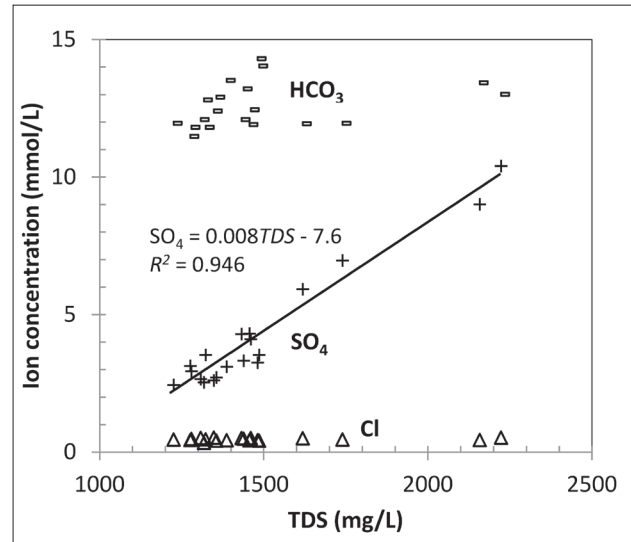


Fig. 14. Concentrations of main anions versus TDS content in mine water samples.

phate, calcium and magnesium are correlated positively. However, bicarbonate anion is negatively correlated with discharge. Statistically significant positive correlation is found also for secondary major ions as sodium and potassium, as well as for minor ions as arsenic (Fig. 8) and iron. On the other hand, manganese is negative correlated (Fig. 9). As *Eh* dependence reveals, mine water tends to reflect less oxidizing conditions in time of higher discharge. According to Spearman coefficient of correlation for pH value, mine water reaction is slightly more acidic during higher discharge stages (Tab. 2).

Geochemical calculation and modelling

Calculated SI values show that almost all samples are undersaturated (some of them are near equilibrium) with respect to the main ore carbonate mineral – siderite. Saturation with respect to other present carbonate ore minerals – ankerite and Fe-dolomite – varies around zero (Tab. 3). All samples are supersaturated with respect to possible secondary ore minerals: dolomite (SI = 0.8–2.1), calcite (SI = 0.2–0.8, Fig. 12) and rhodochrosite (SI = 0.4–0.9). Computed values of $\log(\text{PCO}_2)$ range from –2.15 to –1.53, suggesting that water composition is formed in open carbonate system, with relatively stable CO_2 partial pressure corresponding to conditions typical for the soil atmosphere (Tab. 4, Fig. 11).

The presented results of speciation calculations relate to most environmentally significant elements. They reveal that SbO_3^- represents almost all mass of total Sb-species in mine water samples (Tab. 5). The HAsO_4^{2-} prevails among As species, making up 77–93 % of total As content. Rest of total As content is represented by H_2AsO_4^- . Manganese is almost exclusively represented by Mn^{II} species, with a

simple ion Mn^{2+} making up about 80 % of its total Mn^{T} concentration and its remaining portion consist of complex $[\text{MnHCO}_3]^+$ cation and neutral $[\text{MnSO}_4]^0$ complex.

Water Quality

Comparing to Slovak drinking water standards (The Decree of the Ministry of Health of the Slovak Republic No. 247/2017), mine water of Rochus gallery exceeds “highest limit value” for antimony and arsenic and “limit value” for water electric conductivity and concentration of manganese, magnesium and sulphate. Limit exceeding for EC, Mn and Mg was documented in all and for SO_4 for almost all samples. From 28 samples taken, Sb content exceeded its limit value 5 $\mu\text{g/L}$ in 21 and As content exceeded its limit value 10 $\mu\text{g/L}$ in 6 samples.

Concerning protection of stream water quality (Regulation of the Slovak Government No. 96/2010 Coll.), mine water of Rochus gallery is risky due to its high Mn, As, Mg, SO_4 and TDS content. Contamination risk by manganese is most significant, as Mn concentration in mine water is permanently 3.0–5.5 times higher than limit for surface water. Recorded SO_4 values mostly slightly – but during high discharge seasons up to 4-times – exceeds limit value of 250 mg/L. Limit value for magnesium is exceeded only rarely, maximally 1.4 times. Arsenic concentration is usually (in 22 cases from 28) lower than limit value, its maximum exceedance is 2-fold. TDS values are 1.3–2.3 times higher than respective limit value of 110 mS/m. Antimony is not included in the list of surface water quality indicators. However, for surface water intended for the abstraction for drinking purposes, Sb limit value is 5 $\mu\text{g/L}$ for the best category A1 (only simple physical water treatment and disinfection needed)

and 25 µg/L for categories A2 and A3 (physico-chemical treatment or intensive physico-chemical treatment needed). Only one of the samples taken does not meet the limit for A2 and A3 category.

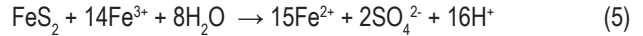
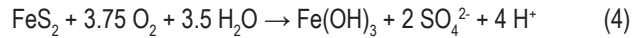
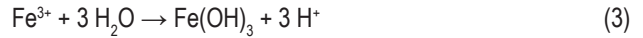
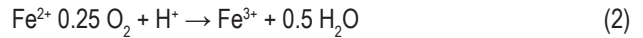
Discussion

Geochemical background of seasonal variability of mine water chemical composition

Variation of TDS content in the Rochus mine water is given mainly by variation of Mg and SO₄ content, while the Ca content fluctuation is less pronounced (Figs. 13, 14). The HCO₃ content is relatively stable. Also sodium content slightly contributes to TDS variation, being positively correlated with sulphate anion.

As gypsum or anhydrite practically absent in rock environment of Rudňany mine, sulphide minerals can be considered as the main source of sulphate anion in studied mine water. Although tetrahedrite and chalcopyrite are the most abundant sulphide minerals present there, pyrite is the most geochemically significant. Chalcopyrite is known as one of the most resistant sulphides to oxidation (Plumlee, 1999), with an oxidation rate of 1–2 orders of magnitude less than pyrite (Rimstidt et al., 1994). Tetrahedrite is reported as mineral whose leaching reaction proceeds slowly in acidic oxidative (Baláž, 2000) and also alkaline (Awe et al., 2010) conditions. Supposed little geochemical importance of chalcopyrite and tetrahedrite at studied site is also indicated by low Cu content in mine water (Tab. 1), as well as a rare occurrence of cuprite, malachite or azurite in oxidation zone of ore veins (Bernard, 1961). Immobilization of released Sb(V) by adsorption on Fe(hydr)oxides may not be significant here, as sorption maxima of Sb(V) occur at low pH values which extent up to pH 7 and desorption of Sb rapidly increases above

pH 7 (Tighe et al., 2005). Many studies presented that sulphide oxidation depends on a wide variety of factors, such as oxygen concentration, the presence of water, ferric ion concentration, acidity, microbial population and temperature (Nordstrom & Southam, 1997; Nordstrom & Alpers, 1999). Pyrite oxidation in water with dissolved oxygen may be written according to equation (1), where ferrous cation, sulphate anion and two protons are released. The overall process taking place in an aerobic environment, including, in addition to pyrite oxidation, also hydrolysis of Fe³⁺ and precipitation of iron hydroxide (eq.1 + eq.2 + eq.3 = eq.4), produces 4 protons per mol of pyrite. When present in the system, ferric iron becomes the primary oxidant of pyrite (Nordstrom et al., 1979; Moses et al., 1987; Ehrlich, 1996 (eq.5).



Strong positive correlation of Mg to SO₄ content in mine water (Fig. 13) suggests that pyrite oxidation is accompanied with the Mg-rich ore carbonates dissolution. During this process, the acid produced by pyrite oxidation is neutralized and in addition to magnesium, also calcium, iron and manganese are released into solution. Ore carbonates present in the Droždiak vein in Rudňany have a known typical composition (Cambel & Jarkovský, 1985) and dissolve according to the equations 6, 7 and 8 for siderite, ankerite and Fe-dolomite, respectively:

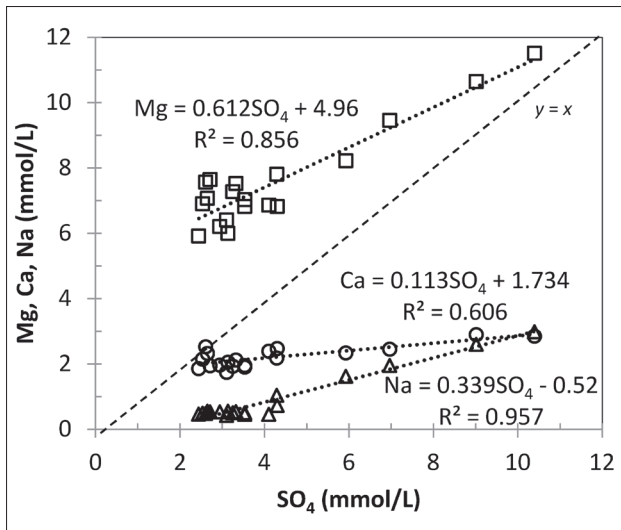


Fig 15. Magnesium, calcium and sodium content versus sulphate concentration in mine water samples.

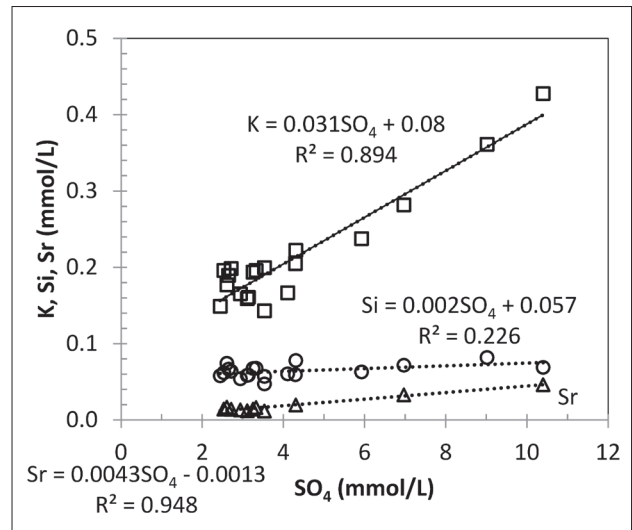
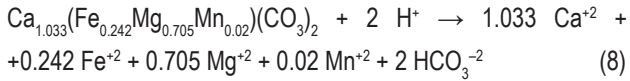
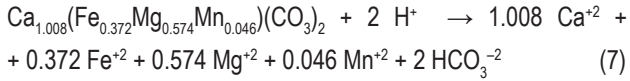
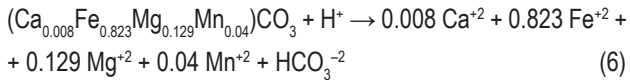


Fig 16. Potassium, silicon and strontium content versus sulphate concentration in mine water samples.



As the positive correlation of Na and K to SO₄ content suggests, also dissolution of aluminosilicate minerals (plagioclases, K-feldspars and micas) participates in this process. Sodium content can be derived from the dissolution of NaCl only at its lowest concentration levels (less than 0.6 mmol/L; Fig. 17). Higher sodium concentrations can be explained as plagioclase (Na-Ca feldspar with variable composition) acidic dissolution. Plagioclase andesine, for example, dissolves according to equation (9). Dissolved SiO₂ as co-product of aluminosilicate dissolution is not significantly correlated with SO₄ content, probably due to precipitation of quartz as suggested by its stable SI values close to zero (Tab. 4).

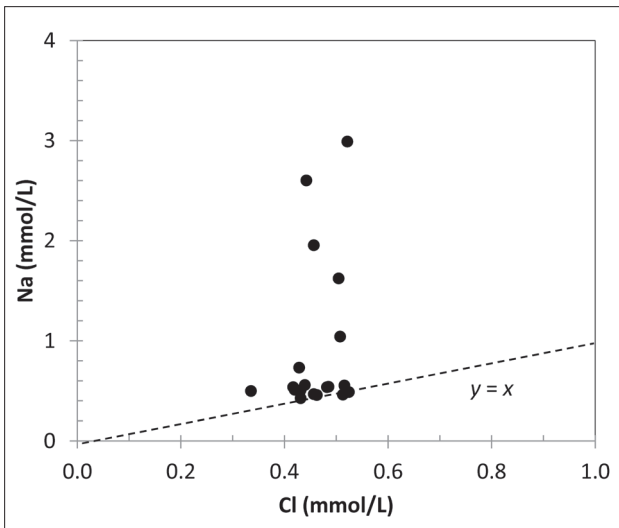
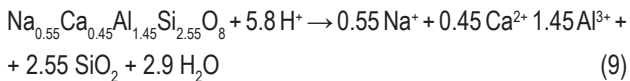


Fig. 17. Sodium versus chloride anion concentrations in mine water.

High content of bicarbonate anion in studied mine water can be considered as a result of ore carbonate dissolution, which can take place in two ways: 1. via sulphuric acid (eq. 1–5) and 2. via carbonic acid (proportional to pCO₂ of underground atmosphere). To determine the relative significance of these processes, it is useful to compare the ratio of relevant ions found in the samples with the ratio derived from governing chemical reactions.

In case the dissolution of carbonates is generated by oxidation of pyrite by oxygen, the ratio of ions HCO₃⁻/SO₄²⁻ released to the solution is 1 : 1 if no solid Fe(OH)₃ precipitate (equation 1), and 1 : 2 if all Fe(II) released from pyrite precipitate (equation 4). Most of mine water samples from flooded Rudňany mine, when shown on the graph, lie around the trend line 4 HCO₃⁻ = SO₄ (Fig. 18). It suggests that dissolution of ore carbonates via sulphuric acid is to a large extent accompanied by their dissolution via carbonic acid.

P(CO₂) values calculated from mine water samples taken from Rochus adit indicate that the conditions of an open carbonate system persist in the zone of water chemistry formation, with relatively stable CO₂ partial pressure of 10^{-2.1}–10^{-1.5} atm (Fig. 11). Such a level of P(CO₂) value is typical for the soil atmosphere conditions. However, P(CO₂) values, obtained from archival mine water samples, representing a mine atmosphere conditions at the time of mine operation (Fig. 7), indicate transition between air and soil atmosphere. Similar character of mine atmosphere can be expected also in the aeration zone of the current mine, which implies that the mine water acquires its final high and stable bicarbonate content in saturated zone of this mine.

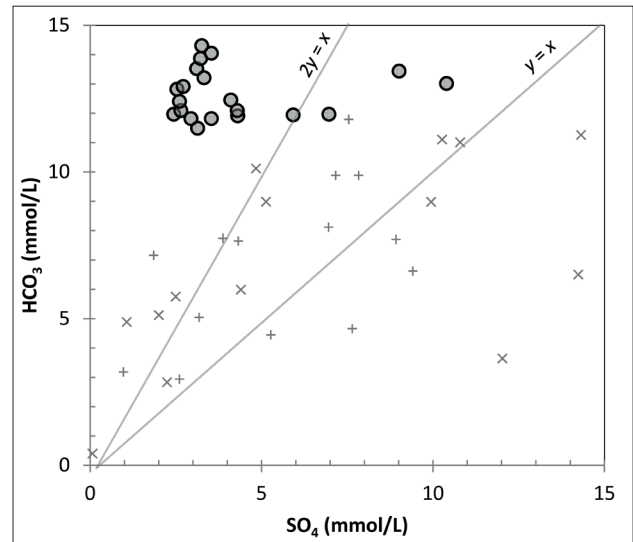


Fig. 18. Scatter plot of bicarbonate and sulphate content in mmol/L.

Forward modelling of mine water chemistry genesis with PHREEQC

For validation of former results and better understanding the evolution of mine water chemical composition at the Rochus mine, a series of simulations has been performed using PHREEQC computer program (Parkhurst & Appelo, 2013). Forward geochemical modelling was used for simulation of the chemical composition of a solution formed on the surface of carbonate minerals occurring

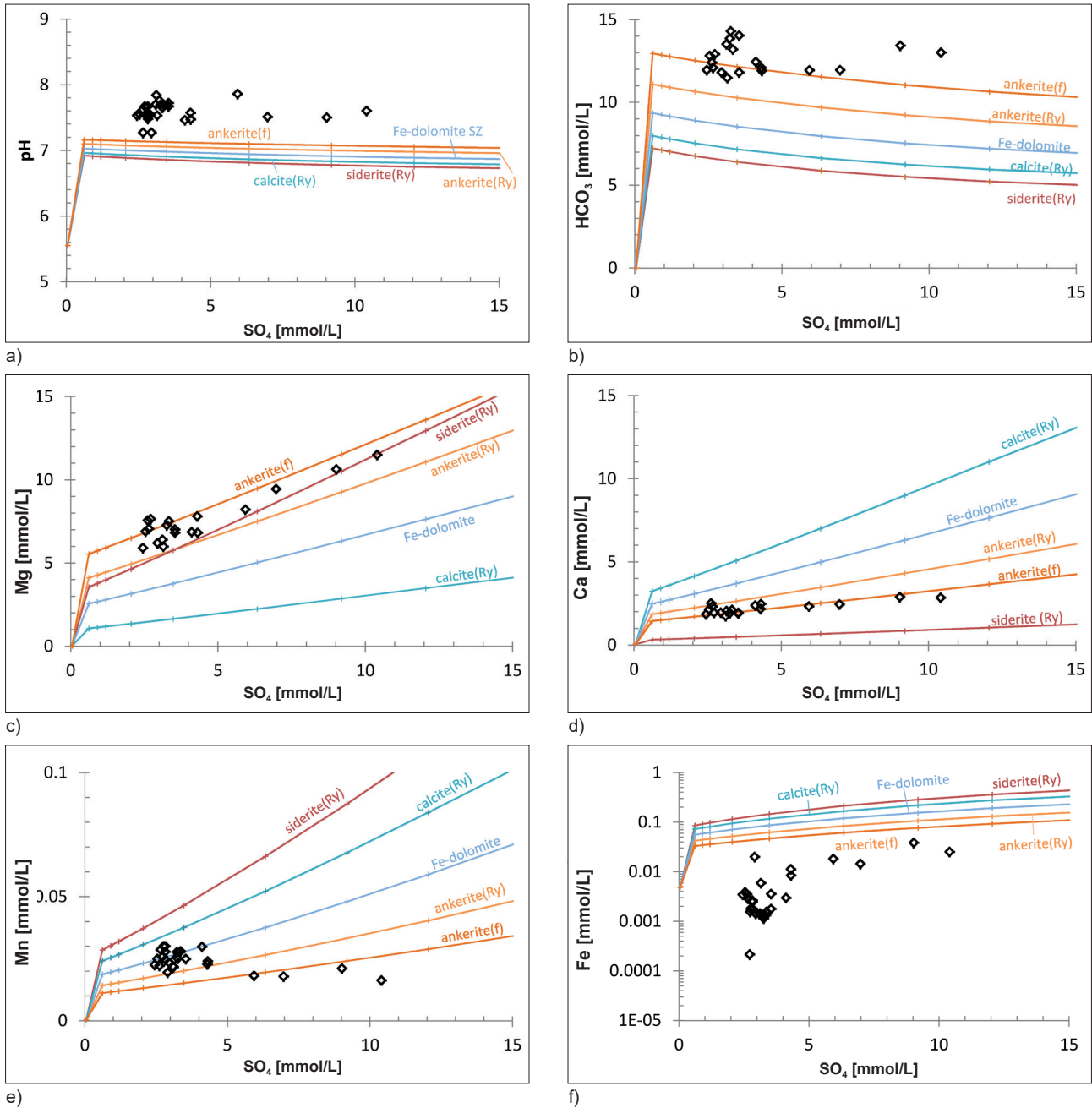


Fig. 19. pH values, bicarbonate, Mg, Ca, Mn and Fe versus sulphate concentrations in mine water samples (points) together with their simulations for variable extent of pyrite oxidation coupled to different ore carbonate minerals dissolution (solid lines), explanation in the text.

in the Droždiak vein, at different intensities of pyrite oxidation, with the possibility of precipitation of various solid phases, under different conditions of CO_2 presence. The simulation results were analysed by comparing them with macro-chemical composition (pH, Mg, Ca, Fe, Mn, SO_4 , HCO_3^-) of mine water samples.

The first series of simulations describes the dissolution of individual ore carbonate minerals via sulphuric acid released under different intensity of pyrite oxidation by oxygen, in open carbonate system (OCS model).

In the simulation, oxygen is added irreversibly to atmospheric water in nine amounts (0, 0.5, 1, 2.5, 5, 10, 15, 20, and 30 mmol). Pyrite and one of local ore carbonate minerals [siderite(Ry), ankerite(Ry), Fe-dolomite(Ry) or calcite(Ry)] are allowed to dissolve to equilibrium and carbon dioxide partial pressure (P_{CO_2}) is maintained at $10^{-1.4}$ atm (expected partial pressure in “main reaction zone” of mine system). In addition, calcite, siderite, rhodochrosite, nesquehonite, goethite, manganite and gypsum are allowed to precipitate if they become supersaturated.

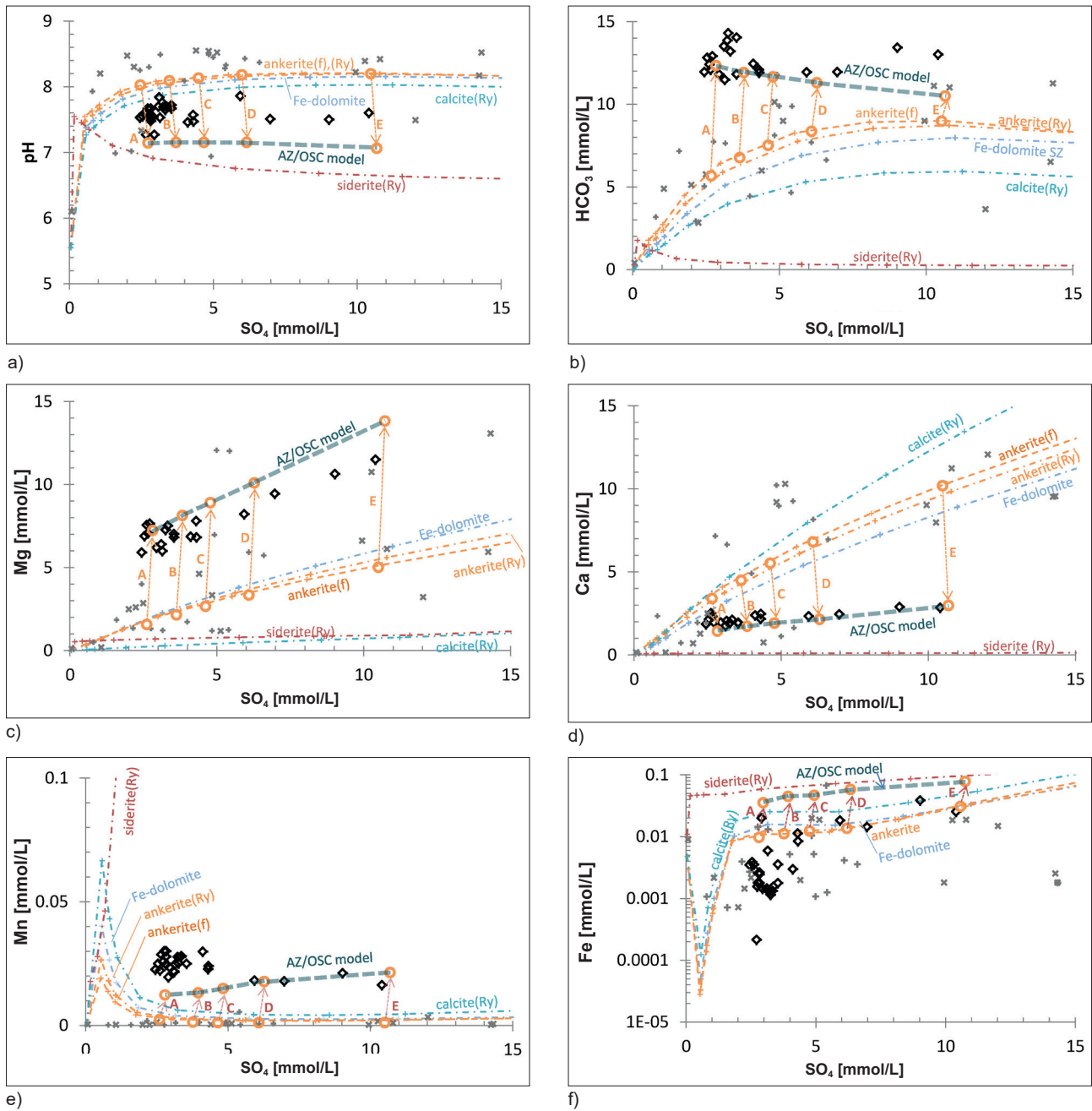


Fig. 20. pH values, HCO_3^- , Mg, Ca, Mn and Fe versus sulphate concentrations in mine water samples from the Rochus adit (bold black cross marks), archival samples of pumped mine water (grey plus marks) and water from non-flooded mine rooms on the Droždiak vein (cross marks) together with AZ model (dash dotted line) and AZ/OSC model simulations, for variable extent of pyrite oxidation. Arrows A to E indicate metamorphosis of hypothetical initial solutions, the chemical composition of which is the result of the AZ model, in the saturated zone of the mine (AZ/OSC model). Further explanation is in the text.

Of the model lines constructed from the results of this simulation, the “ankerite(Ry) line” has the best agreement with macro-chemical composition of mine water samples (Fig. 19). As this model slightly underestimates the bicarbonate content (Fig. 19b), the composition of ankerite with a better agreement of the simulation was sought. It was found that the model considering ankerite composition $Ca_{(Fe0.46}Mg_{0.50}Mn_{0.04})(CO_3)_2$ [ankerite(f)] well simulates

the concentration Mg, Ca, HCO_3^- and Mn. The pH and Fe concentration are simulated less accurately, but best compared to other minerals tested. It follows from the above that among the carbonate minerals present, ankerite can be considered crucial in the formation of the chemical composition of studied mine water.

The second series of simulations describes the dissolution of individual ore carbonate minerals via sulphuric

acid released under different intensity of pyrite oxidation by oxygen, in aeration zone of the mine (AZ model). The AZ model is simulated in two steps. In the first of them, oxygen is added irreversibly to atmospheric water in nine amounts (0, 0.5, 1, 2.5, 5, 10, 15, 20, and 30 mmol). Pyrite and one of local ore carbonate minerals are allowed to dissolve to equilibrium. In addition, gypsum, nesquehonite, rhodochrosite, goethite and manganite are allowed to precipitate if they become supersaturated. In the second step, to simulate conditions in aeration zone, P_{CO_2} is maintained at $10^{-2.6}$ atm and goethite, manganite and rhodochrosite is allowed to precipitate after reaching supersaturation. Model lines constructed for individual ore carbonate minerals (Fig. 20) show that the dissolution of none of them, or the mixing of the solutions formed by their dissolution (see $\text{HCO}_3\text{-SO}_4$ and Mg-SO_4 model lines on Fig. 19b, 19c), does not explain the composition of samples from flooded mine. However, the model lines constructed for the individual ore carbonate minerals are in relatively good agreement with concentrations of SO_4 , HCO_3 , Mg, Ca, Mn, Fe and pH (Fig. 20) found in mine water samples representing the aeration zone of the mine. These samples were taken from mine workings and from the water pumped from the mine during its operation (Bajtoš, 1999a). This model assumes that Ca-Mg carbonates do not precipitate from solution in significant amounts due to quick movement of water through mine workings, so water is supersaturated with respect to calcite and dolomite.

Hydrogeological conditions of the flooded Rudňany mine determine that mine water chemistry is formed in two main phases. The first phase takes place in aeration zone, where the water gravitationally descends through mine workings and their chemical transformation is described by AZ model. Due to the large spatial variability of the mineralogical composition of ore veins, a diverse chemical composition of individual effluents can be expected. These numerous small tributaries feed the saturation zone, in which they mix during the flow to the Mier shaft. The processes taking place in saturated zone represent the second phase of the mine water chemistry formation. Since oxygen is present in limited amounts below the water table, pyrite oxidation and subsequent acidity production is not intense here and therefore further dissolution of the carbonates can take place only via carbonic acid. Simulations by OCS model showed that high HCO_3 concentrations in the water flowing out of the Mier shaft can be explained by relatively high and stable CO_2 partial pressure of $P(\text{CO}_2) = 10^{-1.4}$ atm. However, since previous simulations with this model consider atmospheric water as the initial solution, another/third series of simulations was performed in which the chemical composition of the initial solution is derived from the simulations with AZ model. Five hypothetical initial solutions were defined: A and B solutions correspond to simulated smallest amounts

of oxygen consumed by pyrite oxidation, which have been documented at the time of low flow conditions. The C, D and E initial solutions represent middle, higher and highest amounts of oxygen consumed / flow conditions of the mine. Such combination of OCS and AZ model – OCS/AZ model – was used for simulations which assume that ankerite(f) is dominant carbonate mineral considering resulting chemical composition of mine water.

In these models, the relevant initial solution A–E is exposed to $P(\text{CO}_2)$ at $10^{-1.4}$ atm, ankerite(f) dissolve and goethite, manganite and rhodochrosite is allowed to precipitate after reaching supersaturation. Graphical connection of endpoints of individual AZ/OCS-A–E simulations on graphs (Fig. 20) creates AZ/OCS model lines representing expected final water chemical composition. The agreement of these model lines with the projection points of water samples from the Rochus adit is very good (taking into account the complexity of modelled environment) for HCO_3 , Mg and Ca. The measured pH values are 0.3–0.7 units higher than simulated ones, due to the release of free CO_2 from water during flow through Rochus adit from the Mier shaft to its mouth. Observed Mn concentrations (Fig. 20e) correspond well with those simulated for higher SO_4 levels, for lower ones they are approximately 2 times higher. Detected Fe concentrations (Fig. 20f) are in most cases more than 1 order of magnitude lower than simulated ones, probably due to Fe-ochre precipitation from water during the flow through the Rochus adit. As iron is very redox sensitive element, such a weak agreement was expected in given complex conditions.

The studied process of mine water chemistry formation also includes precipitation of solid / mineral phases. If we consider dissolving ankerite(f) as the only carbonate mineral in saturated zone in AZ model – in the range of measured low flow data corresponding to the consumption of 3.9–6.10 mmol/L of oxygen in the oxidation of pyrite – the amount of 1.2–1.9 mmol of pyrite and 3.3–4.6 mmol of ankerite(f) is dissolved and 2.8–4.9 mmol of goethite precipitate and 0.8–1.6 mmol CO_2 per liter of water is released into underground atmosphere. Subsequent mine water chemistry modification/transformation in saturated zone is predicted by AZ/OCS model. According to AZ/OCS-A simulation, 1 liter of initial solution dissolves 11.2 mmol of ankerite(f), 0.1 mmol of pyrite and 5.4 mmol of $\text{CO}_2(\text{g})$, while 13.1 mmol of calcite, 5.2 mmol of siderite and 0.4 mmol of rhodochrosite precipitates. With increasing TDS content in initial solutions (in water entering saturated zone), the amount of dissolved ankerite(f) and precipitated solid phases increases, while amount of CO_2 consumed decreases. The amount of dissolved pyrite is low and stable, as only oxygen brought by advective transport in the initial solution is available.

Most of the evaluated samples (20 of 28) of water discharging through the Rochus adit correspond to low or middle flow conditions, when 20–70 L/s of water flowed out of the mine. The SO_4 content in this group of samples varies from 235 to 340 mg/L (2.44–3.54 mmol/L), which corresponds to simulated conditions when 3.2–5.1 mmol/L (OCS model) or 3.9–6.1 mmol/L (AZ model) of oxygen is consumed in the oxidation of pyrite coupled to ankerite(f) dissolution in aeration zone of the mine. Whereas at water saturated conditions the oxygen concentration is limited to solubility of oxygen in water, or 0.26–0.40 mmol/L at 25–5 °C, such an intensity of oxidation must be forced not only by advective transport of oxygen with atmospheric water, but also by air convection or diffusion.

The presented analysis of hydrochemical data suggests that chemical composition of the flooded Rochus mine water arises in three main phases (Fig. 21). The first (A phase) takes place in aeration zone of the mine, where the oxidation of pyrite by oxygen and the ankerite dissolution dominate. The saturated zone of the mine is probably dominated by the dissolution of ankerite intensified by the supply of deep CO_2 (zone B), which causes an increase and stabilization of HCO_3^- content in the mine water. These two phases of mine water genesis are permanent and during low flow conditions lead to a relatively stable mine water composition. During high flow conditions, mine water of shallow circulation probably mixes with stagnant, higher mineralized water (C phase), which causes an

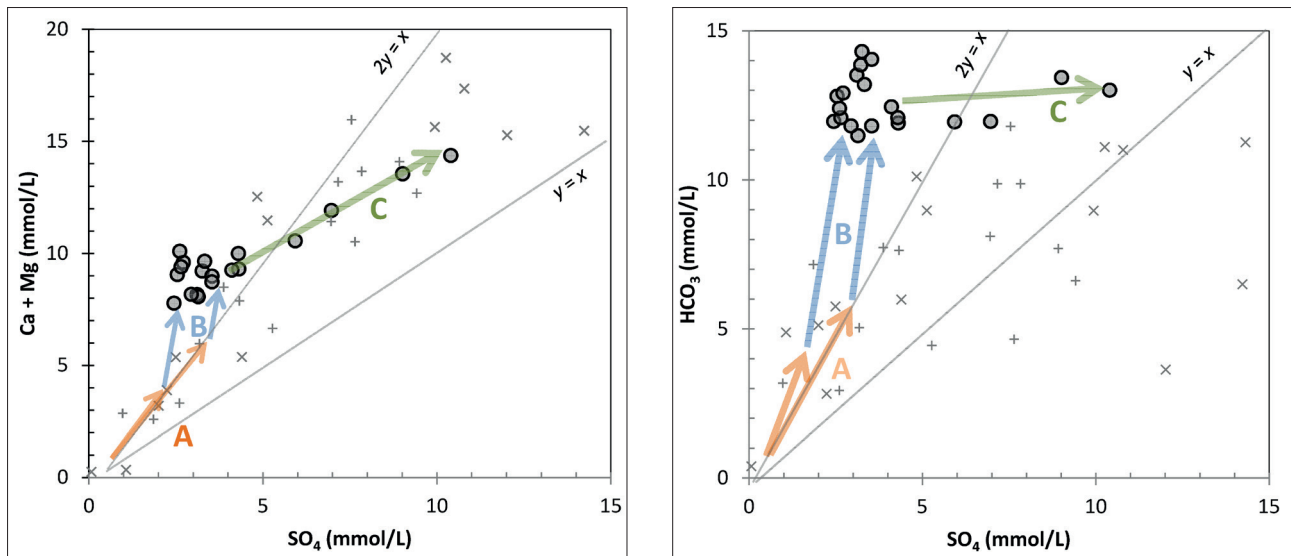


Fig. 21. Concentrations of $\text{Ca}^{2+} + \text{Mg}^{2+}$ and HCO_3^- versus SO_4^{2-} in mine water outflowing from flooded mine (full circles on the chart) as the result of three-phase (A, B, C) evolution. Archival samples of pumped mine water are represented by grey plus marks and water from non-flooded mine rooms on the Droždiak vein by cross marks. Further explanation is in the text.

Only 8 of the evaluated samples correspond to high flow conditions when the SO_4 content reaches up to 1 g/L (10.4 mmol/L). This would correspond to 17 or 20 mmol/L of oxygen consumed, according to models OCS and AZ/SZ, respectively. However, in such flow conditions, the influence of other factors can also be expected. An increase in concentrations of macro-chemical components during high flow rates may be due to rapid dissolution of soluble salts which have gradually accumulated in aeration zone during precipitation-free periods. However, these salts are also a product of sulphide oxidation. Another possible explanation is the mobilization of more mineralized stagnant water from deeper or less hydraulically connected parts of the mine, where water stratification occurs. Taking into account high and relatively stable bicarbonate content in mine water, the second from these options seem to be more likely.

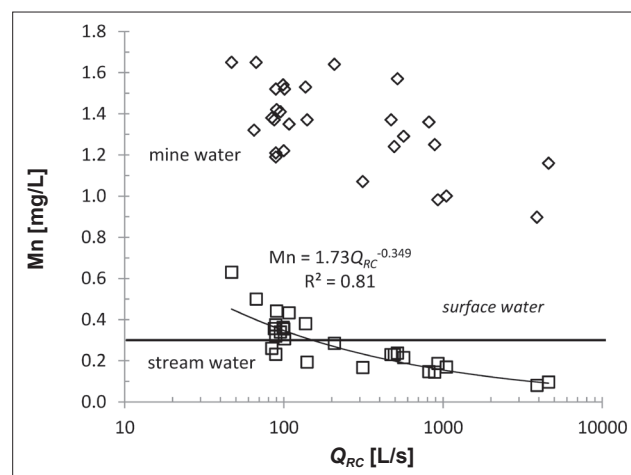


Fig. 22. Manganese concentration in mine water samples (rhombus marks) and calculated manganese concentration in water of the Rudňanský potok creek (square marks) in relation to discharge of this creek (Q_{RC}).

significant increase in SO_4 , Mg, Ca content, as well as to less significant increase in content of other compounds.

The performed simulations show that the concentrations of calcium, iron and manganese in mine water are significantly controlled by precipitation of solid phases. In simulations performed in this study, the choice of calcite precipitation showed better match with observations than aragonite precipitation. However, aragonite is reported to occur in the form of crusts and aggregates on walls of mine workings (Cambel & Jarkovský, 1985). Concerning Fe- and Mn-precipitates, limonite, goethite and psilomelane are mentioned (Bernard, 1961). Regarding the iron content, better simulation results were obtained when considering precipitation of goethite than ferrihydrite. As iron is very redox sensitive element, the achieved low agreement of the simulations with observations was expected in given complex conditions. Manganese is less sensitive in this respect, so the agreement of simulations with measurements is much better – provided that rhodochrosite precipitates (manganite MnOOH is not thermodynamically forced to precipitate according to the simulation results).

Environmental issues

Mine water currently flows out from the Rochus adit directly into the stream, without any treatment. According to SHMI observations, discharge of the Rudniansky creek reaches only 50 L/s during periods of lowest flow conditions. Whereas mine and stream discharges fluctuate almost synchronously (Fig. 4), the mine water with minimum discharge of 13.4 L/s makes up approximately 25 % of the stream discharge in such periods. The proportion of mine water in the stream decreases during higher flow conditions, but positive impact of dilution is partially reduced because of the effect of positive correlation of hazardous substances content with mine water discharge (Tab. 5, Figs. 7, 8 and 10). However, this is not the case with manganese, which correlates negatively (Fig. 9). Manganese concentration in the Rudniansky potok creek in a place under the inflow of mine water, calculated using mixing equation, vary between 0.081 and 0.631 mg/L. It negatively correlates with the Rudniansky potok creek discharge (Fig. 22) suggesting that surface water quality limit is usually exceeded at stream discharges below 150 L/s – which usually last 180 days a year. Concentration of sulphate anion drops to 50–110 mg/L after dilution, well below the limit. Also TDS and Mg content are attenuated by dilution effectively.

Manganese is considered less of an environmental hazard than many others metals and evidence from the literature suggests that the acute and chronic toxicity of Mn to many freshwater biota was low in the mg/L range (Harford et al., 2015). However, more recent studies have reported some particularly sensitive species (Peters et al.,

2010; Harford et al., 2015). Mine water brings manganese to the Rudniansky potok creek mainly in the form of simple Mn^{2+} cation (Tab. 5) which is considered to be more toxic than complex $[\text{MnSO}_4]^0$ and $[\text{MnHCO}_3]^+$ species present. The Mn^{2+} portion in total Mn^{T} concentration is relatively stable over time, but slightly negatively correlates with mine water discharge (Fig. 23).

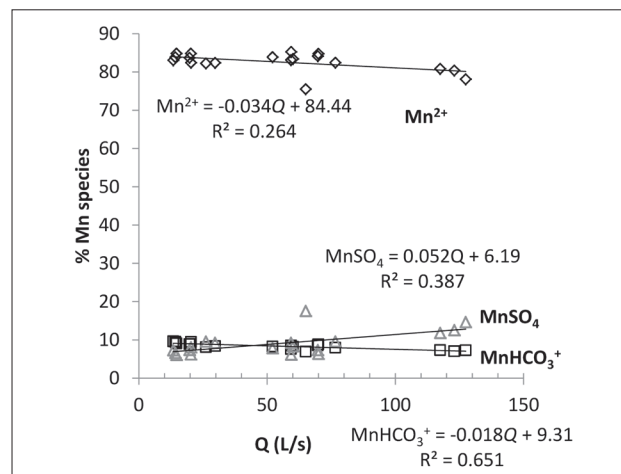


Fig. 23. Distribution of Mn species in mine water samples in relation to mine water discharge.

Arsenic from mine water is diluted in the stream water to concentrations of 2–4 $\mu\text{g/L}$. Speciation modelling suggests that As occurs in mine water in the form of pentavalent arsenate As(V) species, when major species HAsO_4^{2-} (77–93 % of total content) dominates over H_2AsO_4^- (7–23 %; Tab. 5). The proportion of these components is not subject to hydrologic regime or seasonal variation (Fig. 24). After dilution in stream water highly saturated with oxygen, arsenic remains in oxidation state (V). Arsenates are generally less soluble and toxic comparing to arsenites As(III) (Korte & Fernando, 1991) and therefore pose less environmental risk. If water treatment is required, arsenates can be more readily removed from the water than arsenites.

Antimony is considered a metalloid non-essential for optimal functioning of biological processes in an organism which, at high concentrations, is more toxic than As (Elinder & Friberg, 1979; Reimann & Caritat, 1998). The leaching of Sb from Sb-containing minerals and rocks may therefore have important ecotoxicological implications. Sb(III) is reported to be more toxic than Sb(V), inorganic species are generally more toxic than organic ones (Stemmer, 1976; WHO, 2008; Filella et al., 2009). Antimony concentration 3–26 $\mu\text{g/L}$ in the mine water of Rochus adit decreases after mixing with the water of the stream to 3–11 $\mu\text{g/L}$. Such a concentration level classifies this mixed water in category A2 in the classification of surface water intended for the abstraction for drinking purposes (Regulation of

the Slovak Government No. 96/2010 Coll.). As can be expected from previous studies at Sb-contaminated sites (Johnson et al., 2005; Takaoka et al., 2005; Okkenhaug et al., 2011), antimony occurs in studied mine water almost exclusively in the form of pentavalent oxyanion, $\text{Sb}(\text{OH})_6^-$ species (Tab. 5).

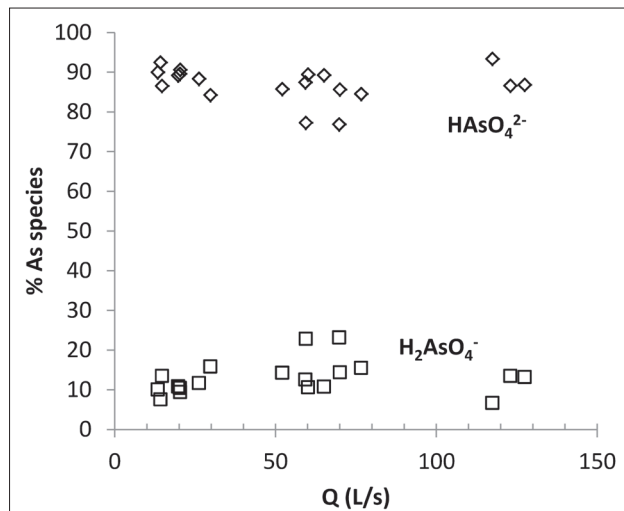


Fig. 24. Distribution of As species in mine water samples in relation to mine water discharge.

Elevated concentrations of Mn, As and Sb caused by the inflow of mine water into the Rudňany potok creek gradually decrease during its downward flow due to natural processes. The most important factors are dilution by hidden karst groundwater inflows and hydrochemical processes such as precipitation of solid phases and sorption. At the discharge gauging site located 2.7 km below the Rochus adit mouth, contents of Mn 0.10–0.15 mg/L, As 2–11 µg/L and Sb 9–15 µg/L were found by state monitoring of mining impact on the environment (www.geology.sk) in stream water in the years 2012–2013.

Conclusions

Observation of mine water hydrochemical regime at the flooded Rudňany mine (Volovské vrchy Mts, eastern Slovakia) connected to siderite-sulphidic veins hosted by Paleozoic metamorphic rocks revealed positive correlation of the macro-chemical components with mine water discharge. Geochemical calculations and forward modelling based on mine water samples suggest that the mine water chemical composition is formed in three main phases. In the aeration zone of the mine, pyrite oxidation coupled to ankerite dissolution and goethite precipitation in relatively low $\text{P}(\text{CO}_2)$ conditions is the main geochemical process (A phase in Fig. 21), although most abundant ore minerals are tetrahedrite and chalcopyrite among present sulphides and siderite among carbonates. In saturated zone

of the mine (phase B), ankerite dissolution combined with calcite and siderite precipitation in stable, relatively high $\text{P}(\text{CO}_2)$ conditions (open carbonate system – deep CO_2 supply?) leads to an increase of magnesium, decrease of calcium and stabilization of high hydrocarbonate ion content in water flowing out of the mine. During high flow conditions, mine water of shallow circulation probably mixes with stagnant, higher mineralized water (C phase), which causes a significant short-term increase in SO_4 , Mg, Ca content, as well as to less significant increase in content of other compounds.

Concerning protection of stream water quality, studied mine water is risky due to its high Mn, As, Mg, SO_4 and TDS content. Water quality of the Rudňany potok creek into which the water from the mine flows is endangered mainly by manganese – presented data suggest that its surface water quality limit is usually exceeded for 180 days a year. Concentration of sulphate anions, magnesium and TDS, as well as arsenic and antimony, drops to levels well below the quality limits after dilution.

Studied mine water is not suitable for drinking purposes due to permanently high TDS, Mn, Mg and SO_4 content, as well as the arsenic and antimony contents occasionally do not meet the limits. Possible future utilization of this mine water for drinking will require, in addition to reducing the concentration of above mentioned elements, also filtration of colloidal ferric (oxy)hydroxides.

The above example clearly demonstrates that detailed knowledge of seasonal hydrochemical regime is necessary for understanding the mine water genesis. It is also indispensable for accurate assessment of the impact of mine water on surface water quality, as well as design of water treatment technologies.

Acknowledgement

The results of this study were obtained owing to the project support of the Ministry of Environment of the Slovak Republic, namely the project “Partial monitoring system – Geological factors”, what is gratefully acknowledged by the author. Suggestions and comments of reviewers Renáta Fľaková and Peter Malík contributed to quality of primary manuscript.

References

- AL, A. A., MARTIN, CH. J & BLOWES, D. W., 2000: Carbonate-mineral/water interactions in sulfide-rich mine tailings. *Geochim. Cosmochim. Acta*, 64, 23, 3933–3948.
- AWE, S. A., SAMUELSSON, C. & SANDSTRÖM, A., 2010: Dissolution kinetics of tetrahedrite mineral in alkaline sulphide media. *Hydrometallurgy*, 103, 167–175.
- BAJTOŠ, P., 1993a: The northern part of the Rudňany ore field, hydrogeological study (in Slovak). *Manuscript. Bratislava, archive SGIDŠ*.

- BAJTOŠ, P., 1993b: Novoveská Huta – Rudňany, mine waters. Hydrogeological survey report (in Slovak). *Manuscript. Bratislava, archive SGIDŠ*.
- BAJTOŠ, P., 1999a: Mine water genesis in the Rudňany ore field (Podmienky tvorby banských vôd Rudňanskeho rudného poľa). *Podzemná voda, 2, 74–80*.
- BAJTOŠ, P., 1999b: Impact of mine working on the hydrogeological conditions of the Rudňany ore field. Proceedings: XXIX. Congress of IAH – Hydrogeology and land use management, Bratislava – Slovakia, 733–738.
- BAJTOŠ, P., PRAMUKA, S. & RAPANT, S., 2012: Partial monitoring system – Geological factors. Subsystem 04: Impact of mining on the environment (in Slovak). *Manuscript. Bratislava, archive SGIDŠ*.
- BAJTOŠ, P., 2016: Mine Waters in the Slovak Part of the Western Carpathians – Distribution, Classification and Related Environmental Issues. *Slovak Geol. Mag., 16, 1, 139–158*.
- BAJTOŠ, P., ZÁHOROVÁ, L., RAPANT, S. & PRAMUKA, S., 2012: Geological monitoring of mining influence on the environment in risk-bearing Slovak areas in years 2007–2011 (in Slovak with English summary). *Miner. Slov., 44, 375–392*.
- BALÁŽ, P., 2000: Extractive Metallurgy of Activated Minerals. *Amsterdam, Elsevier*.
- BERNARD, J. H., 1961: Mineralogie und Geochemie der Siderit – Schwerspatgänge mit Sulfiden in Gebiet von Rudňany (Tschechoslowakei). *Geol. Práce (Bratislava), 58, 1–222*.
- BODIŠ, D., LOPAŠOVSKÁ, M. & RAPANT, S., 2000: Chemical composition of snow pack in Slovakia – the results of 25 years monitoring (in Slovak with English summary). *Podzemná voda, VI, 2, 172–173*.
- CAMBEL, B. & JARKOVSKÝ, J. (Eds.), 1985: Rudňanske rudné pole – geochemicko-metalogenetická charakteristika (The Rudňany ore field – geochemical-metallogenetic characteristics) (in Slovak with English summary). *Bratislava, Veda*.
- DOLD, B., 2010: Basic Concepts in Environmental Geochemistry of Sulfidic Mine-Waste Management. In: Sunil Kumar (ed.): Waste Management. *IntechOpen, 1–242*. ISBN 978-953-7619-84-8.
- EHRlich, H. L., 1996: Geomicrobiology. *New York, Dekker, 719 pp*.
- ELINDER, D. G. & FRIBERG, L., 1979: Handbook on the Toxicology of Metals (Friberg, L., Nordberg, G. F. & Vouk, V. B. – eds.). *Amsterdam, Elsevier, 283 pp*.
- FILELLA, M., WILLIAMS, P. A. & BELZILE, N., 2009: Antimony in the environment: knowns and unknowns. *Environ. Chem., 6, 95–105*.
- GRECULA, P., 1982: Gemerikum – segment riftogénneho bazénu Paleotetýdy (in Slovak with English summary). *Bratislava, Alfa, 1–263*.
- GRECULA, P., KOBULSKÝ, J., GAZDAČKO, L., NÉMETH, Z., HRAŠKO, L., NOVOTNÝ, L., MAGLAY, J., PRAMUKA, S., RADVANEC, M., KUCHARIČ, L., BAJTOŠ, P. & ZÁHOROVÁ, L., 2011: Vysvetlivky ku geologickej mape Spišsko-gemerského rudohoria 1 : 50 000. *Bratislava, Št. Geol. Úst. D. Štúra, 1–308*.
- GRECULA, P. (Ed.), ABONYI, A., ABONYIOVÁ, M., ANTAŠ, J., BARTALSKÝ, B., BARTALSKÝ, J., DIANIŠKA, I., DRNŽÍK, E., ĎUĎA, R., GARGULÁK, M., GAZDAČKO, L., HUDÁČEK, J., KOBULSKÝ, J., LÖRINZ, L., MACKO, J., NÁVESŇÁK, D., NÉMETH, Z., NOVOTNÝ, L., RADVANEC, M., ROJKOVIČ, I., ROZLOŽNÍK, L., ROZLOŽNÍK, O., VARČEK, C. & ZLOCHA, J., 1995: Mineral deposits of the Slovak Ore Mountains. Vol. 1. *Bratislava, Geocomplex, 834 pp*.
- HARFORD, A. J., MOONEY, T. J., TRENFIELD, M. A. & VAN DAM, R. A., 2015: Manganese (Mn) toxicity to tropical freshwater species in low hardness water. *Environ. Toxicol. Chem., 34, 12, 2856–2863*. DOI: /10.1002/etc.3135/.
- JOHNSON, C. A., MOENCH, H., WERSIN, P., KUGLER, P. & WENGER, C., 2005: Solubility of antimony and other elements in samples taken from shooting ranges. *J. Environ. Qual., 34, 248–254*.
- KORTE, N. E. & FERNANDO, Q., 1991: A review of arsenic (III) in groundwater. *Crit. Rev. Environ. Contr., 21, 1–39*.
- Landscape Atlas of the Slovak Republic, 2002: 1st ed. *Bratislava, Ministry Environ Slovak Rep. – Banská Bystrica, Slovak Environ. Agency, 344 pp*.
- MOSES, C. O., NORDSTROM, D. K., HERMAN, J. S. & MILLS, A. L., 1987: Aqueous pyrite oxidation by dissolved oxygen and by ferric iron. *Geochim. Cosmochim. Acta, 51, 1561–1571*.
- MELLO, J., FILO, I., HAVRILA, J., IVANIČKA, J., MADARÁŠ, J., NÉMETH, Z., POLÁK, M., PRISTAŠ, J., VOZÁR, J., KOŠA, E. & JACKO, S., 2000: Geological map of the Slovenský raj – Galmus Mts. and Hornád Depression at a scale of 1 : 50 000. *Bratislava, Ministry Environ. Slovak Rep. – St. Geol. Inst. D. Štúr*.
- NORDSTROM, D. K., JENNE, E. A. & BALL, J. V., 1979: Redox equilibria of iron in acid mine waters. In: Jenne, E. A. (ed.): Chemical modeling in aqueous systems. *Amer. Chem. Soc., Symp. Washington, D.C., 93, 51–79*.
- NORDSTROM, D. K. & ALPERS, C. N., 1999: Geochemistry of acid mine waters. In: Plumlee, G. S. & Logsdon, M. J. (Eds.): The Environmental Geochemistry of Mineral Deposits. *Rev. Econ. Geol., 6A, Soc. Econ. Geol., 133–160*.
- NORDSTROM, D. K. & SOUTHAM, G., 1997: Geomicrobiology of sulphide mineral oxidation. In: Banfield, J. F. & Nealson, K. H. (Eds.): Geomicrobiology: Interactions between Microbes and Minerals. *Rev. Miner., 35, 361–390*.
- OKKENHAUG, G., ZHU, Y.-G., LUO, L., LEI, M., LI, X. & MULDER, J., 2011: Distribution, speciation and availability of antimony (Sb) in plants from an active Sb mining area. *Environ. Pollution, 159, 2427–2434*.
- PARKHURST, D. L. & APPELO, C. A. J., 2013: Description of input and examples for PHREEQC version 3 – A computer program for speciation, batch-reaction, one-dimensional transport, and inverse geochemical calculations. *U.S. Geol. Surv. Techn. Methods, 6, A43, 497 p*. (available only at <http://pubs.usgs.gov/tm/06/a43/>).
- PETERS, A., CRANE, M., MAYCOCK, D., MERRINGTON, G., SIMPSON, P., SOROKIN, N. & ATKINSON, C., 2010: Proposed EQS for Water Framework Directive Annex VIII substances: manganese (total dissolved). *Bristol, United Kingdom, Environ. Agency*.
- PLUMLEE, G. S., 1999: The environmental geology of mineral deposits. In: Plumlee, G. S. & LOGSDON, M. J. (Eds.): *Rew. Econ. Geol. The environmental geochemistry of ore deposits. Part A: Processes, Techniques Health Iss., 6A, 71–116*.
- PLUMMER, L. N., 1992: Geochemical Modeling of Water-Rock Interaction: Past, Present, Future. In: Kharaka, Y. K. & Maest, A. S. (Eds.): *Water-Rock Interaction, 1, Balkema, Rotterdam, Brookfield, 858 pp*.

- RADVANEČ, M. & GONDA, S., 2019: Genetic model of Permian hydrothermal mineralisation in Gemeric unit (W. Carpathians) from the deep-seated zone of anatectic melting to volcanic-exhalative SedEx mineralisation on the surface. *Miner. Slov.*, 52, 109–156.
- Regulation of the Slovak Government No. 96/2010 Coll. laying down requirements for achieving good water status.
- REIMANN, C. & DE CARITAT, P., 1998: Chemical elements in the environment – Factsheets for the Geochemist and Environmental Scientist. *Berlin – Heidelberg, Springer*.
- RIMSTIČ, J. D., CHERMAK, J. A. & GAGEN, P. M., 1994: Rates of reaction of galena, sphalerite, chalcopyrite and arsenopyrite with Fe(III) in acidic solutions. In: Alpers, C. N. & Blowes, D. W. (Eds.): Environmental geochemistry of Sulfide Oxidation. ACS Symposium Series. *Washington, DC*, 550, 2–13.
- STEMMER, K. L., 1976: Pharmacology and toxicology of heavy metals: antimony. *Pharm. Ther.*, A, 1, 157–160.
- TAKAOKA, M., FUKUTANI, S., YAMAMOTO, T., HORIUCHI, M., SAKATA, N., TAKEDA, N., OSHITA, K., YONEDA, M., MORISAWA, S. & TANAKA, T., 2005: Determination of chemical form of antimony in contaminated soil around a smelter using X-ray absorption fine structure. *Analyt. Sci.*, 21, 769–773.
- The Decree of the Ministry of Health of the Slovak Republic No. 247/2017 on requirements for drinking water quality, drinking water quality control, monitoring and management risk of drinking water supply).
- TIGHE, M., LOCKWOOD, P. & WILSON, S., 2005: Adsorption of antimony(V) by floodplain soils, amorphous iron(III) hydroxide and humic acid. *J. Environ. Monit.*, 7, 1177–1185.
- VOZÁROVÁ, A. & VOZÁR, J., 1988: Late Paleozoic in the West Carpathians. *Bratislava, Geol. Úst. D. Štúra*, 314 pp.
- WHO World Health Organisation, 2008: Guidelines for Drinking-water Quality. 3rd ed. incorporating the 1st and 2nd addenda. 1, *Recommendations*, 668 pp.

Využitie analýzy sezónneho hydrochemického režimu vody v zatopenej rudnej bani Rudňany na lepšie pochopenie jej genézy a presnejší odhad jej vplyvu na kvalitu vody v povrchovom toku

Na Slovensku sa nachádzajú stovky opustených hlbinných baní, ktoré sú pozostatkom historickej, ale aj nedávnej ťažby nerastov. Spomedzi 14 vyčlenených banskoložiskových oblastí je najväčšie gemerské pásmo so Spišsko-gemerským rudohorím. Bol v ňom zdokumentovaný výskyt 656 zdrojov banskej vody so sumárnou výdatnosťou 663 L/s (Bajtoš, 2016). Až 535 z nich s celkovou výdatnosťou 456 L/s sa sprístupnilo na ťažbu sideritovo-sulfidických žíl vyvinutých v metamorfovaných horninách paleozoika gemerika. Keďže chemické zloženie týchto zdrojov banskej vody je pomerne variabilné, niektoré z nich môžu slúžiť ako zdroje pitnej vody. Mnohé však predstavujú environmentálne riziko, a to najmä pre anomálny obsah As, Sb, Mn a SO₄. Poznatky o chemickom zložení týchto zdrojov sú zatiaľ založené len na opakovaných laboratórnych analýzach, takže ich hydrochemický režim je zdokumentovaný len čiastočne. Poznanie rozsahu kolísania rizikových prvkov v čase je dôležité pri hodnotení z hľadiska praktického využitia aj pri hodnotení ich environmentálneho rizika. Navyše, môže významne prispieť k pochopeniu geochemických procesov prebiehajúcich v banskom kolektore, ktorých výsledkom je chemické zloženie vody vytekajúcej z bane. Preto sa v rokoch 2012 a 2013 sledoval hydrochemický režim banskej vody zatopenej bane Rochus v Rudňanoch, jednej z najväčších baní v Spišsko-gemerskom rudohorí. Monitoring bol zameraný na dokumentáciu intenzity sezónnych zmien chemického zloženia banskej vody vytekajúcej do Rudňanskeho potoka. Interpretácia získaných údajov smerovala k prevencii závislosti zmien koncentrácie zložiek rozpustených

v banskej vode od jej meniacej sa výdatnosti, identifikácii geochemických procesov prebiehajúcich v banskom kolektore a hodnoteniu miery ovplyvnenia kvality vody Rudňanskeho potoka banskou vodou.

Regresná analýza vzťahu medzi koncentráciou prvkov rozpustených v banskej vode (nezávislé premenné) a jej výdatnosťou (závislá premenná) ukázala, že koncentrácia hlavných iónov Mg, Ca, SO₄ a vedľajších iónov Na, K a As štatisticky významne rastie s rastúcou výdatnosťou (tab. 2, obr. 7, 8). Obsah HCO₃ a Mn (obr. 9) s rastúcou výdatnosťou mierne klesá. Z hľadiska požiadaviek na pitnú vodu najvyššiu medznú hodnotu vo väčšine vzoriek presahuje obsah Sb a vo viacerých vzorkách obsah As. Medznú hodnotu presahujú hodnoty EC a obsah Mn, Mg a SO₄.

Geochemické výpočty a úvahy naznačujú, že pri tvorbe chemického zloženia banskej vody sa uplatňuje rozpúšťanie prítomných rudných karbonátov ako ankerit a siderit (rovnice 1 – 8, obr. 15 a 16) a rozpúšťanie alumosilikátov (rovnica 9), intenzifikované oxidáciou pyritu, ale aj oxidom uhličitým v otvorenom karbonátovom systéme (obr. 11 a 18). Simulácie vývoja chemického zloženia banskej vody tieto predpoklady potvrdzujú, pričom identifikujú ankerit ako geochemicky dominantný rudný karbonát (obr. 19, 20). Výsledkom geochemickej analýzy je predkladaný trojfázový model tvorby chemického zloženia banskej vody vytekajúcej z bane Rochus. Prvá fáza prebieha v nenasýtenej zóne bane, pričom najvýznamnejšími procesmi sú rozpúšťanie ankeritu a oxidácia pyritu. Druhá fáza prebieha v nasýtenej zóne bane, pričom dominuje roz-

púšťanie ankeritu, ktoré je pravdepodobne intenzifikované prínosom hlbinného CO₂. Uvedené dva procesy prebiehajú permanentne počas nižších vodných stavov a vedú k relatívne stabilnému chemickému zloženiu banskej vody. V období vyšších vodných stavov významne narastá koncentrácia SO₄, Mg, Ca, ale aj Na a As, pravdepodobne ako dôsledok primiešania vyššie mineralizovanej vody stagnujúcej v hlbších alebo hydraulicky viac izolovaných častiach zatopenej bane.

Banská voda vyteká z bane do miestneho Rudnianskeho potoka a negatívne ovplyvňuje jeho kvalitu hlavne

prínosom mangánu. Jeho obsah v toku prevyšuje environmentálny limit v obdobiach, keď je prietok toku nižší ako 150 L/s. Zvyčajne to trvá 180 dní v roku. Anomálny obsah SO₄, Mg, As a Sb v banskej vode je po jej vstupe do potoka dostatočne zriedený a neprekračuje environmentálne limity.

Doručené / Received: 2. 6. 2022

Prijaté na publikovanie / Accepted: 21. 6. 2022

Relation of groundwater quality and peat deposits in Tay Ninh province, Vietnam

HUYNH PHU¹, LE CANH TUAN^{2*}, NGUYEN LY NGOC THAO¹ and HUYNH THI NGOC HAN³

¹ HUTECH University; 475A Dien Bien Phu Street, Ward 25, Binh Thanh District, Ho Chi Minh City, Vietnam; h.phu@hutech.edu.vn; nln.thao@hutech.edu.vn

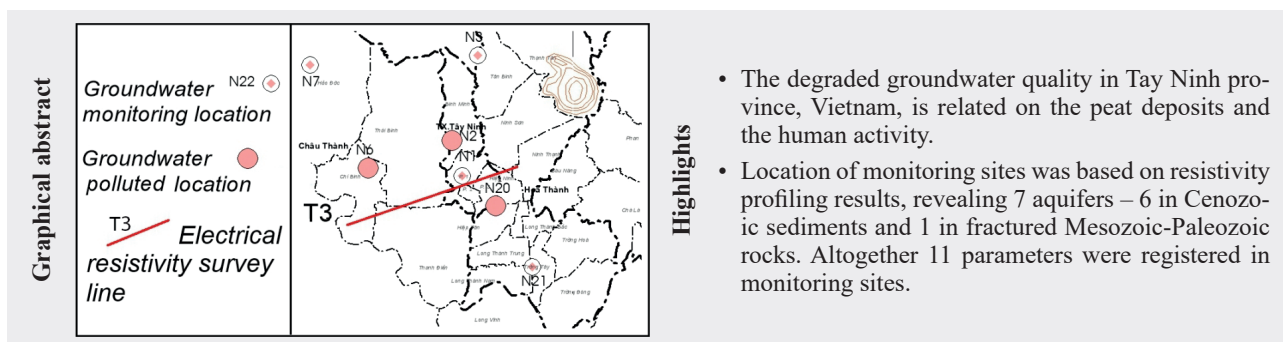
² Hanoi University of Natural Resources & Environment; 41A Phu Dien Street, Ward Phuc Dien, Bac Tu Liem District, Hanoi City, Vietnam; lctuan@hunre.edu.vn

³ Hochiminh City University of Natural Resources & Environment; 236B Le Van Sy Street, Ward 1, Tan Binh District, Ho Chi Minh City, Vietnam; htnhan_ctn@hcmunre.edu.vn

* Correspondence: lctuan@hunre.edu.vn; Tel.: +84-983806463

Abstract: The groundwater quality of Tay Ninh province was studied applying monitoring of 24 wells from 2016 to 2019. Based on this research there were determined 8 sites with very bad water quality, mostly due to the low pH index, high iron and ammonium contents. The remaining 16 wells preserve very good water quality. To determine the relationship between groundwater quality and peat deposits, the authors studied the map of these deposits in Tay Ninh province and compared it with monitoring points. The results show source of pollution mainly related to peat deposits and human activity. Due to the sustainable development, Tay Ninh province needs planning and the reasonable exploitation of the groundwater in the next 30–50 years, as well as the water resources partition and their management in each district.

Key words: groundwater, groundwater protection, Groundwater Quality Index (GWQI), Tay Ninh Province



Highlights

- The degraded groundwater quality in Tay Ninh province, Vietnam, is related to the peat deposits and the human activity.
- Location of monitoring sites was based on resistivity profiling results, revealing 7 aquifers – 6 in Cenozoic sediments and 1 in fractured Mesozoic-Paleozoic rocks. Altogether 11 parameters were registered in monitoring sites.

1 Introduction

The study area in Tay Ninh province is located in Southwest Vietnam in polygon approximately between North latitudes $10^{\circ} 57' 24.86''$ to $11^{\circ} 45' 41.09''$ and East longitudes $105^{\circ} 48' 5.09''$ to $105^{\circ} 51' 20.75''$ as shown in Fig. 1. Water here is extremely important for sustainable development, people's lives and health, so the water demand increases day by day. To guarantee the sufficiently high water quality, the monitoring of water quality is extremely necessary. The authors have studied groundwater quality in Tay Ninh Province from 2016 to 2019. Their aim was the determination the relationship between groundwater quality and mineral extraction (peat extraction in Tay Ninh province, Vietnam). The analyses results of water samples were evaluated on the basis of drinking water standard of Vietnam Ministry of Health and handled by Groundwater Quality Index (GWQI). The conclusions of the authors about the water quality serve to

Sustainable Development on Water Resources in Tay Ninh Province.

2 Materials and methods

2.1 Sampling collection methods

The material presented in article is a result of groundwater research in Tay Ninh province from 2016 to 2019. Collected material was processed applying standard methodology and the referred literature aiming to clarify the distribution rules of aquifers and confining beds, determination of groundwater reserves and factors affecting water quality (Chaterjee & Raziuddin, 2002; Dinh, 1992; Dung, 2005; Hoa et al., 1992; Hung, 1999; Institute of Environmental Technology Promotion and Water Resources Phu My, 2019; Mary & William, 1992; Vietnam Environment Administration, 2011; Vietnam Environment Administration, 2010; Loke, 2015).

2.2 Geophysical methods

The resistivity survey followed the methodology developed by Wenner (Loke, 2015, <http://web.gps.caltech.edu/classes/>). The layout diagram of the multipolar Wenner system, the order of measurement and recording of the outdoor resistivity survey values are described in Figure 2. The electrodes were evenly arranged along a straight line with the initial distance (measurement step) of 20 m. Ex-

tending the multipolar system on the measuring profile (to the left, to the right, or both sides), we obtained a sequence of measured resistivity survey values along the study route. The results allow to determine the aquifers.

We have designed 5 sub-parallel geophysics measurement lines (Fig. 3). The geophysics measurement results were verified by boreholes. See line T1 through borehole N15 (Fig. 2A) and lithological profile constructed owing to results of geophysical measurements (Fig. 2B)

Fig. 2. The arrangement of electrodes for a 2-D electrical survey.

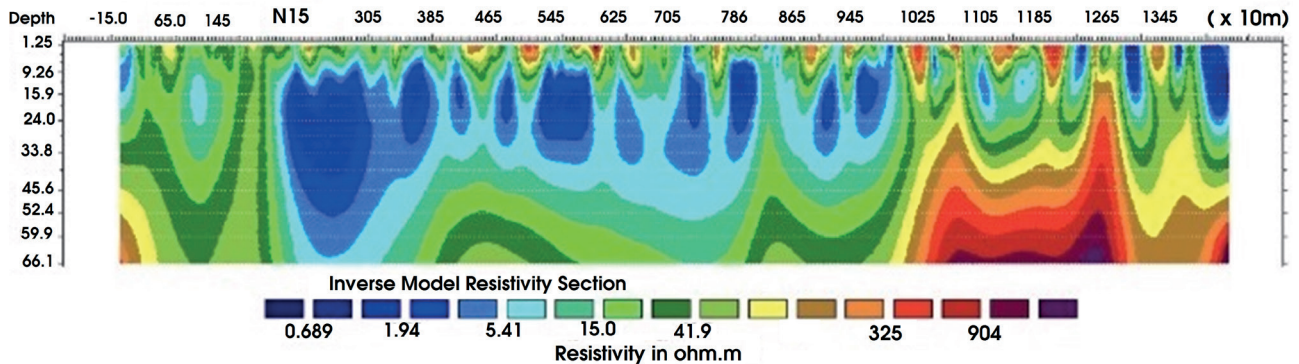
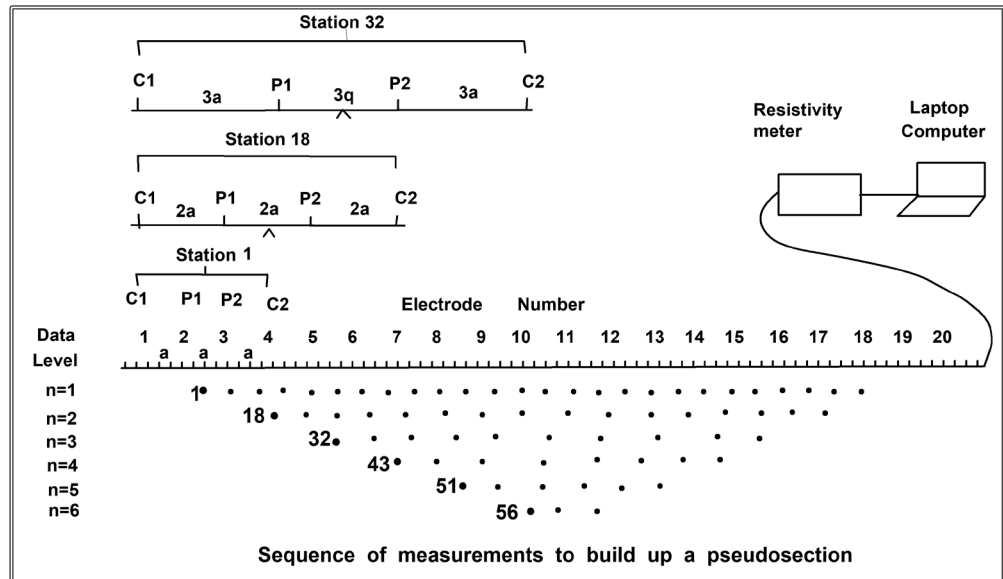


Fig. 2A. The results of geophysical measurement passing through the borehole N15.

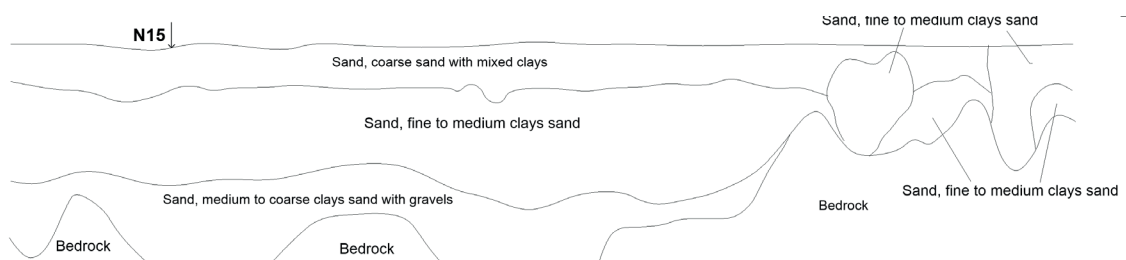


Fig. 2B. Lithology revealed by geophysical profiling.

2.3 Methods of boreholes location and their monitoring

The location of the boreholes was based on results of geophysical methods. Besides we collected data about the amount of rain, amount of vaporizing, flow, the flow of water outlet points, as well as oscillated water table. Monitoring works in pits and boreholes, including pump and suck water experiments, helped us to determine relatively accurately the total amount of groundwater that can be exploited in the entire study area. For Tay Ninh Sustainable Development and Environmental Protection, the groundwater exploits must ensure, the total amount of the groundwater exploit is always less than or equal to the amount of water replenished for groundwater, and can be calculated by the following water balance equation:

$$V_{kt} \leq 365 \times 103 \times S \times R; R = k_f \times (I - ET - SR)$$

Where: R is the average amount of replenishment groundwater/year,

V_{kt} is the total amount of exploitable groundwater, m³/year,

$$k_f = 0.7 \div 0.85$$

is the coefficient for the amount of water due to absorption by vegetation,

I is the average rainfall/year,

ET is the average evaporation/year,

SR is the average amount of flow on the face/year. SR is determined from digital hydrological models (mm/day). S is the acreage of the study area (km²).

Precipitation total I and evapotranspiration total ET data

are provided by national meteorological and hydrological monitoring stations.

The water samples were taken from water for drinking water sources such as wells, boreholes, located in Tay Ninh province. Method of groundwater sampling was done according to the guidance of Vietnamese standards: 6663-11: 2011 (ISO 5667-11: 1991) (Department of Environmental Management – Ministry of Health, 2016; Ministry of Health, 2009; Ministry of Natural Resources and Environment, 2015; National standards, 2011) (Tab. 2).

2.4 Sample analysis methods

Water samples were analysed for 11 criteria: pH, TDS, Hardness, CaCO₃, Chemical Oxygen Demand (COD), Ammonia (N-NH₄⁺), Nitrate (N-NO₃⁻), Fe, Chloride, Pb, *Escherichia coli* and Coliform bacteria (Standards and methods – Tab. 2).

Convenient Portable pH Meter for Wherever Work Takes-ST300 (STARTER)

Measurement Range

0–100 °C; 0.00–14.00 pH; 0–1999 mV

Measurement Resolution:

0.1 °C; 0.01 pH; 1 mV

Accuracy:

± 0.5 °C; ± 1 mV; ± 0.01 pH

Samples were analysed at National Lab – Phumytech (Tab. 2) (Ministry of Health, 2018; Ministry of Natural Resources and Environment, 2015).

Tab. 2

Parameter and Standard (Ministry of Health, 2009).

N°	Parameter	Units	Standard and methods	Vietnamese standards 01-1: 2018/MOH
1	pH	–	TCVN 6492: 2011	6.0–8.5
2	TDS	mg/L	TCVN 9462: 2012 ASTM D5284-09	1 000
3	Hardness, CaCO ₃	mg/L	TCVN 6224: 1996	300
4	Chemical Oxygen demand (COD)	mg/L	SMEWW 5220C: 2012	2
5	Amoni (N-NH ₄ ⁺)	mg/L	SMEWW 4500-NH ₃ ,B&F: 2012	0.3
6	Nitrate (N-NO ₃ ⁻)	mg/L	SMEWW 4500-NO ₃ ⁻ .E: 2012	2
7	Fe	mg/L	SMEWW 3111B: 2012	0.3
8	Chloride	mg/L	TCVN 6194: 1996	0.2–1
9	Pb	mg/L	SMEWW 3113B: 2012	0.01
10	<i>Escherichia coli</i>	CFU/100 ml	SMEWW 9222G: 2012	< 1
11	Coliform bacteria	CFU/100 ml	TCVN 6187-2: 1996	< 3

2.5 Assessment of groundwater quality with concern to drinking water standards

The analysis results are compared with the allowable limit according to Vietnamese standards 01-1: 2018/MOH, regulated by the Ministry of Health on National Technical Regulations on clean water quality used for domestic purposes (Tab. 1) (Ministry of Health, 2009; Ministry of Natural Resources and Environment, 2015; National standards, 2011). Besides, the locations of polluted wells were compared by the authors with the locations of mineral deposits to determine the nature of pollutant emission sources (Figs. 2–3).

2.6 Method of assessing groundwater quality from Groundwater Quality Index results

Based on the study Determination of Groundwater Quality Index (GWQI) by Ahmad (2014), the assessment scale of groundwater quality has five levels: A, B, C, D and E (Tab. 3) (Ahmad, 2014; Chaterjee & Raziuddin, 2002; Mary & William, 1992; Ministry of Health, 2009; Ministry of Natural Resources and Environment, 2015; National standards, 2011).

Analytical methods: Water samplings were done twice at two different sampling periods. Samples were

collected in rainy as well as dry seasons of years 2016, 2017 and 2018, using acid washed 0.5 liter polypropylene (PET) bottles to avoid unpredictable changes in characteristic of water according to standard procedures (APHA et al., 1998).

Step 1: Monitoring groundwater quality with Parameters (Tab. 2)

Step 2: Calculation of Water Quality Index (WQI – Tab. 3)

Tab. 3

Water Quality Index (WQI) and status of water quality (Chaterjee & Raziuddin, 2002).

Water Quality Index Level	Water quality status	Grading
0–25	Excellent water quality	A
26–50	Good water quality	B
51–75	Poor water quality	C
76–100	Very poor water quality	D
> 100	Unsuitable for drinking	E

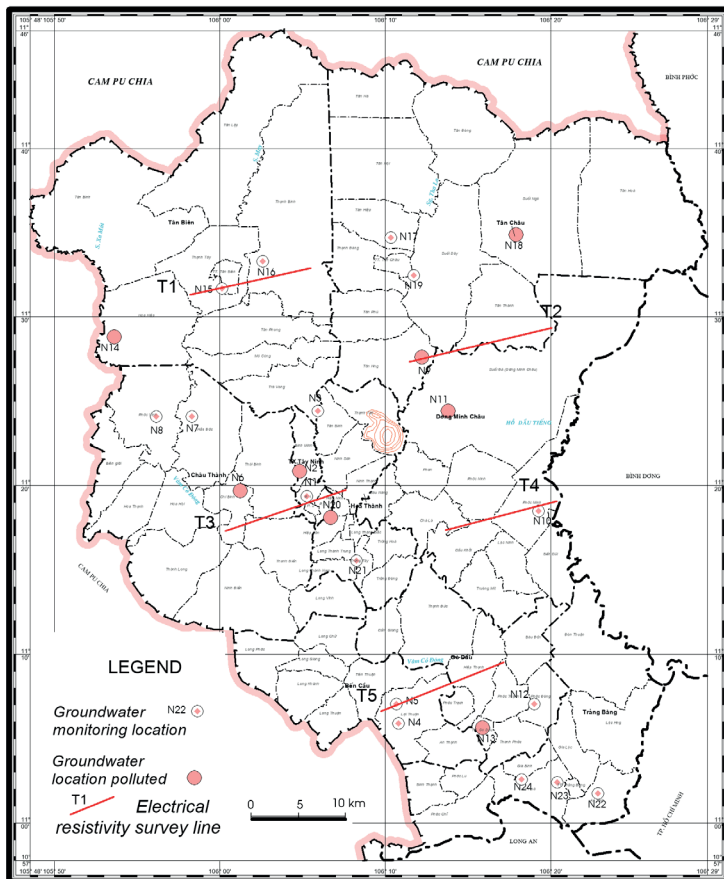


Fig. 3. Wells monitoring groundwater quality and location of polluted wells.

a) Calculation of Sub Index of Quality Rating (qn)

Let there be *n* water quality parameters, where the quality rating or sub index (*qn*) corresponding to the *n*th parameters is a number reflecting the relative value of these parameters in the polluted water with respect to its standard permissible value. The value of *qn* is calculated using the following expression.

$$qn = 100 [Vn - Vio] / [Sn - Vio], \quad (1)$$

Where *qn* – Quality rating for the *n*th water quality parameters,

Vn – Measured value of the *n*th parameter at a given sampling station,

Sn – Standard permissible value of the *n*th parameters,

Vio – Ideal value of *n*th parameter in pure water.

b) Calculation of Quality Rating for pH

For pH the ideal value is 7.0 (for natural water) and a permissible value is 8.5 (for polluted water). Therefore, the quality rating for pH is calculated from the following relation:

$$qpH = 100 [(VpH - 7.0)/(8.5 - 7.0)], \quad (2)$$

Where VpH = observed value of pH during the study period.

The quality rating $qn = 0$ means complete absence of pollutants,

Value $0 < qn < 100$ implies that the pollutants are within the prescribed standard.

Value $qn > 100$ implies that the pollutants are above the standards.

c) Calculation of Unit Weight (Wn)

Calculation of unit weight (Wn) for various water quality parameters are inversely proportional to the recommended standards value Sn of the corresponding parameters.

$$Wn = K/Sn, \quad (3)$$

Where Wn = Unit weight for the n^{th} parameters,

Sn = Standard value for n^{th} parameters.

K = Proportional constant, this value considered (1) here, also can be calculate using the following equation:

$$K=1/\sum (1/Sn). \quad (4)$$

The overall Water Quality Index was calculated by aggregating the quality rating with the unit weight linearly. If Water Quality Index (WQI) is less than 50 such water is slightly polluted and fit for human consumption. When WQI is between (51–80), water is moderately polluted, WQI between (50–100) indicates the excessively polluted and WQI above 100 severely polluted water (Sinha et al., 2004).

$$WQI = \sum_{n=1}^n qn Wn / \sum_{n=1}^n Wn \quad (5)$$

3. Results

3.1 Aquifers

Research results show that Tay Ninh province has 7 aquifers (6 porous aquifers in Quaternary sediments, 1 in fractured aquifer in Mesozoic-Paleozoic sequences) (Chan et al., 1998; Cuong, 2005; Dung, 1999, 2001; Nghi, 2002; Tay Ninh monitoring resources and environment Center, 2019; Tri, 2000; Tuan et al., 1998):

- Upper Pleistocene porous aquifer (qp³),
- Middle–Upper Pleistocene porous aquifer (qp²⁻³),
- Lower Pleistocene porous aquifer (qp¹),
- Middle Pliocene porous aquifer (n₂²),
- Lower Pliocene porous aquifer (n₂¹),
- Upper Miocene porous aquifer (n₁³),
- Mesozoic–Paleozoic fractured aquifer (ps-ms).

In which, there are 5 porous aquifers: (qp²⁻³), (qp¹), (n₂²), (n₂¹), and (n₁³) capable of large scale exploitation. Porous aquifer (qp³) and fractured aquifers (ps-ms) meet the needs of exploiting in retail scale to medium size.

3.2 Position of boreholes

The location of boreholes was determined based on geophysical results, combined with field investigation. Based on the geophysical results we have determined the position and thickness of the aquifers. This result has been verified by boreholes (Tab. 4).

3.3 Monitoring results and groundwater quality

At wells, the registered monitoring parameters represented the water level, pumped quality and targets for the quality of groundwater. The information collected is used to assess the status, change in amount, quality, and other impacts to the groundwater source. The results of groundwater quality analyses in Tay Ninh province are shown in Tab. 5.

Tab. 4
Parameters of porous aquifers.

Aquifers	Roof of the aquifer	Wall of the aquifer	Thickness
Upper Pleistocene porous aquifer (qp ³)	0.0–22.0 m	5.0-46.0 m	4.3–27.0 m
Middle–Upper Pleistocene porous aquifer (qp ²⁻³)	0.0–66.5 m	21.0–82.0 m	5.3–48.0 m
Lower Pleistocene porous aquifer (qp ¹)	13.0-92.0 m	31.5-121.0 m	13.5–50.0 m
Middle Pliocene porous aquifer (n ₂ ²)	45.0–153 m	73.0–195.0 m	6.5–91.5 m
Lower Pliocene porous aquifer (n ₂ ¹)	79.5–207.0 m	120.0–243.5 m	17.5–99.5 m
Upper Miocene porous aquifer (n ₁ ³)	143.5–237.0 m	160.0–302.0 m	16.5–68.0 m

Tab. 5
Analyses results of groundwater samples expressed by the range of obtained values.

TT	pH	Ammonium mg/L	Arsenic mg/L	Chloride mg/L	Chemical Oxygen Demand COD mg/L	Fe mg/L	TDS mg/L	Total hardness mgCaCO ₃ /L	Coliforms bacteria CFU/100 ml	<i>Escherichia coli</i> CFU/100ml
N1	4.91–5.78	0.5–1.46	0	22.5–38.1	0–0.71	0–0.04	32.9–183	29.4–59.9	3–240	0–3
N2	4.75–5.83	ND	ND	ND	0–1.04	ND	ND	ND	3–240	ND
N3	4.33–5.69	0–0.79	ND	4.04–21.45	0–0.61	0–0.26	25.3–70.3	0.37–8.8	3–43	0–15
N4	5–5.96	0–0.2	0–0.005	5.2–45.5	ND	0–1.26	23.9–69.4	1.39–133	3	0–3
N5	4.2–5.63	ND	ND	ND	0–0.6	ND	ND	ND	2–93	ND
N6	4.81–5.61	0.17–13.35	0–0.009	10.91–95.23	0–2.02	0–2.9	34.4–329	3.26–51.5	3–460	0–43
N7	5.09–6.01	ND	0–0.003	ND	0–1.3	ND	ND	ND	3–4	ND
N8	4.63–5.81	ND	ND	ND	ND	ND	ND	ND	3–23	ND
N9	5.06–6.53	0–0.3	ND	ND	0–1.11	ND	ND	ND	3–110	ND
N10	4.76–6.46	0–0.3	ND	ND	ND	ND	ND	ND	3–9	ND
N11	4.82–5.89	0–0.1	ND	ND	0–0.6	ND	ND	ND	3–240	ND
N12	5.2–5.88	0–0.04	ND	0–9.17	0–0.66	0–0.02	18.2–50	0–7.82	3–43	0–3
N13	4.59–5.71	0–0.4	ND	ND	0–0.6	ND	ND	ND	0–460	ND
N14	5.01–6.51	ND	ND	ND	0–2.13	ND	ND	ND	0–240	ND
N15	4.15–5.71	ND	ND	ND	0–0.5	ND	ND	ND	3–43	ND
N16	4.15–5.61	ND	ND	ND	ND	ND	ND	ND	3	ND
N17	4.72–6.01	0–0.1	ND	ND	0–0.7	ND	ND	ND	3	ND
N18	4.38–5.51	0.11–6.2	0	0–20.6	0–1.68	0–4.02	30–107.0	7.44–16.8	3	0–3
N19	4.59–5.62	ND	ND	ND	ND	ND	ND	ND	3	ND
N20	4.42–5.55	0.02–5.9	0	5.9–91.0	0–0.59	0–0.08	22–100.9	16.14–25.67	0–460	0–3
N21	4.15–5.28	0–0.14	ND	ND	ND	ND	ND	ND	3–110	ND
N22	5.06–5.73	0–0.2	ND	ND	0–1.0	ND	ND	ND	3	ND
N23	5.04–5.71	0–0.2	ND	ND	0–0.6	ND	ND	ND	3	ND
N24	4.46–5.64	0–0.3	ND	7–76.4	ND	0–0.04	28–198	7.2–27.3	3	0–3

Note: ND (not detected) – the parameter has been not detected during analysis

- (i) **pH:** According to the Ministry of Health standard, the pH value should be from 6.0 to 8.5. All monitoring groundwater samples focused on pH concentration in Tay Ninh province are not responding to this standard. An acidic pH (pH < 6) affects human health, corroding equipment and water containers. It is possible to overcome the pH value by increasing the ventilation level of the groundwater after exploiting, to eliminate CO₂ in the water. When the pH is in accordance with the allowable threshold, it can be used for domestic or drinking water.
- (ii) **Ammonium:** The maximum allowable limit of the Ministry of Health for Ammonium is 0.3 mg/L. Ammonium monitoring results of all groundwater samples throughout Tay Ninh province from 2016 to 2018 show that the areas of Bencau district, Duongminhchau district, Tanbien district, Trangbang district are unpolluted. Tay Ninh City, Chau Thanh district, Godau district, Tan Chau district, Hoatthanh district areas are affected by ammonium from 8.3 % to 58.3 % (rate of water samples for analysis and monitoring). The Tay Ninh city has the highest ammonium contamination.

- (iii) **Arsenic:** The maximum allowable limit of the Ministry of Health for arsenic content is 0.01 mg/L. The results of monitoring of the arsenic content of all groundwater samples of Tay Ninh province from 2016 to 2018 showed that none of the samples was polluted by arsenic.
- (iv) **Pb:** According to Ministry of Health standards, Pb content allowed in groundwater is 0.01 mg/L. The Pb monitoring results of all groundwater samples of Tay Ninh province from 2016 to 2018 showed that none of the samples is polluted by Pb.
- (v) **Chloride:** According to Ministry of Health standards, dangerous chloride content is 300 mg/L. The results of monitoring the chloride of all groundwater samples of Tay Ninh province from 2016 to 2018 supplemented in 2019 showed that only Tan Bien district is unpolluted, other areas of Tay Ninh province were polluted from 33.3 % to 66.6 %. In which, Tay Ninh city has the highest pollution to 66.6 % (12/18 samples).
- (vi) **Chemical Oxygen Demand (COD):** The maximum COD content is 2 mg/L (Standard of Vietnam 02: 2009/MOH). The results of monitoring the COD of all groundwater samples of Tay Ninh province from 2016 to 2018 showed that groundwater samples from Chau Thanh district and Tan Bien district are polluted by 5.5 %, all other areas of Tay Ninh province reached the allowable threshold.
- (vii) **Fe:** The maximum limit by the Ministry of Health allows 0.3 mg/L. The results of monitoring the Fe of all groundwater samples of Tay Ninh province from 2016 to 2018 showed that the groundwater samples from the Chau Thanh district and Tanchau district are polluted from 5.6 % to 22.2 %. The rest of the areas of Tay Ninh province is unpolluted.
- (viii) **TDS:** The maximum limit by the Ministry of Health allows 1,000 mg/L; The results of monitoring the TDS of all groundwater samples of Tay Ninh province from 2016 to 2018 showed that 100 % of groundwater samples from this province met the allowable limit for TDS content.
- (ix) **Hardness:** The maximum limit allowed by the Ministry of Health is 300 mg/L. The hardness monitoring results of all groundwater samples from Tay Ninh province from 2016 to 2018 showed that 100 % of the groundwater samples from this province met the allowable limit for hardness.
- (x) **Coliforms bacteria:** The maximum limit allows by the Ministry of Health is < 3 CFU/100 ml; The results of monitoring the Coliform bacteria of all groundwater samples of Tay Ninh province from 2016 to 2018 showed that Tayninh City, Bencau district, Chau Thanh district, Duongminhchau district, Godau district, Tanbien district, Hoatthanh district are affected by 8.3–55.5 %. In Tay Ninh City, the Coliform pollution

is the highest (56 %). Tanchau and Trangbang districts are unpolluted by Coliforms.

- (xi) **Escherichia coli:** The maximum limit allowed by the Ministry of Health is < 1 CFU/100 ml; The *E. coli* monitoring results from all groundwater samples of Tay Ninh province from 2016 to 2018 show that Tayninh City, Bencau district, Chau Thanh district, Godau district, Tan Chau district, Hoatthanh district, Trangbang district are affected from 27.7 % to 55.5 %. Tay Ninh city is the most damaged by *E. coli* (56 %). Duongminhchau and Tanbien districts are unpolluted by *Escherichia coli*. In Bencau district, Chau Thanh district, Godau district, Tan Chau district, Hoatthanh district, Trangbang district and Tay Ninh city the *Escherichia coli* and Coliforms are increased due to the characteristics of these districts having livestock farms, but the treatment is not thorough, wastewater overflows, water supply and drainage infrastructure system are not thoroughly synchronized.

The water sources are infected by microbes (*Escherichia coli* and Coliforms bacteria) due to the wastewater seeping into the groundwater resources, by running water from the ground into wells, or by less guaranteed water storage hygiene. When the *E.coli* and Coliform groups of bacteria are identified in the water, it shows that the water source has been affected by human or animal faeces (Ministry of Health, 2009; Ministry of Natural Resources and Environment, 2015; Phu & Phuong, 2019).

3.3 Evaluation of the groundwater quality with Groundwater Quality Index

Based on monitoring of 24 boreholes and groundwater samples analyses results in the Tay Ninh province from 2016 to 2018 the authors calculated the GWQI values applying formula (5) (Tabs. 2 and 6). Obtained results allow authors to conclude that the groundwater quality in Ben Cau district and Trang Bang district reaches 100 % of A “Very good” level. In Tayninh city, borehole N2 has a GWQI of 819. In Chauthanh district, borehole N6 has a GWQI of 267. In Duongminhchau district, borehole N9 has a GWQI of 3753. In the Godau district, borehole N13 has a GWQI of 159, in Hoathanh town, borehole N20 has a GWQI of 106. These are areas where good groundwater quality has not been indentified by GWQI.

In general, groundwater quality in research areas changed many times over time and space. Parameters such as pH, ammonium ion, chloride, coliform bacteria, *Escherichia coli* in some places have exceeded the allowed values. This is a threat to the health of community. Besides, the strong development of industrial zones, the evolution of the mining industry and irresponsible behaviour of people represent threats to the health of community and environment.

3.4 Some causes of affecting groundwater quality in Tay Ninh province

3.4.1 Human causes

Currently, Tay Ninh's population is about 1,171.7 million people (People's Committee of Tay Ninh Province statistical yearbook, 2019). The population increases every year. The land of Tay Ninh province is a constant area (about 4,041 km²). During development with growing industrial zones, the water demand also increases. Most people's wells, when not in use, are left blank. The people should fill the wells with clay to protect the aquifer. Otherwise the wells will become path for potential contamination from the surface to contaminate the groundwater. Moreover, people pollute the environment by waste. Further contributing to environmental pollution are livestock farms, enterprises of mineral processing, as well as the animal feed processing.

Tab. 6
GWQI values.

Sampling locations	2016	2017	2018	GWQI	Area
N1	41	42	29	37	Tayninh city
N2	2 456	1	2	819	
N3	15	24	7	15	
N4	8	9	65	27	Bencau district
N5	1	1	10	4	
N6	294	230	275	267	Chauthanh district
N7	1	1	29	10	
N8	3	1	1	2	
N9	11 256	1	1	3 753	Duongminhchau district
N10	5	1	2	3	
N11	247	1	1	83	Godau district
N12	5	10	11	9	
N13	475	1	1	159	
N14	1	247	10	86	Tanbien district
N15	1	1	5	2	
N16	1	1	1	1	
N17	2	1	1	1	Tanchau district
N18	105	87	38	76	
N19	1	1	1	1	
N20	142	149	26	106	Hoathanh town
N21	12	113	1	42	
N22	4	1	1	2	Trangbang town
N23	3	1	1	2	
N24	8	7	6	7	

3.4.2 Groundwater quality affected by geological reasons

Most of the area of Tay Ninh province represents a delta environment, being formed of Quaternary sediments.

The geological studies show that Quaternary sediments have many different origins (DGMVN, 2006; Hoa et al., 1992; Tri, 2000; Tuan et al., 1998). The sedimentary facies strongly affecting groundwater quality are represented by lake facies and marshy facies, having a reducing environment, closely related to the peat mines. Favourable places to form sedimentary sequences of lake and marshy facies are areas of subsidence in the past. There are 9 peat mines in Tay Ninh province (Cuong, 2005). These peat mines are distributed in alluvium and marshy sediments along the Vam Co Dong valley and rivers of Chau Thanh and Ben Cau districts. The peat beds have a thickness of about 2.0 m. The peat mines are located there, being monitored in points N2, N6, N9, N11, N13, N14, N18 and N20. To determine relationship of affected wells and geological environment, the authors have overlaid the location of the wells on the map of mineral resources in Tay Ninh province. All polluted wells are located nearby peat mines. So, the diffusion of elements from peat mines to surroundings has affected the groundwater quality of Tay Ninh province (Figs. 3–4).

One of the environmental impacts of peat mining is water pollution, the decrease in pH in peat is caused by humic acids from organic matter rather than by dissolving sulphate.

In addition, in Tay Ninh province, there are mineral deposits such as kaolin clay, brick-tile clay and cement limestone, building stone, limestone clay, pebble, gravel, building sand, laterite and mineral water – hot water (Fig. 4). Exploiting these minerals also affects the water environment of Tay Ninh province. However, in this article we dominantly mention only peat.

The formation of sediment lake and marshy faces is associated with the cycles of transgression and regression. The areas with lake and marshy faces represent favourable places for the accumulation of organic matter. Quaternary sediments in Tay Ninh have been identified by groundwater monitoring wells being up to 87 m thick (Borehole 5-NB, Tan Thanh – Tan Chau). Boreholes located in thick Quaternary sediments will contain also thick lake and marshy faces. We have discovered, analysing the Mineral map of Tay Ninh province, that the boreholes with contaminated groundwater resources are located in areas with marshy deposits. Besides, monitoring points N9, N11, and N18 were polluted due to related deposit points contain Ti and Fe.

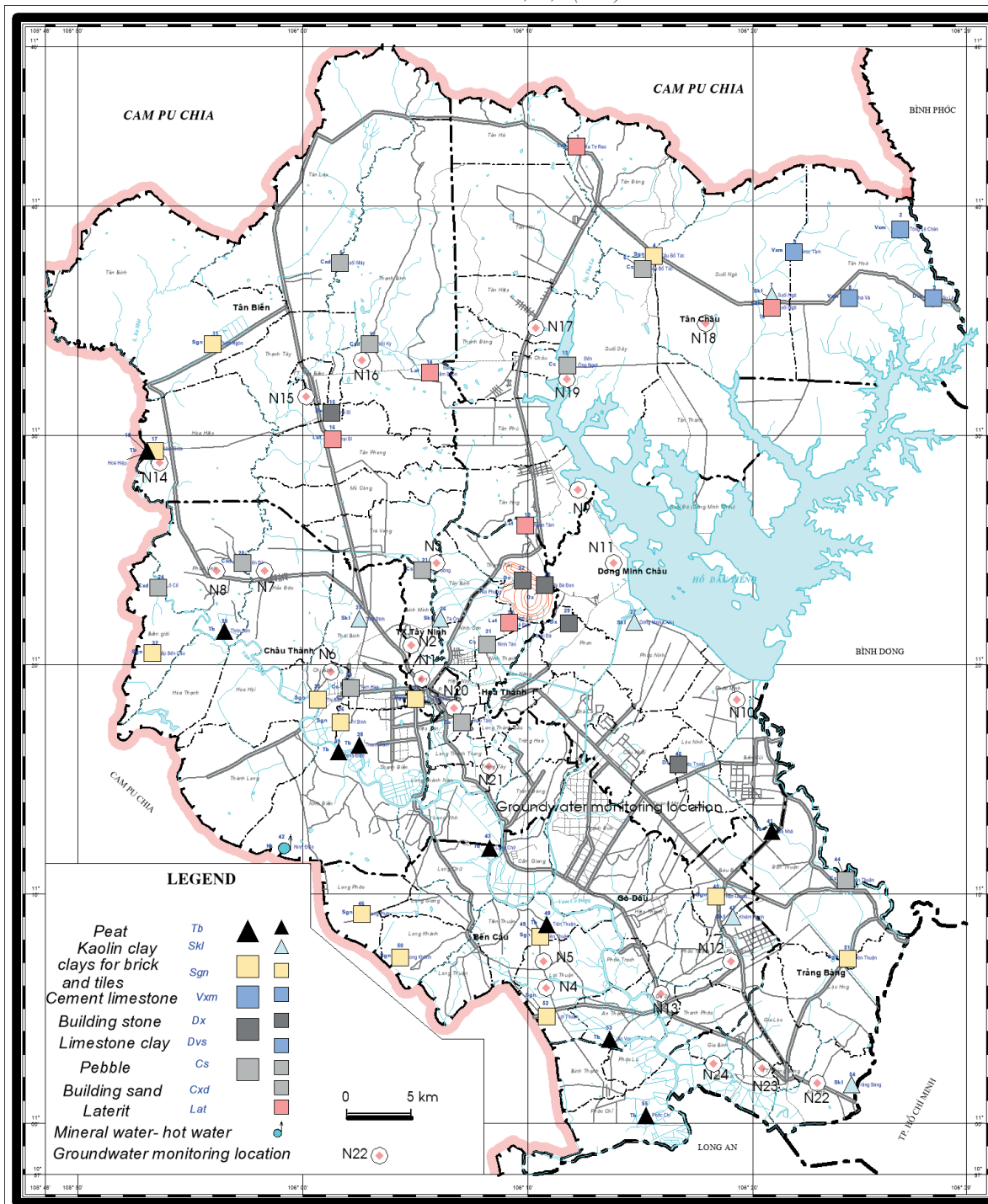


Fig. 4. Map of mineral deposits in Tay Ninh province (DGMVN, 2006).

4 Conclusions

Research results have determined that Tay Ninh province has 7 major aquifer types. Groundwater is mostly super fresh water. Most groundwater has a low pH. In many places, the content of iron, ammonium, coliforms bacteria, Escherichia coli and high chemical oxygen demand (COD) was recorded. In many places, the content

of iron, ammonium, permanganate, Coliforms, *E.coli* exceeds the allowable threshold contents. In some places, nitrate content is present in qp3 and qp2-3 aquifers with a high content (> 10 mg/L). The three locations with nitrate increased content are Long Thanh Trung, Long Thanh Nam, and Hoa Thanh towns (the Hoa Thanh district). Based on monitoring results of 24 wells, 8 affected wells

were identified, being associated with the peat area and building stone mine, containing high Ti and Fe contents. Towards sustainable development on the water source, Tay Ninh Province needs to do the following tasks:

- To raise the Community Education and the responsibility sense to environmental protection, especially in the Dền Tưng village (residential group), as well as the commune (Ward).
- Application of penalties for individuals and organizations for polluting the environment. At the same time, rewarding individuals and organizations behaving well in environmental protection.
- If well system stops working, prevent descending pollution to the aquifers.
- Do not exploit groundwater in aquifer polluted by mineral mines.

In addition, the warming climate and sea level may cause the seawater intrusion to coastal groundwater aquifers and is expected to be more severe in the near future. Tay Ninh needs to take this scenario into account.

Acknowledgments

The research was supported by Hutech University and Institute of Environmental Technology Promotion and Water Resources Phu My. The remarks and suggestions of reviewer Peter Bajtoš (ŠGÚDŠ, Slovakia) and one anonymous reviewer contributed to improving quality of primary manuscript.

References

- APHA, AWWA & WEF, 1998: Standard Methods for the Examination of Water and Wastewater. 20th Ed. *Washington*. DC;
- AHMAD, A. B., 2014: Evaluation of Groundwater Quality Index for drinking purpose from some villages around Darbandikhan district, Kurdistan Region, Iraq. *J. Agricult. Veter. Sci.*, 7, 1, 9, 134–41. ISSN 2319-2380, p-ISSN 2319-2372. www.iostjournals.org. DOI: 10.9790/2380-07913441.
- CHAN, N. Đ. et al., 1998: Geological investigation Tay Ninh City – Thudaumot, scale 1 : 25.000. Archived in Tay Ninh province.
- CHATERJEE, C. & AZIIDDIN, M., 2002: Determination of water quality index (WQI) of a degraded river in Asanol Industrial area, Raniganj, Burdwan, West Bengal. *Nat. Environ. pollut. Technol.*, 1, 2, 181–189.
- DGMVN (Department of Geology and Minerals of Vietnam), 2006: Mineral Resources of Tay Ninh Province.
- Department of Environmental Management – Ministry of Health, 2016: Guide Water treatment family by simple measures.
- DINH, B. T., 1992: Mapping Report on hydrogeology – Southern Engineering Geology, scale 1 : Report on 200.000. Archived in Department of Geology and Minerals of Vietnam.
- DUNG, N. Q., 1999: Exploration of natural mineral water in Ninh Dien – Chau Thanh area. Final report. Archived in Tay Ninh province.
- DUNG, N. Q., 2001: Groundwater exploration in Go Dau – Tay Ninh area. Final report. Archived in Tay Ninh province.
- DUNG, N. Q., 2005: Report exploration mining groundwater in Moc Bai – Ben Cau area. Final report. Archived in Tay Ninh province.
- Exploration mining of groundwater in Tan Hoa, Tan Chau for construction of Tay Ninh Cement Factory, 2005: Final report. Archived in Tay Ninh province.
- HOA, N. N. et al., 1992: Geological map of the Southern Delta, scale 1 : 200.000. Archived in Department of Geology and Minerals of Vietnam.
- HUNG, D. T., 1999: Investigation status of reserves, groundwater quality, and use planning up to 2010 in Tay Ninh province. Archived in Department of Geology and Minerals of Vietnam.
- Institute of Environmental Technology Promotion and Water Resources Phu My, 2019: Groundwater Research Report and Sustainable Development orientation for social-economic development in Tay Ninh province.
- LOKE, M. H., 2015: Tutorial for: 2-D and 3-D electrical imaging surveys. Archived in Tay Ninh province.
- MARY, P. A. & WILLIAM, W. W., 1992: Applied groundwater modeling. *New York, Acad. Press*.
- Ministry of Health, 2009: National Technical Regulations about the quality of drinking water (Standard of Vietnam 02: 2009/MOH).
- Ministry of Natural Resources and Environment, 2015: National Technical Regulations about groundwater quality (Standard of Vietnam 09: 2015/Monre).
- National standards, Standard of Vietnam 6663-1: 2011, Sampling – Part 1: Guidance on the design of sampling programmes and sampling techniques, 2011.
- NGHI, V. V., 2002: Exploration mining underground water industrial Linh Trung 3 – Trang Bang area. Archived in Tay Ninh province.
- People’s Committee of Tay Ninh Province, 2017: Report No 375/Report-PC date 03/12/2018 on The implementation Development socioeconomic plan in 2018 and Development socioeconomic plan in 2019.
- People’s Committee of Tay Ninh Province, 2018: Report Assembly series Hydrogeological map (scale 1/500) and IT applications in groundwater management for zoning exploitation of resources in Tay Ninh province.
- People’s Committee of Tay Ninh Province, 2019: Statistical yearbook. *Statistic. Publ. House*.
- PHU, H. & PHUONG, H. T. T., 2019: Applied research of groundwater quality index (GWQI) to assess suitability for domestic use purposes and proposing management and treatment measures in Tay Ninh province. Archived in Tay Ninh province.
- Standard of Vietnam 5944. Standard groundwater quality, Hanoi, 1995.
- Tay Ninh Environment and Natural Resources Department. Tay Ninh environmental quality monitoring plan. Report, 2018.
- Tay Ninh monitoring resources and environment Center. Results from the report on groundwater quality monitoring of Tay Ninh Environmental Monitoring Center in 2016, 2017, 2018, 2019.
- TRI, V. K., 2000: Investigative report on potential, reserves, and quality of surface water in Tay Ninh. Archived in Tay Ninh province.

- TRINH, L., 2008: Research water quality partition according to groundwater quality index (WQI) and assess the ability to use water resources, river canal in Hochiminh area. Archived in Tay Ninh province.
- TUAN, A. T. et al., 1998: Report on hydrogeological mapping – engineering geological map of Tay Ninh. Archived in Tay Ninh province.
- UNEP, 2003: Groundwater and its Susceptibility to Degradation: A global assessment of the problem and options for management. <https://nora.nerc.ac.uk/id/eprint/19395/>
- Vietnam Environment Administration, 2010: Calculation of water quality index method (WQI).
- Vietnam Environment Administration, 2011: No: 879/ Decision-VNA, notebook guide to calculating water quality index.

Vzťah kvality podzemnej vody a ložísk rašeliny na príklade monitorovacieho výskumu v provincii Tay Ninh, Vietnam

Kvalita podzemnej vody v provincii Tay Ninh vo Vietname (obr. 1) sa skúmala v rokoch 2016 až 2019 monitorovaním 24 lokalít (obr. 3 a 4, tab. 1 a 5).

Lokalizovanie miest pozorovania sa zrealizovalo geofyzikálnym profilovaním aplikáciou odporových meraní, na základe ktorých boli následne vyhlbené monitorovacie vrty (obr. 2 a 2A). Odobraté vzorky na miestach monitorovania sa testovali na nasledujúce parametre: pH, obsah amónnych iónov, arzénu, chloridov, COD, Fe a TDS, celková tvrdosť, prítomnosť koliformných baktérií a *Escherichia coli*.

Po spracovaní výsledkov viacročného monitorovania bola kvalita podzemnej vody na jednotlivých lokalitách

vyhodnotená pomocou komplexného klasifikačného indexu (tab. 6). Bolo identifikovaných 8 lokalít s veľmi zlou kvalitou podzemnej vody, predovšetkým pre nízke pH a vysoký obsah železa a amónnych iónov. Zvyšných 16 lokalít si zachovávalo dobrú kvalitu vody. Z porovnania pozície lokalít s nepriaznivou kvalitou podzemnej vody a ložísk rašeliny vyplynulo, že zhoršenú kvalitu podzemnej vody spôsobujú popri ľudskej činnosti hlavne tieto ložiská. Boli navrhnuté zodpovedajúce nápravné opatrenia.

Doručené / Received: 29. 11. 2021
Prijaté na publikovanie / Accepted: 21. 6. 2022

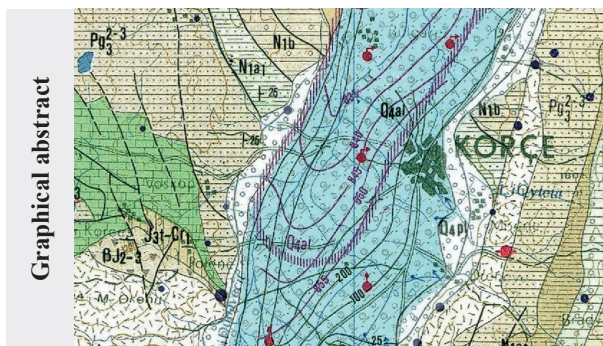
Hydrogeological map of Albania at a scale of 1:200,000, principles of compilation and content – a document of Albanian pioneering hydrogeological research since the 1960s

ROMEO EFTIMI, GUXIM BASHA, IBRAHIM TAFILAJ and XHAVIT SHEGANAKU

Former Hydrogeological Service of Albania, Rr. Kavajes nr. 150, Tirana, Albania

Abstract: The organized hydrogeological investigations in Albania started in 1959, while general hydrogeological prospecting started there in 1963 and finished in 1974. One of the hydrogeological prospecting main goals was the compilation of the hydrogeological map of Albania at a scale of 1:200,000. Hydrogeological maps may differ in content, representation, scale and format, but two main types of these maps are principal: general and/or special hydrogeological maps. The aforementioned map was published in 1985 following principles for general hydrogeological maps as defined in 1970 by IAH/UNESCO, which were subsequently adopted, but also further developed. The areal colours show hydrogeological classification of rocks and the basic elements shown on the map are hydrogeological units. Geological pattern forms the map background, while lithologic units are differed by green colour hatches. Different aquifers and hydrogeological structures identified during the investigations are also shown here, together with important water supply areas of productive drillings and springs. Groundwater quality, thermal springs, seawater intrusion areas and the relation between surface and groundwater can also be recognized. The map published in 1985 can be successfully used until nowadays, not only for the planning purposes, but also as a helping tool in many practical problems of the groundwater use solutions.

Key words: hydrogeological mapping, maps at a scale of 1:200,000, aquifer classification, Albania



Graphical abstract

Highlights

- The only hydrogeological map completely covering the territory of Albania.
- Principles of IAH/UNESCO hydrogeological map legend were further developed to fully describe complex geological settings of the Balkan Dinarides, Albanides and Hellenides.
- The fundamental element of hydrogeological rock classification is transmissivity, reflected by colour of the area – lithology is then illustrated by hatches.

Introduction

Human activity is closely related to groundwater; consequently, the public interest for groundwater is constantly increasing. After the Second World War, hydrogeological investigations and hydrogeological studies were intensified all around the world as humankind was facing both the large demographic development and the intensive development of industry and agriculture in this period. Large quantities of hydrogeological data were accumulated, and the necessity to process them and finally present them on hydrogeological maps of large regions arose. The compilation of hydrogeological maps is the best way to generalize numerous records on groundwater, and these maps then represent a powerful tool for planning, development and environmental protection (Struckmeier, 1989). Hydrogeological maps reflect the natural state of groundwater as well as the possibilities of their exploitation in a conden-

sed form, and therefore can be considered as documents of great practical and scientific value. Basic hydrogeological maps firstly provide information on major groundwater resources, groundwater flow, recharge and discharge zones, groundwater/surface water interactions, location of important springs and pumped wells, vulnerability of groundwater resources, main aquifers and aquitards.

Numerous hydrogeological studies were conducted in Albania during the period of 1960–1985, both those for merely practical purposes (such as water supply of the population and industry, dewatering of mines, use of thermal waters, etc.), as well as those of a practical-scientific character (regional hydrogeological prospecting, groundwater monitoring, application of environmental chemical and isotope tracer methods, etc.). Results of both has been accompanied with data representation that could be depicted on hydrogeological maps.

Necessity of hydrogeological maps compilation was also a consequence of the strong tendency of international hydrogeological community to compile hydrogeological maps of both national and international character.

The purpose of this article is to analyse the principles of compilation of the hydrogeological map of Albania at a scale of 1:200,000 (Eftimi et al., 1985; further on HMA sc. 1:200,000) and to compare it to other international maps, as well as to highlight how these principles serve to reliably reflect Albania's hydrogeological features (Eftimi et al., 1977, 1986).

The HMA sc. 1:200,000 published in 1985 by no doubt reflects the scale of knowledge of the time of publication, nonetheless the basic principles of the compilation of the map are adequate even today and it continues to be a document of great value, both on scientific and practical point of view. The map is produced using traditional printing technologies like this of graving.

Annual mean air temperatures in the coastal regions vary from 15 to 16 °C, and about 10 °C in mountainous areas. Annual mean precipitation in Albania amounts to about 1,450 mm, with more than 3,000 mm in the North Albanian Alps, and about 650–700 mm in the Eastern depressions of Korça and Kolonja.

The hydrographic basin of Albania with a total area of 43,305 km² is about in 50 % larger than the total state territory; for this reasons Albania has abundant surface water resources (Pano et al., 1984). Overall renewable resources amount to 41.7 x 10⁹ m³ or 13,300 m³ per capita, of which 65 % is generated within Albanian territory and the remaining 35 % from upstream countries (Pano et al., 1984). The main river courses in Albania are drained towards the Adriatic Sea. The biggest lakes, namely Prespa, Ohrid and Shkodra, are of transboundary position and of tectonic origin; all of them belong to the Drin River system. Three high dams with large artificial lakes, all in

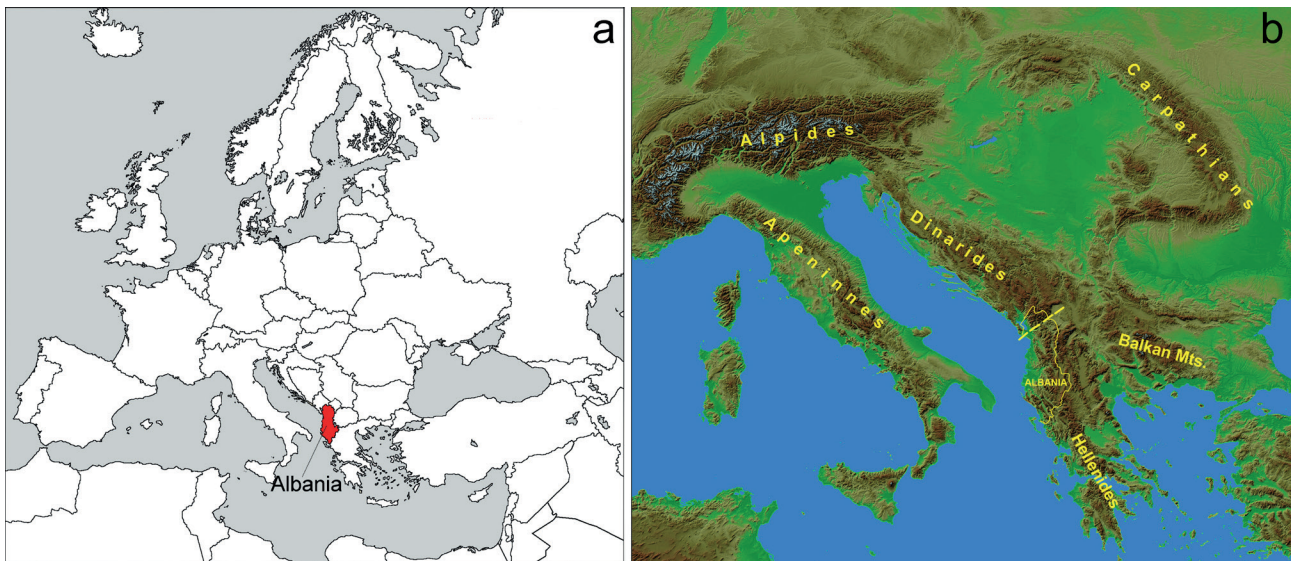


Fig. 1. a) Location map of Albania, b) Tectonic position of Albania.

Basic geographic and geological features of Albania

Albania is situated in the western part of the Balkan Peninsula (Fig. 1a). Many peaks higher than 2,000 m above sea level (a. s. l.) are situated in the northern, eastern and southern parts of Albania. The highest of all is Mt. Korab, reaching an elevation of 2,751 m a. s. l. In the Central Western part of the country along the Adriatic coast, the Adriatic Depression is located consisting of plains and hills which elevations are mostly lower than 200 m a. s. l.

Albania belongs to the Mediterranean climatic belt, which is characterized by hot dry summers and mild rainy winters (Jaho et al., 1975). The moderating influence of the sea is encountered only in the western part of the country, and through valleys it penetrates well inland.

the Drin River system, have been built for flood protection, irrigation and production of hydroelectric power.

From a geological point of view, Albania belongs to the southern branch of the Alpine orogenic system (Fig. 1b). The Shkodra-Peje transversal fault divides the Dinarides from the Albanides and Hellenides. The Northern Albanides extend into the former Yugoslavian territory with Dinarides and the Southern Albanides continue southwards to Greece with the Hellenides (Meçe & Aliaj, 2000; Xhomo et al., 2003). There are some inner and some external tectonic zones successively overthrusting each other towards the west.

Though geographically small, Albania has a variety of geological formations of different ages, origin and composition. Among these are rocks ranging from

Ordovician to Quaternary; they comprise sedimentary and magmatic types together with rather less frequent metamorphic. The carbonate sedimentary rocks are ranging from Devonian to Burdigalian in age and constitute many large and small anticline and syncline structures with the SE-NW orientation found throughout all tectonic zones. The Oligocene to Pliocene molasse sediments are mainly consisting of heterogeneously intercalated sandstone, conglomerate, siltstone, claystone and clay layers that mainly fill the deeper part of the Adriatic depression as well as some inland depressions like the Albanian-Thessaly, which is the largest. Pleistocene-Holocene gravelly clayey deposits are the most widely distributed geological unit in the Adriatic Basin, as well as in some inland mountain plains and river valleys. Magmatic rocks are extensively developed mainly in inner tectonic zones. Most developed is the Jurassic ophiolitic magmatism of Mirdita (Subpaleogonian) zone, which consists mainly of intrusive and less of volcanic rocks (IGI, 1967, 1983; Meçe & Aliaj, 2000; Xhomo et al., 2003).

History of the compilation of the Hydrogeological Map of Albania

During 1961, the former chief hydrogeologist of Albanian Hydrogeological Service (AHS) Spiro Mitro was the first to propose the performance of the regional hydrogeological survey on the territory of Albania, at a scale of 1:100,000 in the mountain areas and at a scale of 1:50,000 on the plain and hilly areas of the country. In 1963, a project was drafted in AHS and the hydrogeological survey of the entire territory of the country started. The final goal of the hydrogeological survey was the compilation of the Hydrogeological Map of Albania at a scale of 1:200,000, which after a persistent work was published in 1985. The completion of this important and complicated task lasted about 12 years, from 1963 to 1974. The realization of this project was very difficult, if one takes into consideration that the technological equipment of that time in Albania were very scarce or outdated. The field survey groups were equipped with the minimum necessary geological equip-

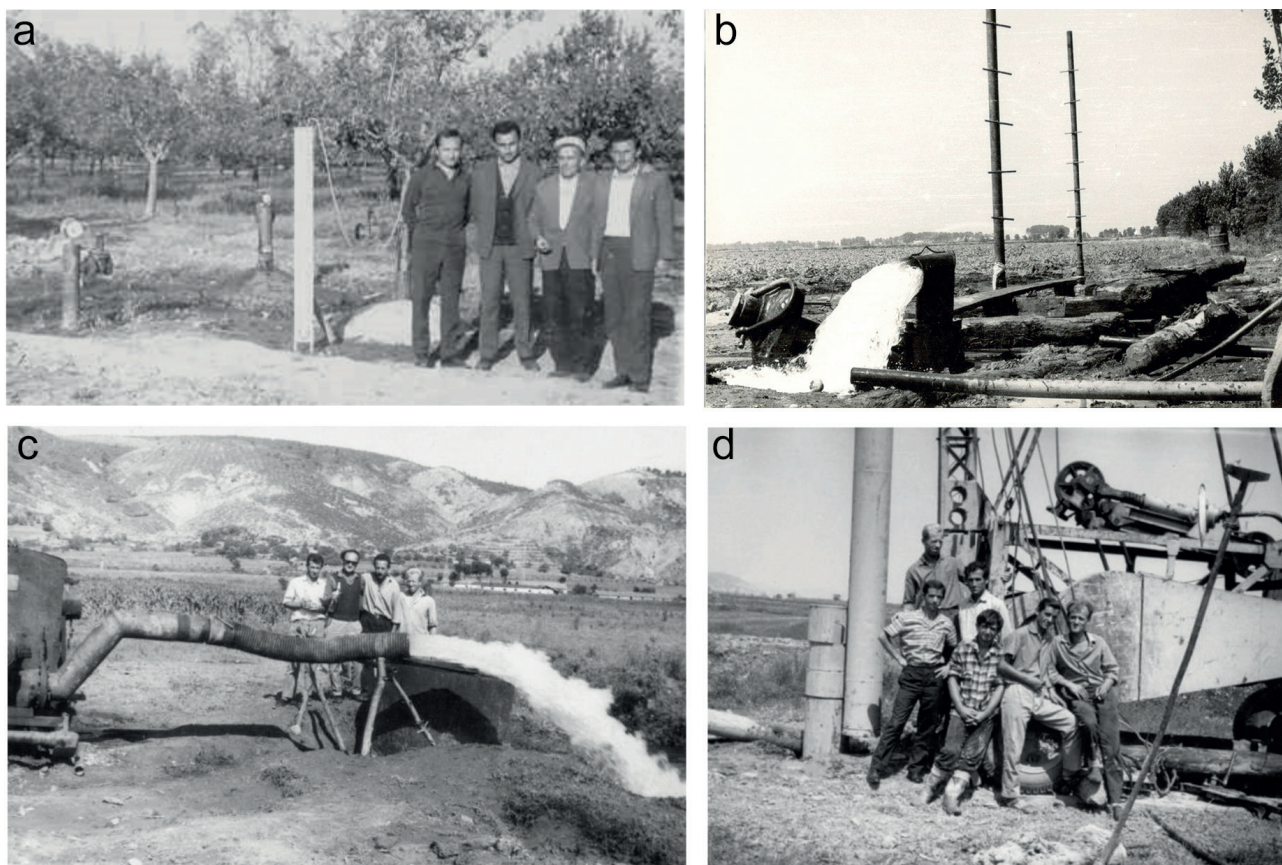


Fig. 2. Historic photos documenting different activities of hydrogeological prospecting of Albania: a – In front of the groundwater monitoring station of Turan, Korça intermountain alluvial basin; manometers are mounted on two wells, while in the third one a primitive instrument with mercury is mounted (photo 1981); b – A free-flowing cable-tool well in Lezha alluvial plain, discharge of about 90 l/s, equipped with two pipe piezometers (in the absence of manometers) for groundwater level observation during the pumping (photo 1970); c – The hydrogeological team during a pumping test, with a centrifugal pump in Elbasan alluvial plain, discharge about 80 l/s (photo 1970); d – The drilling team of a cable-tool drilling machine installed in Elbasan alluvial plain (photo 1976).

ment; at least there was no shortage of paper notebooks and mercury thermometers.

The main results of hydrogeological prospecting of Albania could be summarized as follows:

- a) investigation of 13 gravelly aquifers basins, total surface equal to about 2,300 km²;
- b) investigation of some basins filled with Neogene molasses; total area of about 4,700 km²;
- c) investigation of 25 karst massifs with a total area of 6,750 km²;
- d) drilling of about 1,300 groundwater boreholes to the depths from about 30 to 400 m;
- e) inventory of about 2,500 springs;
- f) groundwater monitoring mainly of the Quaternary intergranular basins;
- g) sampling of about 3,000 groundwater samples for chemical analyses, mainly for macro-components.

Very important data regarding the groundwater and surface water disposed by their institutions of Albania has been also collected. The results of the hydrogeological survey are presented in numerable reports available in the archive of Albanian Geological Service (AGS; Mitro, 1963; Babameto et al., 1965; Babameto & Kondo, 1981; Bisha et al., 1980; Bisha & Prenga, 1981; Gjata, 1968, 1978; Gjata et al., 1967; Keta & Mitro, 1968; Keta et al., 1968, 1970; Lako, 1963, 1968, 1973; Prenga, 1984a, 1984b; Rudi et al., 1969, 1972; Tafilaj, 1960–1985; Tartari, 1979; Tyli, 1971, 1972; Shtrepi, 1972, 1973, and many others). On the other hand, the number of scientific articles published in the journal of Albanian Geological Survey was limited (Eftimi, 1966, 1975, 1982; Eftimi et al., 1977, 1979, 1985, 1986; Kazazi, 1971; Kristo, 1973; Lako, 1973; Tyli, 1976; Tafilaj, 1977). Figure 2 shows some historic photos documenting different hydrogeological activities performed by AHS during the period of 1970–1981. The HMA sc. 1:200,000 was published in 1985 (Fig. 3) – it has passed more than 35 years since the first publication of this map, but it continues to be a document of a great value, correct from the technical point of view and really useful from the practical point of view, as continuously verified by a daily practice.

Principles of compilation of basic (general) hydrogeological maps

Groundwater data interpretation in hydrogeological maps vary greatly regarding their content, quantity and the way of data presentation, map scale, geological features, as well as on the depth of knowledge (Jäckli & Tempf, 1972; Manfredini, 1971; Margat, 1966; Margat & Rogovskaja, 1979; Maurine & Zöl, 1964; Karrenberg et al., 1974; Pfeiffer, 1975; Rogovskaja, 1970; UNESCO, 1970; UNESCO/WMO, 1977; UNESCO, 1983; Guzelovski & Kotevski, 1977). Generally, two types of hydrogeological

maps are distinguished: general hydrogeological maps and special (purpose-built) hydrogeological maps. General hydrogeological maps aim to distinguish different areas and regions according to their hydrogeological character, in close connection with their geological structure. Special hydrogeological maps are of mainly practical character and are constructed in a wide range of display methods, including maps of aquifer permeability/transmissivity, groundwater resources and their utilization, groundwater vulnerability, hydrodynamic maps, groundwater chemistry or paleohydrogeological maps.

Hydrogeological maps differ by their scale, also; the small-scale maps are those with a scale of less than 1:200,000, medium-scale maps are those of scale 1:200,000 and 1:100,000, while large-scale maps are those of scale 1:50,000, 1:25,000 or even more detailed. There is a close connection between the scale of maps and their character: small scale maps usually are general and have mainly scientific character; medium-scale maps have both scientific and practical character, while large-scale maps are more detailed and usually have practical character.

Initially, the geological principle of compiling of the hydrogeological maps prevailed, according to which various important point elements, such as the main springs or drilled wells, were placed on the geological map of a given area (Altovski, 1960; Rogovskaja, 1970). This type of maps was initially used in the practice of Albanian hydrogeological explorations, also (Gjata et al., 1967; Keta et al., 1968, 1970). The regionalization principle of compiling hydrogeological maps, commonly used for small and medium scale maps, has also been quite popular (Bulgarian Academy of Science, 1960; Manfredini, 1971; Penchev, 2002). These maps show the limits of depicted hydrogeological regions, which are distinguished from those of neighbouring regions on the basis of any accepted hydrogeological regionalization principle (Eftimi et al., 1977).

After 1970 the practice of intensive compilation of hydrogeological maps, was mostly oriented to the application hydrogeological principle (Anonymous, 1970, 1983; Institute Geologique du Bucharest, 1961; Jäckli & Tempf, 1972; Karrenberg et al., 1974; Margat, 1979; UNESCO, 1970, 1983; UNESCO/WMO, 1977; IHME, 1970–1980; Takahashi, 1971; Giuliani et al., 1974; Guzelovski & Kotevski, 1977). According to this principle the main elements shown on hydrogeological maps are the lithological-stratigraphic-hydrogeological units (hydrogeological unit), which are distinguished and classified (grouped) based on the knowledge of their lithological composition, porosity and hydraulic parameters. These parameters are responsible for the overall aquifer hydraulic character, for the formation and distribution of groundwater resources and their quality, as well as for the productivity of wells and of the groundwater exploitation features of different

rocks. Water-bearing and non-aquiferous rocks distinct as hydrogeological units, are included in some “groups”, within which some “classes” are distinguished. On hydrogeological maps compiled according to this principle, geology consists the background of the map where each lithological unit is distinguished through ash-coloured ornaments (grey), while hydrogeology is shown more expressively through the areal colours. This principle has served as a basis for compiling the International Hydrogeological Map of Europe (IHME) at a scale of 1:1,500,000 (IHME-UNESCO – Karrenberg, 1970; Karrenberg & Deutloff, 1973; Karrenberg et al., 1974; Karrenberg & Struckmeier, 1979). This method has been also applied by the Albanian Hydrogeological Service for the compilation of hydrogeological maps (Bisha & Prenga, 1981; Eftimi et al., 1977; Prenga, 1984; Tartari, 1979).

The hydrogeological map of Albania at a scale of 1:200,000 is of a general character and for its compilation there are successfully embodied and further enriched the principles of compiling as defined in IHME (Eftimi et al., 1977). The main element contained in this map is the principle of hydrogeological classification of rocks, but is enriched with many original elements (Eftimi et al., 1977). Albania’s hydrogeological map at a scale of 1:200,000 was published in 1985 and is based on Albania’s geological map of the same scale which was finalized in 1983 (IGI, 1983).

Map content

a) Hydrogeological classification of rocks

The hydrogeological classification of the rocks can be considered as the fundamental principle of the compilation of hydrogeological map of Albania at a scale of 1:200,000 and is shown in the first three chapters of the legend. On the map, 46 “hydrogeological units” are distinguished and classified into three “groups of rocks” within which seven “classes” are categorized (Fig. 4).

In each of the seven aforementioned classes of aquifers or “non-water-bearing units” / aquitards / aquicludes (or rocks), several hydrogeological units are included complemented by lithological specification for each unit and respective stratigraphic indications (stratigraphy shown by respective symbols). The stratigraphic units of the basic geological map are in different relationships with the hydrogeological units of the hydrogeological map. They can constitute a hydrogeological unit on the hydrogeological map also, or could be a part of a hydrogeological unit, or – in some case – several hydrogeological units could be distinguished in one stratigraphic unit. Each hydrogeological unit may represent an aquifer or a group of aquifers (hydrogeological complexes). The difference between the aquifers and aquifer complexes has not been shown on the map.

Each group of rocks, and the classes they contain, are characterized in the map Legend with some data regarding hydraulic conductivity (generally high, moderate or variable, frequently high or variable, high to variable, moderate to low, low to very low and very low, while for each class of rocks a short hydrogeological characterization instructive is given (Fig. 4a, b).

Group I – mainly Quaternary aquifers are included, which are classified into two classes:

- Ia – mostly alluvial intergranular aquifers of the western coastal lowland, river valleys and of high elevation intermountain basins. The hydraulic conductivity is generally high and the yield of wells usually varies from about 10 l/s to about 100 l/s.
- Ib – mainly fluvial deposits of high river terraces, glacial deposits (moraines) and slope debris. The hydraulic conductivity is moderate or variable and discharge of springs is usually less than 5 l/s.

Group II – rocks of different ages and various lithology are included and classified into two classes:

- IIa – carbonated deposits of Paleozoic to Eocene age and Perm-Triassic gypsum deposits. Their hydraulic conductivity is generally high, but very non-uniform (nonhomogeneous rocks), so the yields of wells are practically is unpredictable.
- IIb – differently cemented sandstone-conglomerate of Neogene molasses, limestones with schist and heterogeneous sandstone-schists-limestone deposits of the Low Triassic, usually having moderate to low hydraulic conductivity and the yield of wells usually varies from 0.2 to 4 l/s.

Group III – various rocks in terms of genesis, lithology and stratigraphy such as sedimentary, magmatic and metamorphic are included and classified into three classes:

- IIIa – intrusive rocks characterized by low to average hydraulic conductivity mainly related to the tectonic fault zones. The yield of wells varies from about 2 l/s to more than 10 l/s.
- IIIb – both fissured and porous Neogene deposits, with prevailing clayey-claystone deposits and to a lesser extent of sandstone-conglomerate deposits, as well as volcanic and volcanogenic-sedimentary rocks; generally of low hydraulic conductivity. The yield of wells is usually less than 0.3 l/s
- IIIc – mainly Quaternary and Neogene flysch to flyshoid deposits and Paleozoic to Paleogene metamorphic rocks with very low hydraulic conductivity.

In HMA sc. 1:200,000, the hydrogeological classification of rocks has been enriched related to that of Interna-

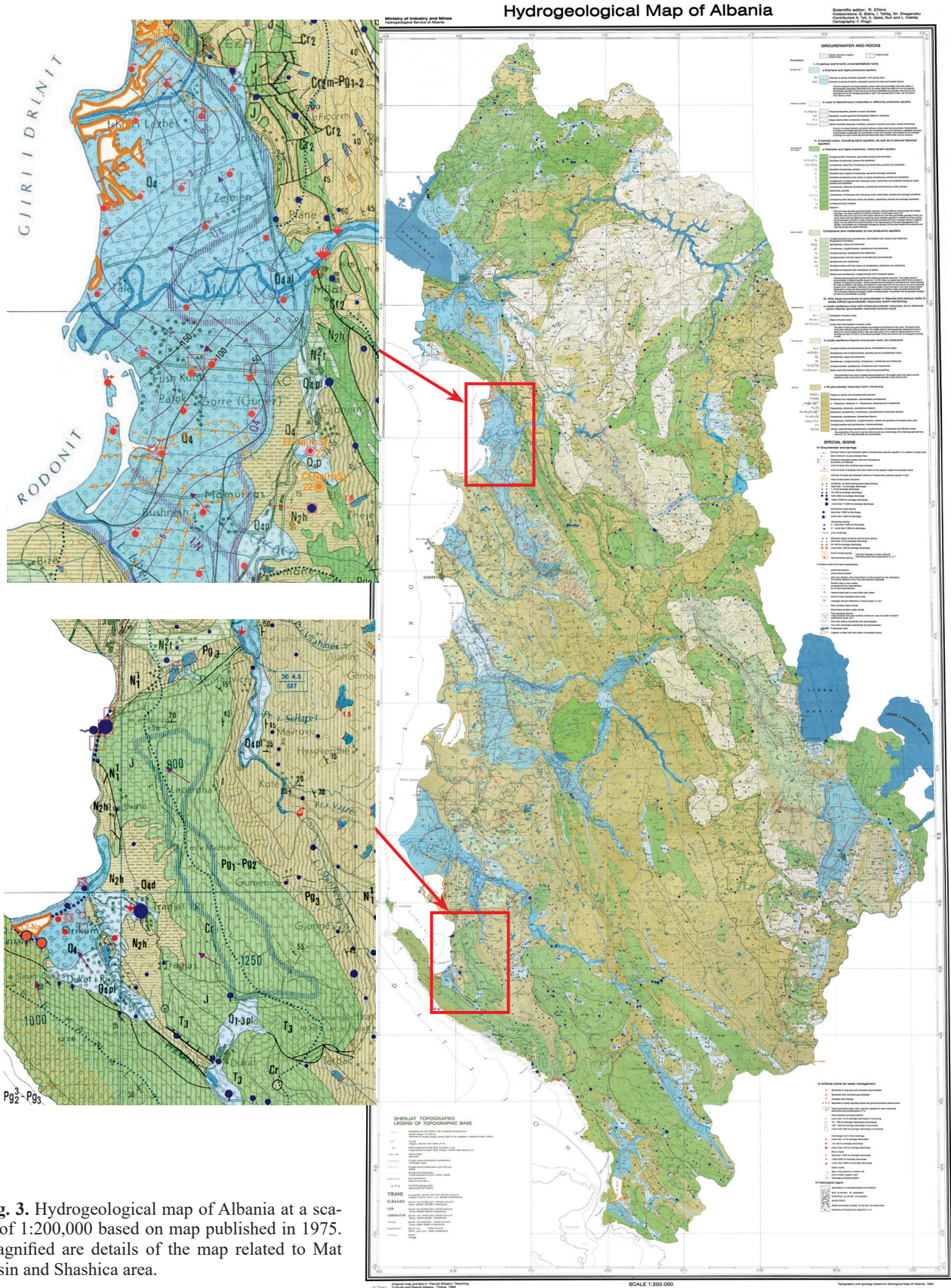


Fig. 3. Hydrogeological map of Albania at a scale of 1:200,000 based on map published in 1975. Magnified are details of the map related to Mat basin and Shashica area.

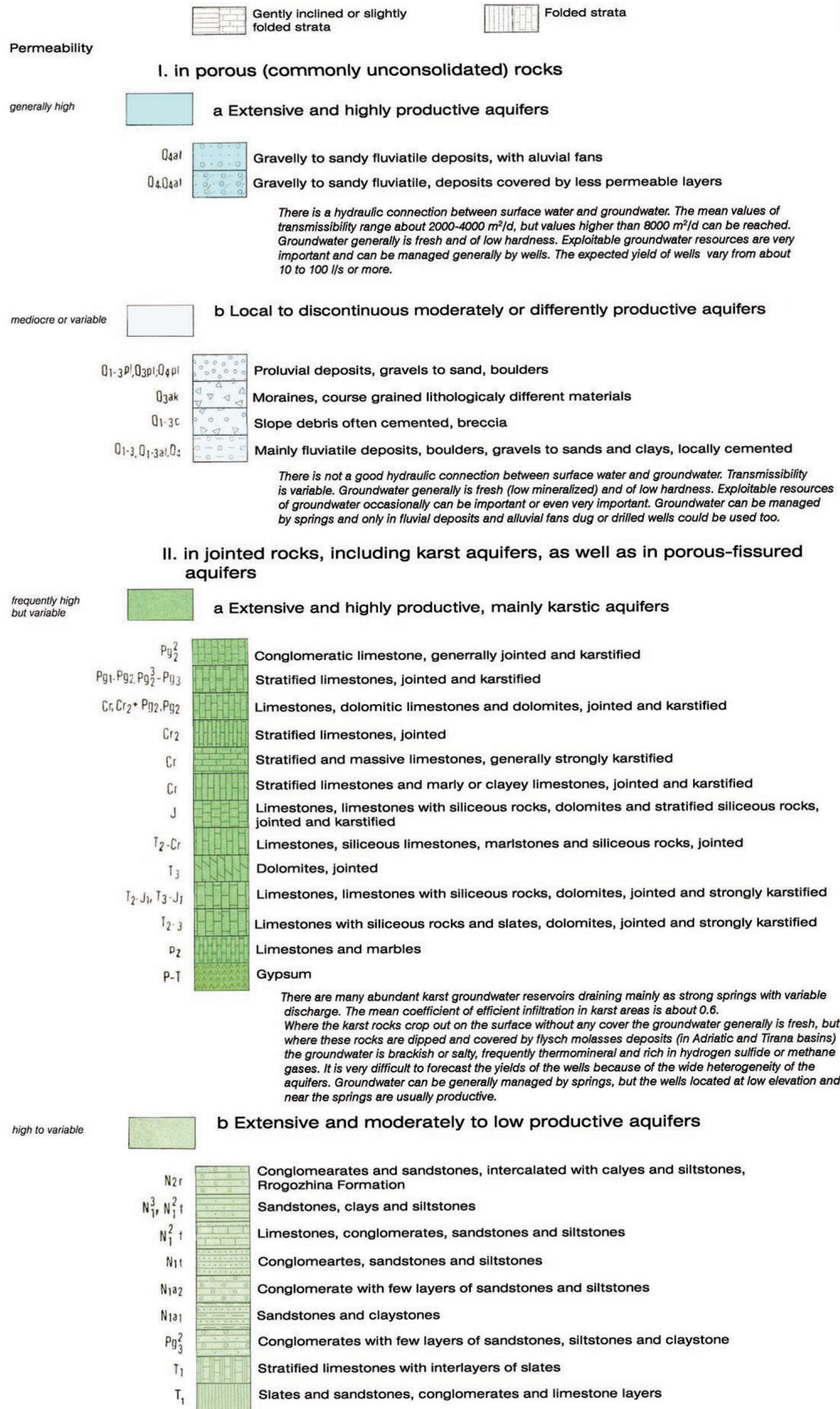
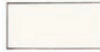


Fig. 4a. Hydrogeological map of Albania sc. 1:200,000; hydrogeological classification of the rocks – first part.

Fissured and porous-fissured aquifers with variable groundwater resources. The median values of transmissibility of different aquifers range from 1 to 50 m²/day, but values about 200 m²/d are present in aquifers of Progozhina Formation. The groundwater at all the aquifers is confined and on broad territories the wells are artesian, free flowing. The capacity of wells varies from 0.2 l/s to about 4 l/s, and occasionally to about 10 l/s. To a depth of 300-400 m the groundwater is brackish or salty, frequently thermomineral, rich in bromide, iodide and hydrogen sulfide of methane gases. Groundwater can be generally managed by wells and subordinately by springs.

III. Only local occurrence of groundwater in fissured and porous rocks or areas without groundwater resources worth mentioning

mediocre to low



a Locally aquiferous rocks with limited groundwater resources, but in fractured zones important groundwater resources could be found

- 6J₂₋₃  Ultrabasic intrusive rocks
- VP₂, VJ₂₋₃  Basic intrusive rocks
- Є-P-T₁, YJ₃, YCr₁  Acidic and intermediate intrusive rocks

The yields of wells show great variations accordingly to the fracturing of the rocks. The tectonic fault zones have distinctly higher productivity. The median yield for wells penetrating marked fault zones is about 2 l/s, and the highest yield of wells may reach about 10 l/s, while the highest yields from mine workings can reach 70-100 l/s. Groundwater generally is fresh and soft and can be managed by springs or wells.

low to very low



b Locally aquiferous fissured and porous rocks, low productive

- N₂, O₁  Conglomerates and sandstones poorly consolidated and clays
- N₁¹, N₁², N₁³, N₂  Sandstones and conglomerates, partially poorly consolidated clays
- N₁², h  Sandstones, clays and siltstones
- N₁b  Sandstones, conglomerates, limestones, marlstones and siltstones
- Pg₂, Pg₃²⁻³, Pg₃³  Conglomerates, sandstones, limestones and marlstones
- T₁, T₂a, βJ₂₋₃, J₃ef-s  Basic and intermediate effusive rocks and pyroclastites

The productivity of the rocks is variable being generally low. The median yield of the wells for all the aquiferous rocks is less than 0.3 l/s. The groundwater generally is fresh and low hard.

very low



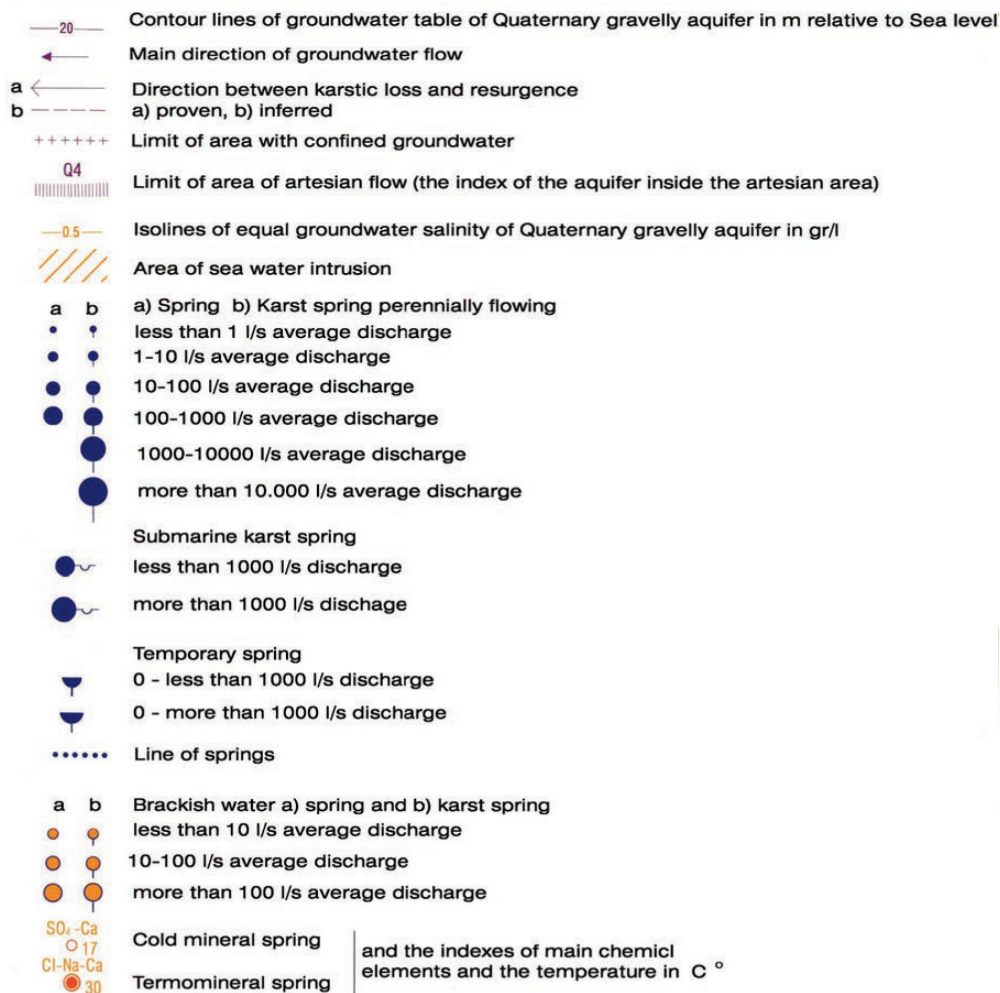
c No groundwater resources worth mentioning

- Q_{4d}, Q₄, Q₁₋₃  Clays to sands and occasionally gravels
- N_{1a1}, N₂, N₂h  Siltstones and claystones, subordinately sandstones
- a - N₁¹, N₁³ b - N₁¹⁺²  a - Claystone, siltstone, b - Claystones, siltstones and marlstones
- Pg₃, Pg₃¹  Claystones, siltstones, sandstones (flysch)
- Cr₂m - Pg₁₋₂, Pg₁₋₂, Pg₂²⁻³  Siltstones, sandstones, marlstones, subordinately limestones (flysch)
- Cr₂-m, Pg₁₋₂, Pg₂²  Claystones, sandstones, limestones (flysch)
- J₃-Cr₁, J₃l - Cr₂cm  Sandstones, marlstones, conglomerates, shales and gravels of variable grain size
- P - T₁  Conglomerates and sandstones, metamorphised
- P₂, P - T₁, T₁  Slates, subordinately sandstones, conglomerates, limestones and effusive rocks

The productivity of the rocks is very low, there are only very small springs with a discharge generally less than of 0.1 l/s. The wells practically are not productive.

Fig. 4b. Hydrogeological map of Albania sc. 1:200,000; hydrogeological classification of the rocks – second part.

IV Groundwater and springs



V Surface water and karst hydrography

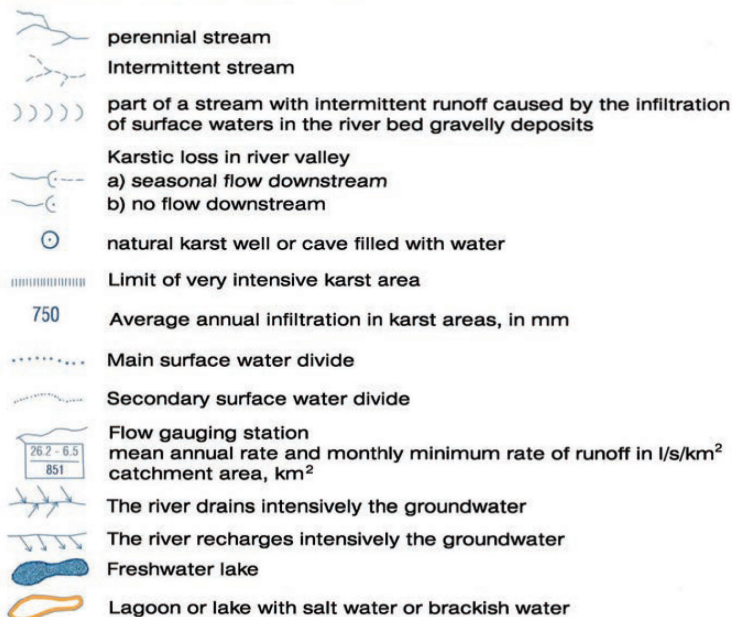


Fig. 5. Hydrogeological map of Albania sc. 1:200,000 – Special signs.

VI Artificial works for water management

- Borehole or dug well with phreatic groundwater
- Borehole with confined groundwater
- Artesian well flowing
- Borehole of deep aquifers below the ground surface sediments
- Thermomineral water well and the indexes of main chemical elements and temperature in °C
- Groundwater pumping station
- Less than 10 l/s average discharge of pumping
- 10 - 100 l/s average discharge of pumping
- 100 - 500 l/s average discharge of pumping
- more than 500 l/s average discharge of pumping
- Discharge from mine workings
- Less than 10 l/s average discharge
- 10-100 l/s average discharge
- more than 100 l/s average discharge
- ↓ River intake
- ↓ less than 1000 l/s average discharge
- ↓ 1000-5000 l/s average discharge
- ↓ more than 5000 l/s average discharge
- Other works
- 1.6 dam, and volume in million m³
- line of water supply main
- drainage pumping station

VII Geological signs

-  geological or hydrogeological boundaries
-  fault a) certain, b) supposed
-  Overthrust a) certain b) supposed
-  gravity block
-  Strike and dip of beds a) normal b) overturned
-  Isopachs of Quaternary deposits, in m

Fig. 6. Hydrogeological map of Albania sc. 1:200,000 – Geologically signs.

tional Legend (Karrenberg et al., 1974; UNESCO, 1970, 1983; IHME, 1970–1981). So, in section III of the hydrogeological map of Albania, an additional class is added, enabling to better distinguish the locally aquiferous rocks, showing a fairly wide distribution and high-water bearing variability. For each class of aquifers and rocks of HMA sc. 1:200,000, a short text of hydrogeological characteristics is given, missing in most of the maps, but helping the map user in better and more rapid understanding of the map content.

b) Special signs

This part of the legend includes the fourth and fifth chapter of the hydrogeological map legend, respectively:

Chapter IV – Groundwater and springs and Chapter V – Groundwater and karst hydrography (Fig. 5).

Chapter IV of the legend contains signs reflecting some point or areal data characterizing the groundwater occurrence and its properties. More in detail are characterized the Quaternary intergranular, mainly gravelly aquifers, through isolines of groundwater levels (hydroisohypses), the directions of groundwater flow movement, the areas with unconfined, confined and those with artesian flow, isolines of groundwater salinity in the ranges of 0.5, 1 and 3 g/l etc. The fresh water springs classified according to their mean discharges are presented in detail in the following ranges: up to 1 l/s, 1–10 l/s, 10–100 l/s, 100–1000 l/s, 1000–10,000 l/s and more than 10,000 l/s; Among the springs, the karst springs, temporary springs, submarine springs, as well as the linear springs are also distinguished by the use of special signs. Brackish water springs, cold mineral springs (water temperature below 20 °C, as well as hot thermal springs (water temperature above 20 °C), are also shown. In the coastal karst areas, the sea water intrusion is shown by a special sign.

Chapter V summarizes hydrological data, starting with the relation of surface water and groundwater. Various symbols are applied for different phenomena, such as the parts of river beds temporarily dry due to the loss of surface water into gravelly

deposits, parts of rivers which serve as intensive groundwater drains (gaining streams), or – in opposite – parts of the rivers which are intensively recharging groundwater resources (losing streams). Important hydrometric data for the main rivers at selected gauging stations, are also given. In karst areas, the limits of intensive rocks' karstification are identified, together with swallow holes (ponors), natural wells (groundwater windows), directions of verified or possible karst water flows, as well as for many karst areas annual values of effective precipitation / recharge are shown in [mm]. The effective precipitation (infiltration) values were calculated using the Turc (1954) formula, but applied only in karst areas without surface runoff (the effective precipitation is considered as the unevaporated part

of precipitation, which directly infiltrates into the subsoil and subsequently recharges groundwater resources).

In the Chapter VI of the legend, the artificial human interventions in water management practices are presented (Fig. 6). In addition to the boreholes, where respective signs differ according to the hydraulic character of the tapped aquifers, deep wells with thermo-mineral groundwater and some key physic-chemical parameters are also given. Discharges of the mining works (mine shafts and mine adits) are shown, classified in the ranges of up to 10 l/s, 10–100 l/s and over 100 l/s. Groundwater pumping stations (groundwater intakes) are distinguished according to the discharges as follows: up to 10 l/s, 10–100 l/s, 100–500 l/s and over 500 l/s. Pumping stations, in the case of springs, represent their capture structure, while in the case of drilling works, these mostly represent the central pumping station collecting water from several drilling wells, and only in particular cases these represent a single pumped borehole. The lines of water supply mains are also shown on the map, as well as river water intakes (mainly for irrigation), which according to their capacities are classified into three groups: up to 1000 l/s, 1000–5000 l/s and more than 5000 l/s.

Geological features are presented in the Chapter VII of the legend (Fig. 6). Here, in addition to the signs of geological boundaries, tectonic contacts, strike and deep of beds, also isolines of the Quaternary deposits thicknesses (isopaches) are also shown, practically marking the maximal effective depths of water wells in these deposits.

Discussion and Conclusions

The hydrogeological map of Albania at a scale of 1:200,000 is a general hydrogeological map and based on the hydrogeological classification of rocks that can be considered as a key element of the map. Such a principle of hydrogeological map compilation is of the same nature as the one used for the compilation of the International Hydrogeological Map of Europe (IHME) at a scale of 1:1,500,000, but another details were further on developed and enriched by additional original signs, particularly those related to groundwater chemistry (Eftimi et al., 2013). In general, respective geological situation represents the background of the map, while hydrogeological features are shown through seven areal colours representing the hydrogeological classification of the aquifers, aquitards and aquicludes formed by the rock environment.

In the HMA sc. 1:200,000, together 46 “lithological-stratigraphical-hydrogeological units” were distinguished, and these were subsequently classified into three “groups of rocks” within which a total of seven “classes” were differed. Comparing with the IHME, an additional class was added, enabling better classification of the local aquifers,

which have a fairly wide distribution in Albania and high-water bearing variability. For each class of aquifers and less-permeable rocks, a short text of hydrogeological characteristics was given, missing in majority of similar hydrogeological maps, but helpful in better and quick understanding of the content.

The principles applied in the process of construction of the Hydrogeological map of Albania at a scale of 1:200,000 can therefore provide important information about location of the aquifers and less-permeable rocks, groundwater resources and their quality, groundwater dynamics, the relationship between surface water and groundwater and the location of important springs and groundwater pumping stations. This map is sufficiently rich in details, so it can be used not only for planning of groundwater exploitation, but even for solving many practical problems of groundwater use and its protection.

The HMA sc. 1:200,000 was published in 1985 and by any doubt it reflects the scale of knowledge in the time of its publication, nonetheless the basic principles of the compilation of the map are adequate even today and it can be considered both as a document of hard work in uneasy times, but still preserving its scientific and practical value (Malik et al., 2015; Duscher et al., 2015).

References

- ANONYMOUS, 1970: International Legend for Hydrogeological maps, UNESCO (IASH/ IAH). *London, Inst. Geol. Sci., 101 pp.*
- ANONYMOUS, 1983: International Legend for Hydrogeological maps 1983, Revised ed., UNESCO Techn. Document, SC-84/W/7. *Paris, 51 pp.*
- ALTOVSKI, M. E., 1960: Metodicheskie ukazaniya po sostavleniju gidrogeologicheskikh kart mashtabov 1:1,000,000–1:500,000 i 1:200,000–1:100,000 (in Russian) (The methods of compilation of hydrogeological maps scale 1:1,000,000–1:500,000 and 1:200,000–1:100,000). *Moskva, 50 pp.*
- BABAMETO, A., 1965: Hydrogeological investigation of Erzen-Shkumbin area, sc. 1:50,000 (in Albanian). *Tirana, archive AGS.*
- BABAMETO, A. & KONDO, M., 1981: Groundwater of Zadrime area (presented in scale 1:25,000). *Tirana, archives AGS.*
- BISHA, G., EFTIMI, R. & ZAÇE, Ë., 1980: Hydrogeological investigation of Vlora area (in Albanian), scale 1:50,000. *Tirana, archive AGS.*
- BISHA, G. & PRENGA, L. I., 1981: Hydrogeological investigation of Lezha plain (in Albanian), scale 1:25,000 *Tirana, archives AGS.*
- Bulgarian Academy of Science – Geological Institute “Strashimir Dimitrov”, 1960: Map of Hydrogeological Division of PR Bulgaria, sc. 1 : 600,000. *Sofia. One sheet. Kartproekt Sofia 1960*
- DUSCHER, K., GÜNTHER, A., RICHTES, A., CLOS, P., PHILIP, U. & STRUCKMEIER, W., 2015: The GIS layers of the “International Hydrogeological Map of Europe 1:1,500,000” in e vector format. *Hydrogeol. J., 23: 1867–1875.* DOI 10.1007/s10040-015-4.

- EFTIMI, R., 1966: Outlook of hydrogeology of the Mat River alluvial Plain (in Albanian). *Përmb. Stud.*, 3, 53–65.
- EFTIMI, R., 1975: Groundwater of Lushnja area (in Albanian). *Përmb. Stud.*, 3, 133–152.
- EFTIMI, R., 1982: A general evaluation of the hydraulic parameters of the intergranular aquifers of PreAdriatic Lowland and capacity of wells. *Bul. Shk. Gjeol.*, 1, 129–139.
- EFTIMI, R., 1985: Hydraulic and yield of wells of sandstone-conglomerate aquifer of Rrogozhina Formation in Albania (in Albanian). *Bul. Shk. Gjeol.*, 2, 1985, 109–127.
- EFTIMI, R., TAFILAJ, I., GJATA, A., TYLI, N., BISHA, G. & HABILAJ, L., 1977: Principles of compilation of hydrogeological map of Albania sc. 1:200,000 (in Albanian). *Përmb. Stud.*, 3, 147–158.
- EFTIMI, R. & TAFILAJ, I., 1979: A short overview of on groundwater of Albania (in Albanian). *Përmb. Stud.*, 1, 133–152.
- EFTIMI, R., BISHA, G., TAFILAJ, I. & HABILAJ, L., 1985: Hydrogeological map of PSR of Albania, scale 1:200,000. *Tirana, Nd. Mjeteve Mësimore Hamdi Shijaku*.
- EFTIMI, R., TAFILAJ, I., BISHA, G. & HABILAJ, L., 1986: Hydrogeological Map of Albania scale 1:200,000. *Bul. Shk. Gjeol.*, 4, 133–147i.
- EFTIMI, R., BISHA, G., TAFILAJ, I. & SHEGANAKU, Xh., 2013: Hydrogeological mapping in Albania: from IHME contribution to larger-scale national maps. Presentation at the International Workshop on Groundwater Systems in Europe, Berlin, 22-23 August 2013. http://www.bgr.bund.de/EN/Themen-/Wasser/Veranstaltungen/workshop_ihm_2013/ihm-2013_inhalt.html?nn=1559030. 201692.710423. DOI 10.13140/RG.2.2.32Stojev V 2021 Hydrogeology.
- GAJTA, A., 1968: Hydrogeology of Fushe Kuqe-Gore artesian basin and the perspective of groundwater exploitations. *Tirana, archive AGS*.
- GJATA, A., 1978: Groundwater of Kavaja area (in Albanian). Internal Report. *Tirana, archive AGS*.
- GJATA, A., TYLI, N., BABAMETO, R. & EFTIMI, R., 1967: Hydrogeological investigation scale 1:50,000 of Fushë Krujë-Koplik area (in Albanian). *Tirana, archive AGS*.
- GUZELOVSKI, D. & KOTEVSKI, G., 1977: Hydrogeological map of Map of Macedonia, scale 1:200,000.
- IGI, 1967: Geological Map of Albania sc. 1:200,000. *Tirana, Inst. Geol. Investig.*
- IGI, 1986: Geological Map of Albania sc. 1:200,000. *Tirana, Inst. Geol. Investig.*
- Institute Geologique du Bucharest, 1961: Carte Hydrogeologique du Rumanie. *Bucharest, Comite d'état geol.*
- IHME-International Hydrogeological Map of Europe 1:1.500,000. *Hanover, Bundesanst Geowiss. Rohstoffe, UNESCO:*
- Sheet C5 Bern (Sci. Ed. Karrenberg, H.), 1970,
 - Sheet C3 Oslo (Sci. Ed. Karrenberg, H., Hornsten, A. & Persson, G.), 1979,
 - Sheet E3 Moskva (Sci. Ed. Egorov, S. V., Karrenberg, H.), 1979,
 - Sheet B3 Edinburg (Sci. Ed. Karrenberg, H., Moseley, R. & Day, B. V.), 1980,
 - Sheet D3 Stockholm (Sci. Ed. Egorov, S. V. & Karrenberg, H.), 1981.
- JAHO, S. (Ed.), 1984: Climate of Albania (in Albanian). *Tirana, Inst. Hydrometeorol.*, 296 pp.
- JÄCKLI, H. & TEMPE, Th., 1972: Hydrogeologische karte der Schweiz 1:100,000, Blatt Bözberg – Bermünster. *sheet. Swiss*
- KAZAZI, M., 1971: Karst springs of Albania, Hidmet. *Tirana. GC, Zurich 24–37 pp.*
- KARRENBERG, H. & DEUTLOFF, O., 1973: Directions for the construction of the International Hydrogeological map of Europe 1:1.500,000. *Bull. Inform. (Paris)*, 15–16, 58–63.
- KARRENBERG, H., DEUTLOFF, O. & STEMPEL, Cv. 1974: General Legend for the International Hydrogeological Map of CV Europe. Published by Bundesanst, Bodenforsch and UNESCO. *Hannover, S.EL.CA Firenze*, 49 pp.
- KARRENBERG, H. & STRUCKMEIER, W., 1979: The hydrogeological Map of Europe. *Episods IUGS (Ottawa)*, 1978, 4, 16–18.
- KETA, Z. & MITRO, S., 1967: Hydrogeology of subartesian basin of Vjosa River (in Albanian). *Tirana, archive AGS*.
- KETA, Z., EFTIMI, R., BABAMETO, A. & RUDI, N., 1968: Hydrogeological study scale 1:100,000 of the area Rrëshen – Peshkopi (in Albanian). *Tirana, archives AGS*.
- KETA, Z., BABAMETO, A. & RUDI, N., 1970: Hydrogeological investigation scale 1:100,000 of the area Elbasan – Librazhd – Prenjas (in Albanian). *Tirana, archive AGS*.
- KRISTO, V., 1973: Some aspects of the karst of Albania (in Albanian). *Përmb. Stud. (Tirana)*.
- LAKO, A., 1963: Hydrogeological investigations of Dobraq explotation area, Shkodra. *Tirana, archive AGS*.
- LAKO, A., 1968: Hydrogeological investigation scale 1:50,000 of Narta-Libofsha area (in Albanian). *Tirana, archives AGS*.
- LAKO, A., 1973: Hydrogeological conditions of Shkumbin River valley of the area Labinot-Fushe Cerrik (in Albanian). *Përmb. Stud.*, 3, 105–133.
- MALÍK, P., ŠVASTA, J., GREGOR, M., BAČOVÁ, N., BAHNOVÁ, N. & PAŽICKÁ, A., 2015: Slovak basic hydrogeological maps at scale of 1:1.500,000 – compilation of methodology, standardized GIS processing and contemporary country coverage. *Slovak Geol. Mag.*, 15, 2, 121–144.
- MANFREDINI, M., 1971: Carta idrogeologica della Piana di Rieti. *Istit. Ricerca Sulle Acque C. N. R.*
- MARGAT, J., 1966: La cartographie hydrogeologique, Chronique d'Hydrogéologie. *Paris, BRGM*, 9, 7–32.
- MARGAT, J. & ROGOVSKAJA, N. V., 1979: Cartographie des ressources en eau souterraine (AIH) Symp. Intern. Vilnius U.S.S.R. juil. 1979. Rapport general theme VIII, Mém. AIH, T. XV-2-Moscou/Doc BRGM 79 SGN 783 HYD J. M., *Orléans*, 18 pp.
- MAURIN, V. & ZÖTL, J., 1964: Hydrogeologie und Vertarstung der Steiermark, Masztab 1:300,0000. *Graz, Akad. rucku Verlagsanst.*
- MEÇE, S. & ALIAJ, Sh., 2000: Geology of Albania. *Berlin – Stuttgart, Gebrüder Bortntraeger*, 246 pp.
- MITRO, S., 1963: Hydrogeological investigation of Elbasan area during 1961. *Tirana, archive AGS*.
- PANO, N. (ed.), 1984: Hydrology of Albania (in Albanian). *Tirana, Inst. Hydrometeorol.*, 434 pp.
- PENCHEV, P., 2000: Groundwater map of Bulgari sc. 1:500,000. *One sheet. Ministry of Environment, Sofia*.
- PFEIFFER, D., 1975: The map of the Islands of Singapore 1:100,000. *Hannover, Geol. Jahrb. Rh. c – Heft 9*.

- PRENGA, LL., 1984a: Groundwater of Ballagat-Rrogzhihës area (in Albanian). *Tirana, archive AGS*.
- PRENGA, LL., 1984b: Hydrogeology of Lushnjë-Peqin-Rrogzhihë area, investigated during 1957–1980. *Tirana, archives AGS*.
- ROGOVSKAJA, N. V., 1970: Obzor i analiz hidrogeologjiçeskikh kart fonda UNESCO po sostajani na 1.11.1969. *Sovjet. Geol.*, 2.
- RUDI, N., 1969: Hydrogeological prospecting scale 1:100,000 of the Kukes area (in Albanian). *Tirana, archive AGS*.
- RUDI, N., 1972: Hydrogeological investigation scale 1:100,000 of the area Shkodra–Puka–Tropoja–Vermosh. *Tirana, archives AGS*.
- SHTREPI, P., 1972: Hydrogeological closeness of Kurvelesh tectonic belt. *Oil Gas, 1, Oil Gas Inst., Fier*.
- SHTREPI, P., 1973: Hydrogeological conditions of Kurvelesh-Berat tectonic belt (in Albanian). *Fier, Oil Gas Inst.*
- STRUCKMEIER, W. F., 1989: Types and uses of hydrogeological maps. In: Memoires of the International Symposium on Hydrogeological Maps as Tools for Economic and Social Development, *Hannover, 1989, 17–30*.
- STRUCMEIER, W. F. & MARGAT, J., 1995: Hydrogeological maps. A Guide and Standard Legend. *Internat. Contr. Hydrogeol.*, 17, *Heise, Hannover, 177 p.*
- UNESCO, 1970: International legend of Hydrogeological Maps. Inst. Geol. Sci, London, A contribution to the International Hydrogeological Decade. *Studies and Reports (Lausanne)*, 20.
- UNESCO, 1983: International legend for hydrogeological map, revised edition. UNESCO, Paris. http://unesdoc.unesco.org/im_andages/0015/001584/158459eo.pdf. Accessed 4 May 2015.
- TAKAHASHI, SH., 1971: Hydrogeological Map of Hino Riner basin. Tottori Prefecture, 1:50,000. *Geol. Surv. Japan*.
- TAFILAJ, I., 1960–1985: Hydrogeological investigations of Albanian mines (in Albanian). *Tirana, archive AGS*.
- TAFILAJ, I., 1977: Hydrogeological classification of mines of Albania (in Albanian). *Përmb. Stud.*, 1, 109–128.
- TARTARI, M., 1979: Groundwater of Berat area (in Albanian). *Tirana, archive AGS*.
- TURC, L., 1954: Le bilan d'eau des sols. Relations entre les precipitations, l'évaporation et l'écoulement. *Ann. Agronomiq.*, 5.
- TYLI, N., 1971: The groundwater of Korça lowland and their importance (in Albanian). *Tirana, archive AGS*.
- TYLI, N., 1972: Hydrogeological conditions of Shkodra area (in Albanian). *Tirana, archive AGS*.
- TYLI, N., 1976: Groundwater regimen based on stationary observations. *Përmb. Stud.*, 4, 131–152.
- XHOMO, A., KODRA, Z., XHAFI, Z. & SHALLO, M., 2002: Geology of Albania (in Albanian). *Tirana, Albanian Geological Service (or AGS), 410 pp.*

Hydrogeologická mapa Albánska v mierke 1 : 200 000, princípy jej zostavenia a obsah – dokument priekopníckeho prístupu k hydrogeologickému prieskumu v Albánsku od šesťdesiatych rokov minulého storočia

Koordinovaný hydrogeologický výskum v Albánsku (obr. 1) sa začal v roku 1959. V rokoch 1963 – 1974 celoštátny prieskum na tomto území (obr. 2) vyústil do zostavenia *Hydrogeologickej mapy Albánska v mierke 1 : 200 000*. Táto mapa bola publikovaná v roku 1975 (obr. 3). Spĺňala kritériá, ktoré definovala Medzinárodná asociácia hydrogeológov a UNESCO v roku 1970 pre generálne hydrogeologické mapy. Tieto kritériá sa ale pri zostavovaní mapy ďalej zdokonaľovali ďalšími originálnymi prístupmi (obr. 4A, B, 5 a 6), týkajúcimi sa predovšetkým chemického zloženia podzemnej vody (Eftimi et al., 2013). Hydrogeologická klasifikácia hornín je vyjadrená siedmimi farbami, čo reprezentuje zdokonalenie dovtedy používanej kvantitatívnej klasifikácie zvodnencov. Hydrogeologická klasifikácia hornín predstavuje základný a inovatívny prvok mapy. Základné chemické prvky zobrazené na mape reprezentujú bázu na vyčlenenie hydrogeologických jednotiek. Na mape je zobrazených celkovo 46 „litologicko-stratigraficko-hydrogeologických“ jednotiek. Tie sú následne klasifikované do troch skupín hornín, v rámci ktorých je definovaných sedem tried. Na rozdiel od *Medzinárodnej hydrogeologickej mapy Európy v mierke 1 : 500 000* bola na *Hydrogeologickej mape Albánska v mierke 1 : 200 000* pridaná ďalšia trieda. Umožnila lepšiu klasifikáciu lokálnych hydrogeologických kolektorov a izolátorov, ktoré majú v Albánsku veľké rozšírenie a majú značnú variabilitu hydraulických vlastností. Pri každej triede zvodnencov a menej priepust-

ných hornín je na mape pridaný krátky vysvetľujúci text o ich hydrogeologickej charakteristike. Napriek tomu, že tento vysvetľujúci text je veľmi užitočný na ľahké a rýchle pochopenie regionálnych hydrogeologických pomerov, na zahraničných hydrogeologických mapách spravidla chýba.

Geologickú stavbu územia reprezentuje na mape spodná vrstva, pričom jednotlivé litologické jednotky sa vzájomne odlišujú šrafovaním zelenej farby. Na mape sú zvýraznené aj rozdielne zvodnence a identifikované hydrogeologické štruktúry a vyznačené aj významnejšie vodárenské zdroje a hydrogeologicky produktívne vrty. Mapa poskytuje informácie o kvalite vôd, termálnych prameňoch, oblastiach ovplyvňovaných prenikaním morskej vody a vyjadruje vzťah medzi povrchovou a podzemnou vodou

Hydrogeologická mapa Albánska v mierke 1 : 200 000 publikovaná v roku 1975 odzrkadľuje nielen rozsah vtedajších hydrogeologických poznatkov. Základné princípy jej zostavovania sú aktuálne aj v súčasnosti a vyjadrujú množstvo kvalitnej zrealizovanej práce a vtedajší vedecký potenciál, ktorý bol využitý pri zostavovaní mapy (Malík et al., 2015; Duscher et al., 2015). Táto mapa sa stále využíva predovšetkým na účely plánovania a ako pomôcka pri riešení mnohých praktických hydrogeologických problémov.

Doručené / Received: 20. 5. 2022

Prijaté na publikovanie / Accepted: 21. 6. 2022

Inštrukcie autorom

Etika publikovania, záväzná pri publikovaní v časopise Mineralia Slovaca:

www.geology.sk/mineralia položka **Publikačná etika**

1. Geovedný časopis Mineralia Slovaca publikuje scientometricky hodnotné recenzované pôvodné vedecké články s vysokým citačným potenciálom. V úvode príspevku musí autor jasne deklarovať, čím konkrétnym je jeho príspevok prínosný pre rozvoj geovied. Rešeršné štúdie sa publikujú len ojedinele.

2. Články na publikovanie (manuskripty) sa do redakcie zasielajú poštou (dva výtlačené exempláre a CD so všetkými súbormi v editovateľnej podobe) alebo e-mailom (editovateľné súbory a kompletná verzia vo formáte PDF).

3. Súčasne s článkom je potrebné redakcii poslať autorské vyhlásenie o originalite textu a obrázkov. Kópie obrázkov z iných publikácií musia byť legalizované získaním práva na publikovanie. Vyhlásenie musí obsahovať meno autora (autorov), akademický titul a trvalé bydlisko.

4. Rozsah manuskriptu na publikovanie je najviac 25 rukopisných strán (MS Word, Times New Roman, veľkosť písmen 12 bodov, riadkovanie 1,5) vrátane literatúry, obrázkov a vysvetliviek. V prípade veľkého odborného prínosu sú v ojedinelých prípadoch povolené aj dlhšie články.

5. Články sú publikované v angličtine alebo v slovenčine. Články v slovenčine musia obsahovať anglický preklad názvu, abstraktu, kľúčových slov, resumé a popisov k obrázkom a tabuľkám. Články písané v angličtine musia obsahovať slovenské resumé.

Text

1. Abstrakt stručne sumarizuje článok. Môže mať najviac 200 slov a nemá obsahovať citácie. Počet kľúčových slov je maximálne 6. Text má mať úvod, charakteristiku (stav) skúmaného problému, použitú metodiku, nové zistenia, ich interpretáciu, diskusiu, záver a zoznam literatúry. Východiskové údaje musia byť zreteľne odlišené od interpretácií. V texte musia byť odvolávky na všetky použité obrázky a tabuľky.

2. Hierarchiu nadpisov v texte je potrebné vyznačiť ceruzkou na ľavom okraji strany manuskriptu: 1 – najvyššia, 2 – nižšia, 3 – najnižšia.

3. V texte sa uprednostňuje citácia v zátvorke, napr. (Dubčák, 1987; Hrubý et al., 1988), pred formou ... podľa Dubčáka (1987).

4. Pozícia obrázkov a tabuľiek v texte sa označí. Nie je vhodné, aby text v editore MS Word obsahoval vložené obrázky, ale náhľadová verzia v pdf ich má obsahovať.

5. Grécke písmená treba identifikovať na ľavom okraji slovom (napr. sigma). Potrebne je odlišovať pomlčku od spojovníka. Symboly, matematické značky, názvy skamenelín a pod., ktoré sa majú vysádzať kurzívou, autor v rukopise podčiarkne vlnovkou.

Obrázky a tabuľky

1. Ilustrácie a tabuľky vysokej kvality bývajú publikované buď na šírku stĺpca (81 mm), alebo strany (170 mm). Optimálna veľkosť písma a čísiel v publikovaných obrázkoch je 2 mm. Články v slovenčine musia mať popisy v obrázkoch a tabuľkách v slovenčine, záhlavie tabuľiek a texty pod obrázkami a tabuľkami sú v slovenčine a angličtine. Články v angličtine majú všetky texty v angličtine. Maximálny rozmer ilustrácie a tabuľky výtlačnej v časopise je 170 x 230 mm. Väčšie (skladané) ilustrácie sú publikované len v ojedinelých prípadoch.

2. Pri počítačovej tvorbe obrázkov odporúčame používať programy s vektorovým zobrazením (Corel Draw, Adobe Illustrator a pod.). Čiary tzv. vlasovej hrúbky, softvérová alebo rastrová výplň plôch (napr. v Corel Draw) nie sú prípustné. Výplne v obrázkoch musia pozostávať zo samostatne vyzádaných objektov.

3. Ilustrácie vrátane fotografií musia obsahovať grafickú mierku v centimetrovej či metrovej škále, prípadne sa rozmer zobrazených objektov vyjadri v popise obrázka. Mapy a profily musia mať aj azimutálnu orientáciu a jednotné vysvetlivky, ktoré sa uvedú pri prvom obrázku. Zoskupené obrázky, napr. fotografie a diagramy, sa uvádzajú ako jeden obrázok s jednotlivými časťami označenými písmenami (a, b, c atď.).

4. Pri zasielaní fotografií vo forme počítačových súborov (formáty JPG alebo TIF) sa požaduje rozlíšenie minimálne 600 DPI. Publikovanie farebných ilustrácií môže byť spoplatnené.

Literatúra

1. Minimálne 50 % citácií musí reprezentovať publikácie od roku 2000. V zozname literatúry sa v abecednom poradí uvádza len literatúra citovaná v danom článku.

2. Spôsob uvádzania literatúry v zozname literatúry

Knižná publikácia: GAZDA, L. & ČECH, M., 1988: Paleozoikum medzevského príkrovu. Bratislava, Alfa, 155 s.

Časopis: VRBA, P., 1989: Strižné zóny v metapelitoch. Miner. Slov., 21, 135 – 142.

Zborník: NÁVESNÝ, D., 1987: Vysokodraselné ryolity. In: Romanov, V. (ed.): Stratifonné ložiská gemerika. Spec. publ. Košice, Slov. geol. spol., 203 – 215.

Manuskript: RADVANSKÝ, F., SLIVKA, B., VIKTOR, J. & SRNKA, T., 1985: Žilné ložiská jedloveckého príkrovu gemerika. Záverečná správa z úlohy SGR-geofyzika. Manuskript. Spišská Nová Ves, archív Št. Geol. Úst. D. Štúra, 28 s.

3. Pri článku viac ako dvoch autorov sa v texte cituje iba prvý autor s dodatkom et al., ale v zozname literatúry sa uvádzajú všetci.

Instructions to authors

Publication ethics, being obligatory for publishing in the journal Mineralia Slovaca:

www.geology.sk/mineralia item **Publication ethics**

1. Geoscientific journal Mineralia Slovaca publishes scientometrically valuable original peer-reviewed scientific articles with a high citation potential. In the introduction of each article the author(s) must clearly declare, which innovative data the paper brings for the development of geosciences. The retrieval studies are published only exceptionally.

2. The articles for publishing (manuscripts) must be sent to Editorial Office by post (two printed copies and CD with editable files), or by e-mail (editable files plus complete preview version in PDF format).

3. Simultaneously with the article the Editorial Office must receive the author's proclamation that no part of the manuscript was already published and figures and tables are original as well. Copied illustrations from other publications must contain a copyright.

4. The extent of the manuscript for publishing is limited to 25 manuscript pages (MS Word, 12 points Times New Roman, line spacing 1.5) including figures, tables, explanations and references. In the case of contribution with a high scientific value, the longer manuscripts for publishing are exceptionally permitted.

5. Articles can be published in Slovak or English languages. The title, abstract, key words, shortened text (resumé), as well as description to figures and tables in Slovak articles are published also in English. Articles published in English contain Slovak resumé.

Text

1. Abstract briefly summarizing the article is limited to 200 words, no references are allowed. The maximum number of key words is 6. Text of the article has to contain the introduction, characterization (state) of investigated problem, applied methodology, obtained new data, discussion, conclusion and references. The obtained data must be distinctly separated from interpretations. All applied figures and tables must be referred in the text.

2. The hierarchy of headings in the manuscript must be indicated by a pencil note: 1 – highest level, 2 – lower, 3 – lowermost level.

3. The references in the text prefer parentheses, e.g. (Dubčák, 1987; Hrubý et al., 1988). The form "according to Dubčák (1987)" should be used only exceptionally.

4. Position of figures and tables must be indicated in the manuscript. Editable text of manuscript sent to editorial office must be without figures and tables, though the preview PDF has to contain them in a correct position.

5. Greek letter in the text must be identified at the left margin of the text (e.g. sigma). The text should strictly distinguish the dash from hyphen. Symbols, mathematic signs, names of fossils, etc., which should be printed in italics, must be underlined by the wavy line in the manuscript.

Figures and tables

1. The high quality figures and tables can be published either in maximum width of column (81 mm) or page (170 mm). The optimum size of letters and numbers in the camera-ready figure is 2 mm. Articles published in Slovak contain the Slovak descriptions in figures and tables, the tables headings and descriptions beneath figures and tables are in Slovak and English. English articles contain all texts in English. Maximum dimension of figures and tables in the journal is 170 x 230 mm. Larger (folded) illustrations are published only exceptionally.

2. For figures drawing the editorial office recommends the vector graphics editors (Corel Draw, Adobe Illustrator, etc.). The very thin lines (hair lines), the pre-defined software or raster fillings of polygons (e.g. in Corel Draw) are not allowed. The filling must consist from separately set objects.

3. Each illustration including photographs must contain graphic (metric) scale, eventually the dimensions of visualized objects have to be stated in the describing text to figure. Maps and profiles must contain also the azimuth orientation, their detail explanations are stated at the first figure. Grouped figures, e.g. photographs and diagrams, are compiled as one figure with separate parts designated by letters (a, b, c, etc.).

4. The photographs sent as JPG or TIF files are required for having minimum 600 DPI resolution. Publishing of colour illustrations can be charged by a fee.

References

1. Minimum 50 % of referred works must represent contemporary publications after 2000. The references in alphanumeric order encompass only literature cited in the article.

2. Examples of referring:

Book: GAZDA, L. & ČECH, M., 1988: Paleozoic of the Medzev nappe. Bratislava, Alfa, 155 p.

Journal: VRBA, P., 1989: Shear zones in the metapelite complexes. Miner. Slov., 21, 135–142.

Anniversary volume: NÁVESNÝ, D., 1987: High-potassium rhyolites. In: Romanov, V. (ed.): Stratiform deposits of Gemericum. Spec. publ. Košice, Slov. geol. soc., 203–215.

Manuscript: RADVANSKÝ, F., SLIVKA, B., VIKTOR, J. & SRNKA, T., 1985: Vein deposits of the Jedlovec nappe of Gemericum. Final report from the project SGR-geophysics. Manuscript. Spišská Nová Ves, Archive Št. Geol. Úst. D. Štúra, 28 p.

3. The article with more than two authors is referred by the name of the first author with the amendment et al., but the list of references contains names of all authors.

OBSAH – CONTENT

PŮVODNÉ ČLÁNKY – ORIGINAL PAPERS

Danková, Z., Bekényiová, A., Čechovská, K., Fedorová, E., Nováková, J., Uhrinová, K., Briančin, J. & Kúšik, D.
Experimental study of polluted sediment and As elimination from the pit water in the locality of Zlatá Idka-Rieka, Slovakia

Štúdium kontaminovaných sedimentov a eliminácie As z podzemnej banskej vody na lokalite Zlatá Idka-Rieka

Valovičová, V., Dolinská, S., Vaculíková, L., Plevová, E., Znamenáčková, I. & Danková, Z.
Characterization of fine-grained montmorillonite fractions for preparing polymer-clay nanocomposites
Charakteristika jemnozrnej frakcie montmorillonitu na prípravu polymérových ílovitých nanokompozitov

Čičáková, C., Tóth, R., Horváthová, H., Drábik, A., Jurkovič, Ľ. & Kravchenko, D.
Electroremediation in low-hydraulic conductivity zones – current stage of knowledge and small-scale laboratory experiment

Elektroremediácia v zónach s nízkou hydraulickou vodivosťou – súčasný stav poznatkov a laboratórny experiment

Bajtoš, P.

Use of analysis of seasonal hydrochemical regime for better understanding of mine water genesis and more accurate estimate of its impact on stream water quality at flooded Rudňany ore mine (North-Gemeric zone, Slovakia)

Využitie analýzy sezónneho hydrochemického režimu vody v zatopenej rudnej bani Rudňany na lepšie pochopenie jej genézy a presnejší odhad jej vplyvu na kvalitu vody v povrchovom toku

Phu, H., Tuan, L. C., Thao, N. L. N. & Han, H. T. N.

Relation of groundwater quality and peat deposits in Tay Ninh province, Vietnam
Vzťah kvality podzemnej vody a ložísk rašeliny na príklade monitorovacieho výskumu v provincii Tay Ninh, Vietnam

Eftimi, R., Basha, G., Tafilaj, I. & Sheganaku, X.

Hydrogeological map of Albania at a scale of 1:200,000, principles of compilation and content – a document of Albanian pioneering hydrogeological research since the 1960s

Hydrogeologická mapa Albánska v mierke 1 : 200 000, princípy jej zostavenia a obsah – dokument priekopníckeho prístupu k hydrogeologickému prieskumu v Albánsku od šesťdesiatych rokov minulého storočia

Indexed / Abstracted / Accessed by SCOPUS, WEB OF SCIENCE and EBSCO
Indexované / abstraktované / sprístupňované databázami SCOPUS, WEB OF SCIENCE a EBSCO

